Alma Mater Studiorum - Università di Bologna

DOTTORATO DI RICERCA IN

SCIENZA E CULTURA DEL BENESSERE E DEGLI STILI DI VITA

Ciclo 34

Settore Concorsuale: 03/D1 - CHIMICA E TECNOLOGIE FARMACEUTICHE, TOSSICOLOGICHE E NUTRACEUTICO - ALIMENTARI

Settore Scientifico Disciplinare: CHIM/08 - CHIMICA FARMACEUTICA

DEVELOPMENT OF ADVANCED ANALYTICAL METHODOLOGIES FOR ALZHEIMER'S DISEASE DRUG DISCOVERY

Presentata da: Lara Davani

Coordinatore Dottorato

Carmela Fimognari

Supervisore

Vincenza Andrisano

Esame finale anno 2022

Abstract

Alzheimer's disease (AD) is the most common type of dementia in the elderly population and it has become a global health concern due to the increase in life expectancy. Currently there are around 50 million people affected by AD worldwide, but in the near future this incidence is expected to rise causing a detrimental effect on the living conditions of AD patients and their families. The drugs currently approved for AD can only ameliorate the symptoms and slow down the cognitive decline for a period of 6-12 months, but they still do not prevent or block the progression of the disease. In this scenario, it is key to develop new strategies towards AD: on one hand, lifestyle has proved to have a central role in primary prevention, as it is able to modulate some of the risk factors of the disease; on the other hand, in order to address the multifactorial nature of the disease and after the recent failure of drug candidates in late-stage clinical trials, drug discovery is focusing on molecules able to interact simultaneously with different pathways involved in the pathogenesis. These compounds are called multi-target directed ligands (MTDLs). The present Ph.D. thesis aimed to develop advanced analytical methodologies suitable for the high throughput screening of natural or synthetic MTLDs candidates on isolated targets involved in the early stages of the pathogenesis. In addition, these methodologies had to be suitable for the characterization of the mechanisms underlying drug-protein bindings and for the study of protein-protein interactions involved in the neurodegenerative pathways.

Accordingly, a high-throughput luminescent assay was applied for screening potential GSK-3β dual inhibitors. The first-in-class of GSK-3β/ HDAC dual inhibitors was characterized towards GSK-3β. Interestingly, their simultaneous inhibition had already proved to give synergistic neuroprotective effects because their activities are strictly connected. The application of a kinase luminescent assay allowed to select an innovative disease-modifying agent among the series, with an activity in the micromolar range both on GSK-3β, HDAC1, and HDAC6. Moreover, this new lead is characterized by promising physicochemical properties. Then the high-throughput luminescent assay was applied in a study carried out in collaboration with the *Department of Pharmaceutical Botany* of Charles University (Hradec Králové, Czech Republic). Professor Cahlikova's research group isolated 28 Amaryllidaceae alkaloids from various Amaryllidaceous plants, and their inhibitory potency was screened against GSK-3β to find new potential natural scaffolds for MTDLs. Indeed, Amaryllidaceae alkaloids have shown to inhibit other serine/threonine kinases involved in carcinogenesis. Until now, despite the absence of studies concerning GSK-3β inhibition, these alkaloids have already been used in the treatment of AD due to their acetylcholinesterase (AChE) inhibitory property. Among the tested compounds, the assay identified the homolycorine and lycorine-type alkaloids as the most active registering IC_{50} values in the micromolar range (around 30 μM). Hence, the method proved able to reliably and quickly select true positive hit compounds, and also to identify in these molecules an interesting natural scaffold for GSK-3β dual inhibitors. Both *in vitro* characterizations provided information to perform structure activity relationship in view of the development and optimization of lead structures with an improved activity and bioavailability. Besides, considering the interest in analytical methods suitable for a preliminary screening, today pharmaceutical analysis is exploring new strategies to pursue two objectives: to further investigate the

structure and conformation of target proteins involved in AD pathogenesis; and to monitor the morphological changes after binding with the selected ligands.

Indeed, the analysis of protein–ligand interactions is important for understanding various biological phenomena and for pursuing drug development. Hence, given the central role of the amyloid pathway in the multifactorial nature of AD, a multi-methodological approach based on mass spectrometry (MS), circular dichroism spectroscopy (CD) and ThT assay was applied to characterize the potential interaction of CO releasing molecules (CORMs) with $A\beta_{1\text{-}42}$. These compounds had already proved to have anti-inflammatory and neuroprotective properties, therefore they resulted interesting in view of discovering molecules able to modulate the amyloid aggregation process and its related toxicity. The comprehensive method provided reliable information on the different steps of the fibrillation process and further details have been obtained regarding the mechanism of action of CORMs. Stable adducts between Ru $(CO)_2$ moiety of CORMs and the histidine residues of the amino acid chain of $A\beta_{1-42}$ were characterized by mass spectrometry. The optimal CORM-3/$A\beta_{1-42}$ ratio in terms of inhibitory effect was identified. When CORM-3 and $A\beta_{1-42}$ are in molar ratio 1:1, the signal of $A\beta_{1-42}$ monomers in mass spectra is still present. CD analysis confirmed that CORM-3 in this condition have a stabilizing effect on the $A\beta_{1-42}$ peptide soluble form, because spectroscopic signature of β-strand structures is not present. ThT Fluorescent Analysis ensured that all the fibrillation process is delayed. In view of MTDL research, CORM-3 emerged as a promising amyloid anti-aggregating agent with neuroprotective properties.

During my exchange period in the research group of Professor Laemmerhofer at *Institute of Pharmaceutical Sciences* (University of Tuebingen, Germany), the investigation of the amyloid aggregation process continued to find a possible correlation with lipid brain alterations that occur in the early stage of AD. In fact, lipidomics, exploiting the latest advances in the field of mass spectrometry, is an emerging tool in the research of new AD pathological mechanisms and clinically relevant biomarkers for AD early diagnosis. An LC-MS method was optimized to evaluate the $Aß_{1\text{-}42}$ oligomers toxic effects in terms of lipid alteration on differentiated human neuroblastoma derived SH-SY5Y cells. The analysis of SH-SY5Y cells lipidic profile was performed through RP-UHPLC system coupled with a high-resolution quadrupole TOF mass spectrometer in comprehensive data-independent SWATH acquisition mode. The lipidomic approach was able to determine potential biomarkers for targeting and testing AD by *in vitro* on cell assays that could be ascribed to $A\beta_{1\text{-}42}$ toxicity. We interpreted the alterations found in PC and LPC levels as caused by Phospholipase A2 (PLA2) enzyme activation that hydrolyses the sn-2 ester bond of the membrane glycerophospholipids to generate MUFAs containing lyso-phospholipids and polyunsaturated fatty acids (PUFAs). Both of them are biologically active lipid mediators, whereas arachidonic acid in particular plays a critical role in neuroinflammation. In the meantime, further alterations in the SM profile were revealed and it was hypothesized that these are due to SM-degrading enzyme Sphingomyelinase (SMase) activation. This enzyme hydrolyses the phosphocholine-headgroup of Sphingomyelins producing proapoptotic ceramides. Accordingly, recent studies have demonstrated the correlation between PLA2, SMase and AD pathogenesis. Therefore, these enzymes could represent interesting targets for AD drug discovery. Furthermore, provided the method is validated, it could also be applied to

monitor the effects of amyloid aggregation inhibitors, which are responsible not only to inhibit the aggregation process, but also to avoid the lipid homeostasis alterations.

List of Content

Aim of the Thesis

In the context of the research of new drugs and natural compounds biologically active towards Alzheimer's Disease (AD), the main goal of the present Ph.D. thesis was developing advanced analytical methodologies capable of evaluating the activity of new potential multi-target directed ligands (MTDLs). In addition, these methodologies had to be suitable for the characterization of the processes underlying drug-protein bindings and for the study of protein-protein interactions involved in neurodegenerative pathways.

This research field is deeply connected with the main purpose of the Ph.D. course, which is the study of the correlation between well-being and lifestyle. A multidisciplinary approach is mandatory in investigating the various aspects of life quality: if on one hand life expectancy is growing, on the other hand the incidence of age-related pathologies like Alzheimer's disease is increasing. [1]Among the elder population, AD reduces life quality and expectancy.[2] In this framework, lifestyle has been proved to have a central role in primary AD prevention, especially in its contribution to the delay of AD onset.[3] But even if non-pharmacological interventions (regular physical exercise, calorie reduction, use of antioxidant supplements and nutraceuticals, and more generally a correct diet) are effective tools in reducing AD modifiable risk factors, the research of drugs for AD therapy is still ongoing.[4 5 6] This is due to the fact that the drugs currently used cannot be considered disease-modifying, since they do not affect AD incidence or the known AD altered pathways. Besides, due to the multifactorial nature of AD, late-stage clinical trials of new drugs designed to address a single target failed. Thus, a promising strategy might be designing multi-target directed ligands (MTDLs) which could interact simultaneously on different pathways. Plants secondary metabolites have been studied as promising multi-target candidates for the treatment of Alzheimer's disease for their ability to interfere with different aspects of the pathogenesis and they could provide natural scaffolds as starting point for the design of semisynthetic derivatives. Nowadays, pharmaceutical analysis is supporting drug discovery by developing analytical methodologies adaptable to large-scale processes. These methodologies should as well be suitable for high-throughput screening on isolated targets involved in the early stages of the pathogenesis. In the meantime, the research is focused on analytical methods able to provide information on structure activity relationships of the molecules tested (SARs). Accordingly, part of the work of the Ph.D project was dedicated to the application of an high-throughput luminescent assay for screening potential GSK-3β dual inhibitors. The in solution assay aimed to characterize the activity towards GSK-3β of the first-in-class GSK-3β/ HDAC dual inhibitors designed by the Medicinal Chemistry group of *Department for Life Quality Studies*, University of Bologna. These enzymes were chosen because GSK-3β and class I–II HDAC inhibitors are able to shift microglia from the neurotoxic activation (proinflammatory) to the neuroprotective (anti-inflammatory) phenotype. This combined inhibition of GSK-3β and HDACs induces synergistic neuroprotective effects.[7] Then the purpose was to evaluate if the proposed kinase luminescent assay could be suitable to screen the activity of natural compounds towards GSK-3β. In detail, a series of Amaryllidaceae alkaloids known for their cholinesterase inhibition in the micromolar range were studied in collaboration with Charles University in Hradec Králové (Czech Republic).

Besides the interest in analytical methods suitable for a preliminary screening, pharmaceutical analysis is exploring new strategies to investigate more deeply the structure and conformation of target proteins involved in AD pathogenesis and to monitor the morphological changes after binding with the selected ligands. Indeed the analysis of protein–ligand interactions is important for understanding various biological phenomena and for pursuing drug development. Hence, the project aimed to apply a multi-methodological approach based on mass spectrometry (MS), circular dichroism spectroscopy (CD) and ThT assay, to characterize the potential interaction of CO releasing molecules (CORMs) with $A\beta_{1-42.}$ These compounds had already proved to have anti-inflammatory and neuroprotective properties, therefore they resulted interesting in view of discovering molecules able to modulate the amyloid aggregation process and its related toxicity.

The last part of my thesis was addressed to further explore the toxic mechanism of amyloid peptide *in vitro* on cell culture, with the final goal to identify potential biomarkers useful to an early diagnosis and targeting of AD patients, in order to overcome the problem of diagnosing the disease after the appearance of symptoms.

MS is one of the main analytical methods applied for a detailed investigation and diagnostic purposes in AD. Thus, during my exchange period at *Institute of Pharmaceutical Sciences* (University of Tübingen, Germany) HR-MS was used in a lipidomic approach to explore the possible connections existing between amyloid aggregation and lipid alterations in neuroblastoma cells, both primary events in AD pathogenesis.[8 9 10 11] The aim was to identify potential changes in the cell treated with the peptide, disclosing potential biomarkers belonging to the cell lipidome, which in a future study on patients could function as precise elements for diagnosis and early targeting of AD patients. Moreover, the discovery of amyloid toxicity related biomarkers could be exploited to candidate drug monitoring.

References:

(1) Oeppen, J.et al. W. Demography: Broken Limits to Life Expectancy. *Science*. **2002,** *360* (6385), 171-175 https://doi.org/10.1126/science.1069675.

(2) Tobore, T. O. On the Etiopathogenesis and Pathophysiology of Alzheimer's Disease: A Comprehensive Theoretical Review. *Journal of Alzheimer's Disease*. **2019**, *68* (2), 417-437 https://doi.org/10.3233/JAD-181052.

(3) Bhatti, G. K.; et al. Lifestyle Modifications and Nutritional Interventions in Aging-Associated Cognitive Decline and Alzheimer's Disease. *Frontiers in Aging Neuroscience*. **2020**, *11* (369), https://doi.org/10.3389/fnagi.2019.00369.

(4) Russell, A. P.; et al. Skeletal Muscle Mitochondria: A Major Player in Exercise, Health and Disease. *Biochimica et Biophysica Acta - General Subjects*. **2014**, *1840* (4), 1276-1284 https://doi.org/10.1016/j.bbagen.2013.11.016.

(5) Hötting, K.; et al. Beneficial Effects of Physical Exercise on Neuroplasticity and Cognition. *Neuroscience and Biobehavioral Reviews*. **2013**, *7* (9 Pt B), 2243-57 https://doi.org/ 10.1016/j.neubiorev.2013.04.005

(6) Schafer, M. J.; et al. Reduction of β-Amyloid and γ-Secretase by Calorie Restriction in Female Tg2576

Mice. *Neurobiol. Aging* **2015**, *36* (3),1293-302 https://doi.org/ 10.1016/j.neurobiolaging.2014.10.043

(7) Bardai, F. H.; et al. Histone Deacetylase-1 (HDAC1) Is a Molecular Switch between Neuronal Survival and Death. *J. Biol. Chem.* **2012**, *287* (42), 35444-35453 https://doi.org/10.1074/jbc.M112.394544.

(8) Jakubec, M.; et al. Fast and Quantitative Phospholipidomic Analysis of SH-SY5Y Neuroblastoma Cell Cultures Using Liquid Chromatography-Tandem Mass Spectrometry and 31P Nuclear Magnetic Resonance. *ACS Omega* **2019**, *4* (25), 21596–21603. https://doi.org/10.1021/acsomega.9b03463.

(9) Xicoy, H.; et al. Lipid Analysis of the 6-Hydroxydopamine-Treated SH-SY5Y Cell Model for Parkinson's Disease. *Mol. Neurobiol.* **2020**, *57* (2), 848–859. https://doi.org/10.1007/s12035-019-01733-3.

(10) Barupal, D. K.; et al. Sets of Coregulated Serum Lipids Are Associated with Alzheimer's Disease Pathophysiology. *Alzheimer's Dement. Diagnosis, Assess. Dis. Monit.* **2019**, *11* (1), 619–627 https://doi.org/10.1016/j.dadm.2019.07.002.

(11) Barupal, D. K.; et al. Generation and Quality Control of Lipidomics Data for the Alzheimer's Disease Neuroimaging Initiative Cohort. *Sci. Data* **2018**, *5*, 180263 https://doi.org/10.1038/sdata.2018.263.

Part I

State of the Art

1. Alzheimer's Disease (AD)

Alzheimer's disease (AD) is the most common type of dementia in the elderly population. It's a severe, chronic and progressive neurodegenerative disorder associated with impaired memory and cognitive faculties that lead to death.

Alois Alzheimer noticed the presence of amyloid plaques and a massive loss of neurons while examining the brain of his first patient who suffered from memory loss and change of personality before dying and described the condition as a serious disease of the cerebral cortex. Later, for the first time, Emil Kraepelin named this medical condition Alzheimer's disease in his 8th edition psychiatry handbook. [1]

At present, there are around 50 million AD patients in the World, but since age is one of the main risk factor for dementia, the AD incidence is projected to increase with the gradual aging of the population worldwide expecting to reach around 152 million of people affected by AD in 2050.[2]

Following this hypothesis, AD is now considered as one of the major public health concerns and an international research priority. Based on what is declared by Airalzh, an Italian association for AD, currently in Italy there are around 600K patients affected by this pathology, and they are in media around 78.8 years old. Once the age of 65 is reached, it has been shown that the chance of experiencing symptoms doubles every 5 years.[3] Several epidemiological studies have highlighted how, compared to men, women are more likely to develop Alzheimer's disease. And after 85 years old the incidence is higher and according to a study conducted by the World Health Organization this prevalence is expected to increase by 0.556% in 2030.[4] AD not only affect individuals and their families but also the global economy, with estimated costs of $ 1 trillion annually, so it has to be considered as a major public health challenge on which to invest resources. [5]

Most of AD cases are classified as late-onset sporadic forms characterized by aging as the major environmental risk factor. However, rare, familial, early-onset autosomal dominant forms, approximately 5 % only of all AD cases, exist and are caused by missense mutations in genes encoding amyloid β (Aβ) precursor protein (APP), presenilin-1 (PS1) and presenilin-2 (PS2).[6 7 8]

1.1 AD Symptoms and Diagnosis

The diagnosis of AD is based on a careful analysis of the clinical features, although it should be confirmed by a depth histopathological examination of patients' brains. Altered stages of the pathology have been identified and they are characterized by a progressive cognitive and functional decline in 5-8 years:

- Initial phase;
- Intermediate phase;
- Final phase;

1.1.1 Initial Phase:

Early symptoms are often erroneously attributed to aging or stress. The difficulty in remembering recently learned facts, the inability to acquire new information, and the lack of mental focus, can be symptomatic of the early stages of Alzheimer's. In this phase, the first neuropsychiatric symptoms also arise: apathy, which will accompany the subject throughout the course of the disease, depression and irritability.

In the initial phase it is often difficult to distinguish the disease from normal aging, then the aggravation of memory loss marks the beginning of the prodromal phase of Alzheimer's disease.

AD does not affect all types of memory equally. Episodic memory, semantic memory, and procedural memory are less affected than short-term memory. Language problems are mainly characterized by a reduction in vocabulary and a decrease in fluency, leading to a general depletion of oral and written language. At this stage, basic communication skills remain. There may be some difficulty in writing, drawing, dressing, coordinating movements and planning complex movements. During AD progress, patients can often continue to perform many tasks independently, but they may need assistance or supervision for more cognitively demanding activities.

1.1.2 Intermediate Phase:

The progression of AD precludes patient independence, they became no longer able to carry out daily activities. Linguistic difficulties become evident due to aphasia, which frequently leads to substituting words with others that are incorrect in that context. Complex motor sequences become less coordinated over time and the risk of falls increases. At this stage, memory problems aggravate, and the person may not recognize close relatives. Now even the long-term memory is impaired. Behavioural and neuropsychiatric changes become more evident, and the patient can quickly show irritability and crying. People also lose awareness of their disease. Urinary incontinence may develop.

1.1.3 Final Phase:

During the final stages of the disease, language is reduced to simple sentences, eventually leading to complete loss of speech. Although aggression may still be present, apathy and fatigue are the most common symptoms. People with Alzheimer's disease are ultimately unable to perform even the simplest tasks independently; muscle mass and mobility deteriorate to the point where they are bedridden and unable to feed themselves. The cause of death is usually an external factor, such as an infection or pneumonia, because as the disease progresses it leads to a deterioration of the immune system and weight loss, increasing the risk of throat and lung infections.

1.2 AD Neuropathology

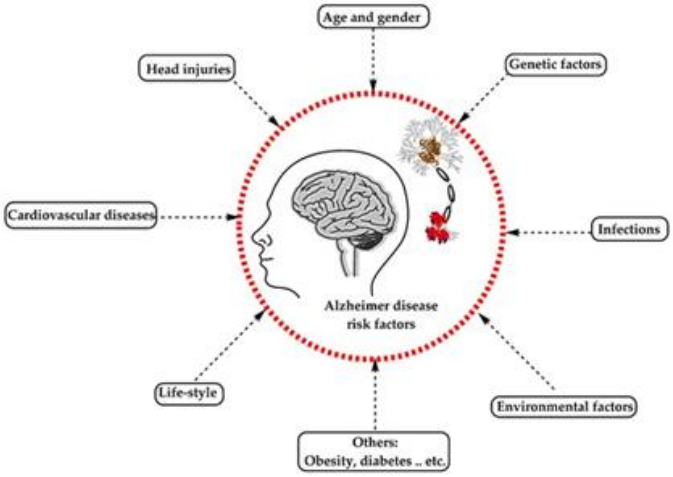

Figure *1.2* -**1** Alzheimer's Disease Risk Factors [2]

In AD brain there two types of neuropathological changes that outline the progression of the disease. The first type is the so called "positive lesions" due to aberrant protein processing in which amyloid β (Aβ) peptide and abnormally hyper-phosphorylated tau (τ) protein, after misfolding and self-assembly, generate respectively the following neurotoxic aggregates: amyloid senile plaques (SPs) and neurofibrillary tangles (NFTs). The second type are called "negative lesions" and correspond to the large brain atrophy due to neuronal, neuropil and synaptic loss caused by neuroinflammation, oxidative stress and cholinergic neurons deficit. Regarding the correlation between these pathological features and the clinical manifestations of AD, what is sure is that the synaptic loss is better correlated to the cognitive decline, and synaptic dysfunction occurs many years before synapses and neurons are lost. [9]

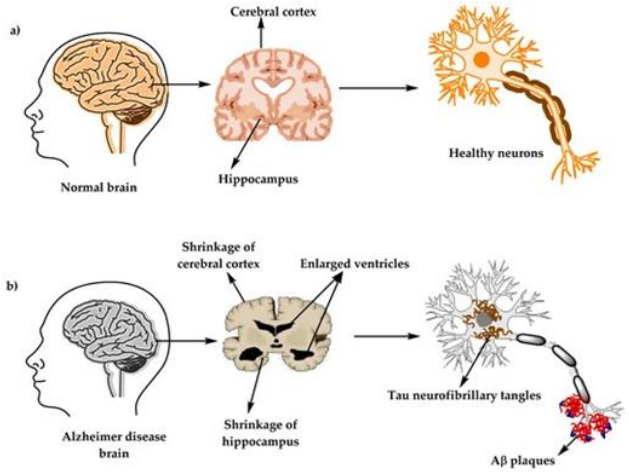

Figure *1.2* **-2** Neuropathological changes in AD brain [2]

Numerous post-mortem studies have been performed in AD patients to understand which areas of the nervous system were most affected by the disease process and therefore outline a series of correlations with symptoms. Initially, attention was focused on observing a series of morphological variations at the cortical level (temporal medial lobe, pre-cuneus and hippocampus) associated with the cognitive and behavioural symptoms typical of the disease.[10] On the contrary, less importance was given to the study of those regions related to neuropsychiatric aspects such as psychosis (38% of cases), affective symptoms (59%, anxiety and depression), hyperactivity (64%, aggression and disinhibition) and apathy (65%).[11] Dates back to May 2015 the first study aimed at investigating morphological changes in the brainstem *in vivo*, using magnetic resonance scans as an investigation tool.[12] Although numerous post-mortem studies had also identified alterations at the level of the brainstem, until then no *in vivo* neuroimaging studies had been performed to confirm these data.

The brain stem contains a series of nuclei involved in functions ranging from the control of homeostasis and emotions to the modulation of the cognitive functions of the cerebral cortex. Therefore, it is important to understand its role in the pathogenesis of AD. The studies carried out showed that patients affected by the disease, when compared with the control group, showed significant deformations in the upper part of the brainstem, the midbrain, where numerous nuclei involved in neurotransmission are located. These findings were in line with previous post-mortem studies, in which several neuropathological variations such as neurofibrillary tangles and a loss of neurons were noted. [10 11 13]

Among the numerous structures of the brainstem, the dorsal nuclei of the raphe (serotoninergic), the locus ceruleus (adrenergic) and the substantia nigra (dopaminergic) have been the most extensively studied as they can be correlated to the various cognitive and emotional symptoms. These nuclei include the isodendritic center which is involved in the modulation of numerous physiological processes and is strongly connected with those areas of the cerebral cortex that undergo neurofibrillary changes in the first phase of the disease.

Precisely, in a previous post-mortem study the presence of neurofibrillary clusters was found in the midbrain, at the level of the raphe nuclei, even before in the transentorinal region.[14] Hence, a new interest arose in studying the brain stem and previous hypotheses were re-evaluated, also considering that the raphe nuclei

produce a large part of the serotonin in the brain. Therefore, their degeneration could explain the neuropsychiatric symptoms associated with Alzheimer's disease such as depression and anxiety.

In support of this new direction of research, in subjects affected by the disease, characteristic lesions, i.e. senile plaques and neurofibrillary tangles, were found at the level of the locus ceruleus, with consequent atrophy of the area.[14] [15]Also in this case this variation morphological could justify the clinical symptom of depression shown by patients. Therefore, comparing the results of the previous studies with those of the *in vivo* study, it can be stated that the deformation present at the level of the midbrain can constitute a marker similar to the hippocampal morphological changes in the progression of the syndrome.[16] In the early stages of the disease it could therefore be responsible for emotional disturbances and irregular sleep, up to, as the disease progresses, to arouse a series of complications related to dysfunction of the autonomic nervous system: difficulty in swallowing, breathing, irregular blood pressure and arrhythmias.

1.3 AD Pathogenesis

The complex Alzheimer's disease pathogenesis is not yet totally deciphered, and the late onset of AD is associated with several risk factors. During years, in the attempt to underly the causes of the pathological changes in Alzheimer's disease (Aβ, NFTs, and synaptic loss), several hypotheses were proposed. Nowadays there is no an accepted theory, but researchers agree in considering AD as multifactorial disorder in which different damaged pathways interact each other. [17] [2]

1.3.1 Cholinergic Hypothesis

Cholinergic Hypothesis was developed in the mid-1970s thanks to post-mortem observations carried out on the brains of subjects with AD. During previous investigations, reduced levels of acetylcholintransferase (CAT) in the brains of dead people affected by AD were highlighted.[18]

Acetylcholintransferase is the enzyme responsible for the synthesis of ACh, a neurotransmitter that in the CNS plays a significant role in the neuromodulation of learning memory and cognitive functions. The reduction of CAT has suggested the idea of a possible role of this depletion in the onset of AD. In addition, drastic reductions in CAT levels were also found in other regions involved in neuro degeneration: the hippocampal and neocortical region.[19] Then, studies on AD have suggested that abnormalities in the cholinergic system such as choline transport, release of ACh, muscarinic and nicotinic receptor expression, and axonal transport can contribute significantly to behavioural dysfunctions. [20]

According to this hypothesis, cholinergic neurons are affected in the initial phase of AD causing the loss of cholinergic functions including the synthesis of ACh in the forebrain basal and consequently cognitive dysfunctions. Therefore, these results indicated that cholinergic replacement therapy should be the primary approach in the treatment of Alzheimer's disease. The cholinesterase (AChE/ BChE) inhibitors, have been used to delay the hydrolytic degradation of acetylcholine into choline and acetic acid, thus increasing the amount of neurotransmitter present in the synaptic cleft. Currently, there are three acetylcholinesterase

inhibitors for the treatment of the moderate form of the disease: donepezil (Pfizer, New York, USA), rivastigmine (Novartis, Basel, Switzerland) and galantamine (Jansesen, Beerse, Belgium).

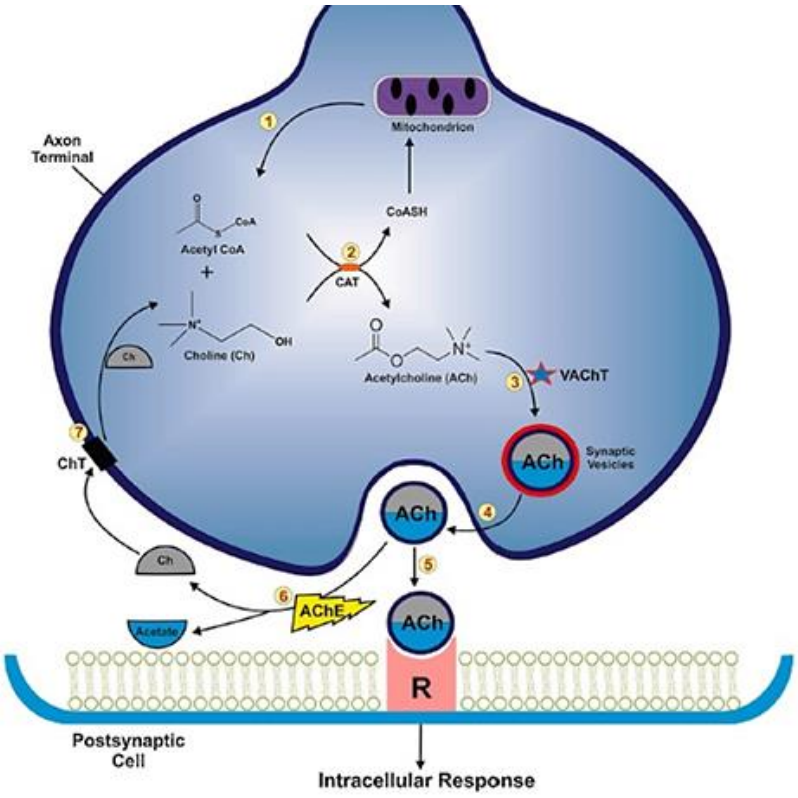

Figure *1..3.1*-**1** Ach synthesis and cholinergic transmission [21]

1.3.2 Tau Hypothesis

Tau is a protein microtubule-associated protein (MAP), that stabilizes the microtubules ensuring the assembly with tubulin. Tau is encoded by the MAPT gene located on chromosome 17 and consists of six isoforms generated by alternative splicing.[22]

In healthy subjects, the tau protein, exists mainly in phosphorylated form and binds microtubules, which within the brain cell act as support structures for the transport of nutrients, vesicles, mitochondria and chromosomes; they also stabilize axonal transport, which is essential for the growth and development of neurons. The tau ability of binding microtubules mainly depends on its phosphorylation status. Therefore, when in AD, tau is hyper-phosphorylated tends to accumulate in the cytoplasm and consequently microtubules disassembly, leading to eventually NFTs formation and neurodegeneration.[23] Eighty-five potential phosphorylation sites (45 Ser, 35 Thr, and 5 Tyr) are present in the longest tau isoform (2N4R) in human brain. Among them, more than 47 phosphorylation sites have been identified by mass spectrometry, which primarily reside in the proline-rich domain and C-terminus.[24]

Tau phosphorylation is regulated by multiple protein kinases and phosphatases. Tau kinases can be classified to two categories: 1) Ser/Thr kinases such as CDK5, glycogen synthase kinase 3β (GSK3β), mitogen-activated protein kinase, Ca2+/calmodulin-dependent protein kinase II, microtubule-affinity regulating kinase, protein kinase A (PKA), protein kinase C, Akt, TTBK1/2, CK1, DYRK1A, and 2) tyrosine kinases including Fyn, Src, Syk and c-Abl [25]

Several molecular factors have been studied to describe the role of tau interactions and its hyperphosphorylation in AD. These factors result in the release of NF-kB and the excessive production of pro-inflammatory mediators such as TNF-α and interleukins, causing inflammatory reactions in brain cells and neuritic lesions.[26] The overproduction of inflammatory mediators therefore leads upon activation of the MAPK, which in turn activates the CDK-5. The activation of these kinases finally leads to the hyperphosphorylation of tau. The ATP binding site is located at N- and C-terminal domains interface and is surrounded by the glycine-rich loop (residues 60-70) and the hinge (residues 134-139). The DFG (Asp200 to Gly202) sequence is the starting motif of the activation loop that ends with the APE motif (Ala224 to Glu226). The activation loop forms one of the edges of the substrate-binding groove, the other one is then constituted by a loop that connects β-strand five with the αC helix. The residues from 330 to 384 form a cluster of helices and loops that pack against the C-terminal domain.[27] In particular, the ATP-binding pocket can be visualized as five distinct regions devoted to specific interactions with the ATP-Mg^{2+} complex. These regions are classified as follow: the phosphate transfer area (highly conserved in kinases), the glycine-rich loop (a flexible lid covering the ATP binding site), the upper and lower hinge regions (the first one is involved in H-bond formation with ATP or other small molecules, while the second forms the edge of the solvent opening) and the hydrophobic pocket (presents a series of sequence variations that can be targeted by newly designed inhibitors to increase selectivity). A large network of hydrogen bonds connects ATP with the phosphorylation substrate facilitating the transfer of the ATP γ-phosphate group. In fact, the backbone atoms of residues Asp133, Val 135, Thr138 and Gln185, located in the upper hinge region of GSK-3β, establish H-bonds with the adenine moiety of ATP. Regarding the regulation mechanism, first, it must be specified that GSK-3 is ubiquitously expressed and constitutively active in unstimulated tissues. Both isoforms are post-translationally regulated or controlled by protein-protein interactions. The catalytic activity is actually regulated through a serie of signalling pathways. The activity of this kinase is functionally expressed through the inactivation of specific substrates by phosphorylation. A strong preference is exhibited in phosphorylating “primed” substrates, that are previously phosphorylated protein substrates. As consequence, the signals that act to suppress the activity of GSK-3 induce the activity of these substrates. In particular, the regulation in both proteins occurs by phosphorylation at their amino-terminal domain. Ser9 and Tyr216 represent the two phosphorylation sites that control the catalytic activity of GSK-3β. Tyr216 is conserved in many kinases and it is located in the GSK-3β activation loop where it plays the role of gate keeper of the substrate-binding groove. PTyr216 is held in place by Arg220 and Arg223 and the phosphorylation of the two independent residues in the activation loop actually controls the catalytic activity of GSK-3 which depends on the correct alignment of the N- and C-terminal domains and greatly increases the enzyme’s catalytic activity.

With regard to substrates phosphorylated by GSK-3β, more than 40 substrates were recognized.[28] It was not possible to establish a common phosphorylation mechanism for all of them. Many substrates are recognized by the canonical phosphorylation motif SXXXpS containing the phospho accepting Ser or Thr separated by three residues from a phosphoserine or phosphor-threonine. In fact, a different kinase must first phosphorylate the substrate at the P+4 position before it can be phosphorylated by GSK-3β at P0 residue. For example, the tau protein is phosphorylated by CDK5 at Ser235 and is then phosphorylated by GSK-3β at Thr23.[29] [30]

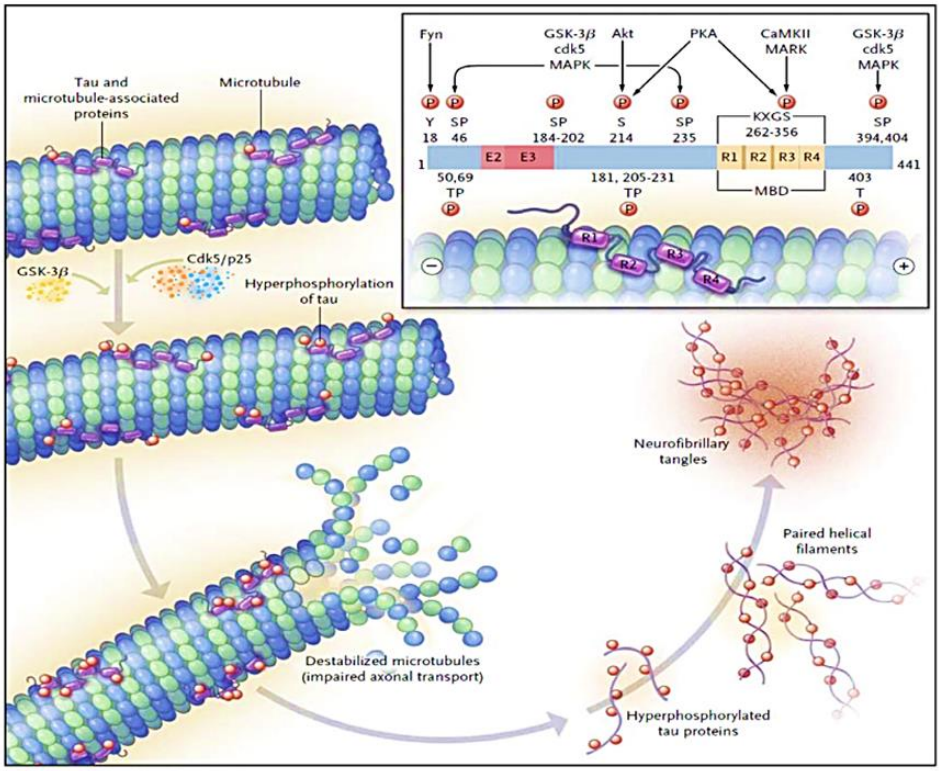

Figure *1.3.2*-**1** Stabilization of microtubule-associated tau protein is controlled by kinases [31]

1.3.3 Epigenetics Hypothesis

Since most of Alzheimer's disease cases are sporadic and occur in elderly population, it seems that environmental factors could take part to AD etiopathogenesis, leading to alterations in gene expression that are not present into the DNA sequence but that can contribute to synaptic signalling alteration and neuronal death. In addition to the activity of transcription factors there is now increasing evidence that epigenetic mechanisms play an important role in memory formation under physiological and pathological conditions.[32] Epigenetics or better epigenesis, as now it is called, deals with these changes in gene expression that occur in response to environmental influences. These alterations typically arise following DNA methylation or hydroxy-methylation, histone post-translational modifications and changes in nucleosome positioning. Nucleosome is an octamer and is the basic unit of chromatin. It is constituted by two molecules of each core

histone [(H) H2A, H2B, H3, and H4] around which is wrapped 147 bp of DNA. Histones are highly conserved basic proteins that act as building blocks of the nucleosome, and they have a flexible N terminus that protrudes from the surface of the nucleosome, the often called the "histone tail". Epigenetic processes correspond to chromatin remodelling and can be divided into 3 major categories: (1) Histone-modifications (2) DNA methylation and the more recently discovered DNA-hydroxy-methylation and (3) non-coding RNAs. Through these processes genetic and environmental factors are combined and contributes to into long-term adaptive changes in gene-expression. Thus, epigenetic mechanisms are key regulatory processes that mediate genome environment interactions (GxE).[33] New evidence suggests that changes in the epigenome during adulthood are crucial for higher cognitive functions such as learning and memory, dysregulation of epigenetic mechanisms are involved neurodegenerative processes. Thus, epigenetics is an emerging field that could drive the design of new therapeutic strategies to improve the cognitive functions and prevent neurodegeneration. Histone tails are the portions more susceptible to the multiple post-translational modifications. Especially, lysine acetylation and lysine methylations are the most common modifications. Histone acetylation is the one of the most investigated epigenetic modifications, that seems strictly associated with memory formation. The addition of acetyl groups to histones is catalysed by histone acetyltransferases (HATs).[34] When histones are acetylated, they are less tight to DNA, in this way it's easier for gene promoters to carry on the transcriptional process. From the first study *in vivo* in a mice, concerning the linking between histone modifications and cognitive functions, emerges that histone acetylation, in single-trial learning, participate to long-term memory acquisition.[35] On the contrary, Histone deacetylases (HDACs) are a family of proteins that acts on nuclear, cytoplasmic, and mitochondrial proteins controlling different cellular events. Specifically, they operate on lysine residues in histones. After this modification the chromatin results more compact and so the transcriptional process is repressed. Vertebrates express 18 HDACs that are organized into four classes based on their similarity to yeast proteins: the Class I RPD3-like proteins (HDAC1, HDAC2, HDAC3, and HDAC8), the Class II HDA1-like proteins (HDAC4, HDAC5, HDAC6, HDAC7, HDAC9, HDRP, and HDAC10), the Class III SIR2-like proteins (SIRT1–7), and HDAC11, which shares sequence homology with both Class I and Class II HDACs and is the sole member of the Class IV subfamily. Although Class I, II, and IV HDACs are zinc-dependent enzymes collectively referred to as classical HDACs, Class III HDACs require NAD^+ for their activity and are referred to as sirtuins. In 1979 for the first time it was demonstrated in an animal model that there is strictly correlation between the acetylation at histones level and the process of memory consolidation.[36] Such studies were later confirmed, showing that specific forms of learning are correlate with increased HAT activity[37] and histone-acetylation.[35] It was shown that when a mice tries a new taste the extracellular signal-regulated kinase (ERK) and mitogen-activated protein kinase (MAPK) are activated and this in turn induces histone acetyltransferases (HATs) at gene promoters in the insular cortex, a brain region that is involved in the new taste memories formation. Accordingly, mice that express a dominant-negative form of cAMP response element-binding protein (CREB)- binding protein (CBP; a HAT and crucial binding partner of CREB) and mice deficient in CBP exhibit deficits in LTP and long-term memory were improved by HDAC inhibitors.[3839]

In humans mutations in the gene encoding for CBP or for its homologue p300 result in Rubenstein-Taybi syndrome, which is an inherited, autosomal dominant disease characterized by severe learning disabilities,[40]

These studies confirmed the role of histone acetylation in synaptic plasticity and memory formation, and it appeared an interesting target that could be modulated to contrast cognitive decline associated with neurodegenerative disease.

1.3.4 Amyloid Cascade Hypothesis

The abnormal proteolytic processing of APP, amyloid precursor protein (APP), a transmembrane glycoprotein containing 695–770 amino acids, causes Aβ formation.[41] In the non-amyloidogenic pathways, APP is cleaved by α-secretase that is a metalloprotease (ADAM) localized to the Golgi complex and the cell membrane and then by γ-secretase. α-secretase cleaves APP at residue L688, located in the middle of the Aβ domain leading to the formation of soluble APP alpha (sAPPα) and a cell-membrane-bound C-terminal fragment 83 (CTF83). At this point γ-secretase cleaves CTF83 and AICD and a small p3 fragment are consequently produced. On the contrary, in the amyloidogenic pathways, APP is cleaved by β- and then γ-secretases. β-secretase (BACE1), that is situated in the luminal side of the membrane, is an aspartic protease long 500 residues and it contains 2 active sites. BACE1 can cleave APP at the N-terminal of the Aβ domain, either at residues Glu682 or Asp672 generating soluble APP β (sAPPβ) and C-terminal fragment 99 (CTF99) that is bound at the cell membrane.[41] On the other hand, γ-secretase is an enzymatic complex of four proteins including presenilin enhancer 2, presenilin (PSEN), anterior pharynx defective 1, and nicastrin. Each subunit is considered as an effective target to increase Aβ clearance or to regulate Aβ generation. γ-secretase cleaves βCTF99 fragment producing the APP intracellular domain (AICD) and Aβ peptides. Various isoforms of Aβ are possible and they are characterized by different numbers of aminoacid residues, among these $A\beta_{1-40}$, the most abundant, and $A\beta_{1-42}$ that is the less soluble, are included. [42]

The Aβ aggregation leads to oligomers, protofibrils and finally fibrils formation, the latter found in the amyloid plaques, that are one of the main hallmarks of AD pathology. Nowadays, Aβ accumulation is considered one of the primary events in AD pathogenesis that occurs initially in the entorhinal cortex and in hippocampus. Since 1991, several independent research groups began to propose Aβ accumulation as one of the main features of AD pathogenesis, but only the year later Hardy and Higgins introduced officially the so called "amyloid cascade hypothesis". Several events are connected to Aβ deposition such as the cognitive decline, the neuronal death, synaptic loss, formation of NFTs, and tau phosphorylation. This theory was supported by the fact that AD onset may be related to the autosomal dominant mutations in the APP gene and these mutations in PSEN1 and PSEN2 can induce the Aβ generation and ultimately mediate the generation of Aβ aggregates and deposits. In fact, in transgenic mouse models that express forms of PSEN proteins or APP containing mutations linked human FAD, it was possible to observe the progressively development of memory impairments and Aβ plaques in the brain. This finding supported the increasing hypothesis that Aβ aggregation could have a crucial role in AD development. Mutations in PSEN seem to be the major cause of FAD with over 150 causative mutations that have been mapped to the genes (PSEN1 and PSEN2) encoding the PSEN proteins.[43] The presence of this

mutations seems to be correlated to increased levels of $A\beta_{1-42}$ in comparison to $A\beta_{1-40}$ promoting the cleavage at residue 639 of APP rather that at residue 637.[44]

On the contrary, the late-onset sporadic AD (SAD), seems to be due to increased activity of BACE1[45] and a decrease of Aβ clearance process. Moreover, the build-up of Aβ is also found to be associated with the apolipoprotein E ε4 (APOE ε4) allele, considered as the strongest genetic risk factor for late-onset SAD.

Post-mortem analyses allowed to verify that even in healthy but elderly individuals an extensive amyloid pathology can be present. Brain imaging analysis supported these findings, Aβ pathology was observed in up to 44% of cognitively healthy older people. The analyses revealed a faster deficit in brain glucose metabolism, a minor brain volume, and a decreased in cognitive performance than in patients without amyloid pathology. It has been estimated that Aβ deposition precede the clinical AD symptoms of 15–20 years.[42]

Given the central role of amyloid pathway, more than half of AD drug candidates in phase III clinical trials are directed to Aβ. Even if in the last years it was registered a decline of 40% in the numbers of anti-Aβ therapies in phase I and II clinical trials. This confirms a change of direction in AD research after the repetitive failures of anti-Aβ candidate drugs. Anti-Aβ molecules include inhibitors designed to target Aβ plaque aggregation, $A\beta_{1-42}$ production, or the clearance rate of Aβ from the brain and CSF.

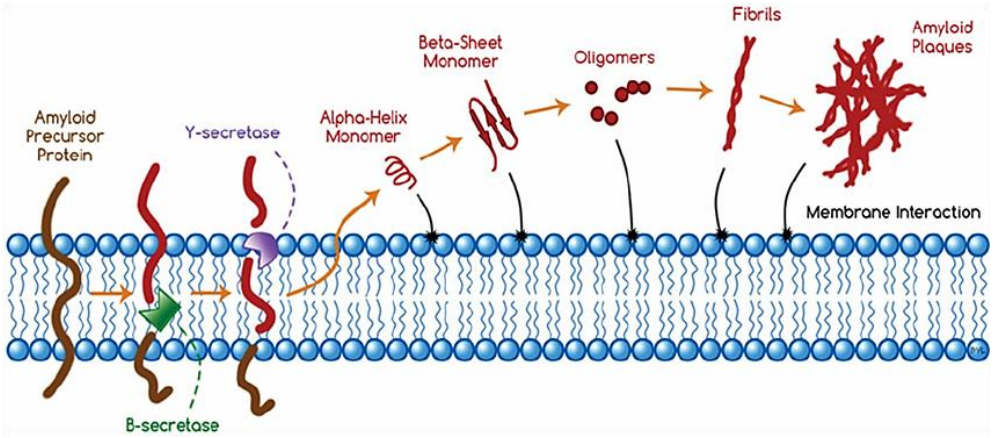

Figure *1.3.4*-**1** APP metabolism [46]

Meanwhile, the brain of an AD patient is endowed with a high oxidative damage index. It is still being debated whether oxidative stress precedes Aß accumulation and may therefore be an incentive of amyloid production, or Aß formation and aggregation is the cause of oxidative stress. Nevertheless, Aß can induce oxidative stress in two main ways. One is carried out through intra-mitochondrial mechanisms, inducing ROS production by disrupting the electron transport chain, decreasing the activity of complexes III and I. The other one involves amyloid oligomers with entrapped redox-active metal ions – such as copper ions –which can produce radical species, harmful to the Aß peptide itself and the surrounding biomolecules. [47] [48] Especially $A\beta_{1-42}$ and lipid peroxidation are intimately associated. A possible explanation for this connection could be ascribed to the fact that $A\beta_{1-42}$ is a relatively hydrophobic peptide as figured out from its aminoacidic sequence, thus the $A\beta_{1-42}$ oligomers solubilize into the hydrophobic environment of the lipid bilayer of the neuronal membrane.

Specifically, in 1994 a model based on Aβ oligomers toxicity and lipidic peroxidation was developed. The proposed mechanism of action was based on the extraction of labile lipid allylic H-atoms by a radical.[49] *In vitro* and *in vivo* models in various studies demonstrated the crucial role of Met-35 of Aβ peptide in AD. This residue is more susceptible to oxidation *in vivo*, especially under conditions of oxidative stress. Indeed, the examination of senile plaque showed a high proportion of methionine sulfoxide present.[50]

The resulting S·+ radical immediately abstracts a nearby labile allylic H-atom from an unsaturated acyl chain of a PUFAs in membrane lipid bilayers. This event leads to a series of reactions that culminate in the production of 4-hydroxy-2-nonenal (HNE), a highly neurotoxic product of lipid peroxidation. This α,β- unsaturated hydroxyl alkenal, mostly formed by the peroxidation of linoleic acid and arachidonic acid (AA), has a strong hydrophobic nature and it is mostly associated with the membranes where it is produced; however, it can also diffuse to different cellular compartments and interact with many different substrates. HNE is indeed a highly reactive moiety forming covalent adducts with membrane, cytosolic and mitochondrial proteins resulting in protein dysfunction and neuronal death. Higher concentrations of HNE cause the alteration of a wide range of biological activities, including the suppression of basal and inducible NFkB activity, disruption of ion homeostasis such as $Ca^{2+,}$ impairment of Na^{+} /K^{+} ATPase activity, activation of caspase pathways, disruption of glutamate transport, altered protein homeostasis. [51] [52] [53] Regarding the correlated excitotoxicity, it is known that amyloid aggregation influences the release of glutamate by astrocytes and the mechanism of re-uptake by the same cells, causing an excessive glutamate concentration in the pre-synaptic space. This excess of glutamate activates ionotropic glutamate receptors acting as Ca^{2+} channels on neuronal membranes, particularly extra synaptic N-methyl-D aspartate (NMDA) receptors.[54] [55] [56] Excitotoxicity is another factor responsible for neurodegeneration and cell death. [57] More recently, it has been demonstrated that Aβ oligomers cause a rapid influx of calcium ions (Ca^{2+}) across the cell membrane by rapidly activation of extra synaptic N-methyl-D-aspartate (NMDA) receptors and, to a lower extent, α amino-3-hydroxy-5-methyl-4-isoxazolepropionic acid (AMPA) receptors without interacting directly with these receptors. These receptors are activated mechanically through a change in membrane tension caused by the alteration carried out by oligomers in the lipid bilayer. [58] Concerning lipids, in the brain 50 % are phospholipids, below 40 % are glycolipids, 10 % cholesterol, cholesterol ester and traces of triglycerides. Long-chain polyunsaturated fatty acids (LC-PUFAs) account for 25–30 % of the total fatty acids (FAs) in the human brain, including docosahexaenoic acid (DHA) and arachidonic acid (AA), this type of FAs (PUFAs) is particularly sensitive to reactive-oxygen species attack. Interestingly, cerebral lipid peroxidation was found to be an early event in AD. [59]

1.4 The Role of a Correct Lifestyle to Prevent AD Late Onset

Worldwide, the average life expectancy is growing, thanks to the improvement of the health system and increasingly early diagnoses.[60] However, as already mentioned, this will lead to an increase in age-related diseases in the next decades. [61]As we know, aging is linked to genetic and molecular mechanisms. Age is one of the risk factors of Alzheimer's disease, which is then joined by the level of education, socio-economic status,

family history, genetic mutations, oxidative stress and neuroinflammation.[62] With the increase in the incidence of the disease and the lack of effective therapy, there is a growing focus on prevention. It is estimated that up to 500,000 cases of dementia can be reduced through prevention in the United States.[63]

The modifiable risk factors are: cigarette smoking, sedentary lifestyle, depression, hypertension, diabetes, dyslipidaemia and obesity. Non-pharmacological interventions including exercise, calorie reduction, the use of antioxidant supplements, diet, nutraceuticals and various plant-based bioactive compounds have been found to be an effective tool in reducing these modifiable risk factors. Specifically, cardio-metabolic risk factors seem to be more involved in the high incidence and cognitive decline of AD.[64] [65] Therefore, lifestyle and nutritional intervention can be effective primary prevention strategies for AD.[66] [67] The Mediterranean diet, considered worldwide as a model of healthy eating, is characterized by the high consumption of foods of plant origin, olive oil as the main source of fat, low to moderate consumption of fish, dairy products and poultry, low red and processed meats, low to moderate wine consumption with meals. Previous studies have shown how the Mediterranean diet plays a preventive role both against cardiovascular diseases but also on neurodegenerative disorders.[68] [69] This is because Mediterranean diet through the bioactive components modulates inflammation and metabolic abnormalities as well as epigenetic changes in histones and chromatin structure. Thus, nutraceutical compounds and dietary models may be promising in preventing cognitive decline or delaying progression to AD.[67] Several components of the diet, such as omega-3 fatty acids, nutraceuticals, minerals, micronutrients and vitamins have been examined for their role in modulating health and disease in order to reduce the prevalence of 2050 by 83% worldwide.[70] [71] Regular exercise activates various cell signalling pathways and helps improve the mitochondrial health in the skeletal muscles.[72] It is known to control blood sugar and body weight, to maintain blood pressure, to reduce dyslipidaemia, and improve muscle and bone health. Another study demonstrated a reduction in cognitive decline and a decrease in the accumulation misfolded in the brains of transgenic animals.[73] Another animal and human study by Hötting and Röder in 2013 confirmed that exercise induces brain neuroplasticity and improves cognitive function.[74] Calorie restriction (CR) is another promising non-drug intervention that is effective in brain aging.[75] CR acts by neutralizing the harmful effects of ROS and oxidative damage.[76] [77] [78] [79] In 2015, a previous study showed that long-term CR reduces amyloid role secretase in female Tg25, thus developing an AD problem.[80] CR exerts these modulations by enhancing their properties by inhibiting vital nutrient-sensing and inflammatory pathways.[81] [82] So, as well as physical activity and exercise, CR may also be considered as a promising nutritional intervention for the prevention of many age-related chronic diseases.

References

(1) Cipriani, G.; et al.Alzheimer and His Disease: A Brief History. *Neurol. Sci.* **2011**, *32* (2), 275-9 https://doi.org/10.1007/s10072-010-0454-7.

(2) Breijyeh, Z.; et al. Comprehensive Review on Alzheimer's Disease: Causes and Treatment. *Molecules (Basel, Switzerland)*. **2020**, *25* (24), 5789 https://doi.org/10.3390/molecules25245789.

(3) Bermejo-Pareja, F.; et al. Incidence and Subtypes of Dementia in Three Elderly Populations of Central

Spain. *J. Neurol. Sci.* **2008**, *264* (1–2), 63-72 https://doi.org/10.1016/j.jns.2007.07.021.

(4) Andersen, K.; et al. Gender Differences in the Incidence of AD and Vascular Dementia: The EURODEM Studies. *Neurology* **1999**, *53* (9), 1992-7 https://doi.org/10.1212/wnl.53.9.1992.

(5) 2020 Alzheimer's Disease Facts and Figures. *Alzheimer's Dement.* **2020**, *16* (3), 391-460 https://doi.org/10.1002/alz.12068.

(6) Tobore, T. O. On the Etiopathogenesis and Pathophysiology of Alzheimer's Disease: A Comprehensive Theoretical Review. *Journal of Alzheimer's Disease.* **2019**, *68* (2), 417-437 https://doi.org/10.3233/JAD-181052.

(7) Lei, P.; et al. The Essential Elements of Alzheimer's Disease. *Journal of Biological Chemistry* **2021**, *296*, 100105 https://doi.org/10.1074/jbc.REV120.008207.

(8) Tiwari, S.; et al. Alzheimer's Disease: Pathogenesis, Diagnostics, and Therapeutics. *International Journal of Nanomedicine*. **2019**, *14*, 5541-5554 https://doi.org/10.2147/IJN.S200490.

(9) Serrano-Pozo, A.; et al. Neuropathological Alterations in Alzheimer Disease. *Cold Spring Harb. Perspect. Med.* **2011**, *1* (1), a006189 https://doi.org/10.1101/cshperspect.a006189.

(10) Grinberg, L. T.; et al. Brainstem: Neglected Locus in Neurodegenerative Diseases. *Front. Neurol.* **2011**, *2*, 42 https://doi.org/10.3389/fneur.2011.00042.

(11) Zec, R. F.; et al.. Non-Pharmacological and Pharmacological Treatment of the Cognitive and Behavioral Symptoms of Alzheimer Disease. *NeuroRehabilitation*. **2008**, *23* (5), 425-38 https://doi.org/10.3233/nre-2008-23506.

(12) Yiannopoulou, K. G.; et al. Current and Future Treatments for Alzheimer's Disease. *Therapeutic Advances in Neurological Disorders*. **2013**, *6* (1), 19-33 https://doi.org/10.1177/1756285612461679.

(13) Eser, R. A.; et al. Selective Vulnerability of Brainstem Nuclei in Distinct Tauopathies: A Postmortem Study. *J. Neuropathol. Exp. Neurol.* **2018**, *77* (2), 149-161 https://doi.org/10.1093/jnen/nlx113.

(14) Grinberg, L. T.; et al. The Dorsal Raphe Nucleus Shows Phospho-Tau Neurofibrillary Changes before the Transentorhinal Region in Alzheimer̈s Disease. A Precocious Onset? *Neuropathol. Appl. Neurobiol.* **2009**, *35* (4), 406-416 https://doi.org/10.1111/j.1365-2990.2008.00997.x.

(15) Zweig, R. M.; et al. The Neuropathology of Aminergic Nuclei in Alzheimer's Disease. *Ann. Neurol.* **1988**, *24* (2), 233-42 https://doi.org/10.1002/ana.410240210.

(16) Albert, M. S.; et al. The Diagnosis of Mild Cognitive Impairment Due to Alzheimer's Disease: Recommendations from the National Institute on Aging-Alzheimer's Association Workgroups on Diagnostic Guidelines for Alzheimer's Disease. *Alzheimer's Dement.* **2011**, *7* (3), 270-9 https://doi.org/10.1016/j.jalz.2011.03.008.

(17) Long, J. M.; et al. Alzheimer Disease: An Update on Pathobiology and Treatment Strategies. *Cell*. **2019**, *179* (2), 312-339 https://doi.org/10.1016/j.cell.2019.09.001.

(18) Perry, E. K.; et al. Neurotransmitter Enzyme Abnormalities in Senile Dementia. Choline Acetyltransferase and Glutamic Acid Decarboxylase Activities in Necropsy Brain Tissue. *J. Neurol. Sci.* **1977**, *34* (2), 247-265 https://doi.org/10.1016/0022-510X(77)90073-9.

(19) Perry, E. K. et al. The Cholinergic Hypothesis-Ten Years On. *Br. Med. Bull.* **1986**, *42* (1), 63-69 https://doi.org/10.1093/oxfordjournals.bmb.a072100.

(20) Terry, A. V.; et al. The Cholinergic Hypothesis of Age and Alzheimer's Disease-Related Cognitive Deficits: Recent Challenges and Their Implications for Novel Drug Development. *Journal of Pharmacology and Experimental Therapeutics*. **2003**, *306* (3) 821-827 https://doi.org/10.1124/jpet.102.041616.

(21) Sharma, P.; et al. Comprehensive Review of Mechanisms of Pathogenesis Involved in Alzheimer's Disease and Potential Therapeutic Strategies. *Progress in Neurobiology*. **2019**, *174*, 53-89 https://doi.org/10.1016/j.pneurobio.2018.12.006.

(22) Takashima, A.; Honda, T.; Yasutake, K.; Michel, G.; Murayama, O.; Murayama, M.; Ishiguro, K.; Yamaguchi, H. Activation of Tau Protein Kinase I/Glycogen Synthase Kinase-3β by Amyloid β Peptide (25-35) Enhances Phosphorylation of Tau in Hippocampal Neurons. *Neurosci. Res.* **1998**, *31* (4), 317-323 https://doi.org/10.1016/S0168-0102(98)00061-3.

(23) Hong, M.; et al. Insulin and Insulin-like Growth Factor-1 Regulate Tau Phosphorylation in Cultured Human Neurons. *J. Biol. Chem.* **1997**, *272* (31), 9547–19553 https://doi.org/10.1074/jbc.272.31.19547.

(24) Li, J. G.; et al. Correction to: A Pharmacological Chaperone Improves Memory by Reducing Aβ and Tau Neuropathology in a Mouse Model with Plaques and Tangles Molecular Neurodegeneration *Molecular Neurodegeneration*. **2021**, *272* (31), 19547-19553 https://doi.org/10.1186/s13024-021-00461-4.

(25) Tapia-Rojas, C.; et al. It's All about Tau. *Progress in Neurobiology*. **2019**, *175*, 54-76 https://doi.org/10.1016/j.pneurobio.2018.12.005.

(26) Wang, W. Y.; et al. Role of Pro-Inflammatory Cytokines Released from Microglia in Alzheimer's Disease. *Annals of Translational Medicine*. 2015, *3* (10), 136 https://doi.org/10.3978/j.issn.2305-5839.2015.03.49.

(27) Johnson, L. N.; et al. Active and Inactive Protein Kinases: Structural Basis for Regulation. *Cell*. **1996**, *85* (2), 149-158 https://doi.org/10.1016/S0092-8674(00)81092-2.

(28) Jope, R. S.; et al. The Glamour and Gloom of Glycogen Synthase Kinase-3. *Trends in Biochemical Sciences*. **2004**, *29* (2), 95-102 https://doi.org/10.1016/j.tibs.2003.12.004.

(29) Ishiguro, K.; et al. Glycogen Synthase Kinase 3β Is Identical to Tau Protein Kinase I Generating Several Epitopes of Paired Helical Filaments. *FEBS Lett.* **1993**, *325* (3), 167-172 https://doi.org/10.1016/0014-5793(93)81066-9.

(30) Sengupta, A.; et al. Potentiation of GSK-3-Catalyzed Alzheimer-like Phosphorylation of Human Tau by Cdk5. *Mol. Cell. Biochem.* **1997**, *167* (1–2), 99–105 https://doi.org/10.1023/A:1006883924775.

(31) Barage, S. H.; et al. Amyloid Cascade Hypothesis: Pathogenesis and Therapeutic Strategies in Alzheimer's Disease. *Neuropeptides*. **2015**, *52*, 1-18 https://doi.org/10.1016/j.npep.2015.06.008.

(32) Hwang, J. Y.; et al. The Emerging Field of Epigenetics in Neurodegeneration and Neuroprotection. *Nature Reviews Neuroscience*. **2017**, *18* (6), 347-361 https://doi.org/10.1038/nrn.2017.46.

(33) Fischer, A. Targeting Histone-Modifications in Alzheimer's Disease. What Is the Evidence That This Is a Promising Therapeutic Avenue? *Neuropharmacology*. **2014**, *80*, 95-102

https://doi.org/10.1016/j.neuropharm.2014.01.038.

(34) Mapstone, M.; et al Plasma Phospholipids Identify Antecedent Memory Impairment in Older Adults. *Nat. Med.* **2014**, *20*, 415–418 https://doi.org/10.1038/nm.3466.

(35) Levenson, J. M.; et al Regulation of Histone Acetylation during Memory Formation in the Hippocampus. *J. Biol. Chem.* **2004**, *279* (39), 40545-40559 https://doi.org/10.1074/jbc.M402229200.

(36) Schmitt, M.; et al [Biochemical Studies on Histones of the Central Nervous System. III. Incorporation of [14C]-Acetate into the Histones of Different Rat Brain Regions during a Learning Experiment]. *Acta Biol. Med. Ger.* **1979**, *38* (4), 683-9

(37) Swank, M. W.; et al Increased Histone Acetyltransferase and Lysine Acetyltransferase Activity and Biphasic Activation of the ERK/RSK Cascade in Insular Cortex during Novel Taste Learning. *J. Neurosci.* **2001**, *21* (10), 3383-3391 https://doi.org/10.1523/jneurosci.21-10-03383.2001.

(38) Alarcón, J. M.; et al Chromatin Acetylation, Memory, and LTP Are Impaired in CBP+/- Mice: A Model for the Cognitive Deficit in Rubinstein-Taybi Syndrome and Its Amelioration. *Neuron* **2004**, *42* (6), 947-959 https://doi.org/10.1016/j.neuron.2004.05.021.

(39) Korzus, E.; et al Histone Acetyltransferase Activity Is a Critical Component of Memory Consolidation. *Neuron* **2004**, *42* (6), 961-972 https://doi.org/10.1016/j.neuron.2004.06.002.

(40) Blough, R. I.; et al Variation in Microdeletions of the Cyclic AMP-Responsive Element-Binding Protein Gene at Chromosome Band 16p13.3 in the Rubinstein-Taybi Syndrome. *Am. J. Med. Genet.* **2000**, *90* (1), 29-34 https://doi.org/10.1002/(SICI)1096-8628(20000103)90:1<29::AID-AJMG6>3.0.CO;2-Z.

(41) Vassar, R.; et al β-Secretase Cleavage of Alzheimer's Amyloid Precursor Protein by the Transmembrane Aspartic Protease BACE. *Science (80-.).* **1999**, *286* (5440), 735-741 https://doi.org/10.1126/science.286.5440.735.

(42) Uddin, M. S.; et al Revisiting the Amyloid Cascade Hypothesis: From Anti-Aβ Therapeutics to Auspicious New Ways for Alzheimer's Disease. *Int. J. Mol. Sci.* **2020**, *21* (16), 5858 https://doi.org/10.3390/ijms21165858.

(43) Ertekin-Taner, N. Genetics of Alzheimer's Disease: A Centennial Review. *Neurologic Clinics*. **2007**, *25* (3), 611-667 https://doi.org/10.1016/j.ncl.2007.03.009.

(44) Lanoiselée, H. M.; et al APP, PSEN1, and PSEN2 Mutations in Early-Onset Alzheimer Disease: A Genetic Screening Study of Familial and Sporadic Cases. *PLoS Med.* **2017**, *14* (3), e1002270https://doi.org/10.1371/journal.pmed.1002270.

(45) Yang, L. B.; et al Elevated β-Secretase Expression and Enzymatic Activity Detected in Sporadic Alzheimer Disease *Nature Medicine***. 2003**, *9*, 3–4 https://doi.org/10.1038/nm0103-3.

(46) Drolle, E.; et al Atomic Force Microscopy to Study Molecular Mechanisms of Amyloid Fibril Formation and Toxicity in Alzheimer's Disease. *Drug Metabolism Reviews*. **2014**, *46* (2), 207-223 https://doi.org/10.3109/03602532.2014.882354.

(47) Cheignon, C.; et al Oxidative Stress and the Amyloid Beta Peptide in Alzheimer's Disease. *Redox Biology*. **2018**, *14*, 450–464. https://doi.org/10.1016/j.redox.2017.10.014.

(48) Reiss, A. B.; et al Amyloid Toxicity in Alzheimer's Disease. *Reviews in the Neurosciences*. **2018**, *29* (6) 613–627. https://doi.org/10.1515/revneuro-2017-0063.

(49) Hensley, K.; et al A Model for β-Amyloid Aggregation and Neurotoxicity Based on Free Radical Generation by the Peptide: Relevance to Alzheimer Disease. *Proc. Natl. Acad. Sci. U. S. A.* **1994**, *91* (8) 3270-3274 https://doi.org/10.1073/pnas.91.8.3270.

(50) Varadarajan, S.; et al A. Methionine Residue 35 Is Important in Amyloid β-Peptide-Associated Free Radical Oxidative Stress. *Brain Res. Bull.* **1999**, 50, (2) 133-141 https://doi.org/10.1016/S0361-9230(99)00093-3.

(51) Di Domenico, F.; et al A. Role of 4-Hydroxy-2-Nonenal (HNE) in the Pathogenesis of Alzheimer Disease and Other Selected Age-Related Neurodegenerative Disorders. *Free Radical Biology and Medicine*. **2017**, *111*, 253-261 https://doi.org/10.1016/j.freeradbiomed.2016.10.490.

(52) Mark, R. J.; et al A Role for 4-Hydroxynonenal, an Aldehydic Product of Lipid Peroxidation, in Disruption of Ion Homeostasis and Neuronal Death Induced by Amyloid β-Peptide. *J. Neurochem.* **2002**, *68* (1) 255-264 https://doi.org/10.1046/j.1471-4159.1997.68010255.x.

(53) Butterfield, D. A.; et al Oxidative Stress, Dysfunctional Glucose Metabolism and Alzheimer Disease. *Nature Reviews Neuroscience*. **2019**, *20*, 148–160 https://doi.org/10.1038/s41583-019-0132-6.

(54) Wang, R.; et al Role of Glutamate and NMDA Receptors in Alzheimer's Disease. *Journal of Alzheimer's Disease*. 2017, 57 (4) 1041-1048 https://doi.org/10.3233/JAD-160763.

(55) Tong, B. C. K.; et al Calcium Signaling in Alzheimer's Disease & Therapies. *Biochimica et Biophysica Acta - Molecular Cell Research*. **2018**, *1865* (11), 1745-1760 https://doi.org/10.1016/j.bbamcr.2018.07.018.

(56) Acosta, C.; et al Astrocyte Dysfunction in Alzheimer Disease. *Journal of Neuroscience Research*. **2017**, *95* (12) 2430-2447 https://doi.org/10.1002/jnr.24075.

(57) Arundine, M.; Tymianski, M. Molecular Mechanisms of Calcium-Dependent Neurodegeneration in Excitotoxicity. *Cell Calcium* **2003**, *34* (4–5) 325-337 https://doi.org/10.1016/S0143-4160(03)00141-6.

(58) Fani, G.; et al Aβ Oligomers Dysregulate Calcium Homeostasis by Mechanosensitive Activation of AMPA and NMDA Receptors. *ACS Chem. Neurosci.* **2021**, *12* (4) 766 78 1https://doi.org/10.1021/acschemneuro.0c00811.

(59) Kao, Y. C.; et al Lipids and Alzheimer's Disease. *International Journal of Molecular Sciences*. **2020**, *21*(4), 1505 https://doi.org/10.3390/ijms21041505.

(60) Oeppen, J.; Vaupel, J. W. Demography: Broken Limits to Life Expectancy. *Science.* **2002**, *296* (5570) 1029-1031 https://doi.org/10.1126/science.1069675.

(61) Beard, J. R.; et al The World Report on Ageing and Health: A Policy Framework for Healthy Ageing. *The Lancet.* **2016**, *387*, (10033), 2145-2154 https://doi.org/10.1016/S0140-6736(15)00516-4.

(62) Bhatti, G. K.; et al Lifestyle Modifications and Nutritional Interventions in Aging-Associated Cognitive Decline and Alzheimer's Disease. *Frontiers in Aging Neuroscience*. 2020, *11*, 369 https://doi.org/10.3389/fnagi.2019.00369.

(63) Feigin, V. L.; et al Global, Regional, and National Burden of Neurological Disorders during 1990–

2015: A Systematic Analysis for the Global Burden of Disease Study 2015. *Lancet Neurol.* **2017**, *16* (11) 877-897 https://doi.org/10.1016/S1474-4422(17)30299-5.

(64) Calder, P. C.; et al Dietary Factors and Low-Grade Inflammation in Relation to Overweight and Obesity. *Br. J. Nutr.* **2011**, *106* (SUPPL. 3), S1 - S78 https://doi.org/10.1017/s0007114511005460.

(65) Bayer-Carter, J. L.; et al Diet Intervention and Cerebrospinal Fluid Biomarkers in Amnestic Mild Cognitive Impairment. *Arch. Neurol.* **2011**, *68* (6) 743-752https://doi.org/10.1001/archneurol.2011.125.

(66) Bhatti, J. S.; et al Therapeutic Strategies for Mitochondrial Dysfunction and Oxidative Stress in Age-Related Metabolic Disorders. In *Progress in Molecular Biology and Translational Science*; **2017**, *146*, https://doi.org/10.1016/bs.pmbts.2016.12.012https://doi.org/10.1016/bs.pmbts.2016.12.012.

(67) Canevelli, M.; et al Nutrition and Dementia: Evidence for Preventive Approaches? *Nutrients*. 2016, *8* (3), 144 https://doi.org/10.3390/nu8030144.

(68) Temple, N. J.; et al The Mediterranean Diet and Cardiovascular Disease: Gaps in the Evidence and Research Challenges. *Cardiology in Review*. **2019**, *27* (3) 127-130 https://doi.org/10.1097/CRD.0000000000000222.

(69) Witlox, W. J. A.; et al. An Inverse Association between the Mediterranean Diet and Bladder Cancer Risk: A Pooled Analysis of 13 Cohort Studies. *Eur. J. Nutr.* **2020**, *59* (1), 287–296 https://doi.org/10.1007/s00394-019-01907-8.

(70) Norton, S.; et al. Potential for Primary Prevention of Alzheimer's Disease: An Analysis of Population-Based Data. *Lancet Neurol.* **2014**, *13* (8), 788-794 https://doi.org/10.1016/S1474-4422(14)70136-X.

(71) Luck, T.; Riedel-Heller, S. G. Prevention of Alzheimer's Dementia in Germany: A Projection of the Possible Potential of Reducing Selected Risk Factors. *Nervenarzt* **2016**, *87* (11), 1194–1200 https://doi.org/10.1007/s00115-015-0045-1.

(72) Russell, A. P.; et al. Skeletal Muscle Mitochondria: A Major Player in Exercise, Health and Disease. *Biochimica et Biophysica Acta - General Subjects*. 2014, *1840* (4), 1276-1284 https://doi.org/10.1016/j.bbagen.2013.11.016.

(73) Pietropaolo, S.; et al. The Impact of Voluntary Exercise on Mental Health in Rodents: A Neuroplasticity Perspective. *Behav. Brain Res.* **2008**, *192* (1), 42-60 https://doi.org/10.1016/j.bbr.2008.03.014.

(74) Hötting, K.; Röder, B. Beneficial Effects of Physical Exercise on Neuroplasticity and Cognition. *Neuroscience and Biobehavioral Reviews*. 2013, 37 (9) 2243 2257 https://doi.org/10.1016/j.neubiorev.2013.04.005.

(75) Wahl, D.; et al. Aging, Lifestyle and Dementia. *Neurobiology of Disease***. 2019**, *130*, 104481 https://doi.org/10.1016/j.nbd.2019.104481.

(76) Barja, G.; Herrero, A. Oxidative Damage to Mitochondrial DNA Is Inversely Related to Maximum Life Span in the Heart and Brain of Mammals. *FASEB J.* **2000**, *14* (2) 312-318https://doi.org/10.1096/fasebj.14.2.312.

(77) Barja, G. Endogenous Oxidative Stress: Relationship to Aging, Longevity and Caloric Restriction. *Ageing Research Reviews*. **2002**, *1* (3), 397-411 https://doi.org/10.1016/S1568-1637(02)00008-9.

(78) Civitarese, A. E.; et al. Calorie Restriction Increases Muscle Mitochondrial Biogenesis in Healthy Humans. *PLoS Med.* **2007**, *4* (3), e76 https://doi.org/10.1371/journal.pmed.0040076.
(79) Zainal, T. A.; et al. Caloric Restriction of Rhesus Monkeys Lowers Oxidative Damage in Skeletal Muscle. *FASEB J.* **2000**, *14* (12), 1825-1836 https://doi.org/10.1096/fj.99-0881com.
(80) Schafer, M. J.; et al. Reduction of β-Amyloid and γ-Secretase by Calorie Restriction in Female Tg2576 Mice. *Neurobiol. Aging* **2015**, *36* (3), 1293-1302 https://doi.org/10.1016/j.neurobiolaging.2014.10.043.
(81) Most, J.; et al. Calorie Restriction in Humans: An Update. *Ageing Research Reviews*. **2017**, *39*, 36-45 https://doi.org/10.1016/j.arr.2016.08.005.
(82) Murphy, M. P. How Mitochondria Produce Reactive Oxygen Species. *Biochemical Journal*. **2009**, *417* (1), 1–13 https://doi.org/10.1042/BJ20081386.

1.5 AD Treatments

The need of finding a preventing strategy is partially related to lack of effective drugs for AD. Currently the treatment offers only a symptomatic relief, since it provides palliative and temporary therapy that only slows down the cognitive decline associated with Alzheimer's disease.[1]

One of the first treatment strategies, used in the more moderate form of AD, consists in the acetylcholinesterase enzyme inhibition, that aims to delay the degradation of acetylcholine into choline and acetic acid and consequently to increase the amount of neurotransmitter present in the synaptic rift.[2] However, recent studies have underlined how it is important starting treatments in the early stages of the disease, immediately after diagnosis. In fact, the therapy delay, just of six months, reduces the efficacy, while it is reported that if the treatment begins soon in three months after diagnosis, there is a slight progress in cognitive functions in the following 3-9 months and the usual decline becomes less rapid: attention, memory, understanding of language and communication are improved.[3]

Currently, three acetylcholinesterase inhibitors are approved and used to treat moderate form Alzheimer's disease: donepezil (Pfizer, New York, USA), rivastigmine (Novartis, Basel, Switzerland) and galantamine (Jansesen, Beerse, Belgium). Following a series of randomized controlled trials (RCTs), their efficacy on the cognitive functions and activities of daily life of moderate AD patients was demonstrated, without detecting any significant difference between the three drugs.[4] Nowadays, Donepezil is authorized for the treatment of severe AD in the USA.[5] In contrast, Tacrine, which was the first drug approved for the disease in 1993, is no longer used due to its hepatotoxicity.[6] For rivastigmine and galantamine, other studies have shown a higher incidence of high gastrointestinal side effects (nausea, vomiting, diarrhea, abdominal cramps) in comparison to donepezil at therapeutical dosage.[7] However, when they are used with caution and with gradual administration for more than three months, it can be said that they have the same tolerability. Among the side effects associated with the use of acetylcholinesterase inhibitors, syncope, bradycardia and the need to use a pacemaker were recorded. Therefore, the adverse effects of these drugs must be carefully considered and

comparable to the benefits found.[8] In moderate and severe forms of the syndrome, memantine represents a therapeutic alternative. Memantine is a non-competitive antagonist with moderate affinity for NMDA receptors (N-methyl-D-aspartate), which therefore protects neurons from excitotoxicity due to excessive release of glutamic and aspartic acid. In both cases they are excitatory neurotransmitters that induce an increase in the amount of free Ca^{2+} at the intracellular level. RCT studies have demonstrated the positive effects of this drug both from a cognitive point of view and on the psychological and behavioural symptoms of dementia on severe and moderate patients.[9] On the other hand, in a small group of subjects memantine caused dizziness, headache, confusion, and agitation.[10] The combination of donepezil and memantine has showed interesting results in patients with a severe and moderate form of the disease, while the same effects were not found in the mildly patients.[11] [12] [13]

Concerning behavioural symptoms, both acetylcholinesterase inhibitors and memantine were less effective than other drugs. For this reason, a series of more specific drugs were used to treat the behavioural and psychological symptoms of dementia in AD. Selective norepinephrine and serotonin inhibitors (mirtazapine, venlafaxine, duloxetine) and the serotonin reuptake inhibitors (fluoxetine, sertraline, paroxetine, citalopram) were administered to address the depression symptoms. These drugs were also taken into consideration for the treatment of agitation and psychosis associated with AD. However, for the treatment of depression, a recent trial concluded that the current practice of use both sertraline and mirtazapine should be reviewed, since no real efficacy data have been recorded. [14]

Psychotic symptoms, agitation and aggressive manifestations are commonly modulated by antipsychotic drugs, among these the preferred agents are atypical agents for the minor Parkinsonian effects: olanzapine, risperidone, quetiapine, aripiprazole.[15] The use of these molecules is a very controversial topic given the cerebrovascular problems and the high mortality recorded in the treated patients. Furthermore, antipsychotics could be responsible for a series of other side reactions, including a high risk of hip fracture, pneumonia and a worsening of cognitive impairment. Benzodiazepines are also used to reduce the anxiety and agitation associated with the syndrome, although they can also lead to increased agitation in the elderly. Finally, an alternative treatment for psychological and behavioural symptoms could be represented by anticonvulsants such as carbamazepine.

But despite the investment in AD research, it is clear that currently the drugs only ameliorate the symptoms and decrease the rate of cognitive decline, for a period of 6−12 months, but none of these are disease-modifying agents.[16]

1.6 AD Drug Discovery

Consequently, today the main purpose is discovering drugs effective in the early stages of Alzheimer's disease. Indeed, as stated above, if treatments are administrated late, the progressive aggravation of symptoms occurs in an irreversible way. The studies are focused on molecules that interfere with the pathways involved in neurofibrillary tangles and amyloid plaques formation.

Starting from tau protein deposition, numerous compounds have been identified through cell culture or in tests *in vitro* as inhibitors of the aggregation of this protein in neurofibrillary clusters. Among the various compounds methylene blue gave, in phase II of clinical trial, demonstrated promising results as a potential drug for AD showing improvements in cognitive functions after six months of administration. But the intrinsic link between phosphorylation and tau aggregation offered the opportunity of considering kinases as potential targets. In spite of the large number of sites for phosphorylation on the tau protein and the ability of multiple kinases to phosphorylate single sites, Glycogen Synthase Kinase 3β (GSK-3β) emerged as the most interesting as potential target.[17]

1.6.1 GSK-3β Inhibitors

The interest in GSK-3β is due to its implication in different but correlated functions, but this in the meantime makes challenging its regulation. So that, many efforts have been put into the discovery and development of new GSK-3β inhibitors during the last few years. Currently, only few compounds such as TDZD-8, Tideglusib, AZD2858, Cazpaullone and Alsterpaullone, TWS119 , CHIR-99021, and SB216763 (fig.1.6.1-**1)** are undergoing clinical trials as GSK-3β inhibitors. Research by both academic centres and pharmaceutical companies has contributed to the discovery of many inhibitors belonging to different chemical families, including organic compounds as well as small cations, showing great chemical diversity.[18] [19] In this context, Lithium represented the first GSK-3β inhibitor applied in clinical practice to the treatment of bipolar disorders and depression. The most common classification for GSK-3β inhibitors is based on their different inhibition mechanisms: ATP-competitive and non-ATP-competitive inhibitors. Most of molecules studied act as ATP-competitive inhibitors, so that the blockage of the enzyme occurs thanks to the molecule's competition with ATP for its binding site. Small molecule inhibitors bind to this site showing very high affinity (concentrations in the nanomolar range). The opportunity to obtain selective ATP-competitive inhibitors endowed with very high affinity may be achieved using structure-based methodologies. Indeed, plenty of ATP-competitive inhibitors have been co-crystallized with the enzyme, giving the opportunity of solving the complex structures by X-ray crystallography. In the meantime, due to the extremely high degree of conservation around this binding site, the opportunity to obtain isoform-selective inhibitors remains remote. Indeed, one of the many issues related to this class of compound is the lack of selectivity.[20] This very important feature can be achieved by molecules that act as non-ATP-competitive inhibitors, capable of interacting with specific kinase sites, such as allosteric sites or substrate-binding domains.

Starting with ATP-competitive inhibitors, the maleimide-based compounds have to be mentioned. Enzyme interactions for these compounds are based on the creation of H-bonds with the carbonyl oxygen of Asp133, located within the hinge region, and the nitrogen atom of the scaffold. Another interaction occurs between one of the two carbonyl oxygens of maleimide group with the backbone nitrogen of Val135 .[19] A further molecule, representing one of the most relevant ATP-competitive inhibitors is the compound AR-A014418 (figure 1.6.1-**1**) whose structure is based on the one of thiazolylureas. This compound shows very high affinity in the nanomolar range, it is highly selective and acts by blocking tau phosphorylation. The interactions established

by this compound occur in the hinge region where three H-bonds are formed: two with Val135 and one with Pro136.[21] The Val135 residue, together with Lys85, is also involved in H-bonds formation with paullones (figure 1.6.1-**1**), such as alsterpaullone (figure 1.6.1-**1**), two potent GSK-3β inhibitors.[22]

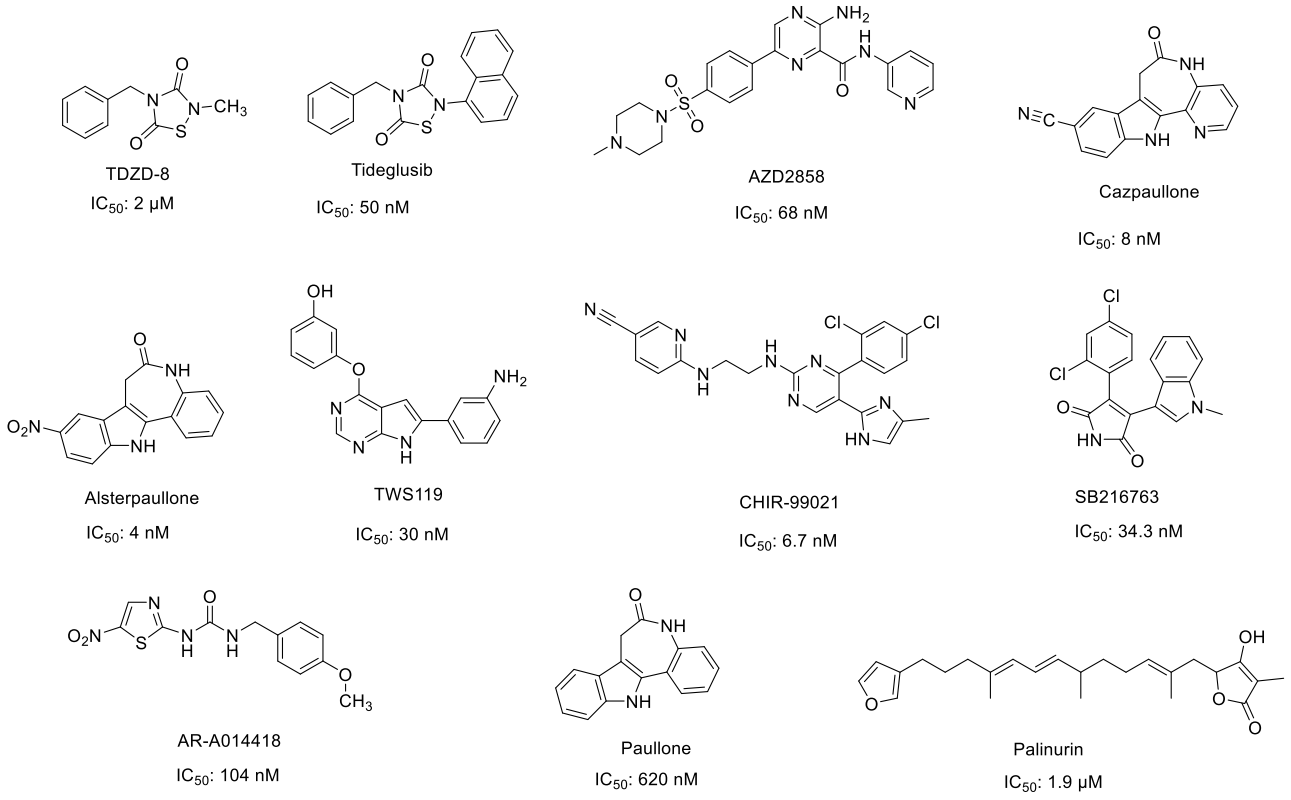

Figure *1.6.1*-**1** Structure of GSK-3β inhibitors

With regard to non-ATP-competitive inhibitors, the most relevant compounds are represented by Tideglusib (figure 1.6.1-**1**) Palinurin (figure 1.6.1-**1**) [23] and halomethyl ketone derivatives which form a covalent bond with the Cys199 residue located at the entrance of ATP binding site.[24] Compared to ATP-competitive inhibitors, these compounds establish weaker interactions with the enzyme and, as a consequence, a lower inhibition rate is reached. This condition is favourable since the therapeutic effect can be achieved by a weak inhibition capable of bringing enzyme activity back to physiological levels and preventing toxic effects.[25]

Regarding organic GSK-3β inhibitors they may be of synthetic origin or derived directly or indirectly from small molecules of natural origin.[26] Many natural compounds were found active towards GSK-3β. In particular, natural alkaloids represent an important source for interesting chemical scaffolds for design new GSK-3β inhibitors.

The bis-indole alkaloid indirubin (1), reported in fig. 1.6.1-**2**, was first described in the 1980s as the main active constituent of Danggui Longhui Wan, a mixture of 11 herbal medicines used in traditional Chinese

medicine for cancer treatment. More specifically, indirubin is the red colored isomer of indigo found in different indigo plant species and marine organisms (gastropod mollusks). Indirubin acts as a potent ATP competitive inhibitor of GSK-3β (IC_{50} values in the 5–50 nM range).

Halogenated indirubins embody an interesting scaffold for exploring specific kinase inhibition. The naturally halogenated indirubin, 6-bromoindirubin (6BI) (2) (figure 1.6.1-**2**), has a selective and strong inhibitory activity for the mammal GSK-3β (0.01 – 0.1 μM) while other 6-substituted synthetic analogues carrying Cl, F and I show similar inhibitory potency, but with loss of selectivity.[27]

Crystallographic data of GSK-3β in complex with various indirubins confirmed that bromine substitution at position 6 is crucial for selectivity while substitutions at 3' are important for the binding activity. The large biding pocket of GSK-3β provides enough space for the bromine atom to be inserted into the back of the cavity, explaining the selectivity of 6BI towards GSK-3β. Halogen substitution at position 5 increases protein kinase inhibition potential, but slightly impairs selectivity[28] whereas, in general, substitution at position 7 decreases the inhibitory activity and brings no benefit in terms of selectivity. 2D-and 3D QSAR studies confirmed that selectivity has a direct correlation with the presence of atoms that electron-withdraw electrons, such as halogens in position 5/6 rather than in position 7/4. Any substitution at position 4, with the exception of hydrogen, causes distortion and loss of the molecular planarity of the structure necessary for the binding, while substitutions at position 7 causes unfavorable contacts with the protein backbone.[29]

Like most inhibitors, that bind through hydrophobic interactions the ATP-binding pocket, indirubins are quite hydrophobic. So that, the conversion of the 3' carbonyl group into an oxime group is an important modification for the modulation of solubility and selectivity properties. The oxime moiety is an ideal site for the introduction of hydrophilic substituents and moreover it provides stabilization of these structures. 6 halogenated substituted indirubins containing the oxime moiety showed greater GSK-3 selectivity and inhibitory potential when compared to other substituted indirubin-3'-oximes. 6-bromoindirubin-3′-oxime (6BIO) (3) is a semi-synthetic cell-permeable analogue of 6BI with a remarkable low nanomolar inhibition range (< 10 nM) currently marketed under the name "BIO" and "GSK-3 inhibitor IX", is considered a prototype inhibitor for the development of selective and potent pharmacological inhibitors of GSK-3.[27]

A series of bis-substituted 3'-oxime indirubins derivates at positions 5 and 6 were synthesized and the best inhibitory activity and selectivity is observed for 5,6-bisubstituted 6-bromoindirubin-3′-oxime analogues bearing CH_3 and NO_2 and 6-cloroindirubin-3'oxime bearing a chloride atom at position 5.[29]

Nevertheless, despite the presence of the oxime group, simple indirubin analogues still suffer from low hydrophilicity (6BIO LogD 2.59 vs indirubin LogD 2.5)[30] Therefore, several 6-bromo-indirubin analogues with different substitutions at the 3' position were synthesized. The introduction of amino-aliphatic chains on the 3' oxime group was essential to obtain a series of compounds with increased solubility with logD values varying from 1.90 to -0.87.[30] Sugar moieties were also introduced to the basic indirubin core at positions 1 and 1′ increasing the solubility of bioactive indirubins.[31] Indirubins consistently are an important molecular scaffold from which very selective and active molecules against GSK-3β emerged. Due to the incredible potential of these compounds as selective GSK-3 inhibitors and possible numerous biological applications, the

research is ongoing for new indirubins characterized by a better water solubility without losing activity and selectivity.

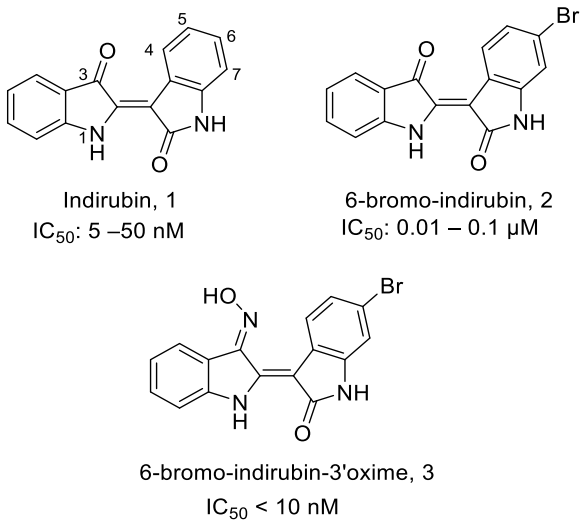

Figure *1.6.1*-**2** Structures of Indirubin and its derivatives

In addition, manzamines (figure1.6.1-**3**) are complex alkaloids isolated from Indo-Pacific sponges and characterized as having an intricate and novel 5-, 6-, 6-, 8-,13-membered heterocyclic ring system coupled to a β-carboline moiety. Manzamine A (4) was first isolated in the late 1980s from the Okinawan sponge of the genus *Haliclona*, and latter from other marine sponge families that also produces manzamine-related alkaloids.[24] [32] Manzamine A inhibits human GSK-3β *in vitro* (IC_{50} value of 10.2 µM) as a non-competitive inhibitor of ATP binding. [33] [34]

Hamman et al. used natural and semi-synthetic analogues to assess the structure-activity relationship in GSK-3 inhibition of some substituents in the carboline moiety and aliphatic heterocyclic system (figure1.6.1-**3**). It emerged that the replacement of hydrogen on the carboline moiety at position 8 with OH and tosylate groups (OTs) generate slightly more active compounds than manzamine A, while other substitutions with hydroxy derivates at position 6 yielded equipotent analogues. Meanwhile, nitrogen substitution at position 9 of the carboline heterocycle with larger groups such as *i*-But, or *t*-BuOCOMe led to inactive derivatives. Regarding the aliphatic heterocyclic system, the double bond between positions 15 and 16 is essential to promote GSK-3 inhibition. Analogues with a carbonyl group on the cyclooctane ring (5) are less potent than manzamine A while an epoxy function restores GSK-3 inhibition (6). In agreement, an increase in GSK-3 inhibition is observed when bulkier moieties at position 9 are combined with a carbonyl group on the cyclooctane ring, indicating the possibility of a pocket in the GSK-3 enzyme where the phenyl ring of the carboline heterocycle should be allocated. In addition, enzyme inhibition is favored by increasing conformational restriction in the aliphatic part of manzamines (4)**.**[34]

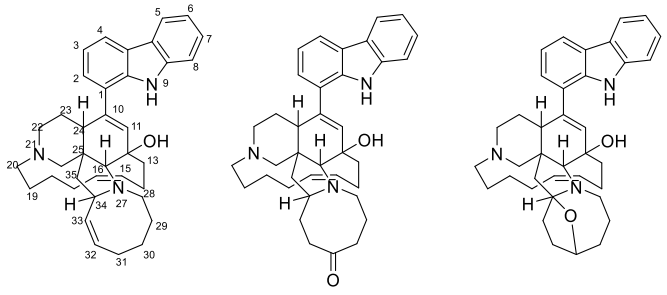

Figure *1.6.1*-**3** Manzamines structures

Among the natural alkaloids the hymenialdisine (HMD) (figure 1.6.1-**4**) is a known metabolite that was isolated for the first time in 1980s from *Hymeniacidon aldis, Axinella verrucosa, and Acanthella aurantiaca.*[35] Chemically, it is a member of the family of tricyclic pyrrole compounds consisting of a brominated pyrrolo[2,3-c]azepine skeleton and a 5-membered glycocyamidine ring system.

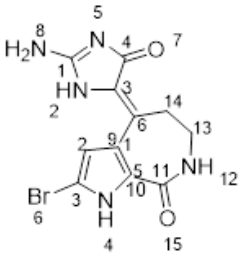

Figure *1.6.1*-**4** Hymenialdisine structure

The interest in hymenialdisine is related to its activity as competitive nanomolar inhibitor towards GSK-3β (IC_{50}: 10 nM). Crystallographic studies revealed that this compound bindes GSK-3β in the ATP binding pocket (figure 1.6.1-**5**).[36]

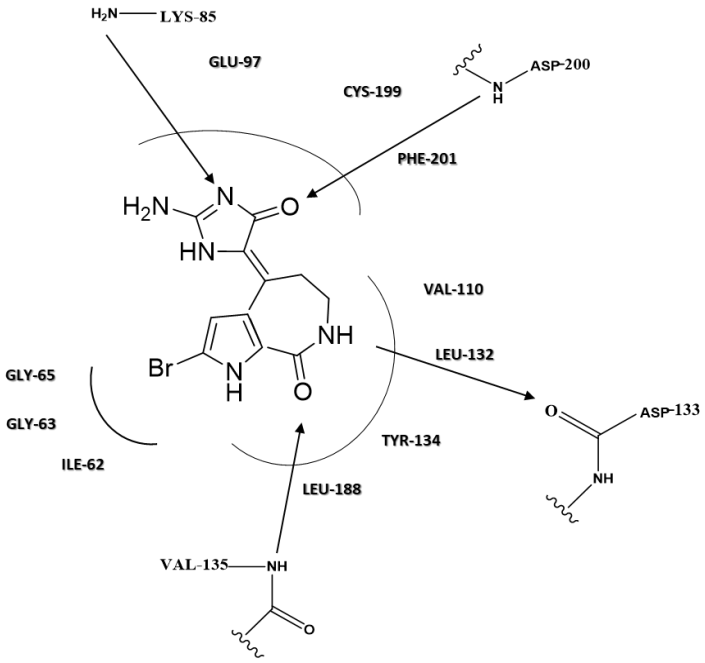

Figure *1.6.1*-**5** Hymenialdisine interactions in the ATP binding pocket

It is easy to deduce that the principal issue related to this very potent natural compound concerns the low selectivity. Indeed, with the intent of improving selectivity some hymenialdisine derivatives were synthetized in 2004 by Gray and coworkers. The design of the new derivatives involved the substitution on the pyrrole ring as well as the replacement of the same one with an indole group with various substituents (figure 1.6.1-**6**).

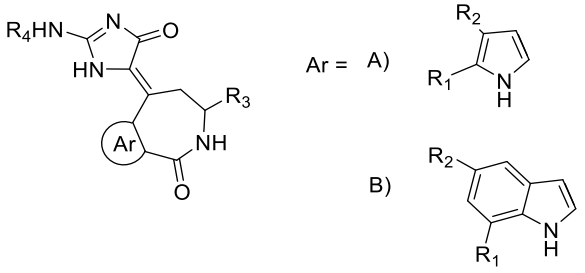

Figure *1.6.1*-**6** Hymenialdisine Pyrrol (A) and Indole (B) analogues

The aim was to optimize the interactions in hydrophobic pocket and to retain important and conserved hydrogen bonds. Regarding the inhibitory activity towards GSK-3β, the compounds showing a chloride or bromide substituent in R_1, R_2 or both the positions maintained the inhibitory activity in the lower nanomolar range. Except for the compound reporting a bromide substituent in R_1 position, these derivatives they showed similar activity towards GSK-3β. Indeed, a decrease in inhibitory activity is detected for those compounds reporting a methyl group in R_3 as well as an ethyl or acetyl group in R_4 position. Regarding the inhibitory activity of indole derivatives, is comparable to that of pyrrole derivatives. Even then, the acylation or alkylation

of glycocyamiadine amide reduces activity. Based on these results it is then possible to deduce that R_3 and R_4 substituents are more influent than R_1 and R_2 in the binding activity.
The substitution of glycocyamidine ring by arylhydrazones was also investigated (Figure 1.6.1-**7**).

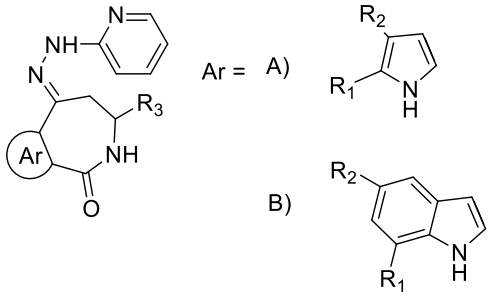

Figure *1.6.1*-**7** Hymenialdisine arylhydrazones derivatives

For compound showing a bromide group in both R_1 and R_2 positions the activity is not improved. The same results are also obtained for analogues reporting a fluoride or chloride substituent in R_1 position. This aspect is not surprising since the glycocyamidine ring contributes to multiple hydrogen bonds to the kinase in the ATP binding pocket.[36]
Once fixed the hydrazone moiety the differences among pyrrolo- or indolo-azepinones was investigated. Compared to pyrrole analogues the indole derivatives show at least a 10-fold improvement in activity. Moreover, the introduction of halogen as R_2 substituent increases the inhibitory activity of derivatives against GSK-3β. In general, compared to the close structural analogues of HMD, the hydrazones obtained show much reduced activity towards GSK-3β.

1.6.2 Amyloid Anti-Aggregating Agents

Regarding the other famous and correlated pathway involved in AD pathogenesis, many compounds were studied to interfere with senile plaques formation. The hypothesis that Aβ aggregation leads to oligomers formation (now considered the most toxic amyloid species) oriented the research towards the study of anti-aggregating agents. The only aggregating inhibitor that arrived in phase III was tramiprosate (3APS) (figure 1.6.2-**1)**, designed to prevent the binding between the Aβ protein and glycosaminoglycans. More recent studies have highlighted the promotion by this compound of an abnormal aggregation of the tau protein, highlighting once again the importance of testing potential drugs for AD on both damaged metabolic pathways, both the amyloid and the tau protein.[37]

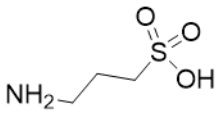

Tramiprosate

Figure *1.6.2*-**1** Tramiprosate structure

Another molecule whose study was stopped in the last clinical stages was colostrinin, a polypeptide complex rich in proline, deriving from sheep colostrum. This compound demonstrated in animal models to inhibit the aggregation of the beta amyloid protein, arresting neurotoxicity and thus improving cognitive functions.

Another compound called scyllo-inositol, tested in the hippocampus of rats, showed the ability to stabilize the oligomeric aggregates of Aβ protein and thus inhibit their toxicity.

Numerous Zn^{2+} / Cu^{2+} chelators have been found to be effective in inhibiting the aggregation of the β-amyloid protein, both *in vitro* and in animal studies. Among these, PBT2 has proved very promising to the point that it will be subjected to subsequent advanced clinical trials.[38]

In the meantime, the search for other therapeutic strategies has been undertaken by focusing the study on the pathological mechanism that leads to the formation of the β-amyloid protein starting from the trans membrane peptide APP. Aβ production could be reduced by inhibiting the β-secretase and γ-secretase enzymes or conversely by inducing the activity of the α-secretase enzyme. γ-secretase is a complex nucleoprotein which, alongside APP, possesses numerous other substrates and transmembrane proteins, including the Notch 1 receptor involved in growth. This caused various side effects (gastrointestinal and haematopoietic) which have hindered the clinical development of inhibitors for γ-secretase. Among γ-secretase inhibitors, the compound semagacestat had shown the ability to decrease the production of the β-amyloid protein.[39] However, this molecule failed the phase III of the clinical trial, conducted on patients with mild and moderate forms of AD, due to the side effects registered. In 2012 the study on avagacestat, another γ-secretase was arrested because it proved to worse cognition and to give greater adverse effects in the treated people compared to those on placebo in Phase II of clinical studies.[40]

On the other hand, the research of drugs designed to enhance α-secretase enzyme activity has led to Etazolate. This compound has shown to be at the same time safe and able to prevent neuronal death induced by the Aβ protein,[41] slowing down disease progression and providing symptomatic relief. However, the most promising target enzyme still appears β-secretase (BACE1).

1.6.3 BACE 1 Inhibitors

The development of BACE1 inhibitors is challenging for two main reasons: firstly, because BACE1 plays a number of physiological roles and therefore its inhibition leads to various toxic side effect; secondly because the active site of the enzyme is quite large and therefore, is difficult to design molecules able to cross the blood brain barrier.

Many efforts have been employed to develop potent BACE1 inhibitors, among them some have reached different stages of clinical trials. However, the latest results of some of the BACE1 inhibitors in clinical trials have led to controversial results. Among the promising compounds that have been developed by the pharmaceutical company Merck MK-8931 (verubecestat) (figure 1.6.3-**1**), which belongs to the non-peptidomimetic guanidine family of BACE-1 inhibitors showed remarkable results for its potency (IC_{50} = 2.2 nM), selectivity, pharmacokinetic and physiochemical properties. However, Merck recently announced that Phase III clinical study in 1958 patients with mild to moderate Alzheimer's disease will be arrested. The failure of this study seems to be related to lack of efficacy, as patients taking verubecestat showed no improvement in their cognitive function compared to the placebo group, despite verubecestat has proved to reduce Aβ levels in the brain and cerebrospinal fluid. Furthermore, different adverse effects associated with the use of verubecestat, were registered such as rashes, falls and injuries. In addition, the failure of verubecestat to achieve the desired effects could be attributed to the fact that the reduction in the level of Aβ production don't lead to clinical benefits when patients are diagnosed with dementia, as Aβ accumulation occurs years before symptoms of dementia appear in AD patients. Another possible explanation for the failure of BACE1 inhibitors to reduce the progression of AD could be due to the complexity of the genetic factors responsible for the progression of AD disease and the inability of the amyloid hypothesis alone to explain the progression of the disease. Another BACE1 inhibitors JNJ-54861911 (atabecestat) (figure 1.6.3-**1**) became famous after it didn't show significant clinical efficacy. This aminodihydrothiazine-containing derivative was tested in a group of asymptomatic high-risk AD patients in study on 1,650 asymptomatic high-risk AD patients. Initially, the results were encouraging the administration of atabecestat to healthy volunteers demonstrated to reduce of 95% Aβ production. However, in May 2018, it was decided to arrest the study due to an abnormal increase in liver enzymes among 600 of the participants. These observations for the progress of BACE1 inhibitors across different clinical trials clearly indicate that safety was the major barrier against the success of many BACE1 inhibitors. For example, two compounds developed by Eli Lilly, LY-2811376 (figure 1.6.3-**1**) and LY-2886721 (figure 1.6.3-**1**), can't have further advances in clinical trials due to liver damage effects registered. Furthermore, BI1181181 developed by Boehringer Ingelheim is a compound that managed to reduce brain levels of Aβ and passed two phase I clinical trials. But again, safety was the main reason that excluded BI1181181 from the market and forced Boehringer Ingelheim to stop its development in July 2015. In addition, for undisclosed causes, the clinical trials of AstraZeneca's AZD-3839 (figure 1.6.3-**1**) and Roche's RG-7129 (figure 1.6.3-**1**) were also terminated.[42]

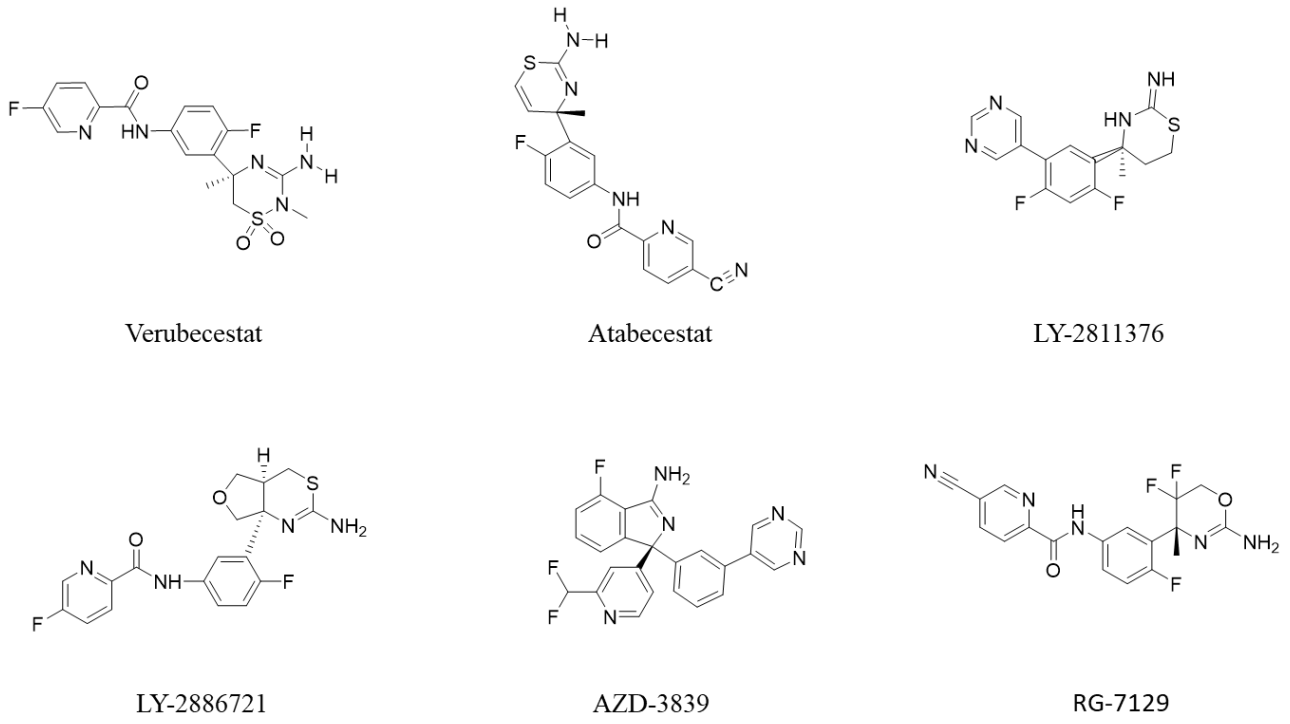

Figure *1.6.3* -***1*** Structure of BACE-1 Inhibitors

1.7 Multi-Target Directed Ligands in AD Drug Discovery

Therefore, till now, we cannot speak of effective treatments for the prevention and modulation of AD, and the failure in clinical trials could be assigned to the strategy of considering the various pathological processes separately in spite of the complex and heterogeneous AD aetiology and pathogenesis.

Accordingly, there is a growing awareness about the multifactorial nature of AD, which could result from the dysregulation of various separate but integrated signalling pathways. So, it seems that the principle of "network medicine", an emerging science that considers the connection between biological effects, could guide the drug discovery. For "network medicine", a disease is nothing other than the result of the breakdown of the physiological network, due to the suppression and activation of certain pathways with a consequent imbalance of inputs and outputs. Therefore, in this context, the therapy aims to re-establishing the physiological network, simultaneously hitting specific key components.[4344]

As mentioned, the efficacy of the therapy is prejudiced if one intervenes only on a single aspect (target protein, metabolic pathway). Hence, the hypothesis that a poly-pharmacological approach could be essential to obtain the desired therapeutic effects.[45]

However, a crucial problem lies in the fact that patients with AD are, in most cases, also subject to a wide range of concomitant co-morbidities (such as hypertension, vascular problems, diabetes). This implies, therefore, that they take multiple drugs. So, from 2008 multitarget-directed ligands (MTDLS) emerged a successful alternative to the use of several specific drugs. They are small organic molecules capable of hitting

different targets simultaneously, that could be a well-tolerated therapeutic tool because it reduces the risks of possible drug interactions.[46] However, the challenging aspects of designing MTLDs were soon clear.[47] Morphy and Rankovic outlined two possible strategies that could be followed, which are still used: the random screening approach and the framework combination approach.[48] In the first case, classes of compounds that are known to be already active towards one of the targets of interest are tested on other targets. On the contrary, the framework combination is an approach that aims to combine two molecular structures into a new single entity. The authors coined the terms linking, fusing and merging to indicate the way in which the two starting molecular fragments were integrated.[47] The ligands obtained by combining two distinct fragments connected by a linker, appeared to have a greater molecular weight and were therefore less suitable for oral administration. On the contrary, ligands designed starting from molecular fragments that were superimposed or intimately integrated (fused or merged), have a lower molecular weight and therefore they have better potential properties as potential drugs. A study carried out in 2006 by the same authors revealed that the selected MTDLs were in themselves larger and more complex than conventional single-target preclinical ligands.[49] For this reason, over the years the strategy of FBDD (fragment based drug discovery) has received increasing consensus as an excellent starting point for the design of multi-target drugs.

In fact, it was discovered that there is a clear correlation between average molecular weight and selectivity, if a molecule has a simple structure, it has a higher possibility to create bonds. Therefore, it is easier for small molecules to establish interactions with multiple targets, having fewer aspects that could negatively affect each other.[50] According to these observations it appeared a good strategy identify a base scaffold, capable of binding multiple targets, with good affinity and binding efficiency. Therefore following the framework combination strategy a series of compounds capable of interacting with AD targets have been designed.

1.7.1 GSK-3β Dual Inhibitors

GSK-3β and BACE1. GSK-3β and BACE1 appeared the ideal targets to design dual inhibitors. In fact, these enzymes, are interconnected: BACE1 promotes the formation of the β-amyloid protein, which exerts its toxic effects in various ways, by inducing GSK-3β. This in turn leads to an increase in tau protein phosphorylation and toxicity linked to NTFs, neuroinflammation, apoptosis, cell cycle dysregulation and damage to acute hippocampal neurogenesis. This correlation lies not only in the response that the GSK-3β enzyme produces to the induction of the β-amyloid peptide, but in the fact that the enzyme in turn regulates the accumulation of the same peptide through the modulation of the enzymes α, β and γ-secretase. According to what has been said, the simultaneous modulation of both BACE1 and GSK-3β enzymes could represent a promising tool in AD treatment. These two enzymes are very different in their nature, and they share the identity sequence for only 19%. For this, a ligand-based approach was followed, combining in a single scaffold the characteristics of the pharmacophore that binds BACE1 and GSK-3β, respectively the guanidine structure and the cyclic amide group in a single scaffold. This conduced to the identification of the 6-amino4-substituted triazinone scaffold as potential starting point (figire 1.7.1-**1**). [51]

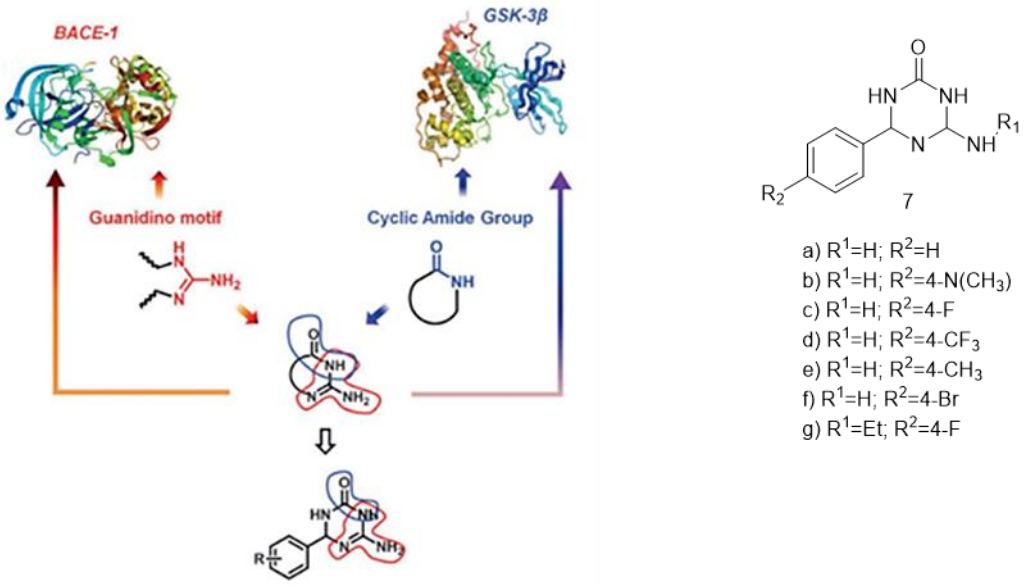

Figure *1.7.1*-**1** Amino-4-substituted triazinone derivatives [51]

Then, a first set of molecules was synthesized and tested against the two enzymes. Compound 7c is the most promising of the series for dual activity demonstrated and additionally demonstrated to be a promising anti-inflammatory and neuro-protective agent. Finally pharmacokinetic data of this derivatives on rats (including the degree of permeability of the blood brain barrier) were collected. Following this new research direction, based on simultaneous modulation of the enzyme BACE1 and GSK-3β, it was rationally synthesized a series of dual inhibitors starting from the pharmacophoric structure of curcumin. Curcumin polyphenol, the first bioactive compound isolated in the rhizome of *Curcuma longa L.*, has been one of the natural compounds more investigated thoroughly following studies that documented its efficacy and safety both for the prevention and for the treatment of various pathologies. This pleiotropic pharmacological behaviour is due to its mechanism of action which consists in the interaction with different protein targets involved in various metabolic pathways. Thus, the neuroprotective activity is the results of the modulation of a wide range of processes: Aβ and tau aggregation, oxidative stress and neuroinflammation. In the curcumin scaffold the central β-ketoenolic core, proved to be exploitable for the interaction with the catalytic dyad of BACE1 (Asp32 and Asp228) while the electrophilic αβ unsaturated carbonyl system was able to covalently bind the GSK3β - Cys199 residue.

In light of this discovery, an attempt was made to synthesize a small library of curcumin analogues (figure 1.7.1-**2**)

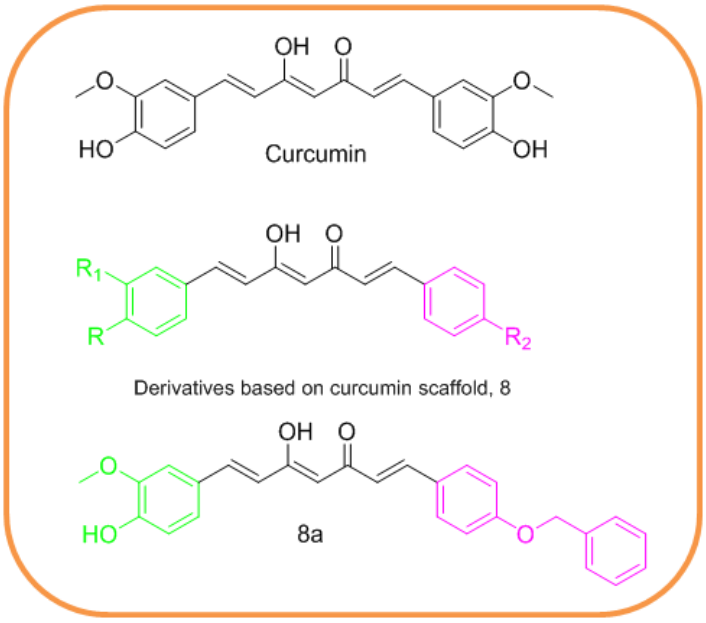

Figure *1.7.1*-**2** BACE1- GSK-3β dual inhibitors based on curcumin scaffold, and the most active of the series (8a)

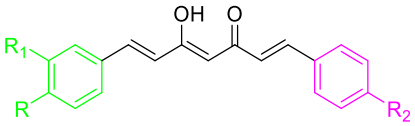

Compound	R	R^1	R^2	BACE -1 IC_{50} (μM)±SEM	GSK-3β IC_{50} (μM)±SEM
a	OH	OCH_3	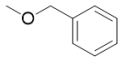	0.97 ± 0.43	0.90 ± 0.38
b	OH	OCH_3	CH_3	0.14 ± 0.03	2.09 ± 0.51
c	OH	H	OH	2.54 ± 0.02	8.39 ± 1.59
d	OCH_3	H	OCH_3	1.65 ± 0.01	0.53 ± 0.27
e	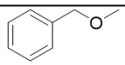	H	OCH_3	2.28 ± 0.64	2.78 ± 0.44
f	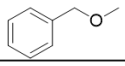	H	OH	2.69 ± 1.01	2.01 ± 0.71
g	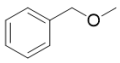	H	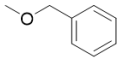	0.04 ± 0.01	2.49 ± 0.82
h	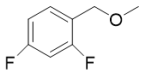	H	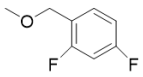	0.40 ± 0.06	9.63 ± 0.21
i	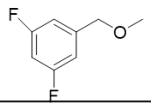	H	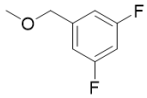	0.39 ± 0.34	8.30 ± 0.54
L	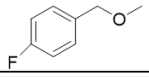	H	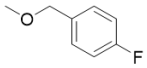	1.04 ± 0.34	12.81 ± 0.14
m	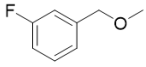	H	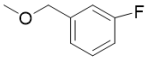	1.08 ± 0.66	16.99 ± 2.68

Table *1.7.1*-**1** Inhibition of BACE1- GSK-3β enzymatic activities by the curcumin based analogues (8a-m) [52]

Values are the mean ± SD of two independent measurements, each performed in triplicate. SEM= standard error of the mean b) N.i.: not inhibiting up to 3 μM c) Data were taken from ref.[53]

Among the various compounds synthesized, a moderate dualistic profile has been demonstrated from 8c and 8d (table 1.7.1-**1**) while 8a, 8e and 8f (table 1.7.1-**1**) turned out to be dual inhibitors active at low molecular concentrations. This is a promising result for multi-target drug discovery. In addition, compounds 8a, 8b, 8e and 8f (table 1.7.1-**1**) induce the NQO1 enzyme, exerting a neuroprotective activity that countered oxidative stress. Given the synergistic effects demonstrated, compound 8a (table 1.7.1-**1**) was considered the promising candidate to work on for the treatment of AD.[52]

GSK-3β and HDACs. Currently, the interest into the role of post-translational modifications, specifically phosphorylation and acetylation, is increasing. Tau phosphorylation is one of the post-translational modifications more deeply investigated in view of AD drug discovery. When tau is hyper-phosphorylated, this conformational change decreases its flexibility and affinity for microtubules, thereby promoting tau accumulation in the cytosol and driving the formation of NFTs. But tau seems to be not only modified by phosphorylation but also by acetylation and these post-translational modifications are strictly connected. Numerous studies demonstrated that the tau acetylation is an encouraging strategy to treat AD. The idea that acetylation was exclusively involved in the regulation the transcriptional process through the modification of histones, was firstly reverted after the discovery that tubulin is the first cytosolic protein acetylated. So, the effects of HDACs inhibition are in part independent from histone-acetylation. HDACs are considered playing a role in the regulation of neuronal survival. Analysing each HDAC protein it was found that isoforms HDAC4, HDAC6, HDAC7, HDRP (a truncated form of HDAC9), and Sirt1 protect neurons rather than promote degeneration. On the contrary, HDAC3 proved to increased toxicity in neurons suggesting that its inhibition might explain the neuroprotective effects of HDAC inhibitors. Tau acetylation and tau phosphorylation appeared strictly connected. HDAC6 activity increases phosphorylation of tau at the 12E8 epitope (pS262/356), a phospho-epitope present within the KXGS motifs of tau's microtubule-binding domain. The phosphorylation of KXGS motifs within tau by the kinase Par-1/MARK2 is required for tau proteotoxicity in Drosophila[54] observed at very early stages of NFT formation in AD brain[55]and appears to prime tau for subsequent phosphorylation events.[54] [55]Tau species phosphorylated on KXGS motifs are not recognized by cellular degradation machinery, including the tau ubiquitin ligase C-terminus of Hsc70 interacting protein (CHIP) and the heat shock protein 70/90 (Hsp70/90) chaperone complex,[56] [57]and are therefore particularly prone to accumulate. Hyperactivation of HDAC6 enzyme would be considered to enhance tau pathology given that tau species phosphorylated on KXGS motifs are resistant to degradation and tend to accumulate in NFTs failing to bind and stabilize microtubules and they are also targets of other kinases. Moreover, it has been recently demonstrated that, in addition to modulating phosphorylation at these critical KXGS motif regions, HDAC6 also regulates their acetylation making them less susceptible to aggregate *in vitro* assays. In addition, it seems that there is competitive relationship between acetylation and phosphorylation on KXGS motifs, so in mouse model HDAC6 inhibitors demonstrated to simultaneously increases acetylation of tau, while blocking phosphorylation. According to these findings, in a Drosophila model of tauopathy, loss of HDAC6 activity caused tau-induced microtubule alteration in both neuronal and muscle cells.[58] This data provides the first *in vivo* evidence that reducing HDAC6 activity in a model of tauopathy is protective. Further emphasizing in the therapeutic potential of HDAC6 inhibitors derives from results demonstrating that loss of HDAC6 expression/activity is also neuroprotective in other neurodegenerative diseases, including AD**.** HDAC1 isoform seems that have a dual role in modulating neuronal viability. It contributes to neuroprotection interacting with other survival-promoting HDACs such as HDRP and neuronal death with HDAC3. Based on a study, HDAC1 translocates from the nucleus to the cytoplasm and this condition is necessary to have the neuronal and axonal degeneration, even this phenomenon has not been detected in other studies. Hence, it was

hypothesized that a small amount of HDAC1 move out of the nucleus, to interact with cytoplasmic HDAC3 and the rest of interaction takes place in the nucleus. HDAC3 is phosphorylated by GSK3β, a modification that is necessary for its neurotoxic effect, so it was supposed that GSK3β phosphorylates HDAC3 to promote its interaction with HDAC1.[59] The hypothesis was confirmed by the fact that inhibition of GSK3β blocks neurotoxicity by HDAC1 expression, although it does not directly phosphorylate HDAC1.So a molecule that inhibits HDAC1-HDAC3 interaction could be useful in preventing neurodegeneration. For this reason, HDAC inhibitors, after having been largely used as mood stabilizers in psychiatric disorders and as anti-epileptics, are now considered interesting as potential therapeutic agents for the treatment of neurodegenerative diseases. HDAC inhibitors can be classified into four main groups in base of their chemical characteristics: the hydroxamic acids (TSA and SAHA), epoxyketones (such as trapoxin), short-chain fatty acids (sodium butyrate, phenylbutyrate and valproic acid) and benzamides.[60] [61]

1.7.2 Amyloid Anti-Aggregating Agents in View of MTDLs

Aβ aggregation, ROS and GSK-3β. Recently, De Simone et al. following the study of Bolognesi and co-workers, started from the scaffold of ferulic acid ethylester (ethyl-4-hydroxy-3-methoxycinnamic acid), a natural antioxidant, to develop potential MTDLs able to target in the meantime Aβ aggregation and GSK-3β (fig. 1.7.2-**1**).[62] The chemical structure of ferulic acid ethyl ester can be easily modified in order to extend its biological activity. In fact, the trans-cinnamoyl scaffold is present in the structures of many compounds that have been evaluated toward many biological targets.[63] So, five trans-cinnamoyl derivatives (9a-e) (fig. 1.7.2-**1**) were designed i) to act as antioxidants thanks to the substituted aromatic moiety obtained from natural products, such as ferulic and caffeic acids and ethylferulate, ii) to interact with GSK-3β through the α, β -unsaturated system and iii) to inhibit $A\beta_{1-42}$ self-aggregation thanks to the substituted aromatic moiety and the presence of an extended planar conjugate system.[62]

a) R^1=OH; R^2=OCH_3
b) R^1=OH; R^2=OCH_2CH_3
c) R^1=OH; R^2=OH
d) R^1=OH; R^2=H
e) R^1=H; R^2=OH

Figure *1.7.2*-**1** Trans-cinnamoyl derivatives [64]

The derivates 9a-e (figure 1.7.2-**1**) were evaluated for their ability to inhibit GSK-3β and $A\beta_{1-42}$ self-aggregation and to counteract reactive oxygen radical (ROS) formation. For the most interesting compound, the ability to chelate copper, a known biometal involved in AD neurotoxicity, was evaluated together with the

neuroprotective activity against glutamate-induced toxicity in cortical neurons. Furthermore, they were tested toward transglutaminase 2. Lastly, their BBB permeability was predicted by BBB-PAMPA assay. During the characterization compound 9c proved to modulate GSK-3β and $A\beta_{1-42}$ self-induced aggregation, to act as copper chelator and, more interestingly, exerted a very high ROS scavenging activity in aqueous medium. Additionally, compound 9c showed to be safe when tested in immature cortical neurons up to 50 mM, and it was able to protect these neurons from toxic stimuli induced by glutamate. Moreover, it was predicted to have a good BBB permeability. Thus, compound 9c emerged as promising tool to investigate AD pathogenesis and may be optimized by further development. It was demonstrated that the introduction of a 3-pyridyl ring allowed to have a better interaction with $A\beta_{1-42}$ growing fibrils, thanks to the extended conjugate system, and in the meantime showed additional interactions with GSK-3β.

Aβ and tau aggregation, AChE and BACE1. Recently the research group guided by Munoz Torrero, has developed a novel class of multi-target hybrid compounds combining the moiety of the natural product rhein, which has moderately potent Aβ and tau antiaggregating effect, and the huprine Y, an alkaloid with potent anti-acetylcholinesterase (AChE) activity.[65]

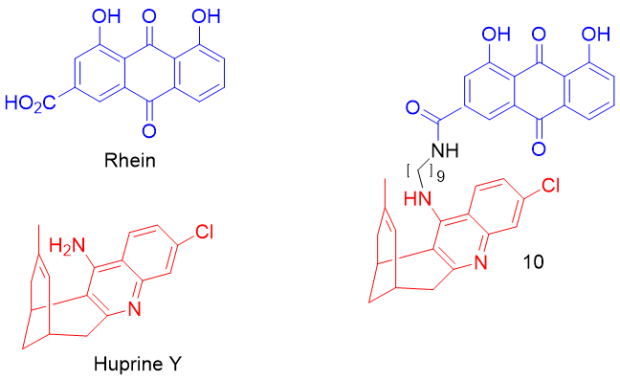

Figure *1.7.2*-**2** Lead compound of the Rhein-Huprine Y serie [65]

The lead compound of the series (compound 10 figure 1.7.2-**2**) showed a very interesting *in vitro* multi-target profile. It proved a good inhibition of human cholinesterases (hAChE, IC_{50} = 3.60 nM; hBChE, IC_{50} = 620 nM), and $A\beta_{1-42}$ and tau anti-aggregating activity (48% and 30% inhibition at 10 μM, respectively, in a cell-based assay that uses intact Escherichia coli cells overexpressing $A\beta_{1-42}$ and tau). Moreover, this compound was tested towards BACE-1 and it showed an IC_{50} of 120 nM. The potent activity toward AChE and BACE1 by the compound 10, was investigated through molecular modelling studies. The dual activity could be ascribed to the presence of two site binding in both enzymes: catalytic anionic site and the peripheral anionic site of AChE, and to the catalytic site and an unexplored secondary site of BACE-1. When is at physiological pH, the huprine moiety of compound 10, is protonated and this allows its interaction in the catalytic site of both AChE and BACE-1. At the level of AChE, cation–π interactions with the indole ring of Trp86 and the benzene ring of Tyr337 occur, and moreover there is a hydrogen bonding with the His447 carbonyl oxygen. In BACE-1, the Asp32 and Asp228 residues of the catalytic dyad are involved in the interaction. The basicity

of the huprine moiety of derivative 10 is therefore crucial for AChE and BACE-1 inhibition, but has to be correctly balanced, because basicity could be associated with a poor permeation through biological membranes and P-gp-mediated efflux. It has been demonstrated that the reduction of the basicity of amidine-based BACE-1 inhibitors has been successfully used to ameliorate permeability and reduce P-gp efflux, enhancing oral bioavailability and BBB penetration. The aim of the subsequent work was to investigate the structural modification and to determine the structural features responsible of the interaction of the huprine moiety of these hybrids to the catalytic site of BACE-1. Then the study wanted to assess the influence of huprine moiety basicity, and hence, of the protonation state of the hybrids, on their multiple biological activities, especially on AChE and BACE-1 inhibition.

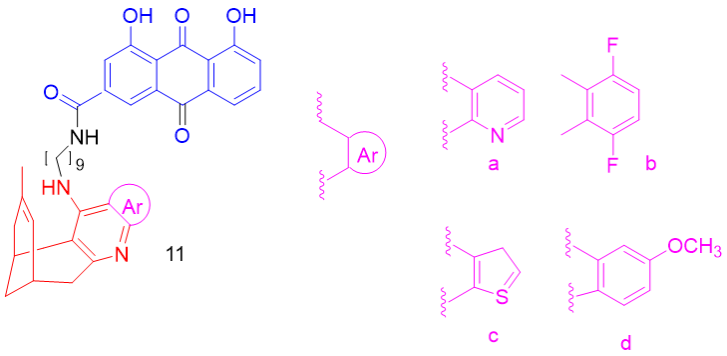

Figure *1.7.2*-**3** Design and synthesis of second-generation of Rhein–Huprine Y hybrids [65]

For the design of the novel rhein–huprine hybrids with various grade of basicity, the chlorobenzene ring of the huprine Y moiety was replaced in the hybrid 10 by other aromatic or heteroaromatic rings. Then novel rhein–huprine hybrids 11a–d (figure 1.7.2-**3**) were selected on the basis of the calculated pKa values of the corresponding molecule obtained. Considering their calculated pKa values, these hybrids have to be protonated in the acidic endosomal compartments protonated in the acidic endosomal compartments (pH 4.5–6.5). This is crucial point because BACE1 works in the endosomal compartments, and in this condition its maximum activity.

The second-generation rhein–huprine hybrids proved to be less active toward hAChE and hBACE-1 than hybrid 3 of the first-generation but they showed an increased inhibitory potency toward as $A\beta_{1-42}$ and tau aggregation. Moreover, some compounds of the series demonstrated an antioxidant activity, higher that the known antioxidants trolox and gallic acid. PAMPA-BBB studies predicted that the novel rhein–huprine hybrids should be able to cross the blood brain barrier and reach the CNS. Among the derivates, the hybrids 11a and 11c in figure 1.7.2-**3** emerged for their interesting multi-target profile having in the meantime potent $A\beta_{1-42}$ and tau anti-aggregating activity, potent antioxidant activity and sub-micromolar hAChE or hBACE-1 inhibitory activity. The least basic hybrid 11c, that should be mostly in neutral form at physiological pH, might overcome the problem of membrane permeability and P-gp efflux liabilities before mentioned.

AchE, BchE and ROS. Starting from these findings, Munoz's research group combined the scaffolds of the cholinesterase inhibitor huprine Y and the antioxidant capsaicin (figure 1.7.2-**4**).[66] Capsaicin is the major bioactive compound in chili peppers. Clinically, it is used for pain relief. But the interest in this molecule derives also to its ability to scavenge reactive oxygen species (ROS), to increase the activity and expression of antioxidant enzymes, and to inhibit protein oxidation and lipid peroxidation, so it could be a potential antioxidant drug for AD. Studies have been already conducted to evaluate its activity *in vivo*, and capsaicin proved to enhance synaptic and cognitive functions in mice and in middle-aged and elderly people. Capsaicin acts on long-term potentiation (LTP), a cellular mechanism involved in learning and memory CA1 area of the hippocampus and reduces oxidative stress and neuroinflammation. So, the hybrid compounds could be potentially active not only in cholinergic deficit and oxidative stress, but also in neuroinflammation, synaptic dysfunction, and cognitive impairment.

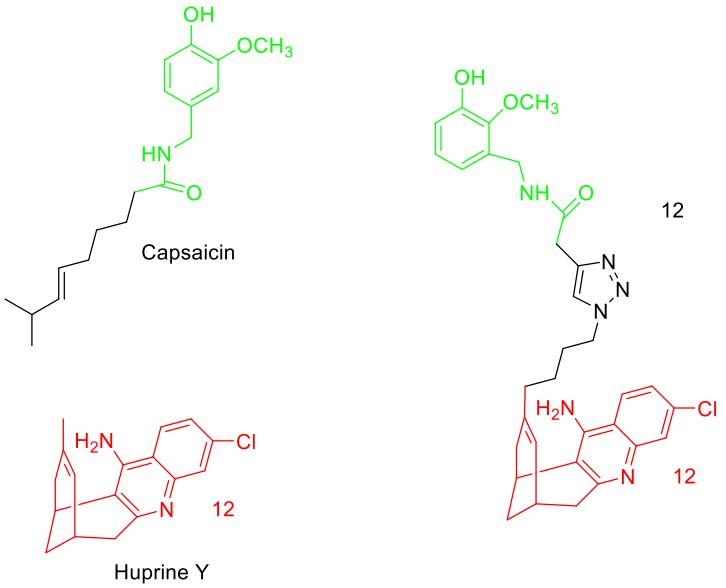

Figure *1.7.2*-**4**

Most active compound of huprine Y-Capsaicin hybrids serie (12)

HC hybrids were synthesised by introduction of various linkers (alkanamide, alkenamide, and benzamide) at position 12 of the huprine scaffold or a triazolylbutyl linker at position 9. The combination of the huprine Y and capsaicin scaffolds results in compounds that showed nanomolar potencies toward human acetylcholinesterase (AChE) and butyrylcholinesterase (BChE) and additionally they retain or improve the antioxidant properties of capsaicin. Their higher activity was investigated through the study of crystal structures of their complexes with AChE and BChE. Biodistribution studies in C57BL6 mice confirmed that they are able to cross BBB, and one of the derivatives (12) whose structure is reported in figure 1.7.2-**4** displayed better brain/plasma ratio than donepezil. After the compound administration to a 10 month-old APP/PS1 mice (2 mg/kg, i.p., 3 times per week, 4 weeks), an improvement in learning and memory was

detected by three different behavioural tests. This confirmed its ability to delay Alzheimer-like pathology progression, as suggested by a significantly reduced $A\beta_{1-42}/A\beta_{1-40}$ ratio in the hippocampus, improved basal synaptic efficacy, and significantly reduced hippocampal oxidative stress and neuroinflammation. It emerged as an interesting anti-Alzheimer lead compound with beneficial effects on cognitive symptoms and on some underlying disease mechanisms.[66]

AchE, BchE, NMDA receptors. Following the idea of designing MTDLs starting from the scaffold of known AChE inhibitors, the same research group synthetized a new series of hybrid compounds obtained by the combination of 6-chlorotacrine with fluorobenzohomoadamantanamine, that is a known NMDA receptor antagonist, using as linkers 4- and 5-carbon-atom ether chain attached at the bridge head amino group or at an additional amino group on the benzene ring of the benzohomoadamantane core (figure 1.7.2-**5**).

The effect of the different linkage position was evident in hBChE inhibition, but didn't have a clear effect on hAChE inhibition and NMDA antagonism. The best hybrids exhibit higher potencies than parent compounds against AChE (IC_{50} 0.33 nM in the best case, 44-fold increased potency over 6-chlorotacrine), butyrylcholinesterase (IC_{50} 21 nM in the best case, 24-fold increased potency over 6-chlorotacrine), and NMDA receptors (IC_{50} 0.89 μM in the best case, 2-fold increased potency over the parent benzohomoadamantanamine and memantine), which suggests an additive effect of both pharmacophoric moieties in the interaction with the primary targets. Moreover, most of these compounds have been predicted to be brain permeable. For these reason they resulted promising lead compounds that could be improved in view of future MTDLs for AD tretament.[67]

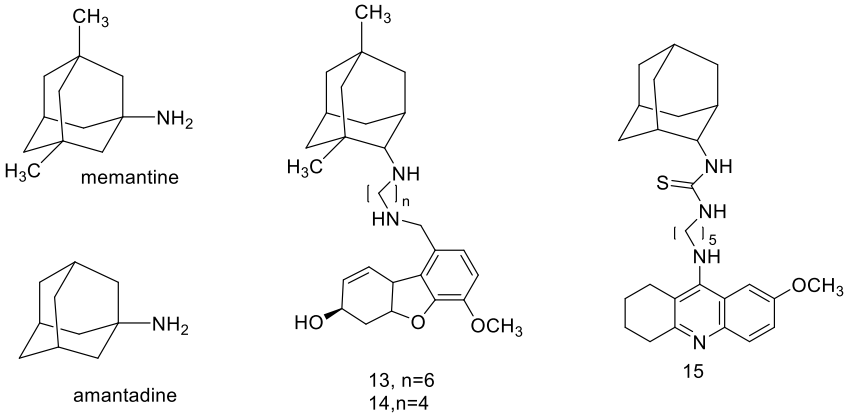

Figure *1.7.2*-**5** Structure of memantine, amantadine, and derivatives with dual activity on NMDA receptors and on AChE [67]

1.7.3 Carbon Monoxide-Releasing Molecules (CORMs) as Potential Aϐ-Antiaggregating Compounds with Neuroprotective Activity

Microglia mediate the brain's innate immune response and are involved in phagocytosis and in the elimination of debris, pathogens and toxins. The correlation between their dysfunction and the increased Aβ accumulation are universally recognized for AD patients. The microglia secrete both pro and anti-inflammatory factors, which can be both beneficial and harmful in neurodegenerative diseases. There is extensive literature that shows inflammation is involved into AD progression, promoting Aβ deposition, neuronal loss, and cognitive deficits. Brains of AD patients and those of mouse models of Aβ pathology uniformly show high expression of pro-inflammatory cytokines and chemokines including TNFα, IFNγ, IL-1β and IL-6.[68] IL-1β and TNFα can impair neuronal function by suppressing long-term enhancement of synaptic transmission (LTP).[69] Multiple interactions as well as high expression of additional cytokines / chemokines and innate immune receptors lead to a state of pro-inflammatory activation in AD. Heme oxygenase-1 (HO-1) is an inducible enzyme known for its anti-inflammatory, antioxidant and neuroprotective effects. Heme oxygenases (HOs), are enzymes responsible for the heme degradation in to biliverdin / bilirubin, free iron and CO. In the normal brain, HO-2 expression is constitutive, abundant, and quite ubiquitous, while HO-1 mRNA and protein are confined to small populations of scattered neurons and neuroglia. In contrast to HO-2, the HO-1 gene (Hmox1) is particularly sensitive to induction by a wide range of pro-oxidants and other stressors. In Alzheimer's disease and mild cognitive impairment, the immunoreactive HO-1 protein is overexpressed in neurons and astrocytes of the cerebral cortex and hippocampus compared to cognitively intact, age-co-located controls and co-localized in senile plaques, neurofibrillary tangles and amylaceous bodies.[70]

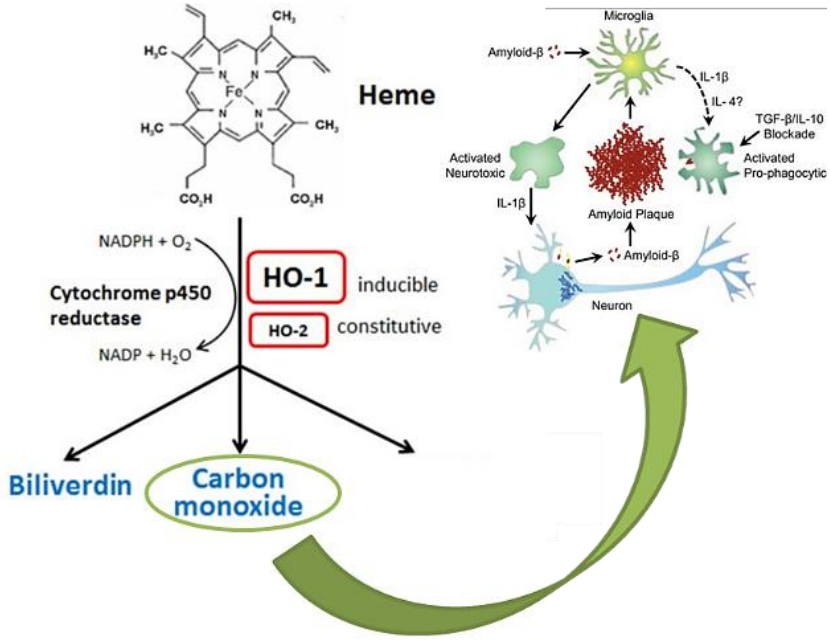

Figure *1.7.3*-**1** Heme oxygenase-1 protects against Alzheimer's amyloid-β1-42-induced toxicity via carbon monoxide production

For this reason, HO-1 overexpression seems clearly a neuroprotective response. It seems that carbon monoxide (CO), produced from heme degradation, has a physiological signal role and affects various systems, including the neuronal one.[71] CO exerts anti-apoptotic, anti-inflammatory, and antioxidant effects, being able to maintain cellular and tissue homeostasis.[72] There is a number of evidences demonstrating the beneficial effects of CO in a range of diseases and among others in neurodegeneration.[71 72 73 74 75 76]

The interesting endogenous properties of CO, but at the same time the impossibility of its administration as such gas for its toxicity, lead Motterlini and collaborators to introduce the concept of CO- released molecules (CORMs), in which CO is chemically bound in a prodrug.[77] Numerous organic compounds were initially explored for their potential as CORMs, including haloalkanes, aldehydes, oxalates and silacarboxylic acids[78] but their CO release rate and the toxicological profile were not favourable to justify further development. Consequently, thanks to the fact that CO is able to bind in a strong but modifiable way the transition metal centres, mostly of CORMs research was focused on metal carbonyl complexes. Only recently, two organic systems have been introduced on unsaturated cyclic 1,2-diketones and xanthene-9-carboxylic acid as the first truly viable simply organic CORMs.[79 80]

However, transition metal-based CORMs still offer the most flexibility in terms of molecular design and they are widely investigated. In fact, by proper selection of the metal centre, the number and spatial arrangement of CO ligands around it, and the nature of the ligands in the coordination sphere of the metal, it is possible to regulate the release properties of CO. Consequently, this "internal" part of the molecule has been called the “CORM sphere” or the “coordination sphere” by Romao et al.[81] The key parameters are the number of CO molecules that can be released from the coordination sphere of the metal, the kinetics of the CO release process and the trigger mechanism required to initiate CO release. Currently, there is no consensus if either a high or a low number of CO ligands per unit of metal complexes would be more desirable and whether CO release would be slow or fast. Monocarbonyl compounds obviously have the simplest release kinetics, while in the case of more than one labile CO present per molecular unit, that could be released consecutively at a different rate, makes the kinetic analysis and identification of potential intermediates very more difficult. Furthermore, it is unclear whether a low but steady release of CO from CORMs would be more beneficial, or rather a rapid release of CO released. In addition to the CORM sphere, which can be adjusted to control the CO release, it is possible to change the periphery of the CO ligand, the so called “outer part”. This is particularly important and it determines the most significant advantages of CORMs over simple CO gas, as it provides the appropriate CORM pharmacokinetic parameters and the ability of targeting specific tissues.[82]

The first CORMs were based on Fe and Mn complex and needed UV activation.[77] Then the most studies today are ruthenium derivatives as CORM-2 ($[Ru(CO)_3Cl_2]_2$) and CORM-3 ($[RuCl(glycinato)(CO)_3]$), they are soluble in H_20 and releases CO in physical conditions, however, with still a fast and non-specific releasing. But in this way compounds for which CO release starts as soon as they are dissolved in the medium, could address only limited targets in base of their half-lives in the circulation after i.v. injection. Recent works are

therefore aimed at developing CORM prodrugs that are stable in serum and only get triggered in the targeted tissue by a very specific stimulus.[82]A CO release quantity control was possible through the use of enzyme input,[83 84 85 86 87 88] a change in pH or through photoinduction. [86 88]

By the way, CORMs today are classified in three main groups: in the first one the CO release starts after ligand reaction with medium, the second group needs an internal or external stimulus, the third release CO subsequently to an environment change, such as an enzymatic expression or pH.[71] In 2008, the so called "photo-CORMs" that released CO under specific conditions of photo excitation received particular interest from the scientific community, in this case the CO releasing time was controlled by selecting a specific activation wavelength. But they found little *in vivo* application limited to the surface of the body or to sites of the body close to the surface. A more promising generation of CORMs was the one based on the activation by wavelengths between the visible and near infrared, however from other studies emerged that the photoreaction did not lead to the release of CO. In conclusion, the advantage of this class of compounds consisted in the discovery of a scaffold that provided good optical properties and aqueous solubility that could be exploited.

CORMs-protein interactions. To understand the biological properties of CORMs, their interaction with biological targets was characterized in order to define both the metal binding site and which part of the original ligands remains even after the adduct formation. The way in which CORMs bind to proteins, plays a key role in its activation, transport and excretion *in vivo*. Some studies have already been done on protein-CORMs adduct, but there is still limited knowledge concerning how CORMs are able to recognize the protein and the mechanism of CO release. Crystallographic studies on protein-CORMs adduct (using HEWL, lysozyme of egg white, as model protein and CORM3, complex with Ru) showed that the Ru complex could bind to the surface of His15 residues and aspartic residues (Asp18 / Asp52 / Asp101 / Asp113) with consequent release of chloride ion, glycinate ion and CO ligand. The rapid formation of the adducts between the protein and the remaining Cis-Ru$(CO)_2$ fragments was monitored applying various methodologies (LC-MS / IR / X-ray crystallography). Three coordination bonds between CORM-3 and the protein were observed. In particular, the site most occupied by Ru shows the following structure: (His15)Ru$(CO)_2(H_2O)_3$.[89]

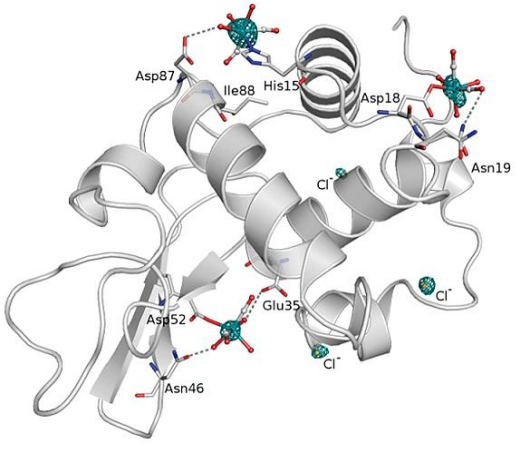

Figure *1.7.3*-**2** Overall structure of HEWL bound to three CORM-3 moieties [89]

In addition, recently, a structural characterization of the adducts between CORM based on Ir ($CsIrCl_5CO$) and Hen Egg-White Lysozyme (HEWL) was also performed. During this study, six different binding sites were identified (His15, Ser24, Asn27, Val120, Asn65, Pro79, Asp18, Asn59, Trp62, Trp63, Ala107, Asn46; Thr 47), thus suggesting multiple binding sites on the surface of the protein for the compounds based on Ir, even if His15 is the primary bond. In the N-terminal amide bond it has been seen that in the first six days neither Cl or CO is lost; it has been disclosed that after 9 days the compounds leave the surface of the protein except than in the first binding site, where the realising of CO occurs after 30 days and it is replaced by a molecule of H_2O. Therefore, in the adduct HEWL- [$IrCl_4CO$ (H_2O)] the CO release process seems associated with a loss of interaction of the molecule on the surface of the protein supporting the idea that CO in these compounds has an important role in the recognition of the ligand protein. These findings are supported by the studies of the X-ray structure in which it has seen that $(IrCl_6)^{3-}$ moiety - binds HEWL on a different site than [$IrCl_4CO(H_2O)$]. Furthermore, it has been found that adducts can be formed through both covalent and non-covalent interactions. This could be an advantage for its clinical use, as it could be exploited to regulate the release of CO. The covalent bonds ensure the stability of the complex and could help the slow release of CO and then only after detachment from the protein, while the non-covalent bonds are more labile and could give the fast release of CO. Therefore, in this way the adducts could release CO in different ways and with different times. In addition, the importance of hydrogen bonds is also evident in obtaining a good bonding affinity between small compounds and pharmacological targets (CORM-residue His interaction).[90]

Continuing the investigation of the interactions between protein and CORMs, studies of the compound ($CsIrCl_5CO$) were also carried out with another protein model, RNase A (bovine pancreatic ribonuclease) using different methods: MS, NMR, X-ray crystallography and circular dichroism. MS allowed to investigate the reactivity of the compound with the model protein. Comparing the spectrum of RNA alone with one obtained after its incubation with $CsIrCl_5CO$, it was possible to detected new peaks due to the adducts between RNAse and fragments $(IrCl_4CO)^-$ / $IrCl_3(H_2O)CO$. This confirmed that more than one fragment can bind the protein. Furthermore, observing the peaks it was evident that CO was retained in the protein binding while Cl^- was released. NMR analysis of CORM-proteins binding verified that CO was bound to the metal core and was not release before two weeks. Furthermore, from the study interaction between $IrCl_5CO^{2-}$ and RNAse A was observed that the binding not only occurs with the histidine residues His12, His, 105, His119 (already known in the binding with other structures) but also with N-terminal amine and Met, never found before. (Sulfide-containing ligands are also often sites for strong bonding to transition metals.) It was also deduced that the formation of the adducts does not significantly affect the structure of the enzyme and the adducts remain stable under the experimental conditions of analysis. In addition, the adduct retains a significant amount of CO for at least 2 months, further confirmation of the fact that the formation of the complex between protein and CORM can be used to modulate the release kinetics of CO.

The binding instead with terminal amine and side chain Met can help to understand the interactions of the Ir compound with biomolecules; it can also be used in the drug design phase. In the "drug design" of CORMs, a series of aspects have to be considered: the main problems are solubility, stability in air and in water,

biocompatibility. Thus, the research is dealing with the effort to find new strategies to overcome the problem of metallic portion toxicity that remains after CO release and to achieve suitable pharmacokinetic parameters. After the optimization of ADME parameters (absorption, distribution, metabolism, excretion), this class of molecules have to be able to reach the right site of action in the body where they can release CO.[91]

The CORMs metabolic destiny after CO realising is not well explored, what is known is that some of them enter cells and here they combine with proteins and cytochromes. Therefore, some other aspects have to be more deeply investigated such as the time in with CO is realised, the toxicity of CORMs at cell level and in animal models, above all the tissue distribution and the consequent effects of metals in kidneys and liver.

What has been noted is that the Ru complexes have very low anti-proliferative activity, therefore low cytotoxicity, while those with Cr and W have a higher toxicity.[92] They have shown do not accumulate in tissues and organs although liver, kidneys and blood are the major storage sites.

However, now various problems avoid that CORMS could be effectively used in therapy. First of all the structure of their metabolites have to be confirmed, and a suitable pharmacological form has to be developed. Moreover, biodistribution seems that is highly dependent on the side substituents of the chain which also influence the release of CO and cytotoxicity. This could therefore be the basis for optimizing future CO complexes. They also have to be enhanced in terms of bioavailability, since they have difficulties to cross the BBB. CORMs in which cobalt is involved in the complex, are promising; they have shown to have low animal toxicity, they do not accumulate but are excreted in the urine (despite the fact that repeated administration damages the liver and kidneys).[9394]

CORMs neuroprotective activity in Aβ-induced toxicity. Accordingly, starting from the evidence of HO-1 remarkably up-regulated in AD patients, in a recent study Hettiarachchi et al. investigated if HO-1 or its product CO, can provide protection against A*β*-induced toxicity in the human neuroblastoma SH-SY5Y cells and in rat primary hippocampal neurones, and whether this involves regulation of K^+ channels. Several lines of evidence suggest that HO-1 provided neuroprotection, reducing the toxic effects of Aβ: thus, chemical induction of HO-1 with protoporphyrins or over-expression of HO-1 reduced the toxic actions of Aβ.[95] Furthermore, protection was provided by hypoxic induction of HO-1, hypoxic treatment can alter the expression of many proteins. The study of Hettiarachchi also indicated that HO-1 protective effect is linked to its ability to generate CO. Hence, although HO-1 activity was not assessed directly (e.g. via measurement of CO or bilirubin production) CORM-2 (but not the inactive form, iCORM) mimicked the effects of HO-1 induction to provide protection against Aβ toxicity. Furthermore biliverdin, that is another HO-1 product, was found without protective effect. Moreover, they show that the activity did not arise from inhibition of apoptosis-associated K^+ efflux, but rather by inhibition of AMPK activation.[95]

1.8 Advanced Analytical Methodologies in Alzheimer's Disease Drug Discovery

Pharmaceutical analysis considerably contributed to AD drug discovery process providing suitable tools and methods to identify AD biomarkers, to assess key parameters of candidate molecules, and to investigate the absorption, distribution, metabolism, excretion and toxicity (ADMET) of drugs in pre-clinical and clinical studies, and to further monitor drugs during the quality control and validation process.[96]

Interesting, in the last few years, advanced analytical methodologies have been increasingly applied at various stages of early drug discovery with applications both in simple *in vitro* assays on single molecules and to complex biological samples analysis. Some of these advanced methodologies exploit the miniaturization, and automated high-throughput screening (HTS) were developed allowing a fast hit identification. Furthermore, these techniques grant the reliable and quickly positive hits determination and the rapid definition of SARs, that is a crucial point to optimize lead structures in terms of activity and bioavailability. The technological improvements in separation sciences, the onset of soft-impact mass spectrometry (MS) methods and the increasing use of bio- physical tools for molecular recognition studies, such as surface plasmon resonance (SPR) allow the characterization in terms of the mechanism of action of new drug candidates. Some of these new approaches investigate the mechanisms involved in molecular recognition processes by examining the structure and folding of the target proteins and monitoring structural and morphological changes upon binding with ligands.

With reference to this, spectroscopic techniques are usually applied to study aggregation kinetics parameters of amyloid aggregation forms (Turbidity, Thioflavin T and Congo Red assay, Fluorescence microscopy) and to quantify them by immunology-based method (Sandwich ELISAs). Electron microscopy (EM) is the technique chosen to study plaque morphology and to obtain structural information on Aβ fibrils; atomic force microscopy (AFM) can be used to visualize $A\beta_{40}$ and $A\beta_{42}$ in different aggregation states, such as sub-fibrillar assemblies, and protofibrils.[97 98 99]

Fourier transform infrared (FTIR) spectroscopy is one of the oldest and well-established experimental techniques for the analysis of secondary structure of polypeptides and proteins because is non-destructive, it requires less sample preparation, and can be used under a wide variety of conditions. FTIR spectroscopy is based on the measurement of wavelength and intensity of the absorption of IR radiation by a sample. The IR spectral data of high polymers are usually interpreted in terms of the vibrations of a structural repeat unit. The polypeptide and protein repeat units give rise to nine characteristic IR absorption bands, namely, amide A, B, and I−VII. Of these, the amide I and II bands are the two most prominent vibrational bands of the protein backbone.[100] The most sensitive spectral region to the protein secondary structural components is the amide I band (1700−1600 cm−1), which is due almost entirely to the C=O stretch vibrations of the peptide linkages (approximately 80%). The frequencies of the amide I band components are found to be closely correlated to the secondary structural element of the proteins. The amide II band, in contrast, derives mainly from in-plane NH bending (40−60% of the potential energy) and from the CN stretching vibration (18−40%), showing much less protein conformational sensitivity than its amide I counterpart. So, amide bonds display distinct IR signals

depending on the different folding of proteins and peptides. Consequently, FTIR spectroscopy has been applied to investigate the mechanism of action of some anti-aggregating molecules. The transition from unordered to β-sheet structure is related to an increase in absorption at 1628 cm^{-1}. A maximum absorbance at 1518 cm^{-1} is detected for the $A\beta_{25-35}$ aggregates, whereas for the treated peptide a shift in the maximum absorbance at 1550 cm^{-1} is detected. The Fourier Transform Infrared (FTIR) spectroscopic analysis allowed to validate the results firstly obtained in vitro using Thioflavin T assay regarding fibril formation inhibition by extracts of marine seaweed Padina gymnospora (ACTPG). Additionally, FTIR spectroscopic analysis was used to investigate the conformational changes in the aggregated and non-aggregated Aβ in the presence of another alga, the Gelidiella Acerosa.[100 101]

Among the other spectroscopic analytical methods, fluorescence correlation spectroscopy (FCS) it has been used for the determination of the protein aggregation and even the soluble oligomeric states of misfolded proteins could be detected. FCS measures the fluctuations in fluorescence intensity caused by the passage of fluorescent molecules through a detection volume in solution and living cell. Indeed, the diffusion depends by the volume/size of the analyte, that changes in base of the aggregation rate. So, this method has been exploited to screen potential AD anti-aggregating compound as in the studies of Hossain and Stark in which the activity of a natural compound from Centella asiatica and a peptidomimetic derivative, respectively, were characterized toward $A\beta_{1-42}$.[102 103]

Interesting, UV resonance Raman (UV-RR) spectroscopy, was exploited to investigate the tau fibrillization process which is characterized by two different stages: the first one that involves the formation of non fibrillar, dye-negative "pre-tangles", and the second stage where mature, dye-positive neurofibrillary tangles are formed. The advantage of UV-RR spectroscopy in comparison to other techniques (ThT fluorescence assays or light scattering-based methods) is that allows the monitoring of fibrils formation in both stages, because the position and the intensities of the amide Raman bands changes in correspondence of the stages of the fibril formation process. In particular, the spectral changes for the Am III3 (the most sensitive frequency of the Am III region) and Am I amide bands give the opportunity of monitoring the aggregation process. For instance, Am III3 bands in the 1240–1279 cm^{-1} region can be assigned to disordered structures, while bands in the 1220–1230 cm^{-1} region can be ascribed to β-sheets. Hence, the change in band position from 1238 cm^{-1} to 1230 cm^{-1} is typically observed upon transition from unordered to β-sheet structures. For the Am I band, a change from 1681 cm^{-1} (monomer in the absence of heparin) to 1670 cm^{-1} (aggregated fibrillar process) occurs during tau fibril formation. That is important for understanding the structural events that occur during the aggregation of tau and give the opportunity of designing and selecting new and specific aggregation inhibitors.[104]

In this context, CD spectroscopy in the far-UV region (260–190 nm) is the technique of choice to study the first steps of aggregation process, since is able to monitor the transition of secondary structure of amyloid monomers from random coil and α-helix to β-sheet before aggregation into soluble oligomers. In particular, the different secondary structures show distinctive CD signatures: disordered proteins are characterized by a negative CD peak at around 200 nm with a broad negative shoulder at longer wavelengths, while β- strands

show a negative CD peak with maximum intensity at 215 nm followed by a positive peak below 200 nm. Therefore CD often provides important information that are not directly available from more conventional spectroscopic techniques, such as fluorescence and absorbance.[105] [106] In the study of new potential drugs able to contrast these processes, CD allows to investigate the effect of ligand binding on the secondary structure of Aβ and tau. These assays are performed by incubating the protein in the absence and in the presence of ligands at single or multiple concentrations. The effect of ligand binding on misfolding can then be determined at a single time after the conformational transition of the isolated protein has taken place, or its change can be evaluated at different times after sample preparation. After CD analysis, the relative contribution of disordered and β-strand structures can be derived using one of the available algorithms for secondary structure estimations (s.s.e.), such as CONTIN or BeStSel.[107] [108] Alternatively, the conformational transition can be described by the evolution of the CD signal at a single wavelength (usually at the maximum of the negative CD peak for β-strands) as a function of time or concentration of ligand. Andrisano research group optimized a reliable and reproducible in-solution assay based on circular dichroism (CD) spectroscopy to perform CD kinetic study in which $A\beta_{1-42}$ initial secondary-structure transition were monitored in the presence of known inhibitors. It was possible collect some very preliminary information about the structural requirements for binding to non amyloidogenic or β-sheet amyloid secondary structure for the development of potent antiaggregating agents and some the molecular events involved in amyloid β (Aβ) aggregation were revealed.[109]

However, oligomers detection is challenging because of their heterogeneity, transient nature and the numbers of their species. The most mentioned biophysical techniques lack the sensitivity and the resolution for their detection and characterization. Recently, a great contribution to the fine characterization of Aβ soluble oligomers and to the assessment of the early-stage mechanism of Aβ aggregation has been offered by the combination of ion mobility and mass spectrometry (IM–MS).[110] [111] [112] [113] IMS-MS can directly sample solution oligomer distributions and size-selected oligomer structures because these vary in m/z and in shape.

But Aβ soluble forms are separated not only based on their m/z value, but also on their mobility through a buffer gas on a millisecond timescale. Depending on the time necessary to pass through the buffer gas in the ion mobility spectrometer, different Aβ oligomers are characterized by different arrival time distributions (ATD). The great advantage of IMS is the possibility to analyse in the same moment various conformational states of Aβ oligomers, this allows to investigate of the potential anti-aggregation mechanism of new molecules.

Moreover the complementary biophysical techniques previously described such as CD and FT-IR, give others details concerning changes in Aβ conformation with the concomitant appearance or disappearance of different oligomeric conformational state during the time.[114] Nowadays many studies are reported in literature in which IM–MS has been applied to investigate new potential anti-Aβ compounds.[115] [116] [117] [118] [119] [103] But mass spectrometry is an important tool of AD investigation also from a diagnostic point of view.[120] Regarding biomarkers used that have to be detected by MS, it seems that Aβ levels in CSF as well as in other biological fluids must occur during disease progression, but it's difficult to confirm this hypothesis through a lab

experiment, because data experiment could be not reliable due the fact that the peptide is difficult to be handle and many factors could invalidate the results: storing conditions, freeze-thaw cycles, standard preparation protocol. The use of CSF $A\beta_{1-42}$ alone or in combination with total tau and phosphorylated tau protein seems to be one of the few biochemical analysis capable to discriminate AD compared with healthy controls. Many methods are currently available to purify/concentrate the Aβ peptides (solid phase extraction (SPE), immunoprecipitation (IP), size exclusion, ultrafiltration and liquid-liquid extraction, immunodepletion, etc.) and the choice depends on the type of analysis. Therefore, it's crucial to carry out preliminary *in vitro* experiments before the real analysis of the biologic samples. Such *in vitro* experiments should mimic the conditions likely to occur *in vivo* (oxidative/nitrosative stress, presence of reactive species, and/or small binding molecules) and are also necessary to properly set up the correct selected reaction monitoring (SRM) or multiple reaction monitoring (MRM) transitions for the quantitative determinations. Assessing the "kind" of Aβ species might be more important than quantifying them. In fact, it seems that plasma Aβ levels reflect peripheral Aβ generation and this is not connected with AD. On the contrary, total tau levels in plasma have been found significantly associated with AD. Moreover, finding an inter-laboratory experimental MS protocol that can assess Aβ levels in a reproducible and reliable way is a very challenging task, due to a much higher presence of contaminants than in the case of CSF. High resolution/accurate mass (HR/AM) analysis is a promising alternative approach to distinguish Aβ peptides from interferences. HR/AM also allowed the development of data independent acquisition (DIA), an MS approach which combines the sequential isolation of a large precursor window with full production spectrum acquisition. MS experiments for proteomic studies on human brain samples post-mortem, are used to elucidate the biomolecular mechanisms involved in AD, with the aim to identify new therapeutic strategies. Two main kinds of MS investigations on AD brain tissue are carried out: (i) MS proteomics studies aimed to identify and/or quantify Aβ peptides as well as other proteins involved with the disease ; (ii) MS imaging studies aimed to obtain Aβ peptides and/or fibril distribution in the various brain regions. In this way, the main isoforms of Aβ in AD brains have been identified, and it was possible to discern between controls and AD patients by comparing specific areas of the brain, the hippocampus, and the cerebellum.[120 121] The experimental method mostly used to analyse molecules directly from brain tissues without any sample pre-treatment apart from matrix deposition is matrix-assisted laser desorption/ionization-imaging MS (MALDI-IMS). MALDI-IMS offers several advantages over other analytical techniques: (i) it does not require homogenization of the brain prior to sample preparation; (ii) possibility to have molecular maps of the different brain areas; (iii)wide range of detectable analytes; ie, not only Aβ peptides, but also lipids, drugs, and metabolites; (iv) label-free; and (v) good lateral resolution (50-200 μm).[122] Other MS approaches have been also used to monitor and determined where Aβ peptides are located in brains, among these the time-of-flight secondary ion mass spectrometry (ToF-SIMS), which can detect small fragments with a spatial resolution down to ~50 nm, and laser ablation inductively coupled plasma mass spectrometry (LA-ICP-MS) and/or nano-secondary ion mass spectrometry (Nano-SIMS).

Then as regards analytical methodologies developed for the screening of potential inhibitors toward the most important AD targets, they are based on spectroscopic measurements. Among these, it is possible to mention

the ultraviolet-visible (UV–vis)-based Ellman's assay for the screening of cholinesterase inhibitors and the assays based on the use of fluorescent dyes such as thioflavin T (ThT) used to identify new active Aβ or tau anti-aggregating molecules.[123] [124] Moreover, due to the urgency of new and more efficient methods able to overcome the radiometric assays, classical assays turned into new spectroscopic methods.

Many fluorescence-based assays were developed adopting the fluorescence resonance energy transfer (FRET) principle, that assumes the energy transfer between a donor and an acceptor when they are in the resonance state. This phenomenon occurs if donor and acceptor groups are in a certain distance. FRET can be applied in a wide range of studies, from the detection of conformational changes for macromolecules to the investigation of ligand-target binding.[125] [126] [127] [128] [129]

Moreover, many in-solution methods for the *in vitro* characterization of BACE1 inhibitors were developed exploiting the FRET principle. For this purpose, synthetic peptides, based on the sequence of the Swedish mutation of the amyloid precursor protein (APP) and bearing a fluorophore (donor group) and a quencher (acceptor group), were used as substrates. When the two groups are positioned within the Förster radius of each other (which is about 3–6 nm and is defined as the distance at which half the excitation energy of the donor is transferred to the acceptor) and the substrate is non-cleaved, the fluorescence of the donor is quenched by the adjacent acceptor so the emission spectrum of the donor well overlaps to the absorption spectrum of the acceptor. But just as, the peptide chain is cleaved by BACE1, the donor-specific fluorescence is no longer quenched and it can be measured.[130] These substrates were adopted furthermore for on-line methods based on the use of immobilized enzyme reactors (IMERs) containing BACE1. These techniques require lower amount of enzyme and substrate than in-solution methods.[131] [132] [133] Moreover, the good reproducibility of results obtained for the evaluation of the inhibitory activity of well-known inhibitors makes this assay suitable for the HTS of BACE1 inhibitors.[134] In 2018, an inkjet printing-based fluorescence assay for high throughput screening of β-secretase inhibitors was developed employing a BACE-1 FRET substrate (Rh-Glu-Val-Asn-Leu-Asp-Ala-Glu-Phe-Lys-Quencher) and validated using known BACE-1 inhibitors. Both the rhodamine-based substrate and the enzyme were printed on parchment paper in same spot. The inhibition was detected by monitoring the fluorescence pro- file obtained by maintaining the substrate concentration constant and by increasing the amount of inhibitor. The good reproducibility of results obtained for the evaluation of the inhibitory activity of well-known inhibitors makes this assay suitable for the HTS of BACE1 inhibitors.[134]

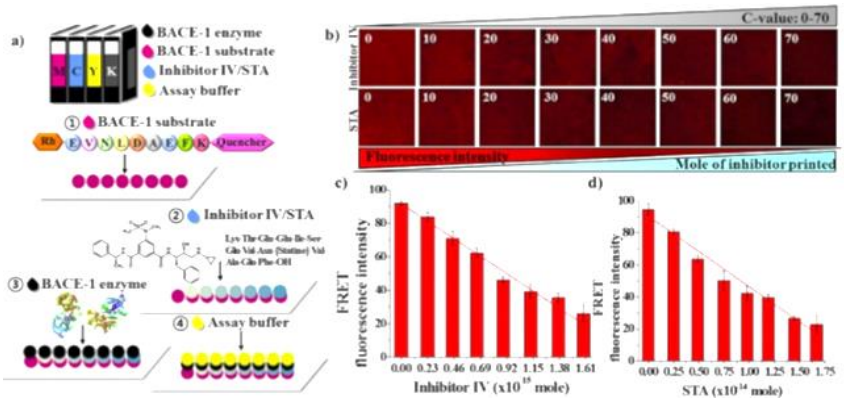

Figure *1.8.2*-**1** Detection of BACE1 inhibitory activities of inhibitor IV and STA using inkjet printing: a) printing order of ink solutions to perform the inhibition assay; b) images of fluorescence produced after the cleavage of FRETpeptide by BACE-1 obtained with different amount of inhibitor printed; quantitative plot of the reduction of fluorescence intensity obtained on the reaction spot for c) Inhibitor IV and d) STA. Fluorescence intensity was measured at Ex/ Em 545 nm/585 nm using a confocal microscope[96]

In the same year Xingguo Chen research group proposed a sensing platform as novel strategy for the BACE1 assay useful also as potential tool for screening drugs. This sensitive fluorescence biosensing platform was based on the interaction between a WS2 nanosheet and a peptide sequence. In the absence of BACE1, a FAM-labeled peptide substrate could be adsorbed on the surface of the WS2 nanosheet, thereby quenching its fluorescence. However, in the presence of BACE1, the hydrolysis of the peptide substrate by BACE1 triggers could occur with the subsequent release of short FAM-linked peptide fragments which could not be adsorbed on the surface of the WS2 nanosheet. This resulted in weak fluorescence quenching, thus restoring the fluorescence signal. By measuring the change in the fluorescence of the FAM-labelled peptide substrate, the fluorescence sensing platform based on the WS2 nanosheet could monitor BACE1.[135]

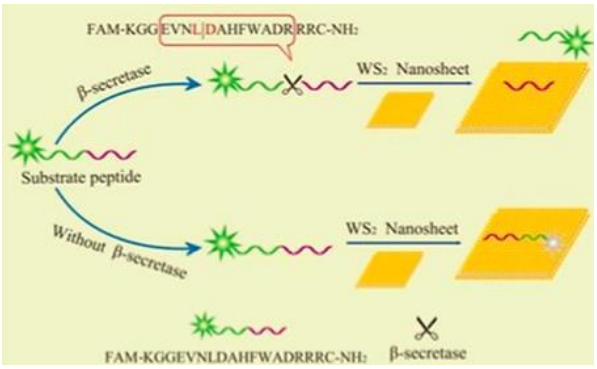

Figure *1.8.2*-**2** WS2 nanosheet-based sensing platform for fluorescent analysis of BACE1 [96]

Additionally, new fluorescence based assays, such as a novel luminescence turn-on assay has been recently developed for the detection of AChE activity. The assay, proposed by Law et al., is based on the supramolecular self-assembly of alkynyl platinum (II) complexes. This assay is founded upon the self-assembly behaviour of

Pt(II) complexes through noncovalent Pt(II) Pt(II) and π π stacking interactions. In the presence of AChE, acetylthiocholine undergoes hydrolysis to thiocholine with the consequent in situ formation of a cationic Ag(I)–thiocholine coordination polymer. The aggregation is then facilitated by the electrostatic interactions between the anionic Pt(II) complex molecules and the cationic coordination polymer, leading to a low-energy red emission turn-on.[136]

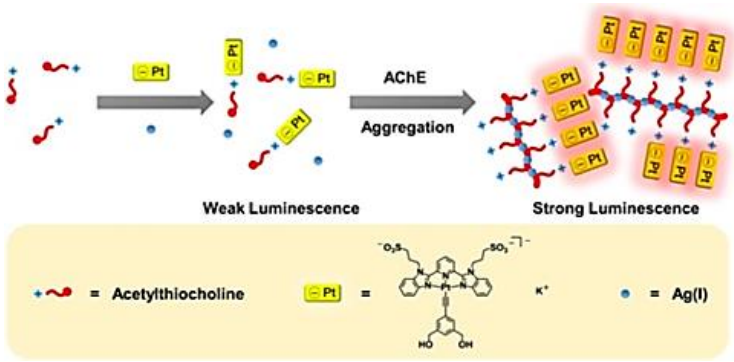

Figure *1.8.2*-**3** Rational for the luminescence Turn-On Assay for AChE using anionic alkynylplatinum(II) [96]

MS is a useful alternative technique to in-solution assays and assess target enzyme activity by monitoring the product formation: it is sensitive, is fast and it requires low amount of sample and it is a label-free method. In particular it is suitable when the substrate is a peptide and the enzymatic reaction works through covalent modification or a cleavage. For this purpose, in 2016 Kennedy group used ESI-MS to perform a label-free HTS assay to screening an 80-compound library toward Sirtuin 1 (SIRT1), which is a s a NAD+-dependent deacetylase.[137] Most of SIRT1 activating compounds (STACs) have been discovered by using a fluorescent screening but in this kind of assays there is the risk of artifact due tauto-fluorescence from test compounds or interference of the bulky fluorophores with the assay. Mass spectrometry ensures of developing the assay using at the same time less reagent and having a lower cost and it could be useful for large-scale application. In the same year, Peng et al. developed a new analytical approach for the evaluation of AChE activity and its inhibition based on the use of acetylcholine-d4 as a surrogate substrate. Another enzyme target activity evaluated by mass spectrometry was presented by De Simone et al.[138] who assayed enzyme activity and inhibition by determining the phosphorylation degree of the substrate, the glycogen synthase muscle (GSM) peptide.

In view of investigating the mechanism of new active compounds against AD, MS has been predominantly used not only to screen anti-Aβ agents but also to characterize the target protein–ligand interactions, and finally identify promising active molecules through HTS. Notwithstanding, some Aβ inhibitors are capable to covalently bind Aβ peptides, most of the tested compounds are involved in noncovalent interactions. The analysis of protein–ligand interactions is important for understanding various biological phenomena and drug development. The physico-chemical parameters that characterize protein–ligand interactions are stoichiometry

and dissociation constant (KD), from which the free energy difference of the interaction is estimated. Meanwhile, recent progress in MS under non-denaturing conditions, mainly led by Robinson's group, has enabled the measurement of total masses of protein–ligand complexes, even for non-covalent interactions Furthermore, recent hydrogen/deuterium exchange MS (HDX-MS) has realized the identification of the interaction site and conformation change of a protein upon ligand binding, providing structural information on protein–ligand interaction. This method is called MS under non-denaturing conditions or native MS and allows the unambiguous determination of protein-ligand interactions. Under a few assumptions, MS has also been applied to determine the dissociation constants for protein-ligand interactions.

Nanoelectrospray ionization mass spectrometry (nano-ESI MS) has emerged as a powerful technique for the detection and characterization of noncovalent interactions.[139] This technique lies has an sensitivity (picomolar quantities of protein and ligand required), speed (as low as 30 s for each analysis), and ability to simultaneously determine binding stoichiometry and dissociation constant and so it could be exploited in fragment-based drug discovery (FBDD) .

Three main mass spectrometry (MS)-based strategies have been used for the targeted and untargeted identification of protein covalent adducts: i) "bottom-up" strategies, involving protein digestion (mainly with trypsin) to peptides followed by MS analysis; ii) protease digestion or acid hydrolysis of proteins to amino-acids followed by MS analysis; and iii) N-alkyl Edman degradation, involving the selective detachment of terminal adducted amino-acids, as hydantoins, upon reaction with isothiocyanates, followed by MS analysis. Nonetheless, the diversity of targets, the huge discrepancy of cellular proteins concentration and the low abundance of the modified protein when compared to the unmodified protein make the detection of protein adducts in a complex matrix a major challenge. Multiple strategies were, therefore, developed to overcome these analytical difficulties involving sample pre-treatment, MS analysis and data analysis procedure.

The covalent modifications that change the structure of proteins can be assessed by top-down and bottom-up approaches, which are often used in combination, providing complementary information. Generally, the top-down approach is at first employed for the detection of the global pattern of modifications affecting the target protein while the bottom-up one allows the identification of specific residues involved in the covalent modifications.[140 141]

In 2012, Fiori et al. in order to go more deeply into the details of Myr inhibition, employed nano-LC-ESI-QTOF, MALDI-TOF, and ESI-IT to highlight the species occurring in during the analysis of $A\beta_{1-42}$ aggregation. Kinetics study of $A\beta_{1-42}$ aggregation by ESI-IT-MS and MALDI-TOF showed, in the presence of Myr, a decreased rate of aggregation, stabilization of the monomer content, and enhanced level of an oxidized $A\beta_{1-42}$ form, which increases only in the presence of Myr and is less prone to aggregation. The $A\beta_{1-42}$ samples with and without Myr were then digested by trypsin at t = 0 and after 24 h of incubation and analyzed by nano-LC-nano-ESI-QTOF to confirm the specific aminoacids targeted involved.[141]

Taniguchi et al demonstrate that catalytic oxygenation of amyloid-β peptides (Aβ) might be an effective approach to treat AD. $A\beta_{1-42}$ was oxygenated under physiologically-relevant conditions (pH 7.4, 37 °C) using a riboflavin catalyst and visible light irradiation, with modifications at the Tyr10, His13, His14, and Met35 residues. The oxygenated $A\beta_{1-42}$ exhibited considerably lower aggregation potency and neurotoxicity compared with native Aβ. At first, MALDI-time-of-flight (MALDI-TOF) MS was exploited to monitor the yield of $A\beta_{1-42}$ oxygenation at selected times. Afterwards, the use of MS allowed the fine characterization of the structural changes induced by the oxidative reaction; indeed, MALDI-TOF analyses performed on $A\beta_{1-16}$, $A\beta_{17-28}$ and $A\beta_{29-42}$, obtained by digestion with the endo- proteinase Arg-C, showed that oxygenation affected mainly Aβ1–16. Finally, the combined use of ESI-quadrupole-time-of-flight (ESI- QTOF) LC–ESI-MS/MS analyses allowed the identification of Tyr10, His13, His14 and Met35 as the sites of the oxidative modifications.[142]

IM–MS analysis allows the preservation of non-covalent protein–ligand complexes, so that the binding interactions of small molecules to target peptides can be observed concomitantly with changes in the relative abundances and distributions of oligomeric species. Moreover, IM–MS can be used for HTS binding assays, with a rate of up to 5000 molecules per day. Ashcroft research group exploited ESI-IMS-MS as a tool for HTS for inhibitors of amyloid aggregation. This approach allowed rapid identification of protein-ligand interactions, using μL sample volumes and mg of protein, and provides information-rich data concerning the identity of the interacting species (monomer or oligomer), the nature of binding (specific, non-specific or colloidal) and the effect of the ligand on protein aggregation (monomer binding, shift in monomer conformational equilibrium, disassembly of oligomers). This method proved to be a robust tool to identify small lead compounds in AD drug discovery.[143]

1.9 Lipidomics in biomarkers research

Lipids, that are essential components in cell membranes, play multiple important roles in biological systems. The lipid bilayer makes the cell as sort of subsystem that is entirely and relatively independent from the external environment. But lipids have various biological functions, indeed they are not only involved in cellular membranes formation, but they also allow energy storage and they take part to cell signalling since numerous lipid molecular species can produce second messengers by enzymatic reactions.[144]

Accordingly, many studies have proven that alteration in lipid homeostasis can lead to various human diseases. Therefore, for discovering potential biomarkers, seems useful monitoring how of the lipid metabolites change in biological samples, after an external stimulus or in the context of pathological processes.[145]

Nowadays, lipid research is moving from the determination in biological samples of the individual lipid molecular structures to the characterization of lipid global changes in view of considering lipidome as part of the entire “biological system”. The concept of “biological system” aims to integrate genetic, transcriptomic, proteomic and metabolomic information with the intent of understanding all the molecular elements within a

cell or organism. So that starting from the information collected, network models can be designed in order to develop hypotheses and predictions about how the system will respond under certain circumstances, such as in specific disorders. Although genomics, transcriptomics and proteomics are critical to the functional integrity of the organism, its metabolites reflect the further downstream effects of gene and protein regulation and thus can provide crucial information on the biological state of the system. In this context, the attempt of lipidomics, is to assign a biological role to lipid changes identified, in order to determine a correspondence between the lipid metabolites or lipid metabolic pathways investigated and the physiological and or pathological conditions.[146]

Thus, lipidomics is a research field that is gaining growing importance[147] and it is widely applied in the study of epidemic diseases (e.g. obesity,[148] diabetes,[144] and cardiovascular disease,[149 150 151 152 153]) in cancers,[154 155] in inflammation,[156] in genetic disorders,[157] in Alzheimer's disease [158 159] and it supports drug development.[160] So that, the combination of lipid profile analysis and multivariate statistics in a lipidomic approach can help to uncover potential biomarkers, to decipher the mechanisms of in-depth lipid-mediated disease and to monitor drug response after pharmacological treatments.[147]

From the analytical point of view, the lipidomic workflow includes multiple steps and each one requires the proper selection of a specific technique. Starting with sample preparation, can potentially include (i) "sub-lipidome isolation" (purification of lipoprotein particles or extracellular vesicles from plasma/serum/urine samples or subcellular separation of the nucleus, mitochondria from tissue or cell samples) (ii) "internal standard addition" for sample normalization and for the "relative" or "absolute" quantitation (iii) sample "homogenization" in case of tissues or cell samples (iv) liquid- or solid-phase lipid "extraction", (v) "derivatization" for enhanced ionization and/or tandem mass spectrometry (MS/ MS) fragmentation (vi) "matrix addition" if mass spectrometry analysis will use MALDI source.[161] Concerning liquid-phase extraction at the moment a standard method has not been established for lipid extraction from biological samples, but alternative to the chloroform-methanol biphasic procedure proposed by Bligh & Dyer have been published.[162] Recently, Laemmerhofer's research group validated a method that adopts 2-propanol as monophasic solvent extraction, that allows at the same time protein precipitation.[163] This extraction protocol has proved to be suitable both for plasma and cell samples. In this last, lipid extraction can be improved by sonication to break cells membrane. Polar lipids are well recovered while results should be improved for apolar lipids (such as TGs, CEs) which are anyway usually highly abundant. The further positive aspect of using 2-propanol is that is compatible with typical plastic vials commonly utilized for collecting clinical samples. But if samples have a high salt content or in case of large aqueous volume of aqueous, the biphasic liquid-liquid extraction using methyl tert-butylether (MTBE)/MeOH has to be choosen.[164]

Then the crude lipid extracts could be either pre-fractionated or kept intact for further separation. Traditional strategies for lipid analysis usually separated lipids into their classes using thin layer chromatography (TLC), normal-phase liquid chromatography (NPLC) or solid phase extraction (SPE). Subsequently in each lipid classes the single molecular species were analysed by high performance liquid chromatography (HPLC)

coupled with ultraviolet or evaporative light scattering detector. The limit of those "classic" techniques was in many cases the lack of sensitivity, the use of large sample volumes and that sample preparation requires multiphase procedures. Moreover, the resolution is also low because only a limited set of individual molecular species was detected.

Alternatively, gas chromatography (GC) has been, and still is, often used for lipid analysis, but time-consuming procedures consisting in hydrolysis and derivatization are usually required since most lipids are otherwise not susceptible to GC. However, by selecting the appropriate GC-based method, it is possible to have an informative analysis about distribution of molecular compositions and physical properties and about lipid concentrations. Nowadays, GC coupled with mass spectrometry is mainly used for full comprehensive fatty acid profiling as fatty acid methyl esters (FAMEs). NMR spectroscopy has demonstrated to be a powerful technology in metabolite analysis of body fluids, cells and intact tissues. It has strong quantitative capabilities, but the sensitivity of NMR is limited compared to MS-based approaches in complex mixtures. Therefore, in lipidomics a shift from NMR to MS-based technologies is clearly observed in recent publications. Indeed, the advent of soft ionization technologies such as matrix assisted laser desorption / ionization (MALDI), electrospray ionization (ESI) and atmospheric pressure chemical ionization (APCI) for MS, possibly coupled to LC, has been the turning point in lipidomics. These methods made possible to analyse most of the lipids in the same assay and in rapid and sensitive way.

MS detection is employed either by using direct infusion of a sample or by chromatographic separation (e.g., GC or LC/UHPLC) of certain or substantial lipid fractions or whole lipid extracts to generate lipid data. In the case of direct infusion, extracts from tissue or mammalian cells are generally resuspended in methanol adding formic acid and ammonium acetate as sample modifiers, to enhance ionization in positive ($[M+ H]^+$, $[M+NH4]^+$ and negative mode $[M-H]^-$, $[M+ Ac]^-$.

In this way, lists of lipid metabolites with absolute or relative concentrations are generated from control and diseased subjects. Next, the data are normalized and subjected to statistical analysis for identifying those lipid metabolites which are discriminatory for diseases. Shotgun lipidomics by direct infusion of the lipid extract from a biological system into a high-resolution mass spectrometer such as Fourier Transform - Ion Cyclotron Resonance Mass Spectrometry (FTICR-MS) or orbitrap-MS is fast and has high-throughput capabilities. The drawback could be related to ion suppression, in-source fragmentation and assay specificity problems if the instruments has lower mass resolving power as in the case of the quadrupole time-of-flight (QTOFs)-MS. [160] In fact, what has to be taken in consideration is that lipids have many isomers, for this reason chromatographic separation prior MS detection may enhance the analysis selectivity. Many techniques have been proposed even if there are still some limits: normal-phase liquid chromatography (NPLC), hydrophilic interaction liquid chromatography (HILIC) and supercritical fluid chromatography (SFC) allow lipid class separation, but lipid species even if having distinct side chains can co-elute or they can elute in a narrow window, while reverse-phase liquid chromatography (RPLC) ensures lipid species separation with some overlaps between lipid classes.

Therefore, liquid chromatography coupled to tandem mass spectrometry has become widely accepted to investigate the metabolome and lipidome in target and untargeted approach. It is clear, that despite all the advances it is still a challenge measuring and identifying all lipids with highly diverse chemical characteristics simultaneously in various biological matrices.

Thus, the choice of the type of MS data acquisition mode plays a crucial role for lipidomics. The so called "data dependent acquisition mode" (DDA) analysis is based on an MS1 full scan experiment (over a certain predefined mass range) and this information is then used to select a small number of precursors whose MS2 spectra linked will be obtained. The drawback of this type of acquisition is that coverage is incomplete and precursor selection derives from a stochastic process that lacks reproducibility between samples because it depends on experimental conditions. Moreover, since MS2 data are not collected continuously, extracted ion chromatograms (EICs) can be obtained only on MS1 level; hence, quantitation is possible only at MS1 level. Thus, from one side limited MS2 coverage restricts identification performance and on the other one lack of fragment ion EICs limits the quantification performance of DDA.

Hence, currently "data-independent acquisition" (DIA) is the favoured one in MS-based lipidomic methods. It consists in the simultaneous comprehensive acquisition of precursor and product ions and it allow to increase the accuracy during unknown lipid identification and during the quantification of known metabolites. Thus, DIA collects MS2 data comprehensively over the entire range m/z and across all samples without dependence on information from the prior full scan (MS1) experiment. The result is a comprehensive view of the sample lipid profile. Therefore, retrospective data analysis can be repeated at later stage without restrictions once new databases will be updated without need for remeasuring samples. Several DIA varieties exist which essentially differ in their precursor isolation width: in all-ion-fragmentation (AIF or MSE) subsequent to a full scan MS experiment (MS1) over a certain mass range, an MS/MS experiment is carried out in which the MS1 (quadrupole) is tuned to all ion transmission (like in full scan) and the collision energy (CE) is more elevated as compared to the MS1 experiment. Briefly, two full scan experiments are performed, first one with low CE and the second one with high CE to fragment the precursor ions. The precursor isolation width is wide (full m/z range) which leads to co-fragmentation of all isolated precursors simultaneously. While sequential window acquisition of all theoretical mass spectra (SWATH) is carried on with the selection of consecutive pre-defined wide overlapping precursor ion windows in the first quadrupole (Q1), followed by fragmentation and simultaneous monitoring of precursors and fragments in the time-of-flight (TOF) or Orbitrap mass analysers. Q1 window widths are typically of 20-25 Da but can be adjusted to optimize specificity and cycle time, and even changed during the analysis. When the SWATH experiment is designed, it is also important that there are enough data points across the chromatographic peak (at least 10) to enable robust and precise quantification. If the chromatographic peak has about 6 s which is a common peak width of UHPLC, then the entire MS cycle (comprising both MS1 and all MS2 acquisition times together) should not take longer than 600 ms. This means that the design of the SWATH windows depends by precursor isolation SWATH windows (preferred in terms of assay selectivity) and long accumulation times (advantageous with regard to sensitivity). Typically, 20-30 SWATH windows with accumulation times of 20-30 ms are programmed per MS cycle.[165]

Finally, data processing is likewise an important part of the entire lipidomic workflow, to obtain useful information from the acquired data. Generally, two distinct strategies can be applied: one is based on the open-source software MS-DIAL, the other one on targeted feature extraction of well-known lipids or lipids listed in databases.[166] MS-DIAL is a software that can deal with DIA data. Data processing involves the steps of peak finding, deisotoping, adduct assignment, back-ground subtraction, feature alignment, and normalization with-user defined settings. It also offers solutions to some problematic issues of DIA, as the presence of contaminating ions in the MS2 spectra of coeluted lipids which are co-isolated in the same SWATH window for fragmentation due to similar m/z and wider precursor isolation window. As discussed above, the link between precursor and fragment ions is lost in DIA acquisition modes such as AIF and SWATH. Both problems can be resolved by a mathematical spectral deconvolution process. The de-convoluted MS2 spectra can be matched against database spectra, such as LipidBlast (an in silico spectral library). The structural annotation (identification) is supported by a scoring system based on retention time similarity (with calculated tR-values from a prediction tool), MS1 (mass accuracy) similarity, isotope similarity, MS2 similarity (calculated as dot product, reversed dot product and fragment presence). The process is fully automated and allows large scale lipid annotation. A certain number of failed deconvolutions and mis-annotations will unfortunately occur, in particular of low abundant lipids, and hence manual curation is still required.

For the case in which lipids are well known, the approach can be found in databases (e.g.Lipidmaps). So, a peak list is used to extract features from the untargeted data file (e.g. using vendor software like MasterView, LipidView or others). In case of SWATH data, this can be done on MS1 and MS2 level. A specific set of precursor and fragment ions for each lipid class are selected and m/z values can be calculated or extracted from LipidBlast database. With the list of m/z values EICs can be extracted from TOF-MS and SWATH-MS/MS experiments in positive and negative ion mode (Fig. 6c). The signals without interferences are then selected for quantitative analysis.

In the last years, many significant efforts have been made to promote research activities in this new-emerging field of lipidomics. For example, the “Lipidomics Expertise Platform” supported by the EU was initiated in 2005 and offers an online resource (http://www.lipidomics-expertise.de), which gathers information on institutions involved in lipidomics and includes databases for lipidomics expertise, lipid standards and methods. Other important websites comprising a wealth of information on lipids, their structures and related technologies are the LIPID MAPS (http://www.lipidmaps.org), LIPID BANK (http://lipidbank.jp), Lipid Data Bank (http://www.caffreylabs.ul.ie), Kyoto Encyclopedia of Genes and Genomes (KEGG) (http://www.genome.jp/kegg/), European Federation for the Science and Technology of Lipids (http://www.eurofedlipid.org), CyberlipidCenter (http://www.cyberlipid.org) and the Lipid Library (http://www.lipidlibrary.co.uk).[161]

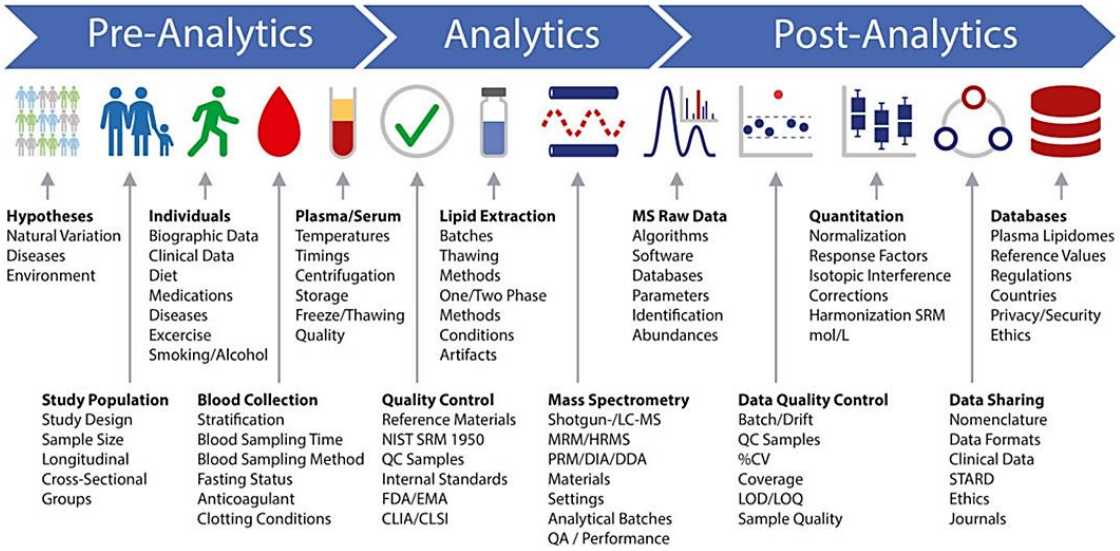

Figure *1.9*-**1** Human plasma lipidomic workflow [167]

1.9.1 Lipid Biomarkers for AD Diagnosis and Therapeutical Monitoring

Adult human brain contains a wide range of lipid classes and lipid molecular species. Lipids seems interact with important proteins involved in Alzheimer's disease pathogenesis, and a concomitant altered lipid metabolism is implicated in AD. Therefore, lipidomics could be an important tool to provide possible biomarkers for the AD diagnosis and therapeutical monitoring. [168]

Nowadays, advancements in analytical chemistry allow efficient, high throughput, and reproducible screening of hundreds of lipid classes [sphingomyelins, ceramides, phosphatidylcholines (PCs), lysophosphatidylcholine (lysoPCs), cholesteryl esters, triacylglycerols (TAGs), diacylglycerols (DAGs), and monoacylglycerols (MAGs), fatty acids]. Few studies have been conducted to investigate lipidomic changes in cerebrospinal fluid (CSF). However, the main limitation of researching CSF biomarkers is that CSF sampling requires a lumbar puncture that is invasive and dependent on considerable medical skill and so it can not be applied to general screening or for repeat measures. Investigating lipidic peripheral changes, they result much more convenient: blood is easier to extract, relatively risk free, unexpensive, and suitable for repeated sampling. Although blood is a secondary compartment for brain related molecules, through the blood–brain barrier (BBB) partition, CSF exchanges metabolites with blood during the reabsorption into the vascular system, moreover BBB permeability may increase in some conditions. Thus, it may be possible to detect brain-related alterations to lipid profiles by examining blood-based biomarkers. So, there is substantial overlap in metabolic changes identified in CSF and plasma. Interestingly some blood lipids may be correlated with tau and amyloid cascade.[169]

For example, high level of serum cholesterol detected in middle age people have been recognized as a risk factor for AD onset.[170] In particular, cholesterol is known to be associated with sphingolipids in membranes

to form organized, detergent-resistant microdomains known as lipid rafts. Lipid rafts anchor many important transmembrane proteins implicated in AD pathogenesis, including BACE1 and γ-secretase. In this way cholesterol takes part to amyloid pathway, by binding amyloid precursor protein and facilitating its processing by those secretases.[171]

Sphingolipids, present in lipid rafts and in myelin, play both structural and signalling roles. Abnormal metabolism of sphingolipids seems contribute to AD. Sphingolipids could be hydrolysed through acid sphingomyelinase (ASM) to produce ceramides that are involved in apoptosis. Then ceramides could be metabolized by acid ceramidase (AC) to sphingosine and further phosphorylated to produce sphingosine-1-phosphate. Increased expression of ASM and AC in membranes of AD brains compared to healthy, age-matched individuals has been identified, and this leads to reduced sphingomyelin and increased ceramide levels in serum/plasma. ASM activity is influenced by Aβ: the addition of Aβ oligomers to neuronal cultures increases ceramide levels.[172] Specifically, two ceramide species (Cer 16:0 and Cer 21:0) were found significantly higher in Alzheimer's disease patients.[173]

Phospholipids, that are the main components of cell membrane, are all altered in AD patients, specifically a decrease in phosphatidylcholines (PC), phosphatidylinositols (PI), phosphatidylethanolamines (PE) and plasmalogens levels was found compared with healthy controls. Regarding phosphatidylcholine, PC 16:0/20:5, PC 16:0/22:6, and PC 18:0/22:6 species resulted reduced in AD patients and in mild cognitive impairment (MCI) individuals in comparison to control patients.[174] The studies revealed that this PC depletion can also be responsible of the poor cognitive performance that occurs in normal ageing, thus indicating a potential association between dysregulated phospholipid homeostasis and cognitive function. Several specific DAGs appeared increased in both plasma and the frontal cortex of AD patients and related to reduced Mini-Mental State Examination (MMSE) scores. A parallel trend was present in MCI individuals, thus emphasizing a possible contribution of DAGs in AD early stages.[175]A studied conducted by Mapstone and colleagues (2014) reported 10-phospholipid biomarkers (primarily PCs, lysoPCs, and acyl carnitine species) that were able to distinguish controls patients from patients who were converting to amnestic MCI (aMCI) or mild AD, and AD patients.[176]

In addition, lipid peroxidation takes place in the AD brain due to the increased level of oxidative stress. The peroxidized products of cerebral lipids include F2-isoprostanes (F2-IsoPs) and isofurans (IsoF), F4-neuroprostanes (F4-NeuroP) and neurofurans (NeuroF), F2-dihomo-isoprostanes (F2-dihomo-IsoP) and dihomoisofurans (dihomo-IsoF), 4-hydroxy-trans-2-nonenal (4-HNE), 4-hydroxy-2-hexenal (4-HHE), acrolein, and malondialdehyde (MDA). IsoPs or isoprostanoids are prostaglandin-like compounds, among which F2-IsoPs are produced by peroxidation of arachidonic acid (AA). Increased level of F2-IsoPs were found in the brain and in CSF of AD patients and could be correlated to disease progression. Therefore, elevated F2-IsoPs are early biomarkers of lipid peroxidation in AD patients even before Aβ depositions. F4-NeuroPs derive from oxidation of docosahexaenoic acid (DHA) and again, their expression showed to be elevated in the CSF and brain of AD patients. Considering other biological samples, peroxidised products in urine samples were

determined by UPLC-MS/MS method. Promising differences in IsoF, PGE2, NeuroP, IsoP levels were identified between patients with mild AD and healthy people. However, further investigations are required because the lipid profiles of plasma and urine were not corresponding with the one in CNS. [177]

References:

(1) Breijyeh, Z.; Karaman, R. Comprehensive Review on Alzheimer ' s Disease : *Molecules* **2020**, *25* (24), 5789 https://doi.org/10.3390/molecules25245789

(2) Sharma, P.; et al. Comprehensive Review of Mechanisms of Pathogenesis Involved in Alzheimer's Disease and Potential Therapeutic Strategies. *Progress in Neurobiology*. 2019, *174*, 53-89 https://doi.org/10.1016/j.pneurobio.2018.12.006.

(3) Qaseem, A.; et al. Current Pharmacologic Treatment of Dementia: A Clinical Practice Guideline from the American College of Physicians and the American Academy of Family Physicians. *Annals of Internal Medicine*. **2008**, *148*, 370-378https://doi.org/10.7326/0003-4819-148-5-200803040-00008.

(4) Farlow, M. A Clinical Overview of Cholinesterase Inhibitors in Alzheimer's Disease. *International Psychogeriatrics*. **2002**, *14* (S1) 93 - 126 https://doi.org/10.1017/S1041610203008688.

(5) Cummings, J.; et al. Effect of Donepezil on Cognition in Severe Alzheimer's Disease: A Pooled Data Analysis. *J. Alzheimer's Dis.* **2010**, *21* (3), 843-851,https://doi.org/10.3233/JAD-2010-100078.

(6) Alfirevic, A.; et al. Tacrine-Induced Liver Damage: An Analysis of 19 Candidate Genes. *Pharmacogenet. Genomics* **2007**, *17* (12), 843-851 https://doi.org/10.1097/FPC.0b013e3282f1f12b.

(7) Alva, G.; Cummings, J. L. Relative Tolerability of Alzheimer's Disease Treatments. *Psychiatry (Edgmont).* **2008**, *5* (11), 27-36

(8) Gill, S. S.; et al. Syncope and Its Consequences in Patients with Dementia Receiving Cholinesterase Inhibitors: A Population-Based Cohort Study. *Arch. Intern. Med.* **2009**, *169* (9), 867-873 https://doi.org/10.1001/archinternmed.2009.43.

(9) McShane, R.; et al. Memantine for Dementia. *Cochrane Database of Systematic Reviews*. **2019**, *18* (4):CD003154 https://doi.org/10.1002/14651858.CD003154.pub6.

(10) Maidment, I. D.; et al. Efficacy of Memantine on Behavioral and Psychological Symptoms Related to Dementia: A Systematic Meta-Analysis. *Ann. Pharmacother.* **2008**, *42* (1), 32-38 https://doi.org/10.1345/aph.1K372.

(11) Tariot, P. N.; et al. Memantine Treatment in Patients with Moderate to Severe Alzheimer Disease Already Receiving Donepezil: A Randomized Controlled Trial. *J. Am. Med. Assoc.* **2004**, *291* (3), 317-324 https://doi.org/10.1001/jama.291.3.317.

(12) Feldman, H. H.; et al. Activities of Daily Living in Moderate-to-Severe Alzheimer Disease: An Analysis of the Treatment Effects of Memantine in Patients Receiving Stable Donepezil Treatment. *Alzheimer Dis. Assoc. Disord.* **2006**, *20* (4), 263-268 https://doi.org/10.1097/01.wad.0000213859.35355.59.

(13) Howard, R.; Donepezil and Memantine for Moderate-to-Severe Alzheimer's Disease. *N. Engl. J. Med.* **2012**, *366* (10), 893-903 https://doi.org/10.1056/nejmoa1106668.

(14) Banerjee, S.; et al. Sertraline or Mirtazapine for Depression in Dementia (HTA-SADD): A

Randomised, Multicentre, Double-Blind, Placebo-Controlled Trial. *Lancet* **2011**, *378* (9789), 403-411 https://doi.org/10.1016/S0140-6736(11)60830-1.

(15) Ballard, C.; Corbett, A. Management of Neuropsychiatric Symptoms in People with Dementia. *CNS Drugs*. **2010**, *24*, 729–739 https://doi.org/10.2165/11319240-000000000-00000.

(16) Tiwari, S.; et al. Alzheimer's Disease: Pathogenesis, Diagnostics, and Therapeutics. *International Journal of Nanomedicine*. **2019**, *2019* (14) 5541—5554 https://doi.org/10.2147/IJN.S200490.

(17) Sayas, C. L.; Ávila, J. GSK-3 and Tau: A Key Duet in Alzheimer's Disease. *Cells*. **2021**, 10 (4), 721 https://doi.org/10.3390/cells10040721.

(18) Kramer, T.; et al. Small-Molecule Inhibitors of GSK-3: Structural Insights and Their Application to Alzheimer's Disease Models. *International Journal of Alzheimer's Disease*. **2012**, *2012*, 381029 https://doi.org/10.1155/2012/381029.

(19) Xu, M.; et al. Structure-Activity Relationship (SAR) Studies of Synthetic Glycogen Synthase Kinase-3β Inhibitors: A Critical Review. *European Journal of Medicinal Chemistry*. **2019**, *164* (15) 448-470 https://doi.org/10.1016/j.ejmech.2018.12.073.

(20) Yu, J. Y.; et al. Simultaneous Inhibition of GSK3α and GSK3β Using Hairpin SiRNA Expression Vectors. *Mol. Ther.* **2003**, *7* (2), 228-236 https://doi.org/10.1016/S1525-0016(02)00037-0.

(21) Bertrand, J. A.; Thieffine, S.; Vulpetti, A.; Cristiani, C.; et al. Structural Characterization of the GSK-3β Active Site Using Selective and Non-Selective ATP-Mimetic Inhibitors. *J. Mol. Biol.* **2003**, *333* (2), 393-407 https://doi.org/10.1016/j.jmb.2003.08.031.

(22) Leost, M.; et al. Paullones Are Potent Inhibitors of Glycogen Synthase Kinase-3β and Cyclin-Dependent Kinase 5/P25. *Eur. J. Biochem.* **2000**, *267* (19), 5983-5994 https://doi.org/10.1046/j.1432-1327.2000.01673.x.

(23) Bidon-Chanal, A.; et al. Evidence for a New Binding Mode to GSK-3: Allosteric Regulation by the Marine Compound Palinurin. *Eur. J. Med. Chem.* **2013**, *60*. 479-489 https://doi.org/10.1016/j.ejmech.2012.12.014.

(24) Palomo, V.; et al. Exploring the Binding Sites of Glycogen Synthase Kinase 3. Identification and Characterization of Allosteric Modulation Cavities. *J. Med. Chem.* **2011**, *54* (24), 8461–8470 https://doi.org/10.1021/jm200996g.

(25) Duda, P.; Akula, et al. Targeting GSK3 and Associated Signaling Pathways Involved in Cancer. *Cells*. **2020**, 9 (5), 1110 https://doi.org/10.3390/cells9051110.

(26) Khan, I.; et al. Natural and Synthetic Bioactive Inhibitors of Glycogen Synthase Kinase. *European Journal of Medicinal Chemistry*. **2017**, *125*, 464-477 https://doi.org/10.1016/j.ejmech.2016.09.058.

(27) Meijer, L.; et al. GSK-3-Selective Inhibitors Derived from Tyrian Purple Indirubins. *Chem. Biol.* **2003**, *10* (12) 1255-1266 https://doi.org/10.1016/j.chembiol.2003.11.010.

(28) Leclerc, S.; et al. Indirubins Inhibit Glycogen Synthase Kinase-3β and CDK5/P25, Two Protein Kinases Involved in Abnormal Tau Phosphorylation in Alzheimer's Disease. A Property Common to Most Cyclin-Dependent Kinase Inhibitors? *J. Biol. Chem.* **2001**, *276* (1), 251-260

https://doi.org/10.1074/jbc.M002466200.

(29) Polychronopoulos, P.; et al. Structural Basis for the Synthesis of Indirubins as Potent and Selective Inhibitors of Glycogen Synthase Kinase-3 and Cyclin-Dependent Kinases. *J. Med. Chem.* **2004**, *47* (4), 935–946 https://doi.org/10.1021/jm031016d.

(30) Vougogiannopoulou, K.; et al. Soluble 3′,6-Substituted Indirubins with Enhanced Selectivity toward Glycogen Synthase Kinase -3 Alter Circadian Period. *J. Med. Chem.* **2008**, *51* (20), 6421–6431 https://doi.org/10.1021/jm800648y.

(31) Libnow, S.; et al. Synthesis of Indirubin-N′-Glycosides and Their Anti-Proliferative Activity against Human Cancer Cell Lines. *Bioorganic Med. Chem.* **2008**, *16* (10), 5570-5583 https://doi.org/10.1016/j.bmc.2008.04.003.

(32) Rao, K. V.; et al. Manzamine B and E and Ircinal A Related Alkaloids from an Indonesian Acanthostrongylophora Sponge and Their Activity against Infectious, Tropical Parasitic, and Alzheimer's Diseases. *J. Nat. Prod.* **2006**, *69* (7), 1034–1040 https://doi.org/10.1021/np0601399.

(33) Hamann, M.; et al. Glycogen Synthase Kinase-3 (GSK-3) Inhibitory Activity and Structure-Activity Relationship (SAR) Studies of the Manzamine Alkaloids. Potential for Alzheimer's Disease. *J. Nat. Prod.* **2007**, *70* (9), 1397–1405 https://doi.org/10.1021/np060092r.

(34) Peng, J.; et al. Structure - Activity Relationship and Mechanism of Action Studies of Manzamine Analogues for the Control of Neuroinflammation and Cerebral Infections. *J. Med. Chem.* **2010**, *53* (1), 61–76 https://doi.org/10.1021/jm900672t.

(35) Skropeta, D.; et al. Kinase Inhibitors from Marine Sponges. *Marine Drugs*. **2011**, *9* (10), 2131-2154 https://doi.org/10.3390/md9102131.

(36) Meijer, L.; et al. Inhibition of Cyclin-Dependent Kinases, GSK-3β and CK1 by Hymenialdisine, a Marine Sponge Constituent. *Chem. Biol.* **2000**, *7* (1), 51–63. https://doi.org/10.1016/S1074-5521(00)00063-6.

(37) Gauthier, S.; et al. Effect of Tramiprosate in Patients with Mild-to-Moderate Alzheimer's Disease: Exploratory Analyses of the MRI Sub-Group of the Alphase Study. *J. Nutr. Heal. Aging* **2009**, *13* (6), 550-7

(38) Summers, K. L.; et al. Copper(II) Binding to PBT2 Differs from That of Other 8-Hydroxyquinoline Chelators: Implications for the Treatment of Neurodegenerative Protein Misfolding Diseases. *Inorg. Chem.* **2020**, *59* (23), 17519–17534 https://doi.org/10.1021/acs.inorgchem.0c02754.

(39) Siemers, E.; et al. Safety, Tolerability, and Changes in Amyloid β Concentrations after Administration of a γ-Secretase Inhibitor in Volunteers. *Clin. Neuropharmacol.* **2005**, *28* (3), 126-132 https://doi.org/10.1097/01.wnf.0000167360.27670.29.

(40) Yiannopoulou, K. G.; et al. Reasons for Failed Trials of Disease-Modifying Treatments for Alzheimer Disease and Their Contribution in Recent Research. *Biomedicines*. **2019**, *7* (4), 97 https://doi.org/10.3390/biomedicines7040097.

(41) Llufriu-Dabén, G.; et al. Targeting Demyelination via α-Secretases Promoting SAPPα Release to Enhance Remyelination in Central Nervous System. *Neurobiol. Dis.* **2018**, *109*, 11-24 https://doi.org/10.1016/j.nbd.2017.09.008.

(42) Moussa-Pacha, N. M.; et al. BACE1 Inhibitors: Current Status and Future Directions in Treating Alzheimer's Disease. *Medicinal Research Reviews*. **2020**, *40* (1), 339-384 https://doi.org/10.1002/med.21622.

(43) Csermely, P.; et al. The Efficiency of Multi-Target Drugs: The Network Approach Might Help Drug Design. *Trends Pharmacol. Sci.* **2005**, *26* (4), 178-182 https://doi.org/10.1016/j.tips.2005.02.007.

(44) Hopkins, A. L. Network Pharmacology: The next Paradigm in Drug Discovery. *Nature Chemical Biology*. **2008**, *4*, 682–690 https://doi.org/10.1038/nchembio.118.

(45) Prati, F.; et al. Two Diseases, One Approach: Multitarget Drug Discovery in Alzheimer's and Neglected Tropical Diseases. *MedChemComm*. 2014, 5, 853-861 https://doi.org/10.1039/c4md00069b.

(46) L. Bolognesi, M. Polypharmacology in a Single Drug: Multitarget Drugs. *Curr. Med. Chem.* **2013**, *20* (13), 1639 - 1645 https://doi.org/10.2174/0929867311320130004.

(47) Hopkins, A. L.; Mason, J. S.; Overington, J. P. Can We Rationally Design Promiscuous Drugs? *Current Opinion in Structural Biology*. 2006, 16 (1) 127-136 https://doi.org/10.1016/j.sbi.2006.01.013.

(48) Morphy, R.; Rankovic, Z. Designing Multiple Ligands – Medicinal Chemistry Strategies and Challenges. *Curr. Pharm. Des.* **2009**, *15* (6), 587 - 600 https://doi.org/10.2174/138161209787315594.

(49) Morphy, R.; Rankovic, Z. The Physicochemical Challenges of Designing Multiple Ligands. *J. Med. Chem.* **2006**, *49* (16). https://doi.org/10.1021/jm0603015.

(50) Hann, M. M.; et al. Molecular Complexity and Its Impact on the Probability of Finding Leads for Drug Discovery. *J. Chem. Inf. Comput. Sci.* **2001**, *41* (3), 856–864 https://doi.org/10.1021/ci000403i.

(51) Prati, F.; et al. Multitarget Drug Discovery for Alzheimer's Disease: Triazinones as BACE-1 and GSK-3β Inhibitors. *Angew. Chemie - Int. Ed.* **2015**, *54* (5),1578-1582 https://doi.org/10.1002/anie.201410456.

(52) Di Martino, R. M. C.; et al. Versatility of the Curcumin Scaffold: Discovery of Potent and Balanced Dual BACE-1 and GSK-3β Inhibitors. *J. Med. Chem.* **2016**, *59* (2), 531–544 https://doi.org/10.1021/acs.jmedchem.5b00894.

(53) Wang, X.; et al. Effects of Curcuminoids Identified in Rhizomes of Curcuma Longa on BACE-1 Inhibitory and Behavioral Activity and Lifespan of Alzheimer's Disease Drosophila Models. *BMC Complement. Altern. Med.* **2014**, *14* (88) https://doi.org/10.1186/1472-6882-14-88.

(54) Nishimura, I.; et al. PAR-1 Kinase Plays an Initiator Role in a Temporally Ordered Phosphorylation Process That Confers Tau Toxicity in Drosophila. *Cell* **2004**, *116* (5), 671-682https://doi.org/10.1016/S0092-8674(04)00170-9.

(55) Augustinack, J. C.; et al. Specific Tau Phosphorylation Sites Correlate with Severity of Neuronal Cytopathology in Alzheimer's Disease. *Acta Neuropathol.* **2002**, *103* (1), 26–35 https://doi.org/10.1007/s004010100423.

(56) Dickey, C. A.; et al. HSP Induction Mediates Selective Clearance of Tau Phosphorylated at Proline-directed Ser/Thr Sites but Not KXGS (MARK) Sites. *FASEB J.* **2006**, *20* (6), 753-755 https://doi.org/10.1096/fj.05-5343fje.

(57) Dickey, C. A.; et al. The High-Affinity HSP90-CHIP Complex Recognizes and Selectively Degrades Phosphorylated Tau Client Proteins. *J. Clin. Invest.* **2007**, *117* (3), 648-58 https://doi.org/10.1172/JCI29715.

(58) Xiong, Y.; et al. HDAC6 Mutations Rescue Human Tau-Induced Microtubule Defects in Drosophila. *Proc. Natl. Acad. Sci. U. S. A.* **2013**, *110* (12), 4604-4609 https://doi.org/10.1073/pnas.1207586110.

(59) Bardai, F. H.; et al. Histone Deacetylase-1 (HDAC1) Is a Molecular Switch between Neuronal Survival and Death. *J. Biol. Chem.* **2012**, *287* (42), 35444-35453 https://doi.org/10.1074/jbc.M112.394544.

(60) Kazantsev, A. G.; Thompson, L. M. Therapeutic Application of Histone Deacetylase Inhibitors for Central Nervous System Disorders. *Nature Reviews Drug Discovery*. **2008**, *7* (10), 854-68https://doi.org/10.1038/nrd2681.

(61) Falkenberg, K. J.; et al. Genome Scale RNAi Screen Identifies GLI1 as a Novel Gene Regulating Vorinostat Sensitivity. *Cell Death Differ.* **2016**, *23* (7), 1209-18 https://doi.org/10.1038/cdd.2015.175.

(62) De Simone, A.; et al. Hydroxy-Substituted Trans-Cinnamoyl Derivatives as Multifunctional Tools in the Context of Alzheimer's Disease. *Eur. J. Med. Chem.* **2017**, *139*, 378–389. https://doi.org/10.1016/j.ejmech.2017.07.058.

(63) Zhuang, C.; et al. Chalcone: A Privileged Structure in Medicinal Chemistry. *Chemical Reviews*. **2017**, *117* (12) 7762–7810 https://doi.org/10.1021/acs.chemrev.7b00020.

(64) De Simone, A.; et al. Hydroxy-Substituted Trans-Cinnamoyl Derivatives as Multifunctional Tools in the Context of Alzheimer's Disease. *Eur. J. Med. Chem.* **2017**, *139*, 378-389 https://doi.org/10.1016/j.ejmech.2017.07.058.

(65) Pérez-Areales, F. J.; et al. Design, Synthesis and Multitarget Biological Profiling of Second-Generation Anti-Alzheimer Rhein-Huprine Hybrids. *Future Med. Chem.* **2017**, *9* (10), 965-981 https://doi.org/10.4155/fmc-2017-0049.

(66) Viayna, E.; et al. Discovery of a Potent Dual Inhibitor of Acetylcholinesterase and Butyrylcholinesterase with Antioxidant Activity That Alleviates Alzheimer-like Pathology in Old APP/PS1 Mice. *J. Med. Chem.* **2021**, *64* (1) 812–839https://doi.org/10.1021/acs.jmedchem.0c01775.

(67) Pérez-Areales, F. J.; et al. A Novel Class of Multitarget Anti-Alzheimer Benzohomoadamantane–chlorotacrine Hybrids Modulating Cholinesterases and Glutamate NMDA Receptors. *Eur. J. Med. Chem.* **2019**, *180*, 613-626https://doi.org/10.1016/j.ejmech.2019.07.051.

(68) Zheng, C.; et al. The Dual Roles of Cytokines in Alzheimer's Disease: Update on Interleukins, TNF-α, TGF-β and IFN-γ. *Translational Neurodegeneration*. **2016**, *10*, 2790 https://doi.org/10.1186/s40035-016-0054-4.

(69) Rowan, M. J.; et al. Synaptic Memory Mechanisms: Alzheimer's Disease Amyloid β-Peptide-Induced Dysfunction. In *Biochemical Society Transactions*; **2007**, *35* (5), 1219–1223.

(70) Schipper, H. M.; et al. Heme Oxygenase-1 and Neurodegeneration: Expanding Frontiers of Engagement. *Journal of Neurochemistry*. **2009**, *110* (2) 469-485 https://doi.org/10.1111/j.1471-4159.2009.06160.x.

(71) Kourti, M.; et al. Aspects of Carbon Monoxide in Form of CO-Releasing Molecules Used in Cancer Treatment: More Light on the Way. *Oxidative Medicine and Cellular Longevity*. **2017**, *2017*, 9326454 https://doi.org/10.1155/2017/9326454.

(72) Kim, H. P.; et al. CO as a Cellular Signaling Molecule. *Annual Review of Pharmacology and Toxicology*. **2006**, *46*, 411-49 https://doi.org/10.1146/annurev.pharmtox.46.120604.141053.

(73) Otterbein, L. E.; et al. Exogenous Administration of Heme Oxygenase-1 by Gene Transfer Provides Protection against Hyperoxia-Induced Lung Injury. *J. Clin. Invest.* **1999**, *103* (7), 1047-54 https://doi.org/10.1172/JCI5342.

(74) Minamino, T.; et al. Targeted Expression of Heme Oxygenase-1 Prevents the Pulmonary Inflammatory and Vascular Responses to Hypoxia. *Proc. Natl. Acad. Sci. U. S. A.* **2001**, *98* (15), 8798-8803 https://doi.org/10.1073/pnas.161272598.

(75) Otterbein, L. E.; et al. Carbon Monoxide Has Anti-Inflammatory Effects Involving the Mitogen-Activated Protein Kinase Pathway. *Nat. Med.* **2000**, *6* (4), 422–428 https://doi.org/10.1038/74680.

(76) Lee, P. J.; et al. Overexpression of Heme Oxygenase-1 in Human Pulmonary Epithelial Cells Results in Cell Growth Arrest and Increased Resistance to Hyperoxia. *Proc. Natl. Acad. Sci. U. S. A.* **1996**, *93* (19), 10393-10398 https://doi.org/10.1073/pnas.93.19.10393.

(77) Motterlini, R.; et al. Carbon Monoxide-Releasing Molecules: Characterization of Biochemical and Vascular Activities. *Circ. Res.* **2002**, *90* (2), e17–e24 https://doi.org/10.1161/hh0202.104530.

(78) Mann, B. E. Carbon Monoxide: An Essential Signalling Molecule. *Top. Organomet. Chem.* **2010**, *32*. 247–285 https://doi.org/10.1007/978-3-642-13185-1_10.

(79) Antony, L. A. P.; et al. Fluorescein Analogue Xanthene-9-Carboxylic Acid: A Transition-Metal-Free CO Releasing Molecule Activated by Green Light. *Org. Lett.* **2013**, *15* (17), 4552–4555 https://doi.org/10.1021/ol4021089.

(80) Peng, P.; et al. Visible-Light Activatable Organic CO-Releasing Molecules (PhotoCORMs) That Simultaneously Generate Fluorophores. *Org. Biomol. Chem.* **2013**, *11* (39), 6671-6674. https://doi.org/10.1039/c3ob41385c.

(81) Romão, C. C.; et al. Developing Drug Molecules for Therapy with Carbon Monoxide. *Chem. Soc. Rev.* **2012**, *41* (9), 3571-3583 https://doi.org/10.1039/c2cs15317c.

(82) Schatzschneider, U. Novel Lead Structures and Activation Mechanisms for CO-Releasing Molecules (CORMs). *British Journal of Pharmacology*. **2015**, *172* (6), 1638-1650 https://doi.org/10.1111/bph.12688.

(83) Romanski, S.; et al. Acyloxybutadiene Tricarbonyl Iron Complexes as Enzyme-Triggered CO-Releasing Molecules (ET-CORMs): A Structure-Activity Relationship Study. *Dalt. Trans.* **2012**, *41* (45),13862-13875 https://doi.org/10.1039/c2dt30662j.

(84) Romanski, S.; et al. Iron Dienylphosphate Tricarbonyl Complexes as Water-Soluble Enzyme-Triggered CO-Releasing Molecules (ET-CORMs). *Organometallics* **2012**, *31* (16), 5800–5809 https://doi.org/10.1021/om300359a.

(85) Botov, S.; et al. Synthesis and Performance of Acyloxy-Diene-Fe(CO)3 Complexes with Variable Chain Lengths as Enzyme-Triggered Carbon Monoxide-Releasing Molecules. *Organometallics* **2013**, *32* (13), 3587–3594 https://doi.org/10.1021/om301233h.

(86) Schatzschneider, U. Photoactivated Biological Activity of Transition-Metal Complexes. *European*

Journal of Inorganic Chemistry. **2010**, *2010* (10), 1451-1467 https://doi.org/10.1002/ejic.201000003.

(87) Schatzschneider, U. PhotoCORMs: Light-Triggered Release of Carbon Monoxide from the Coordination Sphere of Transition Metal Complexes for Biological Applications. *Inorganica Chimica Acta*. **2011**, *374* (1), 19-23 https://doi.org/10.1016/j.ica.2011.02.068.

(88) Rimmer, R. D.; et al. Photochemically Activated Carbon Monoxide Release for Biological Targets. Toward Developing Air-Stable PhotoCORMs Labilized by Visible Light. *Coordination Chemistry Reviews*. **2012**, *256*, (15–16), 1509-1519 https://doi.org/10.1016/j.ccr.2011.12.009.

(89) Santos-Silva, T.; et al. CORM-3 Reactivity toward Proteins: The Crystal Structure of a Ru(II) Dicarbonyl-Lysozyme Complex. *J. Am. Chem. Soc.* **2011**, *133* (5), 1192–1195 https://doi.org/10.1021/ja108820s.

(90) Petruk, A. A.; et al. Interaction between Proteins and Ir Based CO Releasing Molecules: Mechanism of Adduct Formation and CO Release. *Inorg. Chem.* **2014**, *53* (19), 10456–10462 https://doi.org/10.1021/ic501498g.

(91) Caterino, M.; et al. Mapping the Protein-Binding Sites for Iridium(III)-Based CO-Releasing Molecules. *Dalt. Trans.* **2016**, *45* (30), 12206-12214 https://doi.org/10.1039/c6dt01685e.

(92) Wang, P.; et al. Syntheses and Evaluation of Drug-like Properties of CO-Releasing Molecules Containing Ruthenium and Group 6 Metal. *Eur. J. Med. Chem.* **2014**, *74*. 199-215 https://doi.org/10.1016/j.ejmech.2013.12.041.

(93) Gong, Y.; et al. Synthesis, Toxicities and Cell Proliferation Inhibition of CO-Releasing Molecules Containing Cobalt. *Transit. Met. Chem.* **2015**, *40* (4), 413–426 https://doi.org/10.1007/s11243-015-9931-4.

(94) Gong, Y.; et al. Toxicity, Bio-Distribution and Metabolism of CO-Releasing Molecules Based on Cobalt. *Free Radic. Biol. Med.* **2016**, *97*, 362-374 https://doi.org/10.1016/j.freeradbiomed.2016.06.029.

(95) Hettiarachchi, N. T.; et al. Heme Oxygenase-1 Protects against Alzheimer's Amyloid-B1-42-Induced Toxicity via Carbon Monoxide Production. *Cell Death Dis.* **2014**, *5* (12), e1569 https://doi.org/10.1038/cddis.2014.529.

(96) De Simone, A.; et al. Advanced Analytical Methodologies in Alzheimer's Disease Drug Discovery. *Journal of Pharmaceutical and Biomedical Analysis*. **2020**, *178*, 112899 https://doi.org/10.1016/j.jpba.2019.112899.

(97) Lee, S. J. C.; et al. Towards an Understanding of Amyloid-β Oligomers: Characterization, Toxicity Mechanisms, and Inhibitors. *Chemical Society Reviews*. **2017**, *46*, 310-323 https://doi.org/10.1039/c6cs00731g.

(98) Watanabe-Nakayama, T.; Ono, K. High-Speed Atomic Force Microscopy of Individual Amyloidogenic Protein Assemblies. In *Methods in Molecular Biology*; 2018, *1814*, 201-212 https://doi.org/10.1007/978-1-4939-8591-3_12.

(99) Banerjee, S.; et al. Nanoscale Dynamics of Amyloid β-42 Oligomers As Revealed by High-Speed Atomic Force Microscopy. *ACS Nano* **2017**, *11* (12), 12202–12209 https://doi.org/10.1021/acsnano.7b05434.

(100) Kong, J.; Yu, S. Fourier Transform Infrared Spectroscopic Analysis of Protein Secondary Structures.

Acta Biochim. Biophys. Sin. (Shanghai). **2007**, *39* (8), 549–559 https://doi.org/10.1111/j.1745-7270.2007.00320.x.

(101) Syad, A. N.; Devi, K. P. Assessment of Anti-Amyloidogenic Activity of Marine Red Alga G. Acerosa against Alzheimer's Beta-Amyloid Peptide 25-35. *Neurol. Res.* **2015**, *37* (1), 14-22 https://doi.org/10.1179/1743132814Y.0000000422.

(102) Hossain, S.; et al. Medicinal Value of Asiaticoside for Alzheimer's Disease as Assessed Using Single-Molecule-Detection Fluorescence Correlation Spectroscopy, Laser-Scanning Microscopy, Transmission Electron Microscopy, and in Silico Docking. *BMC Complement. Altern. Med.* **2015**, *15* (1), 15:118 https://doi.org/10.1186/s12906-015-0620-9.

(103) Stark, T.; et al. Peptidomimetics That Inhibit and Partially Reverse the Aggregation of Aβ1-42. *Biochemistry* **2017**, *56* (36), 4840–4849 https://doi.org/10.1021/acs.biochem.7b00223.

(104) Ramachandran, G.; et al. Resonance Raman Spectroscopic Measurements Delineate the Structural Changes That Occur during Tau Fibril Formation. *Biochemistry* **2014**, *53* (41) , 6550–6565. https://doi.org/10.1021/bi500528x.

(105) Bertucci, C.; et al. Circular Dichroism in Drug Discovery and Development: An Abridged Review. *Analytical and Bioanalytical Chemistry*. **2010**, *398* (1), 155-66 https://doi.org/10.1007/s00216-010-3959-2.

(106) Pescitelli, G.; et al. Application of Electronic Circular Dichroism in the Study of Supramolecular Systems. *Chemical Society Reviews*. **2014**, *43* (15), 5211-33 https://doi.org/10.1039/c4cs00104d.

(107) Rajaram, H.; et al. "Click" Assembly of Glycoclusters and Discovery of a Trehalose Analogue That Retards Aβ40 Aggregation and Inhibits Aβ40-Induced Neurotoxicity. *Bioorganic Med. Chem. Lett.* **2014**, *24* (18), 4523-4528 https://doi.org/10.1016/j.bmcl.2014.07.077.

(108) Tu, Y.; et al. Hematoxylin Inhibits Amyloid β-Protein Fibrillation and Alleviates Amyloid-Induced Cytotoxicity. *J. Phys. Chem. B* **2016**, *120* (44), 11360–11368 https://doi.org/10.1021/acs.jpcb.6b06878.

(109) Bartolini, M.; et al. Kinetic Characterization of Amyloid-Beta 1-42 Aggregation with a Multimethodological Approach. *Anal. Biochem.* **2011**, *414* (2), 215-225 https://doi.org/10.1016/j.ab.2011.03.020.

(110) Woods, L. A.; et al. Advances in Ion Mobility Spectrometry-Mass Spectrometry Reveal Key Insights into Amyloid Assembly. *Biochimica et Biophysica Acta - Proteins and Proteomics*. **2013**, *1834* (6),1257-68 https://doi.org/10.1016/j.bbapap.2012.10.002.

(111) Young, L. M.; et al. Screening and Classifying Small-Molecule Inhibitors of Amyloid Formation Using Ion Mobility Spectrometry-Mass Spectrometry. *Nat. Chem.* **2015**, *7* (1), 73–81 https://doi.org/10.1038/nchem.2129.

(112) Bleiholder, C.; Bowers, M. T. The Solution Assembly of Biological Molecules Using Ion Mobility Methods: From Amino Acids to Amyloid β-Protein. *Annual Review of Analytical Chemistry*. **2017**, *10* (1), 365-386 https://doi.org/10.1146/annurev-anchem-071114-040304.

(113) Eyers, C. E.; et al. Understanding Protein–Drug Interactions Using Ion Mobility–Mass Spectrometry. *Current Opinion in Chemical Biology*. **2018**, *42*, 167-176 https://doi.org/10.1016/j.cbpa.2017.12.013.

(114) Ashcroft, A. E. Mass Spectrometry and the Amyloid Problem-How Far Can We Go in the Gas Phase? *J. Am. Soc. Mass Spectrom.* **2010**, *21* (7), 1087–1096 https://doi.org/10.1016/j.jasms.2010.02.026.

(115) Lee, S.; et al. Rational Design of a Structural Framework with Potential Use to Develop Chemical Reagents That Target and Modulate Multiple Facets of Alzheimer's Disease. *J. Am. Chem. Soc.* **2014**, *136* (1), 299–310 https://doi.org/10.1021/ja409801p.

(116) Zheng, X.; et al. Amyloid β-Protein Assembly: The Effect of Molecular Tweezers CLR01 and CLR03. *J. Phys. Chem. B* **2015**, *119* (14), 4831–4841 https://doi.org/10.1021/acs.jpcb.5b00692.

(117) Downey, M. A.; et al. Inhibiting and Remodeling Toxic Amyloid-Beta Oligomer Formation Using a Computationally Designed Drug Molecule That Targets Alzheimer's Disease. *J. Am. Soc. Mass Spectrom.* **2019**, *30* (1), 85–93 https://doi.org/10.1007/s13361-018-1975-1.

(118) Kocis, P.; et al. Elucidating the Aβ42 Anti-Aggregation Mechanism of Action of Tramiprosate in Alzheimer's Disease: Integrating Molecular Analytical Methods, Pharmacokinetic and Clinical Data. *CNS Drugs* **2017**, *31* (6), 495–509 https://doi.org/10.1007/s40263-017-0434-z.

(119) Cernescu, M.; et al. Laser-Induced Liquid Bead Ion Desorption Mass Spectrometry: An Approach to Precisely Monitor the Oligomerization of the β-Amyloid Peptide. *Anal. Chem.* **2012**, *84* (12), 5276–5284 https://doi.org/10.1021/ac300258m.

(120) Grasso, G. Mass Spectrometry Is a Multifaceted Weapon to Be Used in the Battle against Alzheimer's Disease: Amyloid Beta Peptides and Beyond. *Mass Spectrometry Reviews*. **2019**,*38* (1), 34-48 https://doi.org/10.1002/mas.21566.

(121) Jia, Y.; et al. Development of Protein Biomarkers in Cerebrospinal Fluid for Secondary Progressive Multiple Sclerosis Using Selected Reaction Monitoring Mass Spectrometry (SRM-MS). *Clin. Proteomics* **2012**, *9* (1), 9 https://doi.org/10.1186/1559-0275-9-9.

(122) Angel, P. M.; Caprioli, R. M. Matrix-Assisted Laser Desorption Ionization Imaging Mass Spectrometry: In Situ Molecular Mapping. *Biochemistry* **2013**, *52* (22), 3818–3828 https://doi.org/10.1021/bi301519p.

(123) Ellman, G. L.; et al. A New and Rapid Colorimetric Determination of Acetylcholinesterase Activity. *Biochem. Pharmacol.* **1961**, *7* (2), 88-90 https://doi.org/10.1016/0006-2952(61)90145-9.

(124) Harry LeVine. Quantification of Beta-Sheet Amyloid Fibril Structures with Thioflavin T. *Methods Enzymol.* **1999**, *309* (18), 274-84

(125) Stryer, L.; Haugland, R. P. Energy Transfer: A Spectroscopic Ruler. *Proc. Natl. Acad. Sci. U. S. A.* **1967**, *58* (2), 719-726 https://doi.org/10.1073/pnas.58.2.719.

(126) Zwier, J. M.; et al. A Fluorescent Ligand-Binding Alternative Using Tag-Lite Technology. *J. Biomol. Screen.* **2010**, *15* (10), 1248-1259 https://doi.org/10.1177/1087057110384611.

(127) Kumar, S.; et al. Click Dimers to Target HIV TAR RNA Conformation. *Biochemistry* **2012**, *51* (11), 2331–2347 https://doi.org/10.1021/bi201657k.

(128) Stryer, L. Exploring Light and Life. *J. Biol. Chem.* **2012**, *287* (19), 5164-15173 https://doi.org/10.1074/jbc.X112.361436.

(129) Antal, C. E.; et al. Intramolecular Conformational Changes Optimize Protein Kinase C Signaling. *Chem. Biol.* **2014**, *21* (4), 459-469 https://doi.org/10.1016/j.chembiol.2014.02.008.

(130) Wu, P. G.; Brand, L. Resonance Energy Transfer: Methods and Applications. *Analytical Biochemistry*. **1994**, *218* (1), 1-13 https://doi.org/10.1006/abio.1994.1134.

(131) De Simone, A.; et al. Liquid Chromatographic Enzymatic Studies with On-Line Beta-Secretase Immobilized Enzyme Reactor and 4-(4-Dimethylaminophenylazo) Benzoic Acid/5-[(2-Aminoethyl) Amino] Naphthalene-1-Sulfonic Acid Peptide as Fluorogenic Substrate. *J. Chromatogr. B Anal. Technol. Biomed. Life Sci.* **2014**, *953–954* (1). https://doi.org/10.1016/j.jchromb.2014.01.056.

(132) Chlebek, J.; et al. Application of BACE1 Immobilized Enzyme Reactor for the Characterization of Multifunctional Alkaloids from Corydalis Cava (Fumariaceae) as Alzheimer's Disease Targets. *Fitoterapia* **2016**, *109*, 241-247 https://doi.org/10.1016/j.fitote.2016.01.008.

(133) De Simone, A.; et al. Immobilized Enzyme Reactors: An Overview of Applications in Drug Discovery from 2008 to 2018. *Chromatographia*. **2019**, 425–441 https://doi.org/10.1007/s10337-018-3663-5.

(134) Lee, J.; et al. Inkjet Printing-Based β-Secretase Fluorescence Resonance Energy Transfer (FRET) Assay for Screening of Potential β-Secretase Inhibitors of Alzheimer's Disease. *Anal. Chim. Acta* **2018**, *1022*, 89-95 https://doi.org/10.1016/j.aca.2018.03.033.

(135) Zuo, X.; et al. A Peptide-WS2 Nanosheet Based Biosensing Platform for Determination of β-Secretase and Screening of Its Inhibitors. *Analyst* **2018**, *143* (19), 4585-4591 https://doi.org/10.1039/c8an00132d.

(136) Sin-Yee Law, A.; et al. A Luminescence Turn-On Assay for Acetylcholinesterase Activity and Inhibitor Screening Based on Supramolecular Self-Assembly of Alkynylplatinum(II) Complexes on Coordination Polymer. *ACS Appl. Mater. Interfaces* **2019**, *11* (5), 11, 5, 4799–4808 https://doi.org/10.1021/acsami.8b18739.

(137) Sun, S.; et al. A Label-Free Sirtuin 1 Assay Based on Droplet-Electrospray Ionization Mass Spectrometry. *Anal. Methods* **2016**, *8* (17), 3458-3465 https://doi.org/10.1039/c6ay00698a.

(138) De Simone, A.; et al. Application of an ESI-QTOF Method for the Detailed Characterization of GSK-3β Inhibitors. *J. Pharm. Biomed. Anal.* **2017**, *144*, 159-166. https://doi.org/10.1016/j.jpba.2017.02.036.

(139) Zhang, S.; et al. Quantitative Determination of Noncovalent Binding Interactions Using Automated Nanoelectrospray Mass Spectrometry. *Anal. Chem.* **2003**, *75* (13), 3010–3018 https://doi.org/10.1021/ac034089d.

(140) Nunes, J.; et al. Mass Spectrometry-Based Methodologies for Targeted and Untargeted Identification of Protein Covalent Adducts (Adductomics): Current Status and Challenges. *High-Throughput*. 2019. https://doi.org/10.3390/ht8020009.

(141) Fiori, J.; et al. Disclosure of a Fundamental Clue for the Elucidation of the Myricetin Mechanism of Action as Amyloid Aggregation Inhibitor by Mass Spectrometry. *Electrophoresis* **2012**, *33* (22), 3380-3386https://doi.org/10.1002/elps.201200186.

(142) Taniguchi, A.; et al. Attenuation of the Aggregation and Neurotoxicity of Amyloid-β Peptides by Catalytic Photooxygenation. *Angew. Chemie* **2014**, *126* (5), 1406-

1409https://doi.org/10.1002/ange.201308001.

(143) Young, L. M.; et al. ESI-IMS-MS: A Method for Rapid Analysis of Protein Aggregation and Its Inhibition by Small Molecules. *Methods* **2016**, *95*, 62-69 https://doi.org/10.1016/j.ymeth.2015.05.017.

(144) Meikle, T. G.; et al. Clinical Lipidomics: Realizing the Potential of Lipid Profiling. *J. Lipid Res.* **2021**, *63*, 100127 https://doi.org/10.1016/J.JLR.2021.100127.

(145) Zhao, Y. Y.; et al. Lipidomics Applications for Disease Biomarker Discovery in Mammal Models. *Biomarkers in Medicine*. 2015, 9(2), 153-68 https://doi.org/10.2217/BMM.14.81.

(146) Watson AD. Thematic review series: systems biology approaches to metabolic and cardiovascular disorders. Lipidomics: a global approach to lipid analysis in biological systems. *J Lipid Res*. **2006**, *47* (10), 2101-11. https://doi.org/10.1194/jlr.R600022-JLR200

(147) Hu, C.; et al. Analytical Strategies in Lipidomics and Applications in Disease Biomarker Discovery. *Journal of Chromatography B: Analytical Technologies in the Biomedical and Life Sciences*. **2009**, *13* (6), 612-632 https://doi.org/10.1016/j.jchromb.2009.01.038.

(148) Yang, Q.; et al. Metabolites as Regulators of Insulin Sensitivity and Metabolism. *Nature Reviews Molecular Cell Biology*. **2018**, *19*(10), 654-672 https://doi.org/10.1038/s41580-018-0044-8.

(149) Chatterjee, M.; et al. Regulation of Oxidized Platelet Lipidome: Implications for Coronary Artery Disease. *Eur. Heart J.* **2017**, *38* (25), 1993–2005 https://doi.org/10.1093/eurheartj/ehx146.

(150) Schlotterbeck, J.; et al. Comprehensive MS/MS Profiling by UHPLC-ESI-QTOF-MS/MS Using SWATH Data-Independent Acquisition for the Study of Platelet Lipidomes in Coronary Artery Disease. *Anal. Chim. Acta* **2019**, *1046*, 1-15 https://doi.org/10.1016/j.aca.2018.08.060.

(151) Cebo, M.; et al. Simultaneous Targeted and Untargeted UHPLC-ESI-MS/MS Method with Data-Independent Acquisition for Quantification and Profiling of (Oxidized) Fatty Acids Released upon Platelet Activation by Thrombin. *Anal. Chim. Acta* **2020**, *1094*, 57-69 https://doi.org/10.1016/j.aca.2019.10.005.

(152) Cebo, M.; et al. Untargeted UHPLC-ESI-QTOF-MS/MS Analysis with Targeted Feature Extraction at Precursor and Fragment Level for Profiling of the Platelet Lipidome with Ex Vivo Thrombin-Activation. *J. Pharm. Biomed. Anal.* **2021**, *205*, 114301 https://doi.org/10.1016/j.jpba.2021.114301.

(153) Kohno, S.; et al. Lipidomic Insight into Cardiovascular Diseases. *Biochem. Biophys. Res. Commun.* **2018**, *504* (3) 590-595 https://doi.org/10.1016/j.bbrc.2018.04.106.

(154) Agarwala, P. K.; et al. Lipidomic Landscape in Cancer: Actionable Insights for Membrane-Based Therapy and Diagnoses. *Medicinal Research Reviews*. **2021**, *42* (2), 983-1018 https://doi.org/10.1002/med.21868.

(155) Andrisic, L.; et al. Short Overview on Metabolomics Approach to Study Pathophysiology of Oxidative Stress in Cancer. *Redox Biology*. **2018**, *14*, 47-58 https://doi.org/10.1016/j.redox.2017.08.009.

(156) Tyurina, Y. Y.; et al. Redox (Phospho) Lipidomics of Signaling in Inflammation and Programmed Cell Death. *Journal of Leukocyte Biology*. 2019, 106 (1), 57-81 https://doi.org/10.1002/JLB.3MIR0119-004RR.

(157) Valianpour, F.; et al. Quantitative and Compositional Study of Cardiolipin in Platelets by Electrospray

Ionization Mass Spectrometry: Application for the Identification of Barth Syndrome Patients. *Clin. Chem.* **2002**, *48* (9),1390–1397https://doi.org/10.1093/clinchem/48.9.1390.

(158) Cuperlovic-Culf, M.; Badhwar, A. Recent Advances from Metabolomics and Lipidomics Application in Alzheimer's Disease Inspiring Drug Discovery. *Expert Opinion on Drug Discovery*. **2020**, *59*(7), 1746-1749 https://doi.org/10.1080/17460441.2020.1674808.

(159) Gonzalez-Riano, C.; et al. Metabolomics Studies in Brain Tissue: A Review. *J. Pharm. Biomed. Anal.* **2016**, *130*, 141-168 https://doi.org/10.1016/j.jpba.2016.07.008.

(160) Dehairs, J.; et al. Lipidomics in Drug Development. *Drug Discovery Today: Technologies*. **2015**, *13*, 33-38 https://doi.org/10.1016/j.ddtec.2015.03.002.

(161) Rustam, Y. H.; Reid, G. E. Analytical Challenges and Recent Advances in Mass Spectrometry Based Lipidomics. *Analytical Chemistry*. **2018**, *90* (1) 374–397 https://doi.org/10.1021/acs.analchem.7b04836.

(162) Bligh, E. G.; Dyer, W. J. A Rapid Method of Total Lipid Extraction and Purification. *Can. J. Biochem. Physiol.* **1959**, *37* (8), 911-7 https://doi.org/10.1139/o59-099.

(163) Calderón, C.; et al. Comparison of Simple Monophasic versus Classical Biphasic Extraction Protocols for Comprehensive UHPLC-MS/MS Lipidomic Analysis of Hela Cells. *Anal. Chim. Acta* **2019**, *1048*, 66-74 https://doi.org/10.1016/j.aca.2018.10.035.

(164) Matyash, V.; et al. Lipid Extraction by Methyl-Terf-Butyl Ether for High-Throughput Lipidomics. In *Journal of Lipid Research*; 2008; 49 (5), 1137-1146 https://doi.org/10.1194/jlr.D700041-JLR200.

(165) Raetz, M.; et al. SWATH-MS for Metabolomics and Lipidomics: Critical Aspects of Qualitative and Quantitative Analysis. *Metabolomics*. **2020**, *16*(6), 71 https://doi.org/10.1007/s11306-020-01692-0.

(166) Tsugawa, H.; et al. MS-DIAL: Data-Independent MS/MS Deconvolution for Comprehensive Metabolome Analysis. *Nat. Methods* **2015**, *12* (6), 523-6 https://doi.org/10.1038/nmeth.3393.

(167) Burla, B.; et al. MS-Based Lipidomics of Human Blood Plasma: A Community-Initiated Position Paper to Develop Accepted Guidelines. *J. Lipid Res.* **2018**, *59* (10), 2001-2017 https://doi.org/10.1194/jlr.S087163.

(168) Wong, M. W.; et al. The Application of Lipidomics to Biomarker Research and Pathomechanisms in Alzheimer's Disease. *Current Opinion in Psychiatry*. **2017**, *30* (2), 65-68 https://doi.org/10.1097/YCO.0000000000000303.

(169) Wong, M. W.; et al. Dysregulation of Lipids in Alzheimer's Disease and Their Role as Potential Biomarkers. *Alzheimer's and Dementia*. **2017**, *13* (2), 196-197 https://doi.org/10.1016/j.jalz.2017.01.008.

(170) Solomon, A.; et al. Serum Total Cholesterol, Statins and Cognition in Non-Demented Elderly. *Neurobiol. Aging* **2009**, *30* (6), 1006-1009 https://doi.org/10.1016/j.neurobiolaging.2007.09.012.

(171) Marquer, C.; et al. Local Cholesterol Increase Triggers Amyloid Precursor Protein-Bace1 Clustering in Lipid Rafts and Rapid Endocytosis. *FASEB J.* **2011**, *25* (4), 1295-1305 https://doi.org/10.1096/fj.10-168633.

(172) He, X.; et al. Deregulation of Sphingolipid Metabolism in Alzheimer's Disease. *Neurobiol. Aging* **2010**, *31* (3), 398-408 https://doi.org/10.1016/j.neurobiolaging.2008.05.010.

(173) Han, X.; et al. Metabolomics in Early Alzheimer's Disease: Identification of Altered Plasma

Sphingolipidome Using Shotgun Lipidomics. *PLoS One* **2011**, *6* (7), e21643. https://doi.org/10.1371/journal.pone.0021643.

(174) Whiley, L.; et al. Evidence of Altered Phosphatidylcholine Metabolism in Alzheimer's Disease. *Neurobiol. Aging* **2014**, *35* (2), 271-278https://doi.org/10.1016/j.neurobiolaging.2013.08.001.

(175) Wood, P. L.; et al. Targeted Lipidomics of Fontal Cortex and Plasma Diacylglycerols (DAG) in Mild Cognitive Impairment and Alzheimer's Disease: Validation of DAG Accumulation Early in the Pathophysiology of Alzheimer's Disease. *J. Alzheimer's Dis.* **2015**, *48* (2), 537-546 https://doi.org/10.3233/JAD-150336.

(176) Mapstone, M.; et al. Plasma Phospholipids Identify Antecedent Memory Impairment in Older Adults. *Nat. Med.* **2014**, *20* (4), 415-8 https://doi.org/10.1038/nm.3466.

(177) Kao, Y. C.; et al. Lipids and Alzheimer's Disease. *International Journal of Molecular Sciences.* **2020**, 21(4), 1505 https://doi.org/10.3390/ijms21041505.

Part II

Development and application of analytical methods for in vitro characterization of new potential MTDLs

II-a

Application of a High Throughput Luminescent Assay for Screening Synthetic or Natural Glycogen Synthase Kinase-3β Dual Inhibitors

Assay principle. In view of developing methods to select HIT compounds towards the main targets involved in the first stage of AD pathogenesis, the *section **a** of the **part II*** of the present Ph.D. thesis focused on the optimization and application of an *in vitro* high-throughput luminescent assay based on the Kinase-Glo™ system for screening GSK-3β inhibitors.

The growing need for a simple, fast and cheaper assay capable of analysing compound libraries in efficient way, and in line with the principles of "High throughput screening" (HTS) has led to the development of the Kinase luminescence assay Glo ™. An ideal HTS assay should be homogeneous, non-radioactive, have relatively short read times, and it must be applicable to different types of kinases, even those using multi-phosphorylated substrates. All protein kinases use ATP as a phosphate donor substrate, which is therefore consumed during the reaction.

Kinase-Glo ™ luminescence assay is based on the measure of the ATP amount left in solution once the kinases have completed the reaction. ATP is quantified by measuring the intensity of luminescence. The luminescence signal is generated after the mono-oxygenation of luciferin substrate by the enzyme luciferase in the presence of Mg2 +, ATP and an oxygen molecule. The luciferase-luciferin reaction consumes one molecule of ATP and produces one photon for each molecule of mono-oxygenated luciferin. The luminescence signal is proportional to the amount of ATP present in solution and inversely proportional to the kinase activity. It is a homogeneous, non-radioactive assay suitable for testing both ATP-competitive and non-competitive GSK-3β inhibitor.

Protocol Kinase-Glo assays are performed in assay buffer containing 50 mM 4-(2-hydroxyethyl)-1-piperazineethanesulfonic acid (HEPES) (pH 7.5), 1 mM ethylenediaminetetraacetic acid (EDTA), 1 mM ethylene glycol tetraacetic acid (EGTA), and 15 mM magnesium acetate. Briefly, in a typical assay, that is executed in white 96-well plates, 10 µL of test compound (dissolved in dimethyl sulfoxide [DMSO] at 1 mM concentration and diluted in advance in buffer to the desired concentration) and 10 µL (20 ng) of enzyme are added to each well in the presence of 20 µL of assay buffer containing GSM substrate and ATP in order to reach a 25 µM and 1 µM final concentration respectively. The final DMSO concentration in the reaction mixture has not to exceed 1%. After a 30 min of incubation at 30°C the enzymatic reaction is stopped with 40 µL of Kinase-Glo reagent. Glow-type luminescence is recorded after 10 min using a multimode plate reader. The activity is proportional to the difference between the total and consumed ATP. The inhibitory activities are calculated on the basis of maximal kinase (average positive) and luciferase activities (average negative) measured in the absence of inhibitor and in the presence of reference compound inhibitor (SB415286 Merck Millipore, IC_{50} = 55 nM)[1] at total inhibition concentration (5 µM). The linear regression parameters are determined and the IC_{50} extrapolated [2]

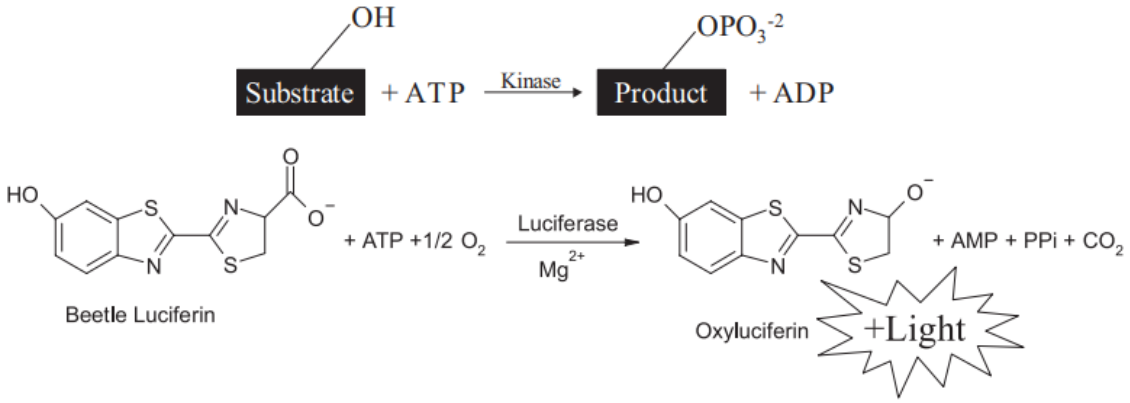

Figure *2*-**1** Assay principle of the Kinase-Glo luminescent kinase assay [2]

2. Characterization of the First-in-Class GSK-3β/ HDAC Dual Inhibitors

2.1 Aim of the work

Several connections between GSK-3β and HDACs have been highlighted. D'Mello and co-workers have shown that the neurotoxic effects of HDAC1 depend on GSK-3β activity, and in turn, the GSK-3β inhibition prevents HDAC1- induced neuronal death in cerebellar granule neurons (CGNs).[3] In hippocampal neurons, GSK-3β and HDAC6 were found in the same protein complex in which GSK-3β phosphorylates HDAC6 enhancing in this way its activity, and the up-regulation of HDAC6 increases tau phosphorylation.[4] Furthermore, it was demonstrated that both GSK-3β and class I–II HDAC inhibitors acts on microglia promoting their anti-inflammatory phenotype. Moreover, it was discovered that the contemporary inhibition of these enzymes produces a greater neuroprotective effect in comparison than the use of single drug specific for one target. Based on the above considerations, the Medicinal Chemistry group supervised by Professor Andrea Milelli at *Department for Life Quality Studies*, of the University of Bologna designed the First-in-Class GSK-3β/ HDAC dual Inhibitors. During the compounds characterization towards targets and the evaluation of their biological effects, the focus of the pharmaceutical analytical group was the application of the *in vitro* high-throughput luminescent assay to assess compounds activity against the enzyme GSK-3β.[5]

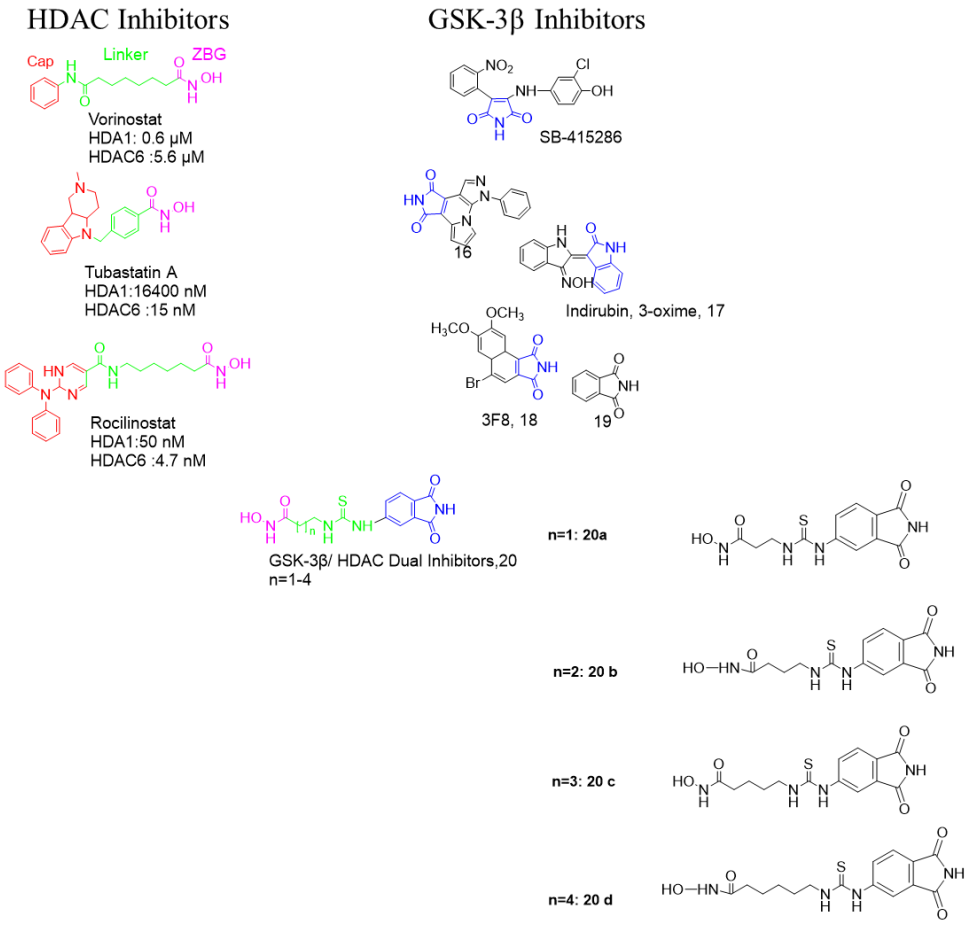

Figure *2.1*-**1** Drug design strategy leading to GSK-3β/ HDAC dual Inhibitors

2.2.1 Design

In order to design dual HDACs/GSK-3β inhibitors, the pharmacophoric groups responsible for binding to GSK-3β and HDACs were combined in a single chemical entity (fig. 2.1-**1**). Looking at known HDAC inhibitors, it was possible to identify some pharmacophore features: the hydroxamic acid as ZBG to chelate the Zn^{2+} located in HDACs active site, an aromatic moiety, named cap group, which occludes the entrance of the pocket, and a linker connecting the two moieties. Particularly, polycyclic aromatic compounds are quite selective toward HDAC6, due to the larger substrate binding pocket. Concerning GSK-3β, many inhibitors, as the aryl-maleimide or the aryl-pyrrolinone, which are known to be able to competitively bind to the ATP binding site of the enzyme, are characterized by a phthalimide-like scaffold. Starting from these findings, a small series of molecules containing both a hydroxamic acid as ZBG and the phthalimide moiety as cap group were designed. The hydroxamic acid has been connected to the phthalimide moiety through polymethylenic linker of different lengths (n=1-4), adding also a thiourea group. The choice of the thiourea group, among several connecting units, was done in view of its synthetic accessibility. The resulted rather large aromatic moiety might possibly fit in both HDAC1 and HDAC6 and bind the GSK-3β enzyme.

2.2.2 GSK-3β Inhibition in Vitro Sssay

Human recombinant GSK-3β, pre-phosphorylated polypeptide substrate and white 96-well plates were purchased from Millipore (Millipore Iberica S.A.U.). Kinase-Glo Luminescent Kinase Assay was obtained from Promega (Promega Biotech Iberica, SL). Adenosinetriphosphate (ATP) and all other reagents were from Sigma-Aldrich. Assay buffer contained 50 mM 4-(2-hydroxyethyl)-1- piperazineethanesulfonic acid (HEPES) (pH 7.5), 1 mM ethylenediaminetetraacetic acid (EDTA), 1 mM ethylene glycol tetraacetic acid (EGTA), and 15 mM magnesium acetate. The in solution experiments for GSK-3β inhibition analysis were performed by following the method developed by Baki et al.[2]

2.2.3 HDACs Activity Assay

The assays were carried out as reported in literature.[6]

2.2.4 Western Blotting Analysis and Antibodies for Immunoblotting

SH-SY5Y cells were washed with cold 1X PBS and were lysed using a lysis buffer (50 mM Tris–HCl pH 8.0, 150 mM NaCl, 1% NP-40, 10 mM NaF, 0.1 mM Na3VO4), supplemented with 40 μg/ml phosphatase and protease inhibitors (Sigma). Cells were then centrifuged at 13000 rpm for 15 min at 4°C, and the protein concentration of supernatant was determined by colorimetric assay (Biorad, Italy). Cell extracts were diluted

1:1 in sample buffer 2X Laemmli (0.217 M Tris-HCl pH 8.0, 52.17% SDS, 17.4% glycerol, 0.026% bromo-phenol blue, 8.7% beta-mercaptoethanol), and then boiled for 3 minutes. Equal amounts of protein (50 μg) were run and separated by SDS-PAGE gel (acrylamidegel). The primary antibody used was Monoclonal Anti-Acetylated Tubulin (SIGMA), diluted 1:1000; anti-ERK1 antibody (Santa Cruz Biotechnology) was used for normalization. Primary antibodies were detected using horseradish peroxidase-linked anti-mouse or anti-rabbit (Amersham Biosciences), conjugates as appropriate and visualized using the ECL detection system (Amersham Biosciences).

2.2.5 Histone Extraction

SH-SY5Y cells were harvested and washed twice with cold 1X PBS and lysed in Triton extraction buffer (TEB: PBS containing 0.5% Triton X-100 (v/v), 2 mM PMSF, 0.02% (w/v) NaN_3) at a cellular density of 107 cells per mL for 10 min on ice, with gentle stirring. After a brief centrifugation at 2000 rpm at 4°C, the supernatant was removed and the pellet was washed in half the volume of TEB and centrifuged as before. The pellet was suspended in 0.2 N HCl at a cell density of 4 × 107 cells per mL and acid extraction was left to proceed overnight at 4°C on a rolling table. Next, the samples were centrifuged at 2000 rpm for 10 minutes at 4°C, the supernatant was removed and protein content was determined using the Bradford assay. The primary antibody used was against acetylated histone H3 on lysine 9 and 14 (Diagenode). Anti H4 antibody (ABCAM) was used for normalization. Primary antibodies were detected using horseradish peroxidase-linked anti-mouse or anti-rabbit (Amersham Biosciences), conjugates as appropriate and visualized using the ECL detection system (Amersham Biosciences).

2.2.6 Tau Phosphorylation Determination

Cell Culture and Neuronal Differentiation. SH-SY5Y cells were maintained in DMEM/F12 medium supplemented with 15% fetal bovine serum, 1% nonessential amino acids, 2 mM L-glutamine, and penicillin/streptomycin in a humidified atmosphere (5% CO_2) at 37 °C. For neuronal differentiation, cells were seeded with a defined medium, containing 1% FBS, 2 mM L-glutamine and 5 μM retinoic acid for seven days.

Pharmacological Treatments. Copper was added to the concentration of 400 μM (in water), based upon dosing studies to find a great induction of tau phosphorylation.[7] SH-SY5Y differentiated were treated with Copper for different times (6, 16 and 24 h). Time-course experiments revealed 16 h as the optimal time of incubation. SHSY-5Y differentiated cells were pre-treated with DMSO (as control) and with the compounds for 1 h, before copper incubation for 26 h. The GSK3β inhibitor LiCl was used at 10 mM as a reference control.[8]The compounds were used at the concentration of 10 μM. At the end of the treatment period, cells were harvested by scraping and the pellet was obtained. Each pellet was suspended in 200 μL of Lysys Buffer with Protease inhibitors,[9] [10] and protein concentration were determined by Bradford assay.

Detection of Phospho-Tau. Phosphorylated tau was detected in SH-SY5Y differentiated cells using an immunoenzymatic assay. Briefly, wells were pre-coated overnight at room temperature with a full length

antibody to tau (sc32274, Santa Cruz Biotechnology), and non-specific sites were blocked using bovine serum albumin (BSA) 14 for 2 h at 37 °C. Pellet (30 μg/100 μL) were captured on wells for 2 h at 25 °C. Purified recombinant protein standards of phospho-tau were assayed in parallel to generate a standard curve. After extensive washing, the samples were probed with a rabbit polyclonal antibody to phospho-tau (Fitzgerald, 70R-32555) and subsequently with an anti-rabbit-HRP antibody. The wells were then washed three times with phosphate buffered saline containing 0.01% Tween 20 (PBS-T), before adding the enzyme substrate 3,3′,5,5′-tetramethylbenzidine (TMB, Thermo Scientific) and leaving the colour to develop for 30 min at room temperature. Absorbance values at 450 nm.

Toxicity and Protection Assays in SH-SY5Y Cell Line

Cell Viability Assay. SH-SY5Y cells (70–75% confluent) were incubated with compound 20d, compound 19 that has the maleimide moiety responsible for GSK-3β inhibition, Vorinostat that is a known HDAC inhibitor and Retinoic Acid (RA) at the concentrations of 0.1 – 10 μM for 24 and 72 h at 37 °C. Cell viability was evaluated by the MTS assay using the CellTiter 96 AQueous One Solution Cell Proliferation Assay kit (Promega). The assay is based on the cleavage of the yellow tetrazolium salt [3-(4,5-dimethylthiazol-2-yl)-5-(3- carboxymethoxyphenyl)-2-(4-sulfophenyl)-2H-tetrazolium] to 15 purple formazan crystals by metabolically active cells. The absorbance at 490 nm was measured in Readwell Touch ELISA Plate Analyzer (Robonik). Cells were seeded on 96-well plates at a density of 10.000 cells/well. The day after, the cells were treated with the desired concentration of compound in presence or absence of H_2O_2 at the chosen concentrations and incubated for 24 or 72 h. At every time point, MTS assay was performed following the manufacture's instruction.

Phase-Contrast Images. In order to check the capability of the compounds to induce neurogenesis, phase contrast photos were taken after 72 h. Briefly, cells were seeded on glass coverslips in 6-well plates at a density of 50.000 cells/well in complete medium and left to adhere for 24 h, then medium was changed with 0% FBS medium and treatments were performed. After 72 h cells were photographed in phase contrast at a 20x magnification.

RNA Extraction and Real-time Polymerase Chain reaction (RT-PCR) Total RNA was extracted (GeneAll Hybrid-RTM miRNA, TemaRicerca S.r.l., Castenaso, BO, Italy) according to the manufacturer directions. RNA was quantified by measuring the absorbance at 260 nm and purity was determined by valuating the absorbance 260/280 nm ratio. The absorbance was measured with an IMPLEN P330 nanophotometer (Carlo Erba, Milan, Italy). cDNA was synthesized using the 1st Strand cDNA Synthesis System for Quantitative RT-PCR (TemaRicerca S.r.l.) with random hexamers. The primers used for PCR are listed in Table 1. PCR was performed with Thermo Scientific Luminaris Color HiGreen qPCR Master Mix (Life Technologies, Milan, Italy) following the product protocol (annealing temperature 60 °C) on instrumentation Thermo Scientific PikoReal 96 (Life Technologies). Measurements were performed in triplicates, and results were analysed by

Thermo Scientific PikoReal Software 2.2. (Life Technologies). using the 2−[[Ct method for relative quantification. Briefly, Ct of gene of interest was16 subtracted by the correspondent Ct of housekeeping gene (GAPDH) obtaining Ct value. The Ct value of every treatment was subtracted by the Ct value of the control obtaining Ct, at the end 2−[[Ct was calculated and plotted.

Western Blotting Analysis in SH-SY5Y Cells. SH-SY5Y cells were seeded on 6-well plates at a concentration of 5×10^5 cells/well and treated with H_2O_2 at 50 μM with or without compound 4 at 10 μM for 24 h at 37 °C. At the end of the treatment the cells were collected with Trypsin/ EDTA, centrifuged for 10 min at 1100 rpm and the pellet was lysed in RIPA Buffer plus 10% of protease inhibitor cocktail. Protein concentration was measured by Bradford assay (Life Technologies). Forty micrograms of total proteins were diluted in Bolt® LDS Sample Buffer (Life Technologies), added with Bolt® Sample Reducing Agent (Life Technologies) and heated at 95 °C for 5 min. Samples and molecular weight markers were separated on Bolt™ 4–12% Bis-Tris Plus Gels and transferred to PVDF membrane using the iBlot® 2 Gel Transfer Device (Life Technologies). After a blocking step using NFDM 5% in PBS 1x plus Tween – 20 0.1% for 2 h at room temperature, blots were washed three times in PBS and the membranes were incubated overnight at 4 °C with mouse anti p53 Monoclonal Antibody (DO-1) (Life Technologies) at the appropriate dilution (1:1000). The next day blots were washed with PBS 1x plus Tween – 20 0.1% and reacted with the secondary antibody goat anti – mouse HRO conjugated diluted 1:5000 (Bethyl Laboratories, Montgomery, AL, USA) for 1 h. Membranes were washed again for three times with PBS 1x plus Tween – 20 0.1% and immunocomplexes were visualized using the enhancing chemiluminescence detection reagent Luminata Crescendo (Millipore, Merck Group, Milan, Italy), digital scansions were obtained with Alliance 9.7 system (UVItec Limited, Cambridge, UK). To determine the equal loading of samples per lane, at the end of each experiment the blots were stripped with ReBlot Plus Strong Antibody Stripping Solution (Merck S.p.a., Vimodrone, MI, Italy) and reprobed with rabbit anti – β-actin polyclonal antibody (Santa Cruz Biotechnology, Santa Cruz, CA, USA), according to manufacturer instructions. Each band was quantified with UVIBAND Image quantification software (UVItec Limited) and the protein expression was calculated as protein expression/β-actin expression ratio normalized for the control.

Neurotoxicity and Neuroprotection in Primary Neurons. Compounds neurotoxicity was evaluated on primary rat cerebellar granule neurons (CGNs), a reliable model for studying neuronal death and apoptosis.[11] [12]All animal experiments were authorized by a local bioethical committee (Protocol n° 17-72-2012) and performed in agreement with the Italian and European Community law on the use of animals for experimental purposes. Cerebella were removed, dissected from meninges and trypsinized. After mechanical dissociation, the cells were washed and plated on 96-well plates, previously coated with 10 mg/L poly-l-lysine at the density of 1.2×1^{05} cells/well in BME with 10% heat-inactivated FBS (Life Technologies), 2 mM glutamine (Sigma-Aldrich), 100 μM gentamicin sulfate (Sigma-Aldrich), and 25 mM KCl (Sigma-Aldrich). Sixteen hours later, 10 μM cytosine arabino-furanoside (Sigma-Aldrich) was added to avoid glial proliferation. After 7 days in vitro (DIV), differentiated neurons were exposed to compounds in serum-free BME medium at different

concentrations (ranging from 0 to 10 μM) for a 6-hour pre-treatment and 24 hour co-treatment with 20 μM 6-OHDA. Then, MTT assay was performed to evaluate cell viability.

Immunomodulation in primary microglial cells. Primary microglial cells were obtained from new born Wistar rat, as previously described.[13] Cerebral cortices were collected, dissected from meninges, trypsinized for 15 min at 37°C and mechanically dissected. The cells were washed, resuspended in Basal Medium Eagle (BME; Life Technologies Italia, Monza, Italy) with 10% heat-inactivated fetal bovine serum (Life Technologies), 2 mM glutamine (Sigma-Aldrich) and 100 μM gentamicin sulfate (Sigma-Aldrich) and plated on flasks (75 cm2, Corning) previously coated with poly-L-lysine (10 μg/ml; Sigma-Aldrich). One week later, microglial cells were harvested from mixed glial cell cultures by mechanical shaking, resuspended in serum-free BME, and plated on 35-mm diameter dishes at a density of 1.5 × 106 cells/2 ml medium/well. 30 minutes later, primary rat microglial cells were treated with increasing concentrations of the compounds (ranging from 0 to 50 μM) in presence of LPS 100 ng/mL, which induces microglial activation. Following 24h, cells were harvested and equal amount of protein were loaded on a SDS-PAGE for western blot analysis.

Western Blot Analysis in microglial cells. Microglial cells were collected in Lysis Buffer (1 % SDS, 50 mM Tris pH 7,4, 1 mM EDTA, 10 μl/ml protease inhibitors and 10 μL/mL phosphatase inhibitors) and protein content was determined by the Lowry protein assay. Cell samples (15 μg total protein) were resuspended with 4X Loading Buffer (0.2 M Tris-HCl pH 6.8; 8 % sodium dodecyl sulfate; 40 % glycerol; 0.4 % bromophenol blue and 0.4 M dithiothreitol; Sigma-Aldrich) and loaded into 10 % sodium dodecyl sulfate-polyacrylamide gels (SDS-PAGE; Bio-Rad). After electrophoresis and transfer to nitrocellulose membranes (GE Healthcare, Milano, Italy), membranes were blocked for 1 h in blocking solution (PBS-0.1 % Tween20 (Sigma-Aldrich), 4 % non-fat dried milk (Bio-Rad) and incubated overnight at 4 °C with primary antibodies in PBS-0.1 % Tween-20. Primary antibodies used were anti-iNOS, anti-MRC1, antiTREM2 and anti-GAPDH (all 1:1000 dilution except for anti-GAPDH used 1:20000 dilution, all from Santa Cruz Biotechnology). Membranes were then incubated with specific secondary antibodies conjugated to horseradish peroxidase (goat anti-rabbit and goat anti-mouse, both at 1:2000 dilution and from Santa Cruz), for 90 minutes at room temperature in PBS-0.1% Tween-20. Labeled proteins were visualized by using the ClarityTM Western ECL Substrate (Bio-Rad) and detected using BioRad Image Lab software with a ChemiDoc™ MP imaging system (Bio-Rad).

In Vivo Activity on Zebrafish Embryos. Wt zebrafish were used to test *in vivo* activity of molecule 11; animals were maintained as described earlier. Ages of embryos are expressed as hours post fertilization (hpf). The embryos were collected and placed into 24-well plates, at least 10 embryos per well, maintained in E2 medium at ∼28 °C. Compound was added 5 hpf (50% epiboly) and the embryos allowed to grow in chemical compound solution up to 2-4 days. The phenotypes were compared using the microscope system from Carl Zeiss at 44−48 hpf.

Animal Husbandry. All animal experiment were conducted and documented according to the local regulation. All embryo testing was stopped at day 5 of embryonic development.

Statistical analysis .Graph-Pad Prism (GraphPad Software Inc., San Diego, CA) was used for data analysis and graphic presentations. All data are presented as the mean ± SEM. One-way analysis of variance (ANOVA)with Bonferroni's corrected t-test for post-hoc pair-wise comparisons was used to perform statistical analysis.

2.3 Results and Discussion:

2.3.1 In Vitro Enzymes Inhibition

Compounds 20 a−d were characterized in parallel for their ability to inhibit GSK-3β, HDAC1, and HDAC6. All the new synthesised compounds resulted able to inhibit the activity of the three enzymes in the low micromolar range of concentration. As reported in table 2.3.1 -**1**, an interesting trend can be defined for compound 20d, that resulted more active than compounds 20a, 20b, 20c and 19 against GSK-3β. Compound 20d proved to be also the most active inhibitor of HDAC6 of the series with an IC_{50} similar to that of Vorinostat (3.19 ± 0.08 vs 5.6 μM), and the inferior homologues are characterized by lower IC_{50} values (20d < 20b < 20c < 20a).

Compound	n	GSK-3β (μM)[a]	HDAC 1 (μM)[a]	HDAC 6 (μM)[a]
Vorinostat		n.a.[b]	0.6(0.31-3.22)[c,d]	5.6(5.31-7.45) [c,d]
SB-415286		0.05 ± 0.01	n.d.[e]	n.d. [e]
20a	1	19.96 ± 1.76	3.75 ± 0.58	18.13 ± 0.17
20b	2	9.85 ± 1.00	2.24 ± 1.17	12.58 ± 0.96
20c	3	4.11 ± 0.01	5.02 ± 1.2	14.71 ± 0.19
20d	4	2.69 ± 0.01	12.78 ± 0.11	3.19 ± 0.08
19		20.22 ± 0.40	n.a.[f]	n.a. [f]

Table *2.3.1* -**1** Compounds 20a−d activity towards GSK-3β, HDAC1, and HDAC6

[a] IC_{50} values are defined as the drug concentration that reduces by 50% the target activity and are reported as a mean value of three or more determinations. [b] n.a.: not active up to 50 μM. [c] Data from ref 25. [d] 95% confidence interval. [e] Not determined. [f] Not active up to 30 μM.[5]

On the contrary, compound 20d is the weakest inhibitor within the series against HDAC1, while compound 20b resulted the most active (IC_{50} 2.24 ± 1.17 vs 12.78 ± 0.11 μM of 20d). These effects are related to the length of the linker between the hydroxamic acid and the phthalimide moieties.

Finally, it is important to note that Vorinostat is not active against GSK-3β and compound 19 with maleimide moiety is not active against HDACs.

For this reason, compound 20d has been selected for a deeper biological investigation due to its high activity against GSK-3β and the two HDAC isoforms. Interestingly, it showed balanced *in vitro* activities against the targets.

2.3.2 Binding Mode Analysis

To gain insights into the mechanism of dual GSK-3β/HDAC inhibition and to elucidate the binding mode of the most active compound 20d, molecular docking calculations were performed using Glide 5.7 in SP mode. As for GSK-3β, an ensemble docking using four representative structures (PDB codes: 1Q3D, 1Q41, 2JLD, 1UV5) suggested two possible binding modes. In binding mode A (fig. 2.3.2-**1**), the maleimide core forms the two typical H-bonds with the hinge region backbone residues V135 and D133, and the thiourea H-bonds, the Q185 backbone carbonyl, and the long aliphatic linker allow the hydroxamic moiety to reach a really polar region of the protein where a deprotonated hydroxamic acid establishes two charge-reinforced H-bonds with the R144 and R141 side chains. On the contrary, in binding mode B (fig.2.3.2-**1**), the hydroxamic acid is found under the nucleotide-binding loop. Looking at the 20 a-d inhibitor profiles in table 2.3.1 -**1**, it is evident that more the linker is shorter lower is the activity, and only the binding mode A seems to be in accordance with this evidence. As regards the docking of 20d into the HDAC1 and HDAC6 [1415]it converged toward a very similar pose in both isoforms (fig. 2.3.2-**1** c, d, respectively), where the hydroxamic acid coordinates the zinc ion and H-bonds a conserved tyrosine (Y303 in HDAC1, Y782 in HDAC6); the aliphatic spacer is found in the acetyl lysine tunnel stacked between two conserved aromatic side chains (F150 and F205 in HDAC1; F620 and F680 in HDAC6). The thiourea forms a bifurcated H-bond with the side chains of D99 in HDAC1 and of S538 in HDAC6, the phthalimide contacts a conserved histidine (H28 in HDAC1, H500 in HDAC6) and H-bonds the E98 in HDAC1 and the D497 in HDAC6. Reasonably, the better accommodation of the phthalimide into the larger HDAC6 substrate binding pocket can explain the superior activity of 20d toward HDAC6 with respect to HDAC1.

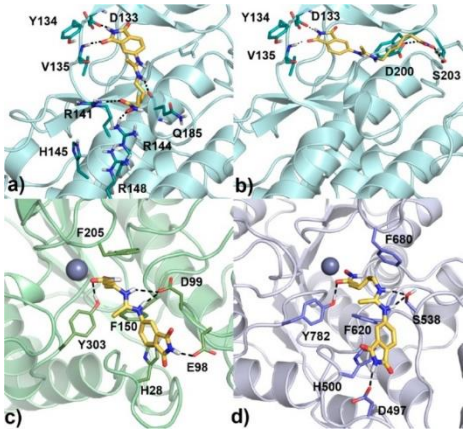

Figure *2.3.2*-**1** Binding modes A (a) and B (b) of 20d (golden sticks) in the active site of GSK-3*β* shown as a cyan cartoon and deep teal sticks. Binding poses of compound 20d into the HDAC1(c;green cartoon) and HDAC6(d; violet cartoon) catalytic domains. H-bonds are represented as black dashed lines [5]

2.3.3 In-Cell Evaluations

In order to evaluate whether the *in vitro* inhibitory activities translate into intracellular inhibition of HDACs, further in-cell-based assays for compound 20d were carried out. Western blotting analysis was performed using human neuroblastoma SH-SY5Y cell line to determine the effects of compound 20d on the acetylation levels of tubulin and histone H3 at lysines 9/14 (H3K9K14ac) (fig. 2.3.3-**1**-a). Cells were treated with compound 20d and its parent compounds, Vorinostat and compound 19 (5 μM), for 30 h at three different concentrations (0.1, 1.0, and 5.0 μM). Compound 20d was able to induce hyperacetylation of α-tubulin although to a lesser extent than Vorinostat. This effect was already visible at 0.1 μM and was concentration dependent. However, it was not able to induce similar increase in the acetylation of histone H3, not even at the highest concentration tested. Since tubulin is a substrate of HDAC6 and acetylated tubulin levels function as a biochemical marker for HDAC6 cellular activity, the increase in the level of acetylα-tubulin compared to H3K9K14ac could be ascribed to an intrinsic cellular selectivity of compound 20d for HDAC6 isoform. Important effects on tubulin and histone H3 were not observed when cells were treated with 19. Then, to assess the effect of compound 20d on tau hyperphosphorylation, the protein's phosphorylation was induced in differentiated SH-SY5Y cells upon incubation with copper. Copper induced a time-dependent tau phosphorylation in differentiated SH-SY5Y cells, with a peak after 16 h of incubation. Conversely, the level of tau phosphorylation returned to control cell value after 24 h of incubation, probably due to compensatory mechanisms. Based on these data, 400 μM copper for 16 h was chosen as experimental conditions. Following, the ability of the compounds to counteract copper-induced tau phosphorylation was examined. LiCl was used as reference control (fig.2.3.3-**1**b). As reported, compound 20d (10 μM) completely counteracted copper mediated tau phosphorylation in a major extent compared to LiCl (10 mM), 19, and Vorinostat (10 μM). Also, the cells were treated with a combination of Vorinostat and 19, and no significant additive/ synergic effect on phospho-tau levels was noticed with respect to single-treated cells (figure 2.3.3-**1**b). Moreover, the percentage of phospho-tau inhibition was markedly lower with respect to that elicited by the dual-target compound 20d. These data suggest that a dual-target molecule may offer advantages in terms of pharmacokinetics and cellular localization that enable an enhancement of its efficacy. Since HDAC inhibitors are used in therapy as anticancer drugs, compound 20d was evaluated for its potential toxicity in SH-SY5Y cell line in comparison to compound Vorinostat and 19 using MTS assay (fig. 2.3.3-**1**c). Compound 20d did not show any toxic effects up to 100 μM. Furthermore, Vorinostat and compound 19 and 20d were tested for their ability to counteract oxidative stress-induced neuronal death (fig. 2.3.3-**1**d).

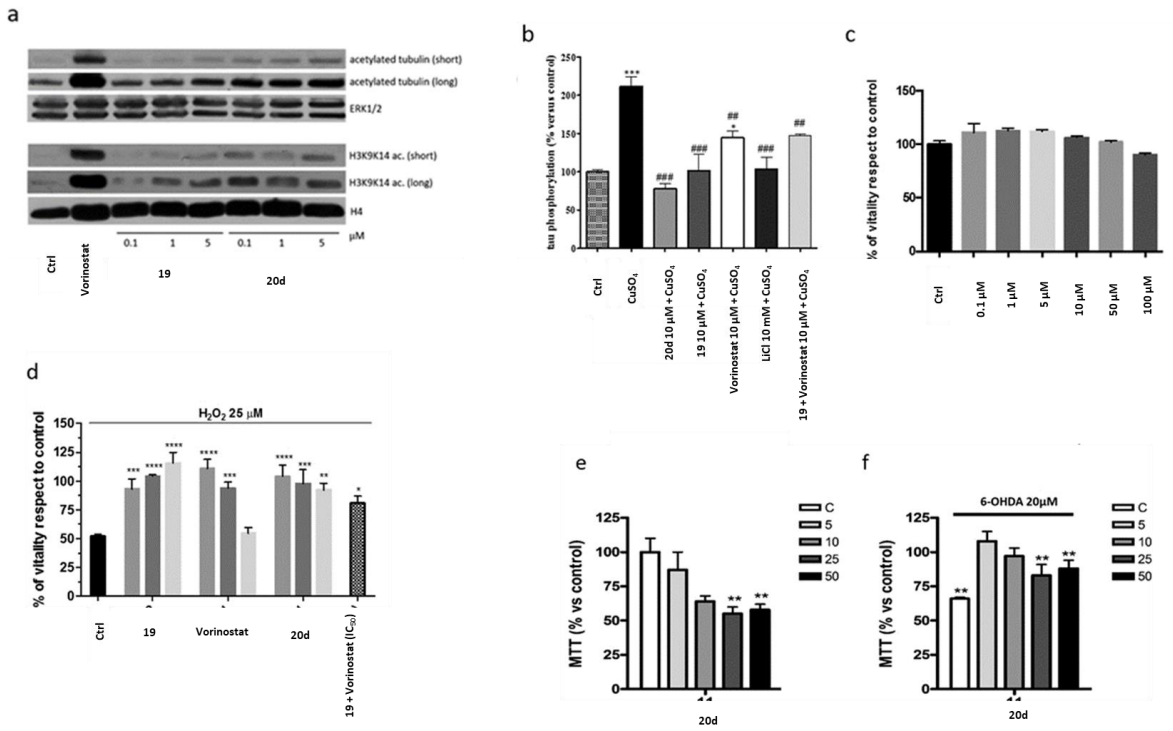

Figure *2.3.3*-**1** Cell-based assay

(a) Western blot probing for acetylated tubulin and histone H3K9K14ac in the SH-SY5Y cell line after 30 h treatment with Vorinostat, 20d, and 19. (b) Effects of the compounds on tau phosphorylation. The cells were pretreated with LiCl (10 mM), Vorinostat, 20d, and 19 (10 μM), or Vorinostat + 19 for 1 h and then with copper (400 μM) for 16 h. Following incubation time, cells were harvest by scraping, and the pellet was obtained. Subsequently, the extent of tau phosphorylation was determined by immunoenzymatic assay. Absorbance was measured at 450 nm. Values represent the mean ± SEM; *p < 0.05, ***p < 0.001 vs control; # p < 0.05, ##p < 0.01, ###p < 0.001 vs cells treated with copper. (c) Effect of compound 20d on SH-SY5Y cell viability after 24 h exposure at 37 °C by MTS assay. Data are expressed as % of vitality respect to control. (d) Effects of Vorinostat, 20d, and 19, and Vorinostat + 19 on SH-SY5Y challenged with H_2O_2. The effect of drugs (0.1−10 μM) on SH-SY5Y cells challenged for 24 h with H_2O_2 (25 and 50 μM) was evaluated by MTS assay. Data are expressed as % of vitality respect to control. *P < 0.05, **P < 0.005, ***P < 0.001, vs H_2O_2. (e,f) Neurotoxicity and neuroprotection on 6-OHDA-induced neurotoxicity in primary differentiated CGNs of compound 20d. Results are the mean ± SE of at least 3 different experiments in quadruplicate; **p < 0.01, ***p < 0.001 relative to untreated CGNs; ##p < 0.01, ###p < 0.001 relative to differentiated CGNs treated with 6-OHDA, Bonferroni's posthoc test following one-way ANOVA[5]

When Vorinostat and compounds 19 and 20d were administered, the viability was restored to almost the control value expected for Vorinostat. For compound 20d, this effect was evident already at the concentration of 0.1 μM. Cotreatment of Vorinostat + 19, at their respective IC_{50}s concentration, did not show any synergism in contrasting H_2O_2-induced cell death. Compound 20d turned out to be more efficient than this combination. To further elucidate the activity of compound 20d, the levels of p53 protein were measured after treatments with H_2O_2 in the presence or absence of compound 20d. Interestingly, in SH-SY5Y cells treated with H_2O_2 (50 μM), p53 expression increases about 30%, and the treatment with compound 20d (10 μM) restored the levels of p53 to control levels. Potential toxic and protective effects of compound 20d were also evaluated on primary differentiated CGNs, and it was found able to completely counteract toxic stimuli induced by 6-hydroxydopamine (6-OHDA) already at 5 μM (fig. 2.3.3-**1** (e,f)) . It is well-known that GSK-3β/HDAC inhibition promotes neurogenesis *in vitro* and *in vivo*. To assess whether compound 20d induces neurogenesis

in SH-SY5Y cell line, the cells were treated with compound 20d for 24 h, and at the end of the treatment, the mRNA expression of recognized markers of neurogenesis including GAP43, N-myc, and MAP-2 was assessed by RT-PCR analysis. The same experiments were performed by using Vorinostat and maleimide based compound (19), and retinoic acid (RA) as positive control (fi. 2.3.3-**2a)**. All the compounds were used at the concentration of 10 μM with the exception of Vorinostat, which was added at the final concentration of 1 μM based on the vitality assay results. All the treatments were able to up-regulate GAP43 and MAP-2, while N-myc was up-regulated by compound Vorinostat, compound 20d, and RA but not by compound 19. Compound 20d increased the expression of MAP-2 and GAP-43 at higher levels than Vorinostat. As expected, RA induced the expression of all the three markers. To confirm the obtained results, the morphology of the differentiated neuronal neurite outgrowth was assessed after cell treatment for 72 h with compounds 20d, 19, and RA (10 μM) used as positive control. As shown in figure 2.3.3-**3b**, compound 19 showed a moderate effect in stimulating neurite outgrowth, whereas compound 20d induced a substantial neurite outgrowth comparable to that caused by RA. It was not possible to analyse the effect of Vorinostat due to compound toxicity after 72 h of treatment.

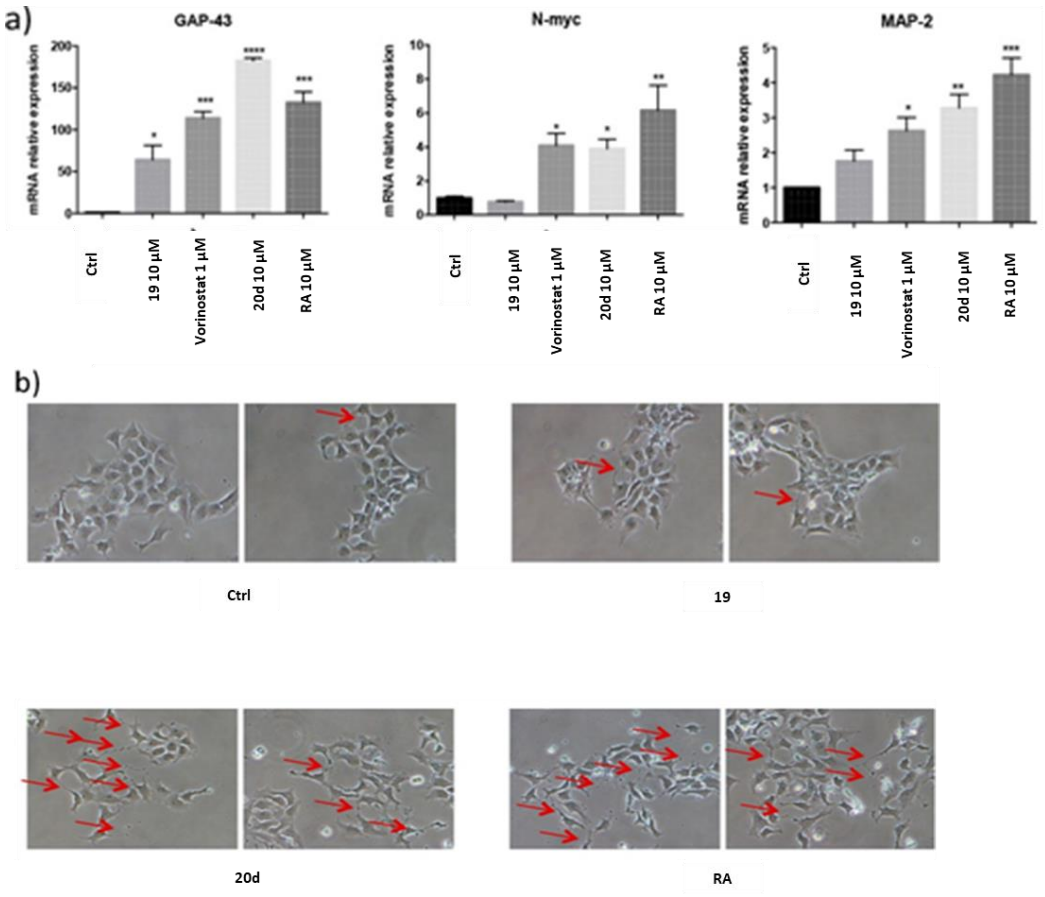

Figure *2.3.3*-**2** (a) Effect of 20d, 19, RA (10 μM), and Vorinostat (1 μM) on neurogenesis markers expression (GAP43, N-myc and MAP-2) in SHSY5Y after 24 h-treatment. The data are expressed as fold of control. (b) Effects of 20d, 19, RA (10 μM for 72 h) on neurite outgrowth. Red arrows indicate cells bearing neurites. Pictures were taken at 20× magnification[5]

Furthermore, the ability of Vorinostat, compound 19 and 20d to modulate the microglial phenotypic switch from the M1 (proinflammatory) to the M2 (anti-inflammatory) type thereby decreasing neuroinflammation was evaluated (Figure 2.3.3-**2**). Indeed, modulation of microglial activation seems to be a valid therapeutic approach in AD and compounds able to modulate the switch from the M1 to M2 phenotype would determine a decrease of neuroinflammation with a parallel increase of neuronal protection and recovery.[16] The immunomodulatory effects of Vorinostat, compound 19 and 20d were evaluated on pure primary cultures of microglia by evaluating the expression of NOS2 and MRC1, which are both markers of M1 microglia, or TREM2, marker of M2 microglia. Western blot analysis clearly shows a more evident decrease in both NOS2 and MRC1 expression in cells treated with the compound 20d than in those exposed to Vorinostat and 19, while TREM2 is unchanged, thus indicating a shift of microglial cells from the M1 neutotoxic to the M2 neuroprotective phenotype and therefore an immunomodulatory activity of compound 20d.

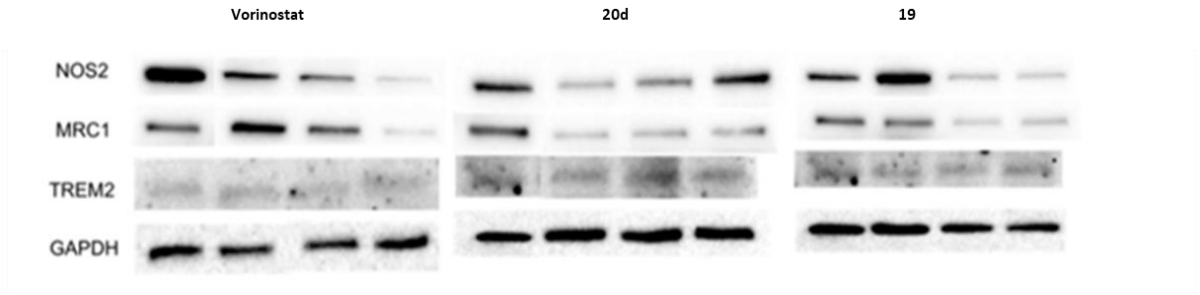

Figure *2.3.3*-**3** Western blot analysis of NOS2, MRC1, and TREM2 expression in primary microglial cells after a 24 h treatment with LPS in presence or absence of Vorinostat, compounds 20d and 19. GAPDH was used as an endogenous control to normalize data

2.3.4 In Vivo wt-Zebrafish Evaluation

Compound 20d was further characterized for its *in vivo* activity in wild-type zebrafish (Danio rerio) (fig. 2.3.4-**1**). Indeed, zebrafish represents an established model system for the *in vivo* validation of GSK-3β inhibitors and assessing drug safety and toxicity. The compounds were added to 5 hpf (50% epiboly), and the embryos were allowed to grow in chemical compound solution up to 2−4 days. Compound 20d showed no lethality in the concentration range (100 μM) Furthermore, it showed no effects on embryos at the concentration of 25 μM, while at the concentration of 50 μM a stunted and crooked tail was observed (fig. 2.3.4-**1**B). This phenotypic effect was more emphasized at 75 μM (fig. 2.3.4-**1**C). At this concentration, some effects on the eyes formation could be observed. The detected effects are consistent with an *in vivo* GSK-3β inhibition.[17] Indeed, the perturbed zebrafish development induced by compound 20d is correlated to the Wnt/β-catenin pathway including GSK-3β. Also, the zebrafish embryo assay provides evidence of exposure and cell penetration of our derivative.

Figure *2.3.4*-**1** Effects on wild-type zebra fish embryos by compound 20d.

A) Control embryo in 2% DMSO. B) Embryo treated with compound 20d at 50 μM. C) Embryo treated with compound 20d at 75μM

2.3.5 Physicochemical Properties of Compound 20d

One of the main challenges in designing multiple ligands is related to the physical−chemical properties of the designed molecules. Pleasingly, compound 20d is characterized by very good water solubility of 53.76 μg/mL (153.42 μM) and fulfills the requirements of the "Lipinski" rule.

2.4 Conclusions

In conclusion, the *in vitro* high-throughput luminescent assay based on the Kinase-Glo™ applied to characterize the novel series of the potential first-in-class GSK-3β/ HDAC dual inhibitors designed by the Medicinal Chemistry group at *Department for Life Quality Studies*, resulted suitable to investigate the activity of the new series of compound towards target GSK-3β, and it allowed to select compound 20d as the most active in the low micromolar range. The luminescent kinase assay gave more insights about the structure activity relationships, that are currently guiding hit-to-lead optimization studies. Thus, compound 20d might be considered a promising hit compound to develop an innovative disease-modifying agent, being active even towards HDAC1, HDAC6 and having suitable physicochemical properties *(*low molecular weight and high water solubility). Moreover, it has demonstrated to be nontoxic and protective against H_2O_2 and 6-OHDA stimuli in SH-SY5Y and in CGN cell lines, respectively and it was no lethality in a wt-zebrafish model (< 100 μM). In addition, it promotes neurogenesis and displays immunomodulatory effects.

References:

(1) Coghlan, M. P.; et al. Selective Small Molecule Inhibitors of Glycogen Synthase Kinase-3 Modulate Glycogen Metabolism and Gene Transcription. *Chem. Biol.* **2000**, *7* (10),793-803 https://doi.org/10.1016/S1074-5521(00)00025-9.

(2) Baki, A.; Bielik, A.; Molnár, L.; Szendrei, G.; Keserü, G. M. A High Throughput Luminescent Assay for Glycogen Synthase Kinase-3β Inhibitors. *Assay Drug Dev. Technol.* **2007**, *5* (1), 75-83 https://doi.org/10.1089/adt.2006.029.

(3) Bardai, F. H.; et al. Histone Deacetylase-1 (HDAC1) Is a Molecular Switch between Neuronal Survival and Death. *J. Biol. Chem.* **2012**, *287* (42), 35444-35453https://doi.org/10.1074/jbc.M112.394544.

(4) Xiong, Y.; et al. HDAC6 Mutations Rescue Human Tau-Induced Microtubule Defects in Drosophila. *Proc. Natl. Acad. Sci. U. S. A.* **2013**, *110* (12), 4604-4609 https://doi.org/10.1073/pnas.1207586110.

(5) De Simone, A.; et al. Discovery of the First-in-Class GSK-3β/HDAC Dual Inhibitor as Disease-Modifying Agent to Combat Alzheimer's Disease. *ACS Med. Chem. Lett.* 2019, 10 (4), 469–474 https://doi.org/10.1021/acsmedchemlett.8b00507.

(6) Giacomini, E.; et al. Novel Antiproliferative Chimeric Compounds with Marked Histone Deacetylase Inhibitory Activity. *ACS Med. Chem. Lett.* **2014**, *5* (9), 973–978 https://doi.org/10.1021/ml5000959.

(7) Cook, C.; et al. Acetylation: A New Key to Unlock Tau's Role in Neurodegeneration. *Alzheimer's Research and Therapy*. **2014**, *6* (3),29https://doi.org/10.1186/alzrt259.

(8) Wang, G.; et al. HDAC Inhibition Prevents White Matter Injury by Modulating Microglia/Macrophage Polarization through the GSK3β/PTEN/Akt Axis. *Proc. Natl. Acad. Sci. U. S. A.* **2015**, *112* (9), 2853-2858 https://doi.org/10.1073/pnas.1501441112.

(9) Leng, Y.; et al. Synergistic Neuroprotective Effects of Lithium and Valproic Acid or Other Histone Deacetylase Inhibitors in Neurons: Roles of Glycogen Synthase Kinase-3 Inhibition. *J. Neurosci.* **2008**, *28* (10), 2576-2588https://doi.org/10.1523/JNEUROSCI.5467-07.2008.

(10) Sharma, S.; Taliyan, R. Synergistic Effects of GSK-3β and HDAC Inhibitors in Intracerebroventricular Streptozotocin-Induced Cognitive Deficits in Rats. *Naunyn. Schmiedebergs. Arch. Pharmacol.* **2015**, *388* (3), 337–349 https://doi.org/10.1007/s00210-014-1081-2.

(11) Lehár, J.; et al. Synergistic Drug Combinations Tend to Improve Therapeutically Relevant Selectivity. *Nat. Biotechnol.* **2009**, *27* (7), 659–666 https://doi.org/10.1038/nbt.1549.

(12) Cuadrado-Tejedor, M.; et al. Defining the Mechanism of Action of 4-Phenylbutyrate to Develop a Small-Molecule-Based Therapy for Alzheimers Disease. *Curr. Med. Chem.* **2011**, *18* (36), 5545 – 5553 https://doi.org/10.2174/092986711798347315.

(13) Polazzi, E.; et al. Microglial Cells Protect Cerebellar Granule Neurons from Apoptosis: Evidence for Reciprocal Signaling. *Glia* **2001**, *36* (3), 271-280 https://doi.org/10.1002/glia.1115.

(14) Pandolfi, F.; et al. New Pyridine Derivatives as Inhibitors of Acetylcholinesterase and Amyloid Aggregation. *Eur. J. Med. Chem.* **2017**, *141*, 197–210. https://doi.org/10.1016/j.ejmech.2017.09.022.

(15) Hai, Y.; Christianson, D. W. Histone Deacetylase 6 Structure and Molecular Basis of Catalysis and Inhibition. *Nat. Chem. Biol.* **2016**, *12* (9), 741–747 https://doi.org/10.1038/nchembio.2134.

(16) Peña-Altamira, E.; et al. Contestabile, A.; Bolognesi, M. L.; Monti, B. Changing Paradigm to Target Microglia in Neurodegenerative Diseases: From Anti-Inflammatory Strategy to Active Immunomodulation. *Expert Opinion on Therapeutic Targets*. **2016**, *20* (5), 627-40

https://doi.org/10.1517/14728222.2016.1121237.

(17) Nishiya, N.; et al. A Zebrafish Chemical Suppressor Screening Identifies Small Molecule Inhibitors of the Wnt/β-Catenin Pathway. *Chem. Biol.* **2014**, *21* (4), 530-540 https://doi.org/10.1016/j.chembiol.2014.02.015.

3. Amaryllidaceae Alkaloids as Potential Glycogen Synthase Kinase-3β Inhibitors

3.1 Aim of the Work

Amaryllidaceae alkaloids are produced exclusively by plants of the Amaryllidaceae family and are characterized by polycyclic nitrogen-containing structures grouped in 12 types of rings. These species grow wildly in the tropical and subtropical regions of the world, but are widespread mainly in Andean South America, South Africa and the Mediterranean coasts.

In traditional medicine, the use of Amaryllidaceae plants dates back to the 4th century B.C., when Hippocrates of Cos used daffodil oil (i.e., *Narcissus poeticus* L.) for the treatment of uterine tumours. Today, Amaryllidaceae alkaloids are being studied for the treatment of drug resistant cancers. For instance, Pancratistatine, Narciclasine, Lycorine, Haemantamine, Distichamine and their derivatives are known for their cytotoxic activity on specific cancer cell lines, and some of them are even involved in different stages of drug development. Amaryllidaceae alkaloids have shown to inhibit other serine/threonine kinases involved in cancerogenesis,[1] but there are not yet studies concerning GSK-3β inhibition, although this enzyme has been found involved in resistant cancers to chemo-, radio-,and targeted therapy.[2] GSK-3β is as potential mediator in contributing to neoplastic transformation, in part because it belongs to the canonical Wnt/β-catenin and to the PI3K/Akt signaling systems, the two major pathways often dysregulated in cancer.[3] Starting from this evidence, it could be possible to think that Amaryllidaceae alkaloids could be active towards GSK-3β. At the same type, these natural compounds have already been used in the treatment of Alzheimer's disease (AD), given their acetylcholinesterase (AChE) inhibitory property. So that, Galantamine that is actually one of the few drugs currently approved by the FDA for the symptomatic treatment of cognitive decline in AD patients,

belongs to this family of natural compounds.[4] Given the pivotal role of GSK-3β in AD, the above mentioned findings guided the present project carried out in collaboration with the Department of Pharmaceutical Botany of the Charles University in Hradec Králové (Czech Republic). Cahlikova research group isolated 28 Amaryllidaceae alkaloids, from various Amaryllidaceous plants and the *in vitro* high-throughput luminescent assay was applied to screen their inhibitory potency against GSK-3β in view of discovery new potential natural scaffolds for AD MTDLs design.[5]

3.2 Materials and Methods

3.2.1 Amaryllidaceae Alkaloids All Amaryllidaceae alkaloids tested have been previously isolated at the Department of Pharmaceutical Botany, Faculty of Pharmacy in Hradec Králové from various Amaryllidaceae plant species (Zephyranthes robusta,[6 7] Chlidanthus fragrans,[8 9] Nerine bowdenii [10] Narcissus poeticus cv. Pink Parasol,[11] and N. poeticus cv. Brackenhurst[12]. The purity of all compounds (98%) was determined by 1H and 13C-NMR spectroscopy.

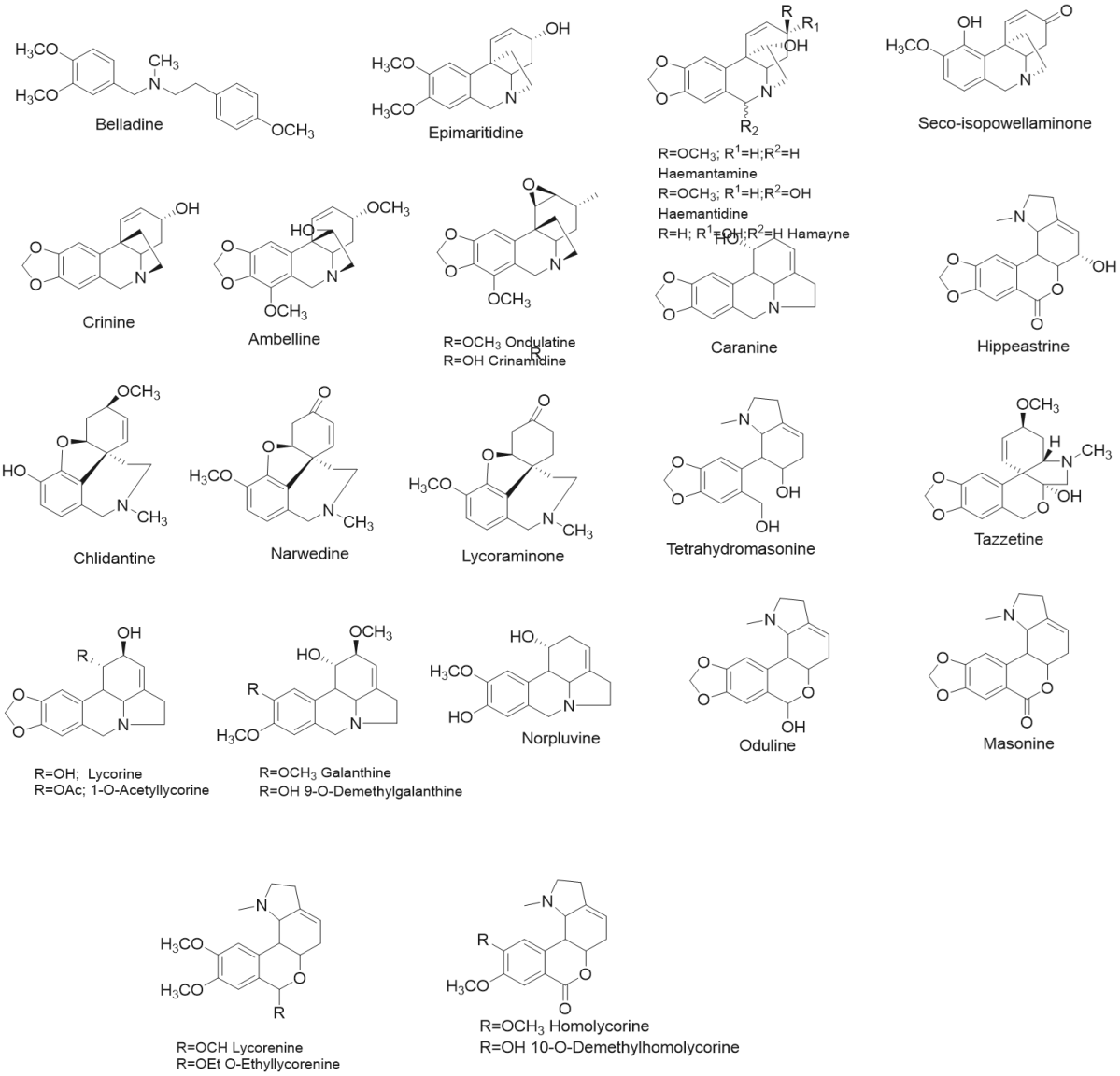

Figure *3.2.1*-**1** Structures of the Amaryllidaceae alkaloids isolated[5]

3.2.2 GSK-3β Assay

Kinase-Glo Kit was obtained from Promega (Promega Biotech Iberica, S.L., Madrid, Spain), and human recombinant GSK-3β and GSM substrate from Merck Millipore (Darmstadt, Germany). Adenosine 5-triphosphate (ATP) disodium salt hydrate, ammonium acetate, ammonium hydroxide, 4-(2-hydroxyethyl)piperazine-1-ethanesulfonic acid (HEPES), ethylene glycol-bis(-aminoethylether)-N,N,N,N-tetraacetic acid tetrasodium salt (EGTA), ethylenediaminetetraacetic acid (EDTA), dimethyl sulfoxide (DMSO), magnesium acetate tetrahydrate, formic acid, and 3-[(3-chloro-4-hydroxyphenyl)amino]-4-(2-nitrophenyl)-1H-pyrrol-2,5-dione were purchased from Sigma-Aldrich (St. Louis, MO, USA). The GSK-3β selective inhibitor SB-415286 ([3-(3-chloro-4-hydroxyphenylamino)-4-(2-nitrophenyl)-1H-pyrrole-2,5-dione]) was purchased from Selleck Chemicals (Houston, TX, USA). Ultrapure water was obtained using a Purite LTD water purification system (Thame, UK). The experiments were carried out using a Victor X3 multimode plate reader (Perkin Elmer, MA, USA).

GSK-3β activity and inhibition were studied according to the luminescent method of Baki et al. using a Kinase-Glo reagent kit.[13]

3.3 Results and Discussion

The best results in preliminary screening were demonstrated by alkaloids of the homolycorin- type. Most of the compounds that belong to this group showed at 50 μM to be able to inhibit more than 50% the GSK-3β activity. After preliminary screening, the most active compounds were selected for IC_{50} determination. The IC_{50} values of the selected alkaloids resulted in the micromolar range (around 30 μM) (figure 3.3-**1**). The highest GSK-3β inhibition potency has been demonstrated by two homolycorine-type Amaryllidaceae alkaloids, Masonine (IC_{50}; 27.81± 0.01 μM) and 9- O-demethylhomolycorine (IC_{50}: 30.00 ± 0.71 μM) , and one lycorine-type alkaloid Caranine (IC_{50}: 30.75 ± 0.04 μM) .The measurements were performed in triplicate and the values given are the average obtained after at least two measurements.

The low number of available homolycorine-type alkaloids precluded a detailed structure-activity relationship (SAR) study, but their general features can still be described. It seems that the presence of hydroxyl substitution at position 2, as in Hippeastrine (figure 3.2.1-**1**), is connected with a distinct reduction of GSK-3β inhibitory activity (10.65% of GSK-3β inhibition at 50 μM) compared with Masonine (66.0% of GSK-3β inhibition at 50 μM), 9-O-demethylhomolycorine (63.6% of GSK-3β inhibition at 50 μM), Oduline (57.7% of GSK-3β inhibition at 50 μM), and O-ethyllycorenine (57.7% of GSK-3β inhibition at 50 μM), where no substituent (e.g., hydroxy or methoxy group, etc.) in position C-2 is present. The opening of the tetrahydropyrane ring in Tetrahydromasonine (figure 3.2.1-**1**) also reduces the GSK-3 β inhibitory potency of homolycorine-type alkaloids. For a detailed SAR study of homolycorine-type of Amaryllidaceae alkaloids, it is necessary to study a wider range of natural or semi-synthetic analogues of active alkaloids

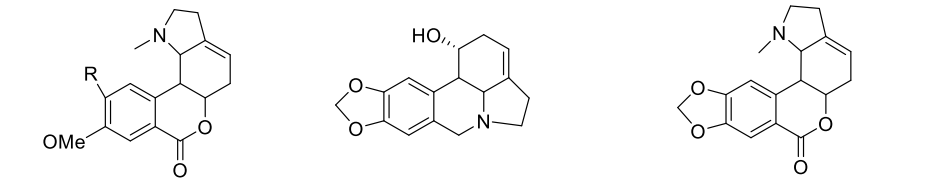

Figure *3.3*-**1** Structures of Amaryllidaceae alkaloids selected for their activity towards GSK-3β

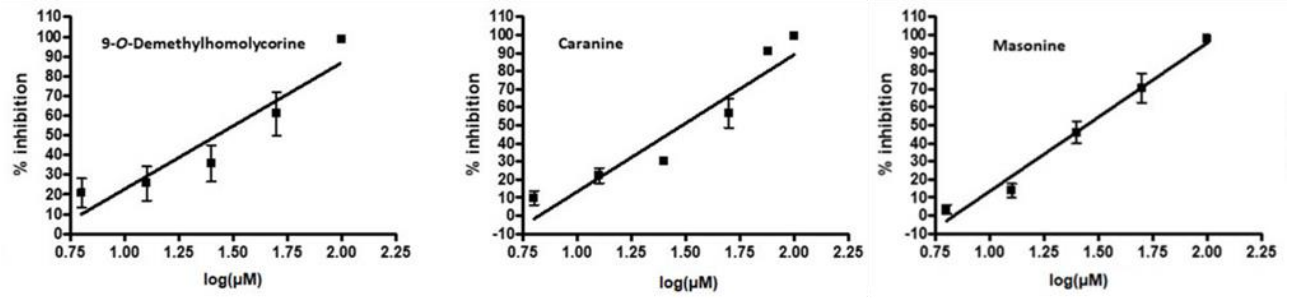

Figure 3.3.-**2** Linear graph of IC_{50} assay of GSK-3β treated with selected Amaryllidaceae alkaloids. Concentrations of alkaloids were 6.25; 12.5; 25; 50 and 100 µM. Activity is presented as % inhibition

3.4 Conclusions and Perspectives

In the present study, the inhibitory potency of Amaryllidaceae alkaloids towards GSK-3β has been studied. The luminescent kinase assay resulted suitable to screen the activity of natural compounds and allowed to recognize in Amaryllidaceae alkaloids an interesting scaffold for GSK-3β inhibitors. In addition, Amaryllidaceae alkaloids are promising, since they can be easily isolated from natural sources in amounts proper for the derivatives preparation. Thus, the active compounds will be used in the design of more potent semisynthetic derivatives. The type of GSK-3β inhibition of active alkaloids, and their semisynthetic derivatives, were examined in next studies.

The year later of the present work, Calichova research group published a study about the characterization of other twenty-one Amaryllidaceae alkaloids of the narcimatuline type isolated from *Narcissus pseudornarcissus* L. cv. Dutch Master.[14] The structure of narcimatuline (21) was elucidated by combining MS, HRMS, 1D and 2D NMR spectroscopic techniques and is reported in figure 3.4-**1**.

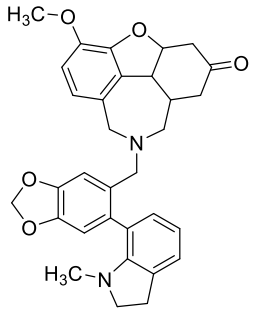

Figure *3.4*-**1** Narcimatuline structure

This compound, which presents in its structure both galanthamine and galanthindole basic scaffold, showed the most interesting biological profile. Indeed, this new isolated compound was found able to inhibit *in vitro* not only GSK-3β (67% of inhibition at 10 µM), but also acetylcholinesterase (AChE), butyrylcholinesterase (BuChE) and propyl oligopeptidase (POP). Despite the multipotent profile showed by narcimatuline, the structure of haemanthamine reported in figure 3.4-**2** (52,4% inhibition at 10 µM concentration toward GSK-3β) was selected as starting point for the preparation of some semisynthetic derivatives. That's because the possibility of isolating a large quantity of this compound. Indeed, some derivatives of hemanthamine alkaloid were developed.[15]

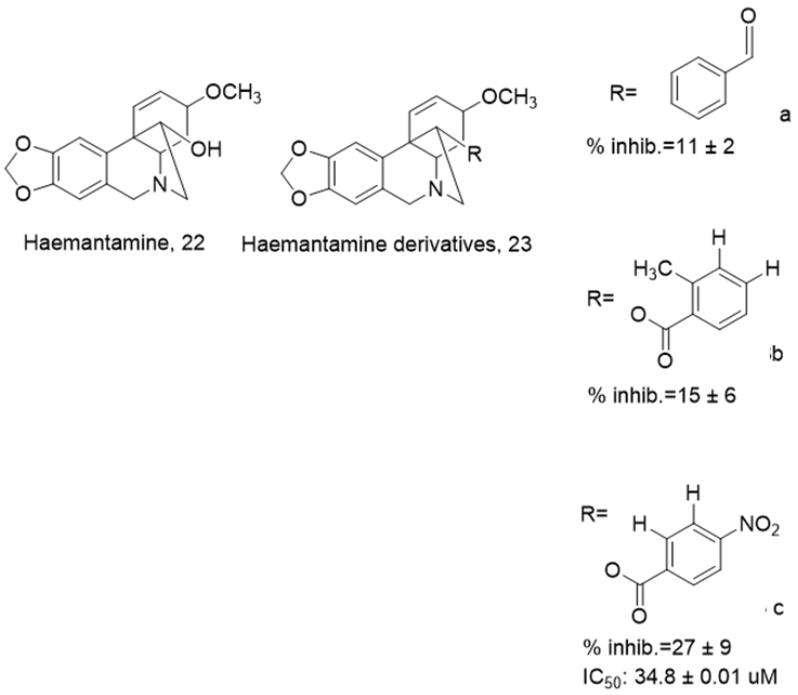

Figure *3.4*-**2** Selected haemanthemine derivatives

All compounds were tested in order to evaluate their antiproliferative activity. Due to the poor considerable results obtained, the interaction of haemanthemine derivatives [15] (structure 23 in figure 3.4-**2**) towards cholinesterases and GSK-3β was investigated. Only three of the tested compounds showed some inhibitory

activity towards GSK-3β (23a, 23b, 23c). The percentage of inhibition obtained at 10 μM concentration was found to be lower than the one obtained for haemanthemine, thus revealing the decrease in inhibitory potency obtained after structural modification. On the other hand, the activity towards cholinesterases was improved for some of them. For compound 23c that showed the most promising profile, a high selectivity towards AchE was detected together with an inhibitory potency (IC_{50} equal to 34,8 μM). Moreover, the assessed BBB permeability makes this compound a promising lead compound.

References

(1) Shawky, E. In-Silico Profiling of the Biological Activities of Amaryllidaceae Alkaloids. *J. Pharm. Pharmacol.* **2017**, *69* (11), 1592–1605 https://doi.org/10.1111/jphp.12794.

(2) Shimura, T. Acquired Radioresistance of Cancer and the AKT/GSK3β/Cyclin D1 Overexpression Cycle. *J. Radiat. Res.* **2011**, *52* (5), 539–544 https://doi.org/10.1269/jrr.11098.

(3) Jope, R. S.; et al. Glycogen Synthase Kinase-3 (GSK3): Inflammation, Diseases, and Therapeutics. *Neurochemical Research*. **2007**, *32* (4-5), 577-95 https://doi.org/10.1007/s11064-006-9128-5.

(4) Masi, M.; et al. Advances in the Chemical and Biological Characterization of Amaryllidaceae Alkaloids and Natural Analogues Isolated in the Last Decade. *Molecules*. **2020**, *25* (23), 5621 https://doi.org/10.3390/molecules25235621.

(5) Hulcová, D.; et al. Amaryllidaceae Alkaloids as Potential Glycogen Synthase Kinase-3β Inhibitors. *Molecules* 2018, *23* (4), 719. https://doi.org/10.3390/molecules23040719.

(6) Kulhánková, A.; et al. Alkaloids from Zephyranthes Robusta Baker and Their Acetylcholinesterase- and Butyrylcholinesterase-Inhibitory Activity. *Chem. Biodivers.* **2013**, *10* (6), 1120-1127 https://doi.org/10.1002/cbdv.201200144.

(7) Šafratová, M.; et al. Revised NMR Data for 9-O-Demethylgalanthine: An Alkaloid from Zephyranthes Robusta (Amaryllidaceae) and Its Biological Activity. *Nat. Prod. Commun.* **2014**, *9* (6), 787-8 https://doi.org/10.1177/1934578x1400900614.

(8) Doskočil, I.; et al. Cytotoxic Activities of Amaryllidaceae Alkaloids against Gastrointestinal Cancer Cells. *Phytochem. Lett.* **2015**, *13*, 394-398 https://doi.org/10.1016/j.phytol.2015.08.004.

(9) Cahlíková, L.; et al. Alkaloids from Chlidanthus Fragrans and Their Acetylcholinesterase, Butyrylcholinesterase and Prolyl Oligopeptidase Activities. *Nat. Prod. Commun.* **2013**, *8* (11), 1541-4 https://doi.org/10.1177/1934578x1300801110.

(10) Vaněčková, N.; et al. Isolation of Amaryllidaceae Alkaloids from Nerine Bowdenii W. Watson and Their Biological Activities. *RSC Adv.* **2016**, *6* (83). https://doi.org/10.1039/c6ra20205e.

(11) Šafratová, M.; Alkaloids from Narcissus Poeticus Cv. Pink Parasol of Various Structural Types and Their Biological Activity. *Arch. Pharm. Res.* **2018**, *41* (2),208–218https://doi.org/10.1007/s12272-017-1000-4.

(12) Havlasová, J.; et al.Chemical Composition of Bioactive Alkaloid Extracts from Some Narcissus Species and Varieties and Their Biological Activity. *Nat. Prod. Commun.* **2014**, *9* (8), 1151-5

https://doi.org/10.1177/1934578x1400900823.

(13) Baki, A.; et al.High Throughput Luminescent Assay for Glycogen Synthase Kinase-3β Inhibitors. *Assay Drug Dev. Technol.* **2007**, *5* (1) 75-84 https://doi.org/10.1089/adt.2006.029.

(14) Hulcová, D.; et al.Amaryllidaceae Alkaloids from Narcissus Pseudonarcissus L. Cv. Dutch Master as Potential Drugs in Treatment of Alzheimer's Disease. *Phytochemistry* **2019**, *165*,112055 https://doi.org/10.1016/j.phytochem.2019.112055.

(15) Kohelová, E.; P et al. Derivatives of the β-Crinane Amaryllidaceae Alkaloid Haemanthamine as Multi-Target Directed Ligands for Alzheimer's Disease. *Molecules* **2019**, *24* (7), 1307 https://doi.org/10.3390/molecules24071307.

II-b

Application of Multi-Methodological Approach Based on MS-CD-ThT Assay to Evaluate Carbon Monoxide-Releasing Molecules (CORMs) Interaction with $A\beta_{1-42}$ Peptide Aggregation

4. Investigating *in Vitro* Amyloid Peptide$_{1-42}$ Aggregation: Impact of Higher Molecular Weight Stable Adducts

4.1 Aim of the Work

Starting from the knowledge of CORMs - protein mechanism of interaction, the present research carried out in collaboration with the University of Reading (UK) wanted to investigate if CORMs could directly react with $A\beta_{1-42}$ peptide.[1] The project aimed to evaluate if the potential chemical interactions with histidine residues of the aminoacid skeleton of $A\beta_{1-42}$ peptide could eventually stabilize the α-helix secondary structure of the peptide delaying the aggregation process. If this hypothesis would be verified it could be possible to assign to CORMs a further mechanism of protection toward $A\beta_{1-42}$ peptide toxicity.[2]

Numerous analytical techniques have already been employed to study amyloid aggregation process *in vitro*, including circular dichroism (CD), NMR, colorimetric and fluorometric methods. The use of mass spectrometry (MS), (CD) and ThT assay in a multi methodological approach has already demonstrated to ensure the study of $A\beta_{1-42}$ aggregation in the various phases.[3] Specifically, the aim of the present research was to apply this comprehensive method to evaluate the kinetics of $A\beta_{1-42}$ aggregation in the presence of CORMs. In detail, MS could be exploited to monitor the changes of molecular weight of the $A\beta_{1-42}$ peptide after incubation with CORMs. At this point, if a new MS signal was detected and corresponds to structural changes, the amino acid residues involved in adduct could be characterized. CD spectroscopy technique could be used to investigate protein secondary structure. In fact, the transition of $A\beta_{1-42}$ peptide from unordered secondary structure to β-sheet, plays a critical role in the conversion of monomers into oligomers. The techniques used before the CD were able to detect only the fibrils already formed not the transient soluble oligomers. On the contrary, CD allows to follow the transition kinetics of the secondary structure during the self-aggregation process, before the precipitation of the fibril. This aspect is crucial and inhibitors of the conformation transition into β-sheet can be designed and tested. Finally, ThT binding for β-sheet structures suggests that this assay could be applied to confirm the compounds capability to interfere even with the fibril formation.

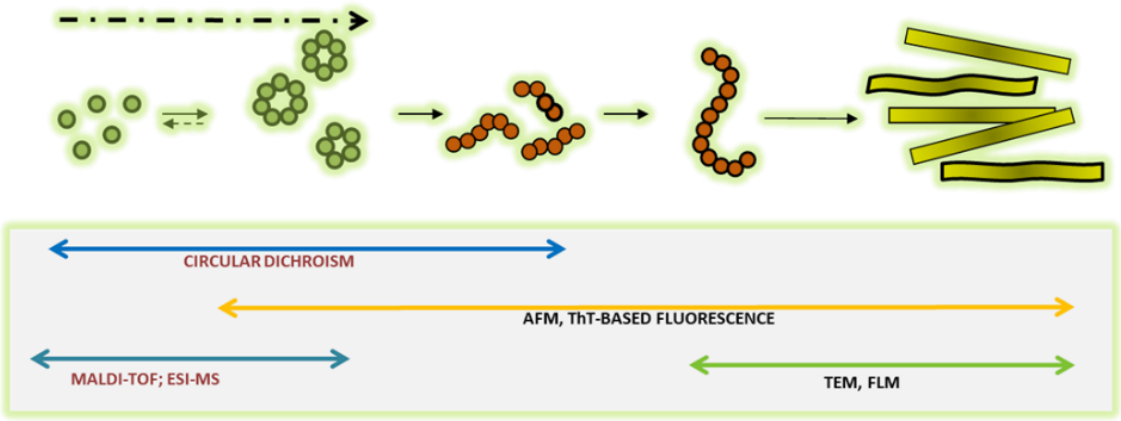

Figure *4.1*-**1** Multi-methodological approach developed to characterize $A\beta_{1-42}$ aggregation mechanism

4.2.1 Materials

1,1,1,3,3,3-Hexafluoro-2-propanol, dimethyl sulfoxide (DMSO), methanol, and acetonitrile (CH_3CN) (Chromasolv) were obtained from Sigma-Aldrich (Milan, Italy). To prepare buffer solutions, potassium dihydrogen phosphate, dipotassium hydrogen phosphate trihydrate, glycine, sodium carbonate, sodium hydroxide, and sodium chloride (Sigma-Aldrich, Milan, Italy) of analysis quality were used. Human $A\beta_{1-42}$ lyophilized powder was purchased from Bachem (AG, Switzerland). Reserpine, myricetin (Myr), CORM-3 and CORM-2, trypsin, and ThT were obtained from Sigma-Aldrich (Milan, Italy). Purified water from MilliRX system (Millipore, Milford, MA) was used to prepare buffers and standard solutions. Nitrocellulose (0.22 μm) and nylon (0.20 μm) membrane filters (Millipore, Carrigtwohill, Ireland B.V.) were employed to filter buffers and solutions. CORM-3 and CORM-2 stock solutions were obtained by dissolving the compounds in water or DMSO, respectively, in order to get the 100 mM starting concentration. Myricetin was solubilized in DMSO at a stock concentration of 1 mg/mL. All compounds were from Sigma-Aldrich (Milan, Italy).

4.2.2 $A\beta_{1-42}$ Preparation

Following the previously published procedure,[4 3 5] 1 mg of $A\beta_{1-42}$ lyophilized powder was pre-treated overnight with 1400 μL of HFIP, portioned, and stored at −20 °C after solvent evaporation

4.2.3 Characterization of $A\beta_{1-42}$-CORMs Adducts

An $A\beta_{1-42}$ aliquot (corresponding to 0.0368 μmol) was solubilized in 69.5 μL of a freshly prepared mixture consisting of CH_3CN/ 300 μM Na_2CO_3/250 mM NaOH (48.3/48.3/3.4, v/v/v) to obtain a 500 μM stock solution. CORM-2 100 mM stock solution was prepared in DMSO, whereas the CORM-3 100 mM stock solution was prepared in water. Stock solutions of the CORMs were kept at −20 °C before use. To study the formation of stable adducts between $A\beta_{1-42}$ and CORM molecules, 3 μL of the $A\beta_{1-42}$ stock solution was diluted with 27 μL of 10 mM phosphate buffer pH 7.7 containing 11 mM NaCl, in the absence and in the presence of CORM-2 or CORM-3 at 5.50, 13.7, 27.5, 55.0, 110, 275, and 550 μM concentrations to achieve final CORM/$A\beta_{1-42}$ MR equal to 0.0, 0.1, 0.25, 0.5, 1.0, 2.0, 5.0, and 10, respectively. Samples were incubated at 30 °C for 3 h and finally diluted 1:1 with water before the LC−MS analysis. Experiments were performed in duplicate

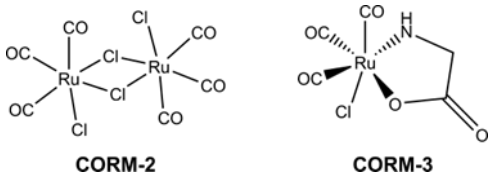

CORM-2 **CORM-3**

Figure *4.2.1*-**1** Chemical structures of CORM-2 and CORM-3

4.2.4 MS-Based Assay.

$A\beta_{1-42}$ stock solution was diluted 1:10 with 10 mM phosphate buffer pH 7.7 containing NaCl 11 mM, in the absence and in the presence of CORM-3 at 55.0 and 275 μM concentrations (to achieve the final CORM-3/Aβ1−42 MR equals to 0.0, 1.0, and 5.0, respectively) and in the presence of 55.5 μM Myr (final Myr/$A\beta_{1-42}$ MR 1: 1). Samples were incubated at room temperature (RT) and, at selected times, 10 μL were diluted 1:1 with reserpine solution (30 μM in water/MeOH, 50/50, v/ v) employed as the internal standard. The analysis was performed by the LC−MS analysis as reported in Section *4.2.6*. Two independent experiments, each one performed in duplicate, were carried out using two different batches of $A\beta_{1-42}$.

4.2.5 ThT-Based Fluorometric Assay

$A\beta_{1-42}$ stock solution was diluted 1:10 with 10 mM phosphate buffer pH 7.7 containing 11 mM NaCl, in the absence or presence of CORM-3 at 27.5, 55.0, and 275 μM concentration to achieve the final CORM-3/Aβ1−42 MR equal to 0.0, 0.5, 1.0, and 5.0, respectively. Samples were incubated at RT for 48 h and finally diluted with the glycine−NaOH buffer (50 mM, pH 8.5) containing ThT (1.5 μM) to achieve the final volume of 2.0 mL. Fluorescence emission was monitored by a Jasco FP-6200 spectrofluorometer (Jasco, Tokyo, Japan) using a 3 mL quartz cell. For each sample, the fluorescence emission signal was monitored at 490 nm (λex = 446 nm) with excitation and emission slits of 2 nm bandwidth. A time scan was performed, and the fluorescence intensity values at the plateau (300 s) were averaged after subtracting the background fluorescence from 1.5 μM ThT.

4.2.6 LC−MS Analysis

LC−MS analyses were performed by an Agilent 1200 Series (Walbronn, Germany) coupled with an ESI-Q-ToF mass spectrometer equipped with a Z-spray ion source (Micromass, Manchester, UK). Flow injection analyses were performed by employing water/acetonitrile/FA (70/30/ 0.1; v/v/v) as the mobile phase at the flow rate of 0.1 mL/min. The injection volume was 5 μL. The capillary voltage was set at 3000 V, the cone voltage was 40 V, the capillary temperature was 100 °C, while the desolvation temperature was 300 °C. Mass spectra were recorded in total ion current (TIC), within 1000 and 2000 m/z, in positive polarity mode. The $A\beta_{1-42}$ baseline subtracted spectrum (m/z 1100−1700) was deconvoluted onto a true mass scale using the maximum entropy (MaxEnt1)-based software supplied with MassLynx software. The output parameters were mass range: 4100−5200 Da and resolution: 2 Da/channel. The uniform Gaussian model was used, with 0.63 Da width at half height. The $A\beta_{1-42}$ (alone or forming a complex with CORMs) relative abundance was calculated by dividing the corresponding form intensity by the sum of all forms intensities and multiplying them by 100. Data were analysed by Excel.

4.2.7 LC-ESI-MS/MS Analysis

A 3 μL aliquot of $A\beta_{1-42}$ stock solution (500 μM) was diluted ten folds with 10 mM phosphate buffer pH 7.7 containing 11 mM NaCl, in the absence and in the presence of CORM-2 or CORM-3 to achieve final CORM/Aβ1−42 MR equal to 5.0 and 10. Samples were incubated for 3 h at 30 °C, then 1 μL of trypsin (1 μg/ μL; Sigma T1426) was added and samples were incubated overnight at 37 °C to allow peptide digestion. $A\beta_{1-42}$ tryptic digest (10 μL), corresponding to 485 pmol, was analysed by using an Agilent 1100 Series system (Walbronn, Germany). Analyses were performed on a C18 column (Aeris peptide XBC18; 150 × 2.1 mm; 3.5 μm; Phenomenex). Mobile phases A [water/acetonitrile/FA (99/1/0.1, v/v/v)] and B [water/ acetonitrile/FA (1/99/0.1, v/v/v)] were used to develop a gradient. The solvent gradient was set as follows: A−B from (98:8, v/v) to (40:60, v/v) in 20 min; (40:60, v/v) for 2 min. The column was equilibrated with the mobile phase composition of the starting conditions for 10 min before the next injection. MS analysis was performed on the Q-ToF Micro hybrid analyser (Micromass, Manchester, UK) with a Z spray ion source. The ESI-Q-ToF source temperature was set at 100 °C, the capillary voltage at 3.0 kV, and the cone voltage at 35 V. Peptide ions within a m/z 400−1700 survey scan mass range were analysed for subsequent fragmentation. 2^+, 3^+, and 4^+ charged ions exceeding a threshold abundance (TIC value: 10 counts/s) were selected for MS/MS analyses. From a single survey scan, 4 ions were selected for subsequent fragmentation. Scan returns to mass survey mode when the ion intensity falls below 5 counts/s or after 8 s. Scan time was 1s for the parent ion and 1 s for the MS/MS ions. The collision energy was selected using charge state recognition.

4.2.8 CD Analysis

CD measurements were carried out at 25 °C in the 260−200 nm spectral range on a Jasco (Tokyo, Japan) J-810 spectropolarimeter equipped with a PTC-423S Peltier-type temperature control system, using QS quartz cells (Hellma Italia, Milan, Italy) with a 0.1 cm path length, a 2 nm spectral bandwidth, a 0.5 nm data interval, a 20 nm min−1 scanning speed, and a 2 s data integration time. $A\beta_{1-42}$ samples (50 μM, 200 μL final volume), either in the absence or in the presence of CORM-3 at both 1 and 5 MR, were prepared as previously described. The CD spectra of all samples were measured at different times after preparation (up to 52 h) to follow the time evolution of the secondary structure of $A\beta_{1-42}$ and evaluate the effect of CORM-3 on the misfolding process. Baseline correction was performed by subtracting the spectral contribution of phosphate buffer (8.7 mM) containing NaCl (10 mM), Na_2CO_3 (14.5 mM), NaOH (0.85 mM), and acetonitrile (8.2%, v/v); CORM-3 was not included in the blank solution, as it shows no CD signal in the spectral range considered in the analysis. Solvent-corrected CD spectra were then converted to molar units per residue (Δεres, M−1 cm−1) and plotted using the Bezier smoothing algorithm provided by the Gnuplot software (version 5.2.2, http://gnuplot. sourceforge.net). The conformational change of $A\beta_{1-42}$ was monitored by plotting the difference between the unsmoothed CD signals at 205 and 218 nm ($\Delta\varepsilon_{res,205} - \Delta\varepsilon_{res,218}$) as a function of time.

The aim of the present work was the development of a multi-methodological approach that could provide further information about CORMs mechanism of interaction with $A\beta_{1-42}$ peptide, and the investigation of their possible antiaggregant and stabilizing capacity. Since $A\beta_{1-42}$ toxicity is related to specific pre-fibrillar species, it is important to follow the amyloid aggregation kinetics.[6 7]

The advantage of this multi-methodological approach is precisely that of being able to study the effect of the CORMs during the different steps of the aggregation, provides a more comprehensive view about CORMs /Aβ interaction. An analogy study had already been done on Myricetin. The antiaggregant properties of myricetin were demonstrated by the ThT fluorescence assay, while its ability to produce structural changes in $A\beta_{1-42}$ peptide was confirmed by CD studies. Furthermore, MS techniques allowed to monitor the first $A\beta_{1-42}$ self-assembly species and to study adducts formed between myricetin-and monomers. The multi-methodological study confirmed of myricetin ability to stabilize the $A\beta_{1-42}$ peptide in the monomeric form, and made it possible to relate this effect to a mechanism of oxidation of the peptide at the level of Met_{35} through the formation of a sulfoxide that is less prone to aggregation, leading to lower cytotoxicity and oxidation rate of proteins.[3 5]

Accordingly, it was decided to apply the same multi-methodological approach taking myricetin as known reference $A\beta_{1-42}$ anti-aggregating agent.

4.3.1 Evaluation of $A\beta_{1-42}$/CORM-3 Interaction by MS

Evidence of CORMs protective effects against $A\beta_{1-42}$ toxicity *in vitro* and capacity to form stable adducts with histidine residues of different proteins[8] prompted to investigate their interaction with $A\beta_{1-42}$ by MS analysis. Following the experimental procedure previously reported by Bartolini et al.[5] $A\beta_{1-42}$ was incubated at 30 °C for 3 h in the absence and in the presence of either CORM-2 or CORM-3 to achieve final CORM/$A\beta_{1-42}$ molar ratios (MRs) ranging from 0.1 to 10 to gain insights into the reaction of CORMs with the His residues of $A\beta_{1-42}$. In figure 4.3.1-**1a**, the characteristic multi-charged mass spectrum of native $A\beta_{1-42}$ is shown. The analysis of the ESI-MS spectra exposed the generation of different charge states of the monomer. The resulting signals were attributed to $A\beta_{1-42}$ charge states ranging from 2 to 5 ions, the most intense being $[M + 4H]^{4+}$ at 1129.3 m/z, $[M + 5H]^{5+}$ at 903.7 m/z, and $[M + 6H]^{6+}$ at 753.3 m/z (4.3.1-**1a**). The deconvoluted MS spectrum of $A\beta_{1-42}$, not treated with CORMs (figure 4.3.1-**1b**) shows an intense signal at 4514 Da, which corresponds to the molecular weight of the native form of the peptide. However, when $A\beta_{1-42}$ was incubated with CORM-3 at higher concentration (CORM-3/$A\beta_{1-42}$ = 10), new species at higher molecular weights were detected and the deconvoluted mass spectra reveal the addition of $Ru(CO)_2$ to $A\beta_{1-42}$ (figure 4.3.1-**1c**). In particular, a mass increment of 156 Da for the interaction of $Ru(CO)_2$ to each His residue is detectable, producing signals at 4670, 4826, and 4982 Da, related to the addition of 1, 2, and 3 $Ru(CO)_2$ moieties, respectively. These species derive from the formation of stable adducts between $A\beta_{1-42}$ and 1−3 $Ru(CO)_2$ groups from CORM-3 (molecular weight of 156 Da). As the primary sequence of $A\beta_{1-42}$ contains three histidine residues and CORMs

are known to form stable adducts with this aminoacid[8] the $A\beta_{1-42}$/CORMs reaction may reasonably occur at this level. The extent of $A\beta_{1-42}$/CORMs adducts formation was found to be proportional to CORM concentrations. Indeed, increased mono-, di-, and tri-modified forms of the peptide (figure 4.3.3-**1**) were detected at increasing CORM-2 and CORM-3 concentration. Indeed, compared to CORM-3, the disappearance of the native form of $A\beta_{1-42}$ requires a lower CORM-2 concentration (MR = 5 instead of 10; figures 4.3.3-**1a-b**). At low CORM molar ratio, only the mono modified form of $A\beta_{1-42}$ is evident, with the native $A\beta_{1-42}$ peptide concomitantly being transformed. By increasing the CORM/$A\beta_{1-42}$ molar ratio, peptide modification was more pronounced, with the modification of the monohistidine-modified form into bis- histidine- and trishistidine-modified $A\beta_{1-42}$ adducts (figure 4.3.3-**1)**. In particular, CORM-2 induced a complete disappearance of the native $A\beta_{1-42}$ form and the concomitant formation of $A\beta_{1-42}$ modified forms in which two or three histidine residues are modified. This higher reactivity of CORM-2 can be explained by the fact that two ruthenium moieties are present in the CORM-2 structure, whereas CORM-3 bears only one.

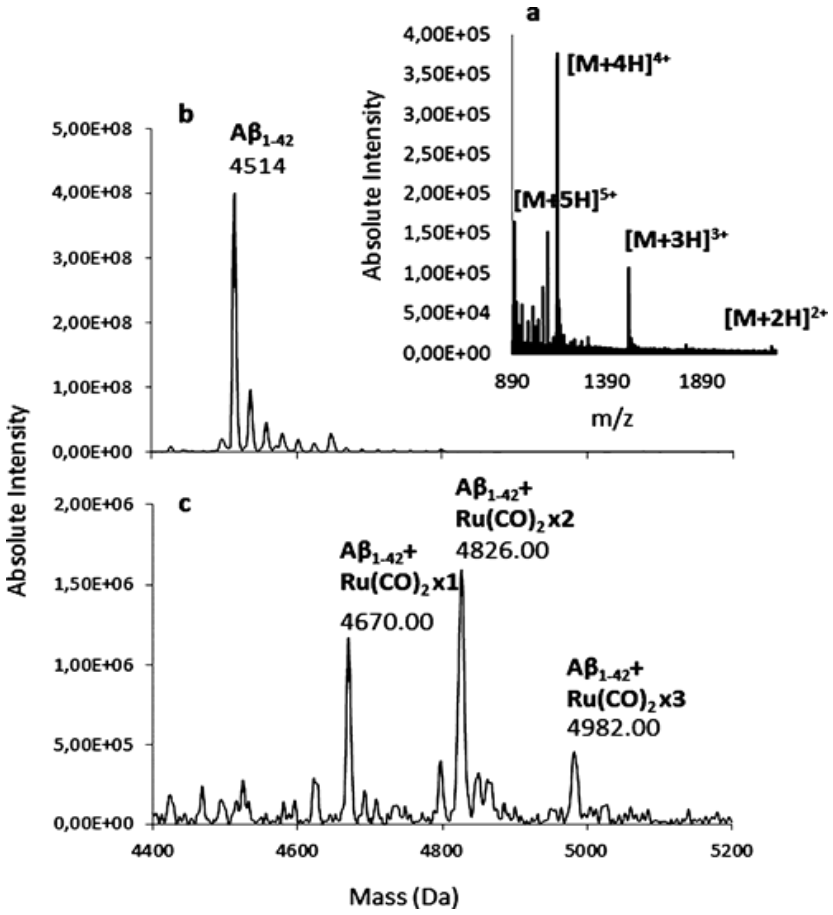

Figure *4.3.1*-**1** Mass spectra of Aβ1−42/CORM assemblies [1]

a) $A\beta_{1-42}$ multicharged mass spectrum (Upper panel)

b) $A\beta_{1-42}$ deconvoluted mass spectrum. (Lower panel)

c) $A\beta_{1-42}$ deconvoluted mass spectrum after its incubation with CORM-3 for 3 h at 30 °C (molar ratio CORM-3/Aβ1−42 = 10)

4.3.2 Identification of $A\beta_{1-42}$ Amino Acids Involved in the Formation of Stable Adducts with CORM-3 and CORM-2

$A\beta_{1-42}$ was incubated for 3 h at 30 °C in the absence and in the presence of CORMs at final CORM/ $A\beta_{1-42}$ molar ratio of 5 or 10 before digestion with trypsin. Peptides from the tryptic digestion of untreated $A\beta_{1-42}$ were all identified. Analysis of the tryptic digests, resulting from incubation with CORMs, highlighted modification only at peptide 6−16, independently from the type of CORM and molar ratio. In particular, the mono-modified form of the peptide 6−16 (as discharged form m/z = 747.5) was detected after incubation with CORM-3 at molar ratio equal to 5. The identity of the adduct was confirmed by the characteristic ruthenium isotope pattern, which perfectly matched that previously reported by Hong and co-workers.[9] MS/MS analysis of this peptide allowed final identification of residue His6 as the amino acid residue involved in $Ru(CO)_2$ binding. This finding confirms the tendency of ruthenium-containing molecules to form adducts with His residues and to interact with binding sites close to Asp and Arg residues as previously reported by others.[10 11 12] The identification of the second amino acid residue involved in the formation of the di-adduct was not possible because the di-modification of the peptide drastically impacts the ionization efficiency and significantly reduces signal intensity. The same phenomenon is also the cause of not detecting the tri-modified peptide. However, as the modifications occur at 6−16 peptide containing three histidine residues and according to the data reported in literature,[12] it is quite reasonable to assume that the second and the third modification involve His 13 and 14.

After assessing the capacity of CORMs to form stable adduct with $A\beta_{1-42}$, their anti-aggregation capacity was evaluated. A reproducible $A\beta_{1-42}$ aggregation protocol has been previously developed, which allows the characterization of different assembly species and a definition of their morphology, molecular weight, and relative abundance.[4] This information is crucial to avoid confusing outcomes from both aggregation studies and screening of inhibitors. Based on this multimethodological approach,[3] the effects on $A\beta_{1-42}$ aggregation of CORM-3 at different concentrations was monitored by different methodologies, using myricetin as the reference inhibitor. ESI-MS was applied for the quantification of monomers; CD spectroscopy was used to obtain information on the secondary structure,[5 13] and a ThT fluorescence assay was applied to assess fibrils formation.[14] The use of different techniques allows for a more comprehensive analysis of increasingly complex interactions involved in prefibrillar species formation during the aggregation process.[15] Indeed, it was established that Aβ toxicity is related to specific intermediates.[6]

4.3.3 ESI-MS Analysis

ESI-MS has been previously used to highlight the non covalent interaction of myricetin and other inhibitors with the native peptide.[4 3 13 16] Using this approach, it was possible to characterize the inhibitors, determining their potency (IC_{50}) and their capacity to maintain the $A\beta_{1-42}$ in its non-amyloidogenic, soluble monomeric form. In the present study, the aim was to verify whether $A\beta_{1-42}$/CORMs interaction could promote the

stabilization of the non amyloidogenic soluble form. Hence, an ESI-MS based approach was exploited for monitoring the decrease of $A\beta_{1-42}$ soluble monomers along with the mono-, di-, and tri $Ru(CO)_2$-modified monomers formation. In detail, $A\beta_{1-42}$ (50 μM) solution was incubated in the presence and in the absence of 50 μM myricetin, 50 μM CORM-3, and 250 μM CORM-3. At selected times, samples were analysed by ESI-MS upon addition of reserpine (30 μM) as an internal standard. In a time course experiment, the aggregation was followed by monitoring the ratio between the sum of all $[M + 4H]^{4+}$ monomer species (native, mono, di-, and tri-Ru(CO)2- modified) and the internal standard ($IA\beta_{1-42}$ monomers/IIs). The charge state 4 was selected as it is endowed with the highest intensity. As a result of the aggregation process, the signal of the $A\beta_{1-42}$ monomer progressively decreases until it almost disappears in 48 h, when incubated alone (Ctrl sample, figure 4.3.3-**2**). Conversely and in agreement with previous reports, myricetin was able to partially prevent monomer inclusion into higher assemblies, slowing down the aggregation process. Interestingly, CORM-3 was also able to interfere with amyloid aggregation (figure 4.3.3-**2**). It is noteworthy that the inhibitory activity of CORM-3 is higher at lower concentrations (1:1 molar ratio). This effect is further elucidated in figure 4.3.3-**3**, where the $A\beta_{1-42}$ relative abundance in the presence of CORM-3 at 5:1 and 1:1 ratio is shown in the time course experiment. The $A\beta_{1-42}$ in its native form is not detectable after 24 h, when incubated in the presence of CORM-3 at higher concentration. In contrast, a 1:1 molar ratio, CORM-3 seems to have an increased stabilizing effect on the $A\beta_{1-42}$ peptide in its soluble form, as its signal is still detectable after 48 h. Taking in account intrinsic variability of amyloid aggregation process, data were collected in duplicate from two independent experiments carried out with different batches of the $A\beta_{1-42}$ peptide.

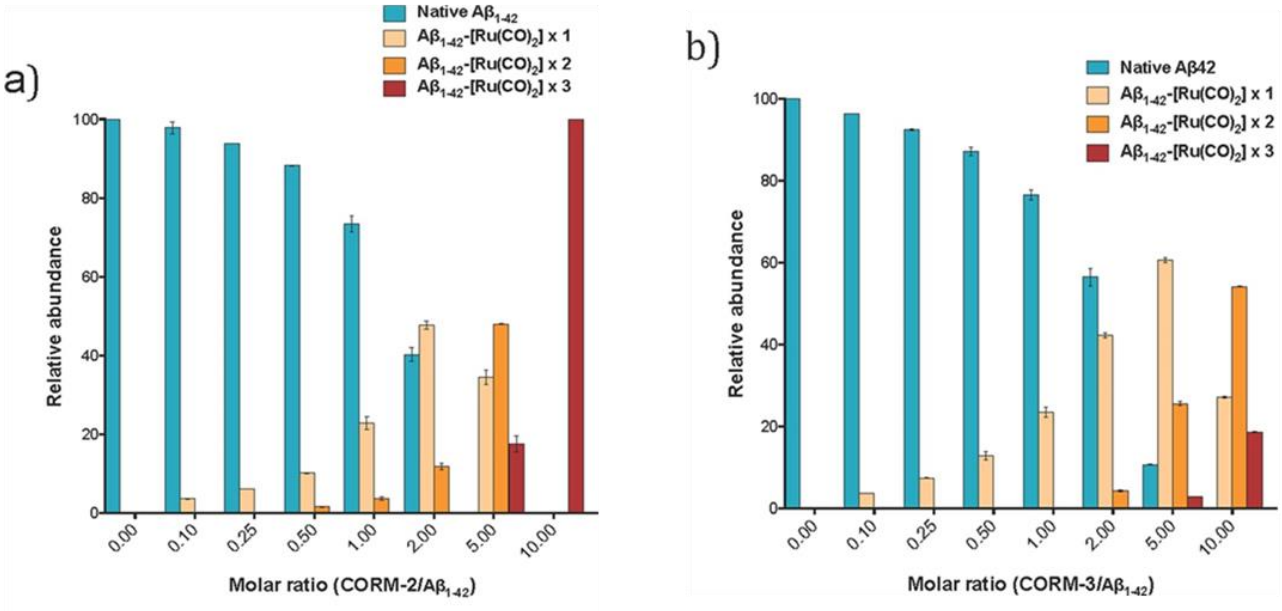

Figure *4.3.3*-**1** CORMs/$A\beta_{1-42}$ adducts abundance as a function of CORMs/$A\beta_{1-42}$ molar ratio. The relative abundance of $A\beta_{1-42}$ species as a function of CORM-2 or CORM-3/$A\beta_{1-42}$ molar ratio is reported in panels a and b, respectively. $A\beta_{1-42}$ (50 μM) and CORMs at different concentrations (0−500 μM) were incubated at 30 °C for 3 h and analyzed by ESI-MS. The $A\beta_{1-42}$ species relative abundances were derived from the deconvoluted ESI-MS spectrum[1]

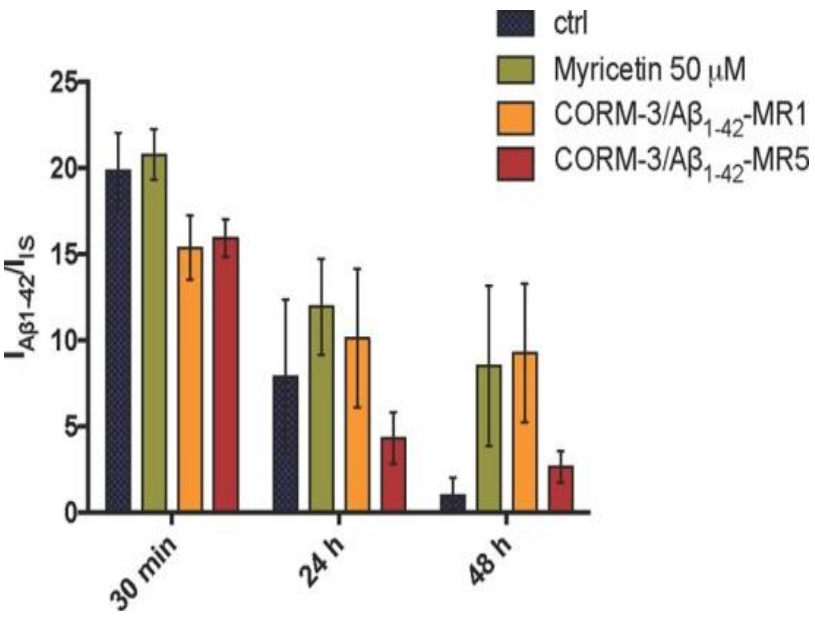

Figure 4.3.3-**2** Time-dependent inhibition of $A\beta_{1-42}$aggregation. $I_{A\beta_{1-42}}$ monomers/I_{IS} values after 30 min, 24 and 48 h incubation. $A\beta_{1-42}$was incubated in the absence (ctrl) and in the presence of myricetin (50 μM), CORM-3 (50 μM), and CORM-3 (250 μM).[1]

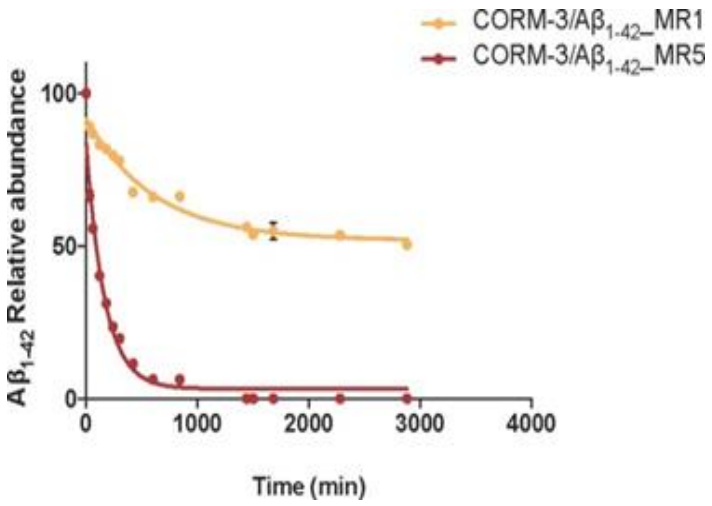

Figure *4.3.3*-**3** Time-dependent disappearance of $A\beta_{1-42}$ monomer in the presence of CORM-3. Relative abundance of native $A\beta_{1-42}$ monomer measured after incubation with CORM-3 at 50 and 250 μM is reported ranging from 30 min to 48 h[1]

4.3.4 ThT Fluorescent Analysis

The selectivity of ThT binding for β-sheet structures suggests that this assay can prove the ability of compounds to interfere with fibril formation.[14] $A\beta_{1-42}$ (50 μM) samples were incubated at room temperature with different amounts of CORM-3 to achieve final CORM-3/$A\beta_{1-42}$ MRs of 0.5, 1.0, and 5.0. After 48 h incubation, the samples were diluted with glycine–NaOH buffer (50 mM, pH 8.5) containing ThT (1.5 μM). Fluorescence

emission intensity was monitored at 490 nm (λexc = 446 nm) for 300 s. Fluorescence intensities (IF) at 300 s were averaged after subtracting the background fluorescence of 1.5 μM ThT solution and of the tested compound. Inhibition of fibril formation is expressed as the percent decrease of fluorescence in comparison with the $A\beta_{1-42}$ control sample. As shown in figure 4.3.4-**1**, CORM-3 at 25 μM strongly inhibited the formation of $A\beta_{1-42}$ fibrils to an extent similar to that by myricetin but at a 2 times lower concentration. In agreement with the MS data (figure 4.3.3-**2**), the inhibitory effect was more pronounced at the lowest CORM-3 concentration (lower IF values) at which the extent of Aβ modification by CORM-3 is lower. This could be explained considering that different degrees of modification could lead to different effects on amyloid aggregation.

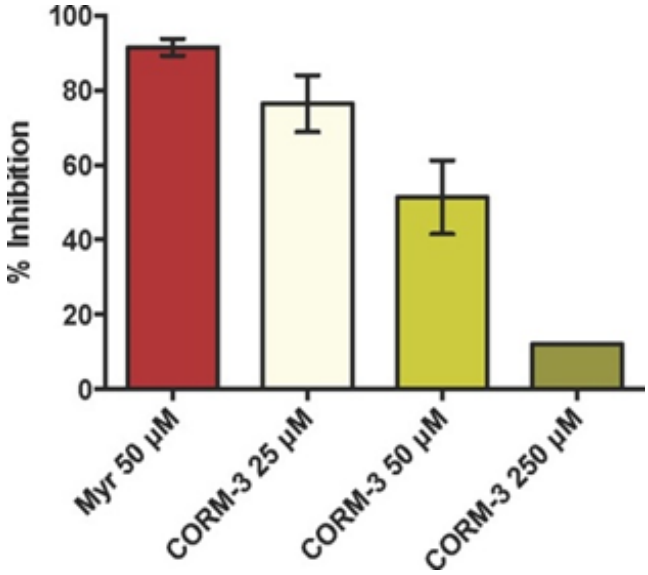

Figure *4.3.4*-**1** Inhibition of $A\beta_{1-42}$ aggregation by ThT fluorescence assay. Inhibition of fibrils formation obtained in the presence of myricetin 50 μM or CORM-3 at different concentrations is expressed as percentage of fluorescence signal recorded in the presence and in the absence of the inhibitor[1]

4.3.5 CD Analysis

Nowadays it is known that $A\beta_{1-42}$ misfolding is the earliest step of amyloid aggregation. For this reason, the change of the $A\beta_{1-42}$ secondary structure was monitored over 50 h by CD spectroscopy [5] in order to evaluate the inhibitory effect of CORM-3 on the formation of amyloid aggregates. The CD spectra of $A\beta_{1-42}$ (figure 4.3.5-**1)** show a clear transition from a prevalently unordered conformation, characterized by two weak negative bands at around 205 and 230 nm, to a β-strand structure, characterized by a stronger negative band centred at 218 nm. Based on this observation, the conformational change was monitored using the difference between the CD signals at 205 nm (unordered) and 218 nm (β-strand) as a function of time (figure 4.3.5-**2**). Under the used experimental conditions, the misfolding of $A\beta_{1-42}$ results completed in 48 h, with the mid-transition point occurring at 23.6 h. CORM-3 demonstrated to strongly interferes with the $A\beta_{1-42}$ folding process. In fact, the CD spectra of the $A\beta_{1-42}$/CORM-3 mixture at 1:1 molar ratio (figure 4.3.5-**1**b) show a

perturbation of the electronic properties of the peptide due to the formation of stable adducts between CORM-3 and a single histidine residue of $A\beta_{1-42}$. The spectroscopic signature of β-strand structures, however, was not observed throughout the considered time frame, indicating that the conformational change was fully inhibited (figure 4.3.5-**2**). Interesting the formation of double and triple Aβ1−42/CORM-3 adducts in the presence of a 5:1 molar excess of CORM-3 (figure 4.3.5-**1**c) induced a conformational change of $A\beta_{1-42}$ toward a β-strand-like arrangement which, nevertheless, did not evolve into an extensive amount of misfolded peptide (figure 4.3.5-**2**). This interpretation of CD data was supported by the relative abundance of $A\beta_{1-42}$/CORM-3 adducts at different times, as shown by the ESI-MS analysis and by the ThT fluorescence assay. Together, this suggests that the inhibition of amyloid aggregation is highest when the interaction of CORM-3 with $A\beta_{1-42}$ involves a single histidine residue. The results obtained via $A\beta_{1-42}$ tryptic digestion confirmed the hypothesis that His6 is the first to be involved by CORM modification.

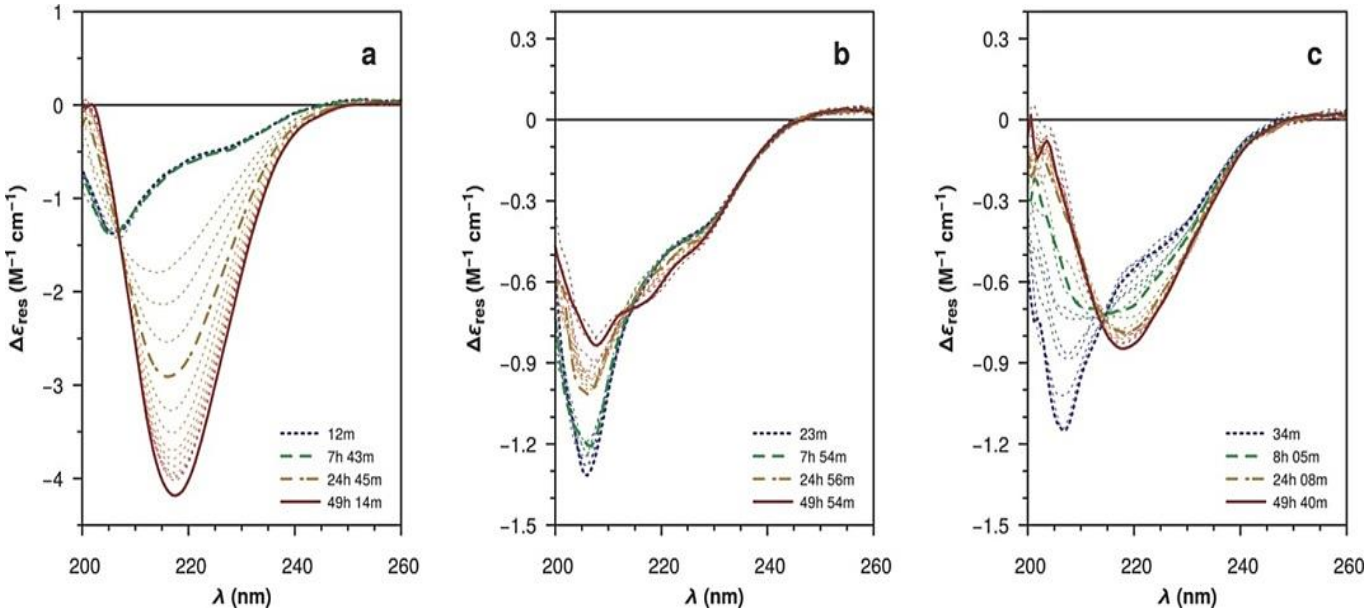

Fig. *4.3.5*-**1** CD spectra of Aβ1−42 samples at different times after sample preparation. [1]

a) Aβ1−42 in the absence of CORM-3.

b) Aβ1−42 in the presence of CORM-3 at 1:1 molar ratio.

c) Aβ1−42 in the presence of excess CORM-3 at 5:1 molar ratio

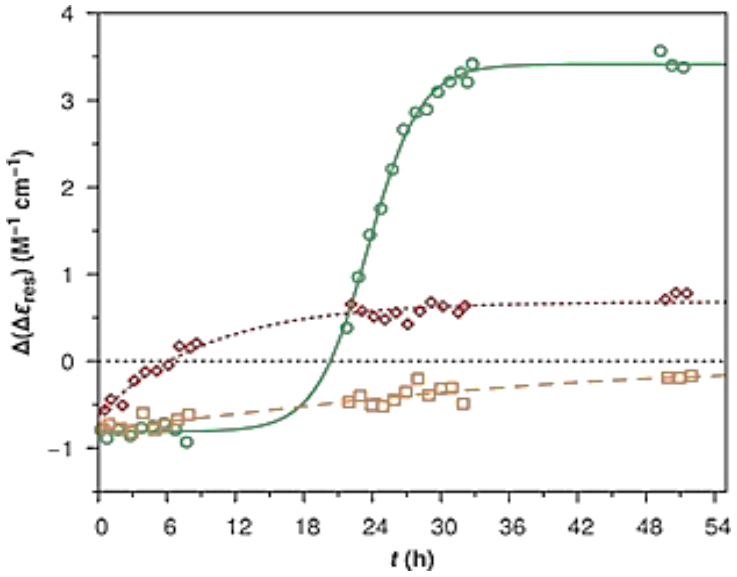

Figure *4.3.5*-**2** Kinetics of Aβ1–42 misfolding as monitored by CD spectroscopy [1]

circles, solid line: Aβ1−42 in the absence of CORM-3.
squares,dashedline: Aβ1−42 in the presence of CORM-3 at 1:1 molar ratio.
diamonds, dottedline: Aβ1−42 in the presence of excess CORM-3 at 5:1 molar ratio

4.4 Conclusions

The aim of this study was the application of a multi-methodological approach based on the combination of the ThT assay, the ESI-MS analysis and the CD studies to get further details regarding the individual phases of the $A\beta_{1-42}$ aggregation kinetics *in vitro* after the incubation with CORMs. It provided reliable information on both the fibrillation process and the identification of new potential inhibitors of aggregation and their mechanism of action. In particular, mass spectrometry has shown that CORM-3 and CORM-2 interact directly with $A\beta_{1-42}$, forming stable soluble adducts. After tryptic digestion, it has been confirmed that adducts are probably formed through modification of histidine residues with the addition of Ru $(CO)_2$ moiety. In fact, the hypothesis that His6 is the first residue of His involved in the modification of $A\beta_{1-42}$ by the CORM studied was proved. Adduct formation depends by CORM-$A\beta_{1-42}$ molar ratio, incubation time and CORM type. Indeed, CORM-2, characterize by two Ru atoms in its structure, modify effectively $A\beta_{1-42}$ in a lower molar ratio than CORM-3. CORM-2 greater reactivity highlighted is certainly related to the different reaction stoichiometry of metal with amyloid. Furthermore, Kumar et al reported a much higher binding affinity of the binuclear complex, $[(bpy)\ 2Ru_2 + (dpp)\ Pt_2 + Cl_2]^{2+}$ instead of the mononuclear $[(dpp)\ Pt_2 + Cl_2]$ towards Aβ.[17] Finally, it has been seen that the greater stabilizing effect is achieved with a lower molar ratio $A\beta_{1-42}$ / CORM-3, therefore when $A\beta_{1-42}$ is modified only at the level of a histidine residue instead of two or three residues, remaining more soluble and less prone to aggregation.

CD study of $A\beta_{1-42}$secondary structure has shown that when the peptide is mono-modified there is a total inhibition of the conformation of the filament. When instead double or triple adducts are formed, i.e. CORM-3 and $A\beta_{1-42}$ are in molar ratio 1: 5, this interaction induces a conformational change of $A\beta_{1-42}$ towards a filament-like disposition which, however, does not evolve into an extensive misfolding of the peptide. The interpretation of the CD data is supported by the relative abundance of $A\beta_{1-42}$ / CORM3 adducts at different times, as observed by ESI-MS analysis and a ThT fluorescence assay, suggesting that inhibition of amyloid aggregation is the higher when only a single histidine is involved in CORM-3-$A\beta_{1-42}$ interaction. In this way, further details have been obtained regarding the mechanism of action of CORMs, confirming that adducts with histidine residues of the amino acid chain of $A\beta_{1-42}$ are stable. CORM-3 emerged as a promising inhibitory agent towards $A\beta_{1-42}$ aggregation. Furthermore, the mass spectrometry and dichroism spectroscopy studies have provided useful data to identify the CORM / $A\beta_{1-42}$ molar ration in which there is the higher anti-aggregating activity. In addition, in view of researching MTDLs, the antiaggregant properties highlighted are complementary to the already known CORM-3 neuroprotective and anti-inflammatory. Therefore, these findings can be used as a further potential mechanism explaining the CORMs-mediated reduction of Aβ toxicity previously reported *in vitro* and additionally *in vivo*. CORM-3 is also promising from the toxicological point of view: CORM-3 does not increase CO levels *in vivo*, that the CO trapped by hemoglobin in therapeutic conditions is below the toxicity threshold (in humans, this threshold is close to 10% COHb). The study has identified CORM-3 as potential drug for further developments. The future aim will be testing the activity of this compound first *in vitro* in a cell model then *in vivo* in transgenic mouse models to have more realistic information about CORMs effects on amyloidogenesis.

References:

(1) De Simone, A.; et al. Investigating in Vitro Amyloid Peptide 1−42 Aggregation: Impact of Higher Molecular Weight Stable Adducts. *ACS Omega* 2019, *4*, 7, 12308–12318 https://doi.org/10.1021/acsomega.9b01531.

(2) Hettiarachchi, N. T.; et al. Heme Oxygenase-1 Protects against Alzheimer's Amyloid-B1-42-Induced Toxicity via Carbon Monoxide Production. *Cell Death Dis.* **2014**, *5* (12), e1569 https://doi.org/10.1038/cddis.2014.529.

(3) Bartolini, M.; et al. Kinetic Characterization of Amyloid-Beta 1-42 Aggregation with a Multimethodological Approach. *Anal. Biochem.* **2011**, *414* (2), 215-225https://doi.org/10.1016/j.ab.2011.03.020.

(4) Fiori, J.; et al. Mass Spectrometry as an Efficient Tool for the Characterization of Amyloid β Peptide 25-35 Self-Assembly Species in Aggregation and Inhibition Studies. *Eur. J. Mass Spectrom.* **2013**, *19* (6), 483-90 https://doi.org/10.1255/ejms.1255.

(5) Bartolini, M.; et al. Insight into the Kinetic of Amyloid β (1-42) Peptide Self-Aggregation: Elucidation of Inhibitors' Mechanism of Action. *ChemBioChem* **2007**, *8* (17), 2152-2161

https://doi.org/10.1002/cbic.200700427.

(6) Sakono, M.; Zako, T. Amyloid Oligomers: Formation and Toxicity of Aβ Oligomers. *FEBS Journal*. **2010**, *277* (6), 1348-1358 https://doi.org/10.1111/j.1742-4658.2010.07568.x.

(7) Findeis, M. A. Approaches to Discovery and Characterization of Inhibitors of Amyloid β-Peptide Polymerization. *Biochimica et Biophysica Acta - Molecular Basis of Disease*. **2000**, *1502*, 76-84 https://doi.org/10.1016/S0925-4439(00)00034-X.

(8) Santos-Silva, T.; et al. CORM-3 Reactivity toward Proteins: The Crystal Structure of a Ru(II) Dicarbonyl-Lysozyme Complex. *J. Am. Chem. Soc.* **2011**, *133* (5), 1192–1195 https://doi.org/10.1021/ja108820s.

(9) Hong, J.; et al. Binding Sites of [Ru(Bpy)2(H2O)2](BF 4)2 with Sulfur- and Histidine-Containing Peptides Studied by Electrospray Ionization Mass Spectrometry and Tandem Mass Spectrometry. *J. Mass Spectrom.* **2005**, *40* (1), 91-99 https://doi.org/10.1002/jms.779.

(10) Pontillo, N.; et al. Ru-Based CO Releasing Molecules with Azole Ligands: Interaction with Proteins and the CO Release Mechanism Disclosed by X-Ray Crystallography. *Dalt. Trans.* **2017**, *46* (29), 9621-9629 https://doi.org/10.1039/c7dt01991b.

(11) Santos, M. F. A.; et al. New Insights into the Chemistry of Fac-[Ru(CO)3]2 + Fragments in Biologically Relevant Conditions: The CO Releasing Activity of [Ru(CO)3Cl2(1,3-Thiazole)], and the X-Ray Crystal Structure of Its Adduct with Lysozyme. In *Journal of Inorganic Biochemistry*; **2012**; *117*, 285-291 https://doi.org/10.1016/j.jinorgbio.2012.06.018.

(12) Valensin, D.; et al. Fac-{Ru(CO)3}2+ Selectively Targets the Histidine Residues of the β-Amyloid Peptide 1-28. Implications for New Alzheimer's Disease Treatments Based on Ruthenium Complexes. *Inorg. Chem.* **2010**, *49* (11), 4720–4722 https://doi.org/10.1021/ic902593e.

(13) Naldi, M.; et al. Amyloid β-Peptide 25-35 Self-Assembly and Its Inhibition: A Model Undecapeptide System to Gain Atomistic and Secondary Structure Details of the Alzheimers Disease Process and Treatment. *ACS Chem. Neurosci.* **2012**, *3* (11), 952–962 https://doi.org/10.1021/cn3000982.

(14) Harry LeVine. Quantification of Beta-Sheet Amyloid Fibril Structures with Thioflavin T. *Methods Enzymol.* **1999**, *309* (18), 274-84 https://doi.org/10.1016/s0076-6879(99)09020-5. PMID: 10507030.

(15) Sengupta, U.; et al. The Role of Amyloid-β Oligomers in Toxicity, Propagation, and Immunotherapy. *EBioMedicine*. **2016**, *6*, 42-49 https://doi.org/10.1016/j.ebiom.2016.03.035.

(16) Fiori, J.; et al. Disclosure of a Fundamental Clue for the Elucidation of the Myricetin Mechanism of Action as Amyloid Aggregation Inhibitor by Mass Spectrometry. *Electrophoresis* **2012**, *33* (22), 3380-3386 https://doi.org/10.1002/elps.201200186.

(17) Singh, S. K.; et al. Overview of Alzheimer's Disease and Some Therapeutic Approaches Targeting A β by Using Several Synthetic and Herbal Compounds. *Oxid. Med. Cell. Longev.* **2016**, *2016*, 7361613 https://doi.org/10.1155/2016/7361613.

Part III

Development of a Lipidomic Method in View of Researching New Potential Biomarkers for Targeting and Monitoring Alzheimer's Disease

5. Aß$_{1-42}$ Peptide Toxicity on Neuronal Cells: a Lipidomic Study in View of Alzheimer's Disease Drug Discovery

5.1 Aim of the Work

Currently not all Alzheimer's Disease (AD) pathological pathways, which lead to cell death and dementia, are completely investigated; among these, the lipid changes in brain tissues that begin years before AD symptoms.[1] While the central role of amyloid aggregation process is well established,[2] more in-depth studies must be conducted to disclose the connections of this process to the alterations in brain lipid metabolism**.** Lipidomic approach could be considered as a viable research method to analyse the lipid profile of cells stressed by $A\beta_{1-42}$ in order to deeply explore the mechanisms of toxicity of the peptide. The current project originated from a series of different studies focused on the β-amyloid aggregation process and its potential inhibition.[3] [4] The most crucial steps of the work concerned SH-SY5Y cells treatment with $A\beta_{1-42}$ and the development of a mass spectrometry analytical method able to detect the related alterations in lipidome. The aim was to disclose some peculiar lipid alterations, suitable as biomarkers, that might be correlated to $A\ss_{1-42}$ different aggregation species to explore the cellular response mechanisms to the toxic stimuli. Finally, the purpose was to achieve an attractive cell model for *in vitro* studies on AD, that can be applied to the elucidation of amyloid aggregation inhibitors mechanism of action, able not only to inhibit the aggregation process, but also to reduce lipid alterations, in view of discovering new AD drugs.[5]

5.2 Materials and Methods

5.2.1 Materials

Mobile phases were prepared with solvents of Ultra LC-MS grade. Acetonitrile (ACN) and isopropanol (IPA) were supplied by Carl Roth (Karlsruhe, Germany). Ammonium formate, formic acid, and IPA of HPLC grade, were purchased from Merck (Darmstadt, Germany). Ultrapure water was obtained by purification with a water filtration system from Elga Purelab (Celle, Germany).

EquiSPLASH™ LIPIDOMIX® containing the following isotopically labeled internal standards (ILIS): 15:0e-18:1(d7)-PC, 15:0-e18:1(d7)-PE, 15:0e-18:1(d7)-PS, 15:0e-18:1(d7)-PG, 15:0e-18:1(d7)-PI, 15:0e-18:1(d7)-PA, 18:1(d7)-LPC, 18:1(d7)-LPE, 18:1(d7)-Chol Ester, 18:1(d7)-MG, 15:0e-18:1(d7)-DG, 15:0e-18:1(d7)-15:0-TG, 18:1(d9)-SM, Cholesterol(d7) was purchased from Avanti Polar Lipids (Alabama, USA). Arachidonic acid-d11 (AA-d11), C18-Ceramide-d7 (d18:1-d7/18:0), and Palmitoyl-L-Carnitine (d3) were obtained from Cayman Chemicals (Ann Arbor, MI, USA). The final concentrations used are specified in table 5.2.2-**1**. Light Splash containing the following standards: 15:0-18:1 PC, 18:1 Lyso PC , 15:0-18:1 PE, 18:1 Lyso PE, 15:0-18:1 PG, 15:0-18:1 PI , 15:0-18:1 PS, 15:0-18:1-15:0 TG, 15:0-18:1 DG, 18:1 MG, 18:1 Chol Ester, d18:1-18:1 SM and C15 Ceramide (d18:1/15:0) was acquired from Avanti Polar Lipids (Alabama, USA); FA 20:4 (AA), Palmitoyl-L-Carnitine, FA 15:0-18:1 (PA), Cholesterol, Chol Ester 18:1, d18:1 Lyso SM and Sphingosine-1-phosphate d18:1 were obtained from Cayman Chemicals (Ann Arbor, MI, USA). The

concentrations of unlabeled standards used as calibrants in QC samples for the method validation are listed in table 5.2.2-**2**

5.2.2 Lipid Extraction and LC-MS Method Validation

Sample preparation In table 5.2.2-**1** the concentrations of internal standards used in QC samples for the method validation and subsequently in SH-SY5Y cell sample analysis are reported.

Internal standard	Final concentration in the reconstituted solution [ng/mL]	Final concentration in the reconstituted solution [nmol/L]
FA 20:4 (AA) (d11)	11	0.035
Palmitoyl-L-Carnitine (d3)	50	0.114
FA 15:0-18:1 (PA) (d7)	50	0.072
d18:1 (d9) Lyso SM	50	0.108
Sphingosine-1-phosphate d18:1 (d7)	50	0.129
15:0-18:1 (d7) PC*	50	0.066
15:0-18:1 (d7) PE*	50	0.070
15:0-18:1 (d7) PS (NH4 Salt) *	50	0.064
15:0-18:1 (d7) PG (NH4 Salt) *	50	0.065
15:0-18:1 (d7) PI (NH4 Salt) *	50	0.059
18:1 (d7) Lyso PC*	50	0.095
18:1 (d7) Lyso PE*	50	0.103
Chol Ester 18:1 (d7) *	50	0.076
18:1 (d7) MG*	50	0.138
15:0-18:1 (d7) DG*	50	0.085
15:0-18:1 (d7) -15:0 TG*	50	0.062
d18:1-18:1 (d9) SM*	50	0.068
C15-Ceramide-d7*	50	0.087
Cholesterol (d7)	200	0.508

*Internal standards prepared from EquiSPLASH Lipidomix

Table *5.2.2* -**1** Final concentrations of internal standards

In table 5.2.2-**2** the concentrations of unlabeled standards in QC samples used as calibrants for the method validation are listed.

Surrogate calibrant	**Cal 1 [nmol/L]**	**Cal 2 [nmol/L]**	**Cal 3 [nmol/L]**	**Cal 4 [nmol/L]**	**Cal 5 [nmol/L]**	**Cal 6 [nmol/L]**
15:0-18:1 PC*	0.001	0.013	0.134	1.340	13.404	40.212
18:1 Lyso PC*	0.002	0.019	0.192	1.917	19.169	57.508
15:0-18:1 PE*	0.001	0.014	0.142	1.421	14.205	42.615
18:1 Lyso PE*	0.002	0.021	0.209	2.085	20.851	62.553
15:0-18:1 PG*	0.001	0.013	0.132	1.321	13.211	39.632
15:0-18:1 PI*	0.001	0.012	0.119	1.190	11.904	35.711
15:0-18:1 PS*	0.001	0.013	0.130	1.299	12.988	38.963
15:0-18:1-15:0 TG*	0.001	0.012	0.124	1.242	12.418	37.253
15:0-18:1 DG*	0.002	0.017	0.172	1.721	17.214	51.642
18:1 MG*	0.003	0.028	0.280	2.805	28.047	84.142
18:1 Chol Ester *	0.002	0.015	0.154	1.536	15.359	46.076
d18:1-18:1 SM*	0.001	0.014	0.137	1.372	13.716	41.148
C15 Ceramide (d18:1/15:0)*	0.002	0.019	0.191	1.909	19.088	57.264
FA 20:4 (AA)	0.003	0.032	0.317	3.170	31.696	95.087
Palmitoyl-L-Carnitine	0.002	0.023	0.228	2.277	22.774	68.322
FA 15:0-18:1 (PA)	0.001	0.014	0.145	1.449	14.494	43.483
Cholesterol	0.003	0.025	0.254	2.540	25.400	76.200
Chol Ester 18:1	0.002	0.015	0.152	1.519	15.194	45.582
d18:1 Lyso SM	0.002	0.022	0.215	2.152	21.523	64.569
Sphingosine-1-phosphate d18:1	0.003	0.026	0.259	2.587	25.873	77.618

*Standards prepared from Light SPLASH Lipidomix

Table *5.2.2* -**2** Concentrations of surrogate calibrants

Three sets of Quality Control samples (QCs) were used for the calculation of Matrix effect (ME %), extraction recovery (RE %) and process efficiency (PE %) and Intra-assay precision and Intra-assay accuracy for 2 QC levels

Series 1 (pre-extraction spiked):

Samples (1 x 10^6 cells) were spiked with 100 µL of calibrant solution with 1:10 diluted IS stock mix to get QCs with only 1 level of IS and 2 levels of unlabeled lipids: low (1000 ng/mL) and high (10 000 ng/mL) level, each one in 3 replicates. Then the lipid extraction procedure has been performed as described in paragraph 5.2.6. The dried lipid extracts were reconstituted in 100 µL of methanol before the injection into the LC-MS instrument.

Series 2 (post-extraction spiked):

1 mL of IPA:H_2O (90:10 v/v) was added to samples (1 x 10^6 cells). After that, the lipid extraction procedure has been carried out as described in paragraph 5.2.6. Finally, the dried lipid extracts were reconstituted in 100 µL of Calibrant solution 1:10 diluted IS stock mix to obtain low and high level (each one in 3 replicates): 1000 ng/mL and 10 000 ng/mL respectively.

Series 3 (neat solution):Calibrants solutions corresponding to concentrations 1000 ng/mL and 10 000 ng/mL with 1:10 diluted IS stock mix (each one in 3 replicates) were directly injected into the LC-MS instrument.

In table 5.2.2-**3**. the concentrations of every unlabeled standard in the 2 levels of QC samples used for the validation are reported.

Lipid	**Endogenous concentration [nmol/L]**	**QC low L [nmol/L]**	**QC high H [nmol/L]**
15:0-18:1 PC	0.004	1.340	13.404
18:1 Lyso PC	0.006	1.917	19.169
15:0-18:1 PE	0.001	1.421	14.205
18:1 Lyso PE	0.001	2.085	20.851
15:0-18:1 PG	0.000	1.321	13.211
15:0-18:1 PI	0.000	1.190	11.904
15:0-18:1 PS	0.000	1.299	12.988
d18:1-18:1 SM	0.001	1.372	13.716
C15 Ceramide (d18:1/15:0)	0.000	1.909	19.088
FA 20:4 (AA)	0.001	3.170	31.696
Palmitoyl-L-Carnitine	0.000	2.277	22.774
d18:1 Lyso SM	0.000	2.152	21.523

Table *5.2.2*-**3**. Concentrations of quality controls (QCs) (prepared by spiking of cell extract from 1×10^6 cells)

LC-MS analysis: Chromatographic conditions In table 5.2.2- **4** the composition of eluent A and B in the mobile phase is described and table 5.2.2-**5** shows the gradient elution program and the change of mobile phase component B during the gradient elution

Component	**A**	**B**
ACN %	60	9
H_2O %	40	1
NH_4HCOO	10 mM	10 mM
HCOOH	0.1	0.1
IPA %	0	90

Table *5.2.2*-**4** Mobile phase composition

Time [min]	% A	% B
0.00	85	15
2.00	70	30
2.50	52	48
11.00	18	82
11.50	1	99
12.00	1	99
12.10	85	15
15.00	85	15

Table *5.2.2*-**5** Mobile phase gradient during LC runs

MS conditions In Table 5.2.2-**6** the parameters used in Sciex Triple-TOF 5600+ Mass Spectrometry for non-targeted MS/MS acquisition are present. DIA by SWATH was used with variable Q1 window size covering the 50-1250 m/z range.

				Positive			**Negative**	
Experiment	**Type**	**Acc.Time [ms]**	**Start *m/z***	**Stop *m/z***	**Collision Energy [V]**	**Start *m/z***	**Stop *m/z***	**Collision Energy [V]**
1	Ms Full SCAN	80	50	1250.0	10	50	1250.0	-10
2	SWATH	31	50	214.6	45 ± 15	49.5	342.2	-46 ± 15
3	SWATH	31	213.6	281.8	45 ± 15	341.2	453.6	-46 ± 15
4	SWATH	31	280.8	390.7	45 ± 15	452.6	450.8	-46 ± 15
5	SWATH	31	389.7	40.4	45 ± 15	479.8	507.8	-46 ± 15
6	SWATH	31	479.4	509.0	45 ± 15	506.8	532.3	-46 ± 15
7	SWATH	31	508.0	536.5	45 ± 15	531.3	566.8	-46 ± 15
8	SWATH	31	535.5	610.6	45 ± 15	565.8	617.4	-46 ± 15
9	SWATH	31	609.6	677.1	45 ± 15	616.4	687.1	-46 ± 15
10	SWATH	31	676.1	709.0	45 ± 15	686.1	715.0	-46 ± 15
11	SWATH	31	708.0	735.1	45 ± 15	714.0	744.1	-46 ± 15
12	SWATH	31	734.1	759.1	45 ± 15	743.1	755.1	-46 ± 15
13	SWATH	31	758.1	773.1	45 ± 15	754.1	776.0	-46 ± 15
14	SWATH	31	772.1	790.2	45 ± 15	775.0	794.6	-46 ± 15
15	SWATH	31	789.2	811.2	45 ± 15	793.6	807-6	-46 ± 15
16	SWATH	31	810.2	827.2	45 ± 15	806.6	830.3	-46 ± 15
17	SWATH	31	826.2	856.2	45 ± 15	829.3	840.1	-46 ± 15
18	SWATH	31	855.2	884.3	45 ± 15	839.1	859.2	-46 ± 15
19	SWATH	31	883.3	915.9	45 ± 15	858.2	889.1	-46 ± 15
20	SWATH	31	914.9	983.7	45 ± 15	888.1	924.6	-46 ± 15
21	SWATH	31	982.7	1250.0	45 ± 15	923.6	1050.5	-46 ± 15

Table 5.2.2-**6**. MS-settings of Sciex Triple-TOF 5600+ mass spectrometry: SWATH design

5.2.3 $A\beta_{1-42}$ Peptide Preparation

1 mg of $A\beta_{1-42}$ lyophilized (Bachem; Switzerland) powder was pretreated overnight with 1400 µL of hexafluoroisopropanol (HFIP) (Merck Life Science S.r.l, Milan, Italy), portioned, and the resulting unaggregated $A\beta_{1-42}$ peptide film was stored at −20 °C after solvent evaporation, as previously described.[4 6 7] Before cell treatment, $A\beta_{1-42}$ film was dissolved in 40 µL of DMSO (Merck Life Science S.r.l, Milan, Italy) and left at room temperature for 1 h, then diluted in Phosphate Buffer Solution (PBS) (Euroclone, Milan, Italy) to reach the final concentration of 500 µM.

5.2.4 Cell Culture and Cell Treatment

The cells used throughout these experiments are human neuronal cells, SH-SY5Y (Merck Life Science S.r.l, Milan, Italy) cells were grown in Dulbecco's modified Eagle's Medium (DMEM) supplemented with 10% heat-inactivated fetal bovine serum (FBS), 1% 2 mM L-glutamine solution and 1% penicillin/streptomycin solution (Euroclone, Milan, Italy). Cells were incubated at 37° C in a humidified incubator with 5% CO_2. To maintain exponential growth, the medium was changed every 2–3 days and cells were split using 0.025 % Trypsin-EDTA solution (Euroclone, Milan, Italy). Cells were then seeded in 24 well culture plate at a concentration of 2.5-5-10-15 x 10^4 cells/well. Cells were used for experiments after inducing their differentiation with RA. After 4h from seeding, Retinoic Acid (AR) (Euroclone, Milan, Italy) at final concentration of 10 µM in DMEM was added. Cells were incubated for a total of four days with RA, changed every 48h. Human brain derived neurotrophic-factor (BDNF) (Euroclone, Milan, Italy) at the final concentration of 50 ng/mL was added in fresh DMEM without FBS for at least two days. The cells differentiated were then used for the treatment with $A\beta_{1-42}$ at different concentrations (2-5-10-25-40-50 µM).
After 24h or 48h incubation (different treatment time), the cell viability was evaluated and then the cells were washed with 500 µL of PBS. Afterwards, the cells were incubated with 100 µL of Trypsin solution (0.025%) at 37°C. After 3 min, cells were washed by adding 300 µL of DMEM supplemented with 10% fetal bovine serum.
The suspension was transferred into 1.5 mL reaction tubes and centrifuged at 1200 rpm for 5 min at 25 °C; the supernatant was withdrawn. The remaining cell pellets were frozen at –20 °C until extraction.

5.2.5 Cell Viability Measurement

Cell viability was evaluated using the PrestoBlue™ HS Cell Viability Reagent. It is a ready-to-use resazurin-based solution that works as a cell health indicator by using the reducing power of living cells to quantitatively measure viability. This reagent has been optimized for the fast and reliable detection of mammalian cell viability. Resazurin-based reagent enters the living cells that continuously converts resazurin to resorufin, resulting in a pronounced color change. Thus, the cell viability can be detected using absorbance-based plate readers. Since no lysis is required, the diluted PrestoBlue HS solution can be removed and replaced with complete growth medium, for further culturing of the cells. So, briefly, at the end of each experiment, the cell

medium was removed, and replaced by a mix of 450 µL of complete growth media and 50 µL of PrestoBlue™ HS Cell Viability Reagent in each well of the 24-well plate. After 3h of incubation at 37 °C and 5% CO_2, the absorbance at 570 nm was detected through microplate spectrophotometer (VICTOR3 V Multilabel Counter; PerkinElmer, Wellesley, MA, USA) using 600 nm as reference wavelength. Data are reported as percentage with respect to controls. Control cells are considered as 100 % cell viability. (Figure 5.2.5-**1**)

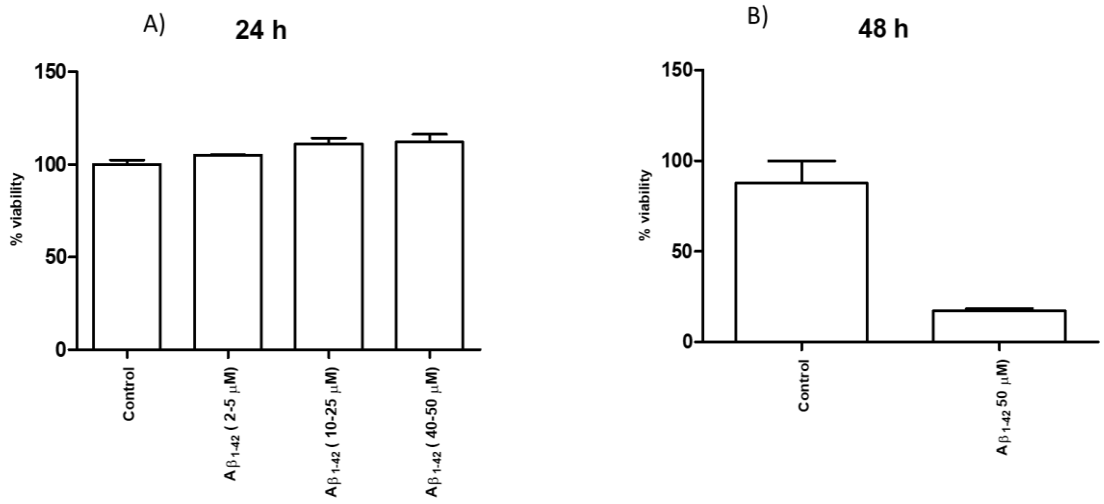

Figure *5.2.5*-**1** Percentage Viability of SH-SY5Y cells treated with Aβ1-42. SH-SY5Y cells were incubated with Aβ1-42 (A) at increasing concentrations (2-50 µM) for 24 h (B) at highest concentration (50 µM) for 48 h. Data are expressed as percentage with respect to untreated cells, considered as 100 % cell viability. Each bar represents means ± SEM of three independent experiments

5.2.6 Lipid Extraction of Samples with IPA: H_2O (90:10 v/v)

Cell pellet was suspended in 1 mL of IPA:H_2O (90:10 v/v) solution, then 100 µL of internal standard (IS) mix was added and samples were finally vortexed (30 s) for mixing. Five (5) cycles (x 10 s and 30 s of pause between each other, 4°C) in Precellys® evolution homogenizer (Bertin GMBH, Frankfurt am Main, Germany) was applied for the cell cryo-lysis. Then samples were incubated on ice on an orbital shaker (500 rpm, 60 min) to have a complete protein precipitation and lipid extraction. After the lipid extraction, centrifugation at 12200 rpm for 10 min was applied and supernatant was transferred to a 1.5 mL reaction tubes. Samples were dried overnight in centrifugal evaporator under nitrogen protection. The lipid extract was resuspended in 100 µL of methanol followed by vortexing (30 sec) and sonication (2 min). Centrifugation at 3500 rcf for 3 min at 4°C was performed and the supernatants were transferred into vials for MS-measurements. During the last step, 10 µL aliquot from each sample was removed and transferred into another vial to prepare the pooled QC sample.

5.2.7 LC-MS/MS Untargeted Analysis

Analysis were performed by Agilent 1290 Series UHPLC instrument (Agilent, Waldbronn, Germany) coupled to Sciex Triple-TOF 5600+ MS (Sciex, Concord, Ontario; Canada) with duo-spray source and Pal HTC-xt

autosampler from CTC (Zwingen, Switzerland). All samples were analyzed in both positive and negative ion mode with electrospray ionization with the same chromatographic separation conditions.

Acquity UPLC CSH C18 (130 Å, 1.7 µm, 2.1 mm × 100 mm) column was used with Acquity UPLC CSH C18 VanGuard pre-column (130 Å, 1.7 µm, 2.1 mm × 5 mm) (Waters, Eschborn, Germany) for chromatographic separation.

About the mobile phase, eluent A was composed of 60:40 ACN:H_2O (v/v) containing 10 mM ammonium formate and 0.1% formic acid (v/v) and eluent B of 90:9:1 IPA/ACN/H2O (v/v/v)containing 10 mM ammonium formate and 0.1% formic acid (v/v). The gradient elution started with 15% B; then it was increased to 30% B in 2 min followed by further increase to 48% B within the next 0.5 min. In the following 11.00 min the gradient was elevated to 82% B and then quickly reached 99% B in the next 0.5 min, and stayed at this percentage for 0.5 min; Afterwards, the percentage of B was back to starting conditions (15% B) in 0.1 min to re-equilibrate the column for the next injection (2.9 min). The flow rate was 0.6 mL/min and column temperature was 65 °C. The injection volumes were 3 µL and 5 µL for positive and negative ion mode, respectively.

LC-ESI-MS/MS experiments were measured firstly in positive polarity mode and then in negative polarity mode. The mass spectrometry parameters were set as follows: curtain gas (CUR) 35 psi, nebulizer gas (GS1) 60 psi, drying gas (GS2) 60 psi, ion-spray voltage floating (ISVF) + 5500 V in positive and - 4500 V in negative mode, source temperature (T) 350 ° C, collision energy 45 V, collision energy spread 15 V, declustering potential (DP) 80 V, mass range m/z 50-1250 in ESI (+) and 50-1050 in ESI (-), and RF Transmission (RF) m/z 40: 50% and m/z120: 50%.
MS/MS experiments were acquired by using sequential window acquisition of all theoretical fragment ion spectra (SWATH). The MS cycle time was always 720 ms. More details on MS and MS/MS experiments are reported in the table 5.2.2-**6**.
The sample order was randomized. The sequence started with three injections of IS mixture as system suitability test and was controlled by regular injection of the QC sample after every 5 samples to control the performance of the instrument throughout the sequence. Finally, a dilution series of calibrant solution has been injected at the beginning and in the end of the sequence.

5.2.8 Lipidomic Data Processing

Identification based on different MS and MS/MS signals. MultiQuant 3.0 software was used to calculate the peak height of the IS while data pre-processing, identification and relative quantification of the unknown lipids were performed using MS-Dial software (RIKEN, version 4.24).[8] Data raw files (.wiff format) were converted into Analysis Base Files (.abf format) via the ABF converter (Reifycs, Tokys, Japan) in order to perform peak detection, deisotoping, adduct assignment, feature alignment, MS2 data deconvolution, and

compound identification through all the samples. After conversion, the MS-DIAL projects were created separately for each ionization mode.

The identification was achieved by comparison of experimental spectra with those in the LipidBlast library (tR tolerance for Lipid-Blast based identification: 0.5 min) using both accurate mass and MS/MS fragmentation data (identification score cut-off: 85%;)

Processing parameters were adjusted to the following settings: peak finding between 0 and 15 min; precursor m/z range from 50 to 1250; TOF-MS and SWATH-MS/MS tolerance for peak profile were set to 0.01 and 0.025 Da, respectively; Smoothing level: 1; minimum number of points per peak: 5; minimum peak height: 1000 cps. Blank subtraction was exerted for signals that had a fold change <5 in the average samples compared to the average blank signals. A quality control pooled sample (QC, a mix of all samples in the batch) was prepared and injected several times (every five samples) during the batch analysis to test the instrumental variability. Peak alignment was based on the 5th QC sample with a tR tolerance of 0.2 min. TOF-MS tolerance of m/z 0.05.

Identification with a retention time prediction model. In reversed phase chromatography the different lipid species of the same class elute with a regular characteristic order. For this reason, retention time prediction models can be utilized to confirm lipid identification and check for misannotations, respectively. The retention time prediction model used here was based on two main observations. First, lipids of the same class with the same number of double bonds in the FAs elute in order of increasing carbon number (as sum of carbon atoms in FA chains). Secondly, lipids of the same class and the same number of carbons in FA chains elute in order of decreasing double bond number. All lipid classes were analyzed separately. In each class, lipids were divided into groups with the same number of double bonds. For each class, a spotting map, a plot of m/z of precursor ions versus retention times was prepared (figure 5.3.3-**2**). Then, the empirical correlation of the given m/z and RT was calculated for each group. A correlation coefficient > 0.95 was required to consider that all the found lipids were correctly identified. However, if the correlation coefficient was lower or elution order was not correct, outliers were removed

Relative quantification. Data of the lipids were normalized to the lipid class-specific IS. The relative abundance of every lipid species has been calculated as percentage distribution in its lipid class (sum of the total lipid signals identified in the same class).
Non-parametric Mann-Whitney U Test (U-test) was performed at significance level P=0.05. Fold changes were also calculated in the paired manner to find significantly regulated lipids between the two groups of treated cells and untreated control samples.

5.3.1 Results of the Lipid Extraction and LC-MS Method Validation

Quantitative analysis was based on peak area ratios of precursor ion EICs of target analytes to precursor ion EICs of internal standards. Quantitative analysis was performed using MultiQuant 3.0 software in the three sets of Quality Control samples (QCs) at two concentration level (low-high)

For LC-MS method validation in positive and negative ionization mode recovery (ER) matrix effect (ME) and process efficiency (PE) and intra-assay precision and accuracy have been calculated.

Positive polarity ionization mode analysis:

	ER [%]		**ME [%]**		**PE [%]**	
Lipid	**Low**	**High**	**Low**	**High**	**Low**	**High**
15:0-18:1 PC	117	106	N/A	90	N/A	95
15:0-18:1 PE	104	96	95	107	99	103
18:1 Lyso PE	90	95	108	108	98	103
15:0-18:1 PI	104	97	91	90	95	87
18:1-18:1 SM	94	95	84	96	79	90
C15 Ceramide	104	90	84	89	88	80
Palmitoyl-L-Carnitine	99	105	101	99	100	104

ER (%) = A/B x 100 (A= pre-extraction spiked set; B= post-extraction spiked set); ME (%) = B/C x 100 (B= post-extraction spiked set; C= neat solution standards); PE (%) = A/C x 100 = (ME x RE) /100

Table *5.3.1*-**1** Validation of extraction recovery (ER) matrix effect (ME) and process efficiency (PE)

	Intra-assay precision		**Intra-assay accuracy**	
Lipid	**Low**	**High**	**Low**	**High**
15:0-18:1 PC	N/A	2	104	100
15:0-18:1 PE	2	5	101	100
18:1 Lyso PE	0	0	93	92
15:0-18:1 PI	4	13	101	100
18:1-18:1 SM	10	5	107	100
C15 Ceramide	6	9	109	100
Palmitoyl-L-Carnitine	1	3	112	100

The precision of the method was determined by the replicate analyses (n=3) of the 2 level of 3 set of samples containing each one of every standard while the accuracy was expressed by [(mean observed concentration) / (spiked concentration] x 100 corrected for endogenous levels

Table *5.3.1*-**2**, Validation of intra-assay precision (CV%; acceptance criteria ± 15%) and intra-assay accuracy (% recovery; acceptance criteria 100 ± 15%)

Negative polarity mode analysis:

	ER [%]		ME [%]		PE [%]	
Lipid	**Low**	**High**	**Low**	**High**	**Low**	**High**
18:1 Lyso PC	100	106	94	105	94	111
15:0-18:1 PG	99	93	100	98	99	90
15:0-18:1 PS	110	89	N/A	79	N/A	70
20:4 AA	88	127	93	90	82	115
LysoSM d18:1	95	89	107	115	101	102

Table *5.3.1*-**3**. Validation of extraction recovery (ER), matrix effect (ME), and process efficiency (PE)

	Intra-assay precision			**Intra-assay accuracy**	
Lipid	**Low**	**High**		**Low**	**High**
18:1 Lyso PC	23	N/A		N/A	N/A
15:0-18:1 PG	7	4		99	100
15:0-18:1 PS	9	10		90	100
20:4 AA	35	18		106	100
LysoSM d18:1	19	18		95	100

Table *5.3.1*- **4** Validation of intra-assay precision (CV%; acceptance criteria ± 15%) and intra-assay accuracy (% recovery; acceptance criteria 100 ± 15%)

5.3.2 Background and Study Design

In the present work differentiated neuroblastoma cells were treated with $A\beta_{1\text{-}42}$ peptide at increasing concentrations (2-50 µM) for 24 h and at 50 µM for 48 h, respectively, in the first and in the second case studies. The $A\beta_{1\text{–}42}$ peptide concentration and time of incubation were fixed in agreement with other previous studies.[9 10 11]

The human SH-SY5Y cell line is widely used as a model for different neurodegenerative diseases. Due to their dopaminergic character, SH-SY5Y cells are generally considered as a model for Parkinson's disease.[12] However, their phenotype can be changed by different protocols of neural differentiation and to obtain dominantly cholinergic phenotype suitable for AD studies.[13] So far, the in *vitro* toxic effects of amyloid peptides are most commonly examined using the human neuroblastoma derived SH-SY5Y cell line. However, in most of the publications non-differentiated cells are used. According to a recent study differentiation is a crucial step to achieve most accurate results for translation and comparison to in *vivo* models.[13] For this reason, in the present experiments, SH-SY5Y cells were treated with retinoic acid (RA) and brain-derived neurotrophic

factor (BDNF), following the same protocol described by Krishtal et al.[14] In fact, differentiated neuron-like SH-SY5Y cells are more sensitive to amyloid peptides than non-differentiated cells, because the latter lack long neurites. It is known that the toxic effect of exogenous soluble $A\beta_{1-42}$ is related to its tendency to cover cell bodies and whole neurites in differentiated cells with dense fibrils, causing neurite beading and fragmentation. When SH-SY5Y cells are undifferentiated, they rapidly proliferate and appear to be non-polarized, with very few, short processes. They often grow in clumps and express markers indicative of immature neurons. Nevertheless, currently there are only a few studies examining Aβ-induced toxicity in differentiated SH-SY5Y cells. Moreover, only in a recent study Aβ-induced toxicity has been investigated in RA/BDNF differentiated SH-SY5Y cells.[14]

Another important investigated issue concerns the exact nature and secondary structure of the toxic forms of Aβ. In 1994 Lambert and colleagues proved that the toxic effect of $A\beta_{1-42}$ on RA pre-treated SH-SY5Y cells could be attributed to the peptide oligomers (DMSO-induced).[15] In agreement, in the study of Krishtal et al the preformed $A\beta_{1-42}$ fibrils had no toxic effects. The Andrisano research group investigated through circular dichroism spectroscopy the influence of experimental conditions in determining the conformation and the solubility of Aβ *in vitro*, which in turn affects the rate of amyloid aggregation.[7] They also showed that the change of secondary structure towards β-sheets can be reverted by inhibitors.[7] They proved that the kinetic of the amyloid aggregation process is strongly related to the peptide and salt concentration in solution, the temperature, the pH value and solvent properties and concentration of active inhibitors. The storing conditions of the solid-state peptide were found to significantly affect its conformation too. For all these reasons, we used the validated method by Bartolini et al. to prepare $A\beta_{1-42}$ peptide with a high non-amyloidogenic conformation content. This is a crucial point to ensure that aggregation starts from the same Aβ conformation conditions. For this purpose, the Aβ peptide was solubilized in HFIP which represents an ideal solvent to stabilize the Aβ peptide in its α-helix secondary structure conformation even after 24 h. Then the resulting $A\beta_{1-42}$ film obtained by solvent evaporation was stable when kept at -20 °C and could be stored and used for further studies. Before the incubation with SH-SY5Y neuroblastoma cells, the unaggregated $A\beta_{1-42}$ film was dissolved in DMSO, then the solution was diluted in PBS. The purpose was to have the shift towards the β-sheet structure, which eventually leads to oligomerization and insoluble fibril formation, only during the incubation with the differentiated neuroblastoma cells.

5.3.3 Lipidomics and Lipid Identification

After incubation of the SH-SY5Y cells with the peptide, the lipid extraction of washed cells was performed by using a monophasic solvent extraction protocol with IPA 90%, as previously reported.[15] It represents a convenient, less time consuming, less toxic and cheaper protocol in comparison to extraction methods performed with methyl tert-butyl ether (MTBE), Chloroform/MeOH ($CHCl_3$) such as of the classical Folch and Bligh&Dyer protocols.[16] This method produced an improved yield of recovery and higher precision, accuracy and reproducibility, especially for more polar lipids.

For the analysis of the lipid extract, RP-type UHPLC lipid species separation was selected and coupled to ESI-QTOF-MS/MS detection. Data-independent SWATH acquisition provided comprehensive MS1 and MS2 data across all studied samples

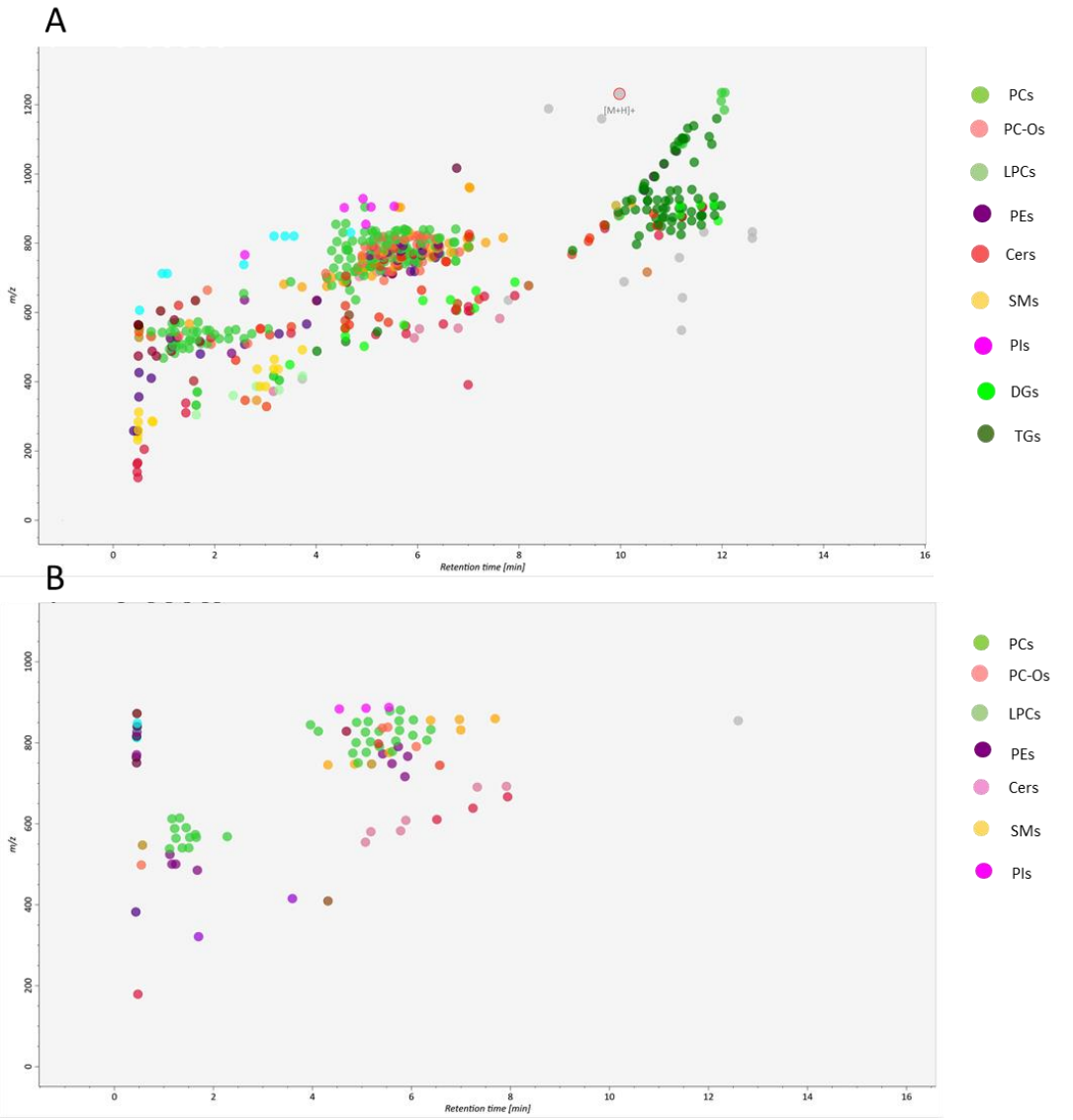

Figure *5.3.3*-**1** Lipid identification: Peak spotting map. (A) corresponds to the spotting map of the lipid species identified in positive ionization mode (ESI+), while (B) depicts the lipid species determined in negative ionization mode

Table 5.3.3-**1** summarizes the identified lipids by showing the experimental and theoretical precursor ions of PCs, LPCs, PC-O, SMs, Cers, PEs, TGs, PIs, DGs and TGs as automatically annotated by MS-Dial software (RIKEN, version 4.24) using the LipidBlast library, followed by verification with retention model for outlier detection, and manual curation through checking the MS2 spectra of the lipids with low scores in MS-DIAL

	t_R [min]	**Adduct type**	**Precursor ion m/z**	**Theoretical m/z**	**Mass error [ppm]**
PC 28:0	4.308	[M+H]+	678.50891	678.50684	-3
PC 30:0|PC 14:0_16:0	4.94	[M+H]+	706.53748	706.53815	-1

PC 30:2|PC 15:1_15:1	4.208	[M+H]+	702.5097	702.50684	4
PC 31:1|PC 14:0_17:1	4.933	[M+H]+	718.53772	718.53815	-1
PC 32:0|PC 16:0_16:0	5.074	[M+H]+	734.56946	734.56946	0
PC 32:1|PC 16:0_16:1	5.079	[M+Na]+	754.53754	754.53571	2
PC 32:2|PC 16:0_16:2	5.073	[M+H]+	732.5520	732.55377	-2
PC 32:2|PC 16:1_16:1	4.819	[M+H]+	730.54114	730.53815	4
PC 33:0	4.348	[M+H]+	728.5224	728.52246	0
PC 33:1|PC 18:0_15:1	5.933	[M+H]+	748.58759	748.58508	3
PC 34:0|PC 16:0_18:0	5.35	[M+H]+	746.57141	746.56946	3
PC 34:1|PC 16:0_18:1	6.311	[M+H]+	762.60541	762.60071	6
PC 34:2|PC 16:1_18:1	5.68	[M+H]+	760.5871	760.58508	3
PC 34:3|PC 18:1_16:2	5.179	[M+H]+	758.56543	758.56946	-5
PC 34:4	4.909	[M+H]+	756.56073	756.55377	9
PC 35:1|PC 17:0_18:1	4.447	[M+H]+	754.53876	754.53815	1
PC 35:2|PC 17:1_18:1	6.03	[M+H]+	774.60333	774.60071	3
PC 36:0	5.438	[M+H]+	772.59082	772.58508	7
PC 36:1|PC 18:0_18:1	7.004	[M+H]+	790.6319	790.63202	0
PC 36:2|PC 18:1_18:1	6.381	[M+H]+	788.61694	788.61639	1
PC 36:3	5.751	[M+H]+	786.60095	786.60071	0
PC 36:3|PC 16:0_20:3	5.543	[M+H]+	784.58337	784.58508	-2
PC 36:4|PC 16:0_20:4	5.343	[M+H]+	784.59033	784.58508	7
PC 37:1	5.069	[M+H]+	782.56793	782.56946	-2
PC 37:2	6.714	[M+H]+	802.63715	802.63202	6
PC 38:1	4.59	[M+H]+	792.55457	792.55377	1
PC 38:2	7.035	[M+H]+	816.65417	816.64771	8
PC 38:3	6.052	[M+H]+	814.62451	814.63202	9
PC 38:3|PC 18:0_20:3	6.247	[M+H]+	812.61353	812.61639	-4
PC 38:4	6.039	[M+H]+	812.62317	812.61639	8
PC 38:4|PC 18:0_20:4	5.412	[M+H]+	810.5976	810.60071	-4
PC 38:4|PC 18:0_20:4	5.56	[M+H]+	810.60266	810.60071	2
PC 38:5|PC 16:0_22:5	5.74	[M+H]+	810.59967	810.60071	-1
PC 38:6	5.122	[M+H]+	808.58679	808.58508	2
PC 38:6|PC 16:0_22:6	4.716	[M+H]+	806.57019	806.56946	1
PC 38:7	4.909	[M+H]+	806.57416	806.56946	6
PC 39:5	4.411	[M+H]+	804.55365	804.55377	0
PC 39:6	5.435	[M+H]+	822.60504	822.60071	5
PC 40:3	5.222	[M+H]+	820.59259	820.58508	9
PC 40:4	6.751	[M+H]+	840.64777	840.64771	0
PC 40:7	5.559	[M+H]+	834.60175	834.60071	1
PC 40:8	4.959	[M+H]+	832.58301	832.58508	-2
PC 42:9	4.653	[M+H]+	830.56885	830.56946	-1
PC 42:10	4.39	[M+H]+	854.56958	854.56946	0
LPC 14:0	0.99	[M+H]+	468.31094	468.30847	5
LPC 15:0	1.211	[M+H]+	482.32617	482.32413	4
LPC 16:0 (1)	1.369	[M+H]+	496.33951	496.33978	1
LPC 16:0 (2)	1.499	[M+H]+	496.3414	496.33978	3
LPC 16:1	1.111	[M+H]+	494.32425	494.32413	0
LPC 17:0 (1)	1.729	[M+H]+	510.35443	510.35541	2
LPC 17:0 (2)	1.856	[M+H]+	510.35815	510.35541	5

LPC 18:0	2.277	[M+H]+	524.37463	524.37109	7
LPC 18:1 (1)	1.519	[M+H]+	522.3595	522.35541	8
LPC 18:1 (2)	1.651	[M+H]+	522.35706	522.35541	3
LPC 18:2	1.246	[M+H]+	520.33826	520.33978	3
LPC 19:0 (1)	2.733	[M+H]+	538.38824	538.38672	3
LPC 19:1 (2)	1.999	[M+H]+	536.37329	536.37109	4
LPC 20:0	3.055	[M+H]+	552.40314	552.40234	1
LPC 20:1	2.417	[M+H]+	550.38922	550.38672	5
LPC 20:2	1.851	[M+H]+	548.36993	548.37109	2
LPC 20:3	1.439	[M+H]+	546.35706	546.35541	3
LPC 20:4	1.213	[M+H]+	544.34265	544.33978	5
LPC 20:5	0.969	[M+H]+	542.3255	542.3241	3
LPC 22:5 (2)	1.315	[M+H]+	570.3559	570.35541	1
LPC 22:5 (1)	1.24	[M+H]+	570.354	570.35541	2
LPC 22:6	1.162	[M+H]+	568.34259	568.33978	5
LPC 26:0	4.779	[M+H]+	636.49457	636.49628	3
PC O-30:0	5.337	[M+H]+	692.56055	692.5589	2
PC O-32:4	4.191	[M+H]+	712.52765	712.52759	0
PC O-34:1	6.098	[M+H]+	746.60358	746.60583	3
PC O-34:2	5.558	[M+H]+	744.59454	744.59015	6
PC O-36:1	6.823	[M+H]+	774.6424	774.63715	7
PC O-36:2	6.157	[M+H]+	772.62561	772.62146	5
PC O-36:4	5.464	[M+H]+	768.59247	768.59015	3
PC O-36:6	4.908	[M+H]+	764.55939	764.5589	1
PC O-37:5	5.194	[M+H]+	780.58435	780.59015	7
PC O-38:4	5.99	[M+H]+	796.62585	796.62146	6
PC O-38:4	6.149	[M+H]+	796.62585	796.62146	6
PC O-38:6	5.394	[M+H]+	792.59216	792.59015	3
PC O-38:7	4.963	[M+H]+	790.57672	790.57452	3
PC O-38:7	5.165	[M+H]+	790.57239	790.57452	-3
PC O-40:5	6.033	[M+H]+	822.63513	822.63715	-2
PC O-40:7	5.326	[M+H]+	818.60858	818.60583	3
SM 32:1;2O	675.5452	[M+H]+	675.54517	675.54358	2
SM 33:1;2O	689.5598	[M+H]+	689.55981	689.5592	1
SM 34:1;2O	703.5794	[M+H]+	703.57452	703.57483	0
SM 34:2;2O	701.5618	[M+H]+	701.56183	701.5592	4
SM 35:1;2O	717.5928	[M+H]+	717.59283	717.59052	3
SM 36:1;2O	731.6106	[M+H]+	731.6106	731.60614	6
SM 36:2;2O	729.5942	[M+H]+	729.59418	729.59052	5
SM 38:1;2O	759.6412	[M+H]+	759.64117	759.63745	5
SM 38:2;2O	757.6254	[M+H]+	757.62537	757.62183	5
SM 39:1;2O	773.6434	[M+H]+	773.64679	773.65308	-8
SM 40:1;2O	787.6688	[M+H]+	787.66882	787.66876	0
SM 41:1;2O	801.688	[M+H]+	801.68805	801.68439	5
SM 41:2;2O	799.6765	[M+H]+	799.67371	799.66876	6
SM 42:1;2O	815.7042	[M+H]+	815.70422	815.70007	5
Cer 34:1;2O|Cer 18:1;2O/16:0	5.773	[M+H]+	538.51898	538.51935	1
Cer 36:1;2O|Cer 18:1;2O/18:0	6.516	[M+H]+	566.55096	566.55066	1

Cer 42:2;2O|Cer 18:1;2O/24:1	7.916	[M+H]+	648.63184	648.62891	5
PE 34:1	5.862	[M+H]+	718.53888	718.53815	1
PE 36:2|PE 18:1_18:1	5.93	[M+H]+	744.55261	744.55377	-2
PE 38:4|PE 14:0_24:4	5.916	[M+H]+	768.55225	768.55377	-2
PE 38:5	5.298	[M+H]+	766.53931	766.53815	2
PE 38:6|PE 16:1_22:5	5.03	[M+H]+	764.5235	764.52246	1
PE 40:4|PE 20:2_20:2	6.411	[M+H]+	796.58344	796.58508	-2
PE 40:6|PE 16:1_24:6	5.723	[M+H]+	792.55463	792.55377	1
PE 40:7|PE 16:1_24:6	5.123	[M+H]+	790.5368	790.53815	2
PI 38:3	5.538	[M+NH4]+	906.60852	906.60663	-2
PI 38:4	5.082	[M+NH4]+	904.59473	904.59094	-4
PI 38:5	4.551	[M+NH4]+	902.57507	902.57532	0
DG 22:1	3.482	[M+Na]+	449.32153	449.32376	5
DG 28:2	4.575	[M+Na]+	531.40515	531.40198	6
DG 30:5	4.577	[M+Na]+	553.3866	553.38635	0
TG 24:0|TG 8:0_8:0_8:0	4.015	[M+NH4]+	488.39594	488.39456	-3
TG 48:0|TG 14:0_16:0_18:0	11.191	[M+NH4]+	824.76917	824.77014	-1
TG 48:2	10.373	[M+NH4]+	820.74182	820.73889	4
TG 50:1|TG 16:0_16:0_18:1	11.201	[M+NH4]+	850.78857	850.78583	3
TG 50:2|TG 16:0_16:1_18:1	10.805	[M+NH4]+	848.77386	848.77014	4
TG 52:0|TG 16:0_18:0_18:0	11.853	[M+NH4]+	880.83691	880.83276	5
TG 52:0|TG 16:0_18:0_18:0	11.603	[M+NH4]+	880.83185	880.83276	-1
TG 52:1|TG 16:0_18:0_18:1	11.591	[M+NH4]+	878.8197	878.81714	3
TG 52:2|TG 16:0_16:0_20:2	11.21	[M+NH4]+	876.80554	876.80145	5
TG 52:3	10.835	[M+NH4]+	874.78461	874.78583	1
TG 52:3|TG 14:0_18:0_20:3	11.031	[M+NH4]+	874.78784	874.78583	2
TG 52:4|TG 16:0_16:0_20:4	10.696	[M+NH4]+	872.77301	872.77014	3
TG 54:3|TG 18:0_18:1_18:2	11.22	[M+NH4]+	902.81635	902.81714	-1
TG 54:4|TG 16:0_18:0_20:4	11.155	[M+NH4]+	900.80658	900.80145	6
TG 54:5|TG 16:0_16:0_22:5	10.718	[M+NH4]+	898.78918	898.78583	4
TG 54:6|TG 16:0_16:0_22:6	10.516	[M+NH4]+	896.77277	896.77014	3
TG 54:7|TG 16:0_16:1_22:6	10.089	[M+NH4]+	894.75916	894.75452	5
TG 56:5|TG 18:0_18:1_20:4	11.157	[M+NH4]+	926.82294	926.81714	6

Table *5.3.3*-**1** Peak list of lipids identified

Data processed were then exported as peak list with peak heights and were then normalized by use of internal standards. The structural assignments of the most abundant lipids were afterwards confirmed through the evaluation of peak spotting plots of m/z vs RT (figure 5.3.3-**2**)

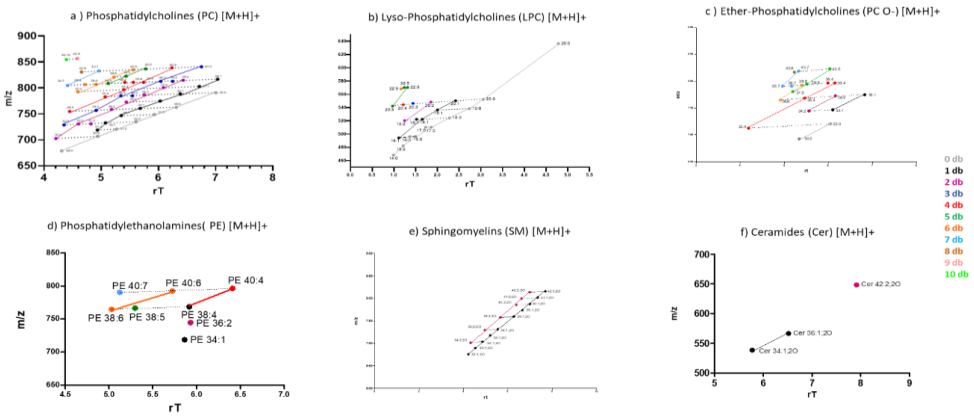

Figure 5.3.3-**2**

Spotting maps showing relationship of precursor m/z and RT for 7 different lipid classes: PC, LPC, ePC, PE, PE, SM, Cer. The same colors represent lipids with the same number of double bonds. In every graph the m/z of precursor ions of the identified specie was plot versus retention times. Then, the empirical correlation of the given m/z and RT was calculated for each group of lipids with the same number of carbons.

A correlation coefficient > 0.95 was required to consider that all the lipids found were correctly identified

It is known that lipid species of the distinct lipid classes elute in regular patterns in accordance with their homology principle; lipids with more double bonds elute earlier while lipids with longer acyl chains elute later always shifted by regular increments per structural repeat element if the gradient is linear. Hence, this empirical correlation was helpful to identify misidentifications which was based on the most abundant, easily identified lipids in a class, or on added internal standards.

The lipid composition of SH-SY5Y, is still not yet known in detail. In 2019, for the first time, Halskau research group characterized the whole cell and plasma membrane lipid isolated from the neuroblastoma cell line SH-SY5Y.[17] In the same year, Xicoy et al. performed a lipidomic study, based on LC-MS analysis to determine Parkinson Disease-linked changes in the lipid profile of SHSY5Y cell line, in that case treated with the neurotoxin 6-hydroxydopamine (6-OHDA) to confirm the validity of cultured 6-OHDA-treated SH-SY5Y cells as an attractive cell model for *in vitro* studies on PD.[12] In the present study, 138 lipids from 9 lipid classes were identified in SHSY5Y cell culture, normally used to study neurodegeneration and for evaluation of active compounds capable of halting amyloid toxicity.[18 19 20 21]

Regarding the distribution of all identified lipid species according to their lipid classes, most of the lipids belonged to Phosphatidylcholines (PCs), that covered 35.51% of all identified lipids (both polarities combined). SMs were detected in the positive mode in a lower percentage distribution compared to that there would be (10.90%).[17] Moreover, it was not possible to identify the exact SMs FA acid composition because

most observed SM lipid species lacked FA-specific fragments. The latter finding is in line with a previous ^{31}P NMR phospholipid analysis of SH-SY5Y whole cell and plasma membrane lipid isolated. The abundance of PEs is lower than the one reported by Jakubec et al. (5.80%). Other widely identified lipid classes were Lyso-Phosphatidylcholines (LPCs) (15.94 %) Triglycerides (TGs) (14.49 %) and Ether-Phosphatidylcholines (PC-O) (11.60%), not described in their study. Moreover, a small number of Ceramides (Cers) (2.17%), Diglycerides (DGs) (1.44%) and Phosphatidylinositols (PIs) (2.17%) were found (Figure 5.3.3-3).

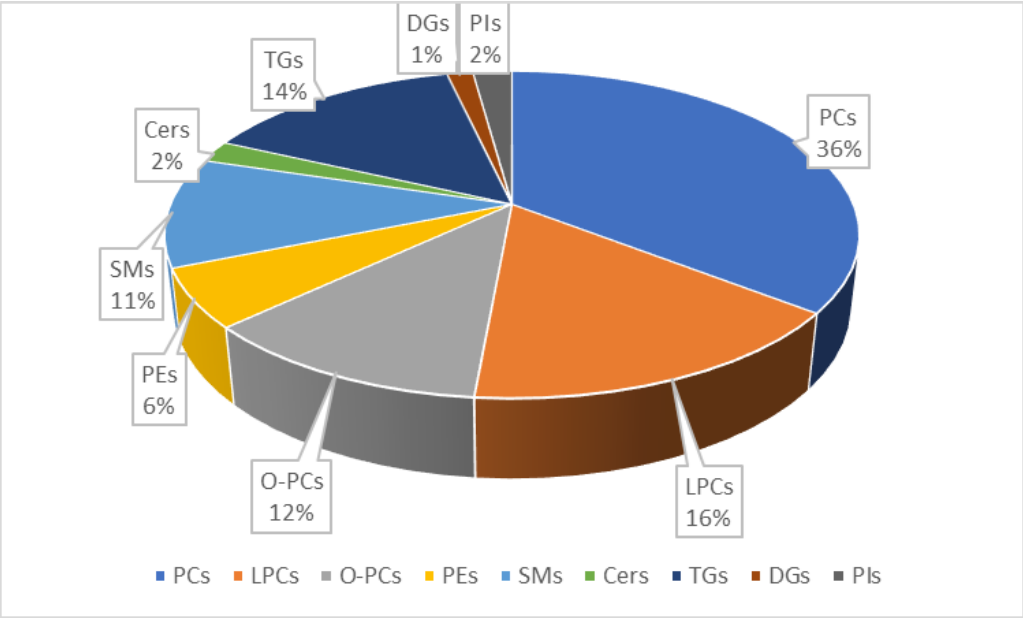

Figure *5.3.3*-**3**

Percentage distribution in 9 lipid classes of the 138 lipids identified in SH-SY5Y cell culture

5.3.4 Validation of Precision of LC-MS Analysis of the Identified Features in the QC in Positive Ionization Mode (ESI+)

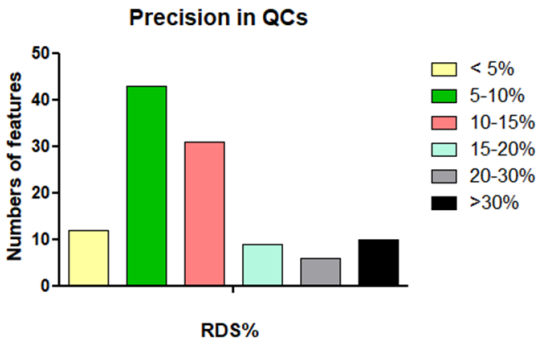

Figure *5.3.4*-**1**. Quality control of analytical batch with pooled QC

Distribution of CVs (%) for the identified lipids in the pooled QC embedded during the analytical batch (injection after every fifth sample); yellow (CV < 5%), green (CV 5 - 10%), red (CV 10 %- 15%), light blue (15-20%) and grey (20-30%) bars show acceptable data, while black bar show lipids that have to be removed because of CV > 30%

5.3.5 Relative Quantification of Lipids

Concerning the relative quantification, in this preliminary study we focused on the lipid classes of Phosphatidylcholine (PC), Lyso-Phosphatidylcholine (LPC) and Sphingomyelins (SM), because Glycerophospholipids (GPs) and Sphingolipids (SPs) perturbation, more than others, may be associated with neuronal injury, neuroinflammation and neurodegeneration.

The current study originates from evidence collected in previous lipidomic analysis in AD patients that showed decreased brain levels of ether-sterols, PCs, SMs and total phospholipids compared to healthy control group.[22]

GPs are the major type of lipid defining the cell membrane and Phosphatidylcholine (PC) is the predominant form in the human brain, accounting for 32.8 % [1]. In AD brain PCs were found significantly decreased, in particular the three PC species: PC (16:0-20:5), PC (16:0-22:6) and PC (18:0-22:6). It seems that the depletion could identify cognitively normal individuals who will convert to AD within 2-3 years.[23] According to these prior evidences, in the present study, a significant decrease in percentage distribution of the following PCs species: PC (18:1-16:2); PC (18:0-20:3); PC (18:0-20:4); PC (16:0-22:5) and PC (16:0-22:6) was measured when differentiated neuroblastoma cells were treated with low (2-10 µM) and medium concentration (10-25 µM) of $A\beta_{1\text{-}42}$ peptide for 24 h [figure 5.3.5-**1** (A)].

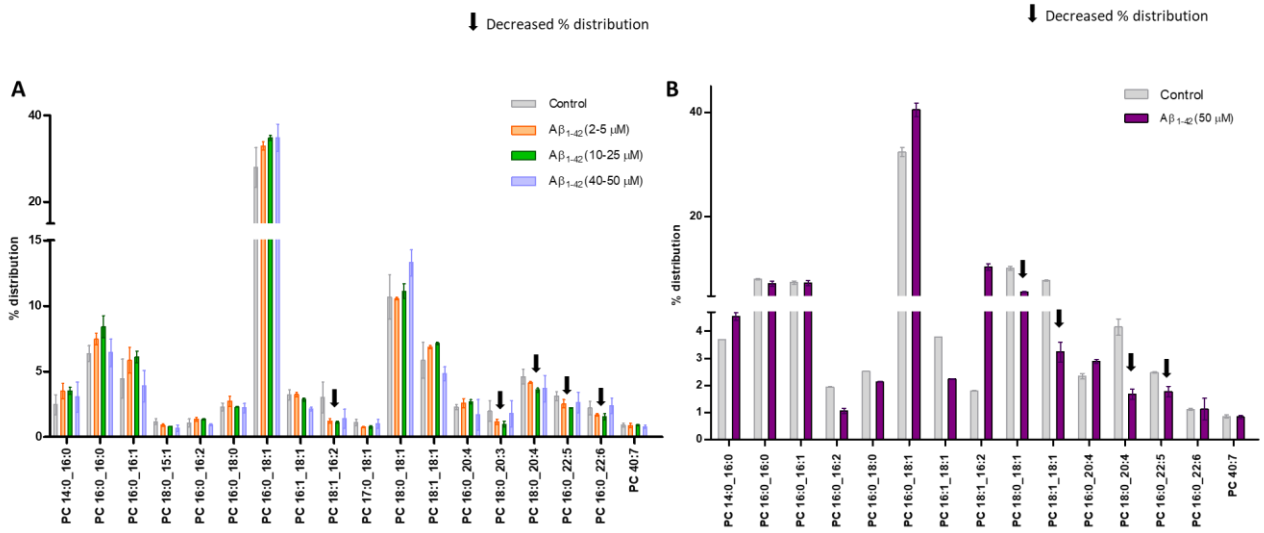

Figure 5.3.5-**1** Relative Phosphatidylcholine (PC) distribution in the lipid extract of differentiated. SH-SY5Y cells treated with Aβ1-42 SH-SY5Y cells were incubated with $A\beta_{1\text{-}42}$ (A) at increasing concentration (2-50 µM) for 24 h (B) at highest concentration (50 µM) for 48 h. Each bar represents means ± SEM of three independent experiments

In fact, it has already been proposed that amyloid causes toxic effects through membrane interactions.[24] This mechanism of toxicity may include the induction of membrane channels or pores, activation of calcium

channels such as N-methyl-D-aspartate (NMDA), membrane thinning and/or membrane destabilization. It has been shown that amyloid peptides, mostly oligomers, incorporating into lipid bilayer may exhibit detergent-like properties, destabilizing the membrane by removing lipid molecules [25] [26]. This mechanism has further been supported by observation of pore-like activity predominantly causing an increase in the neuronal influx of Ca^{2+}. In particular, a recent study demonstrated that oligomeric Aβ peptide induces accumulation of free PUFAs and Lyso-Phosphatidylcholine containing a saturated or monounsaturated FA in the sn-1 position [27]. This seems due to the activation of cytosolic phospholipase A2 (cPLA2), that in the presence of Ca^{2+} gets activated and binds to substrates in the cell membrane. It is highly specific for PC cleavage and arachidonic acid (AA) release (figure 5.3.5-**2**) [27].

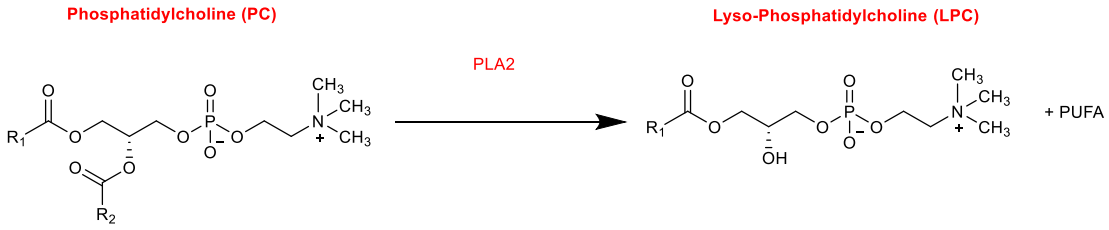

Figure *5.3.5*-**2** Cytosolic phospholipase A2 (cPLA2) catalyses PC cleveage at sn-2 position. PUFAs and Lyso-Phosphatidylcholine containing a saturated or monounsaturated FA in the sn-1 position are released

The results from the first case study [$A\beta_{1-42}$ (2-50 uM) treatment for 24 h] are in agreement with these previous findings. In fact, the PC species that decreased their percentage distribution were those containing PUFA while the PC species that increased were those containing saturated FAs or MUFAs [figure 5.3.5-**1** (A)].

A concomitant correlated increased percentage for the MUFA-containing LPC species can be found: LPC 16:0 (1) (sn1 lyso form), LPC 16:0 (2) (sn 2 lyso form) and LPC 18:0 and a diminished percentage for PUFA-containing LPC [figure 5.3.5-**3** (A)]. These results are in line with accumulation of free PUFAs and Lyso-Phosphatidylcholine containing a saturated or monounsaturated FA in the sn-1 position reported in Palavicini's study [27].

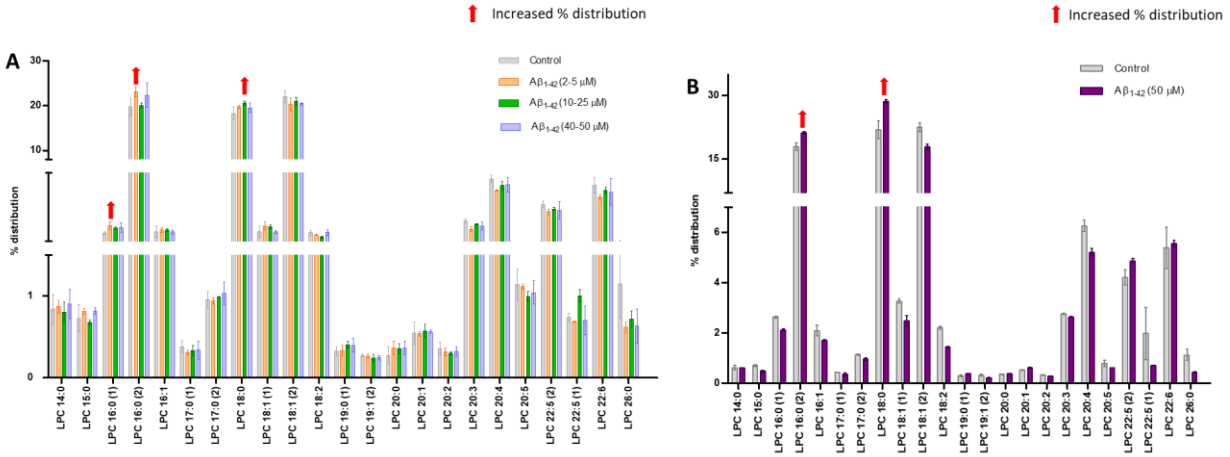

Figure *5.3.5*-**3** Relative Lyso-phosphatidylcholine (LPC) distribution distribution in the lipid extract of differentiated SH-SY5Y cells treated with $A\beta_{1-42}$. SH-SY5Y cells were incubated with $A\beta_{1-42}$ (A) at increasing concentration (2-50 μM) for 24 h (B) at highest concentration (50 μM) for 48 h. Each bar represents means ± SEM of three independent experiments.

Concerning SMs, they are the most abundant SPs in the brain and they are important components of lipid rafts. We found that the percentage distribution of most of the SMs species is reduced upon $A\beta_{1-42}$ treatment in comparison to control samples. In particular, the SM 38:1;2O; SM 40:1;2O; SM 41:1;2O have a reduced percentage distribution under low and medium $A\beta_{1-42}$ peptide treatment for 24 h; SM 42:1;2O specie is decreased as well at high $A\beta_{1-42}$ peptide treatment concentration for 24 h [figure 5.3.5-**5** (A)]. According to studies on mouse model,[28] intracerebral injection of Aβ promoted neutral Sphingomyelinase (SMase) activity and increased ceramide levels. SMase is the enzyme responsible of catalysing the hydrolysis of phosphodiester bond in SM that results in the formation of phosphocholine and ceramide (Cer) (figure 5.3.5-**4**).

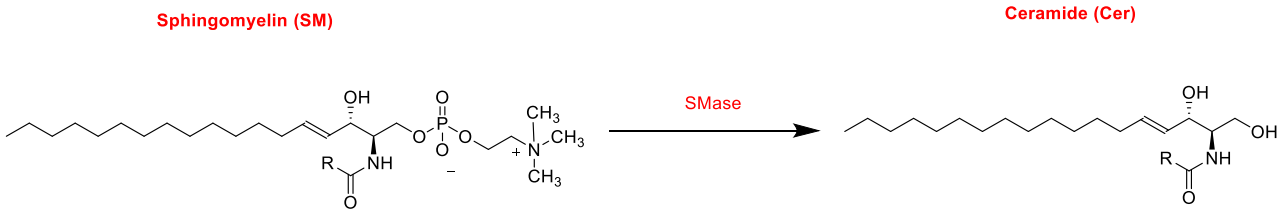

Figure *5.3.5*-**4** Sphingomyelinase (SMase) catalyses sphingomyelin to ceramide by hydrolysis

In base of the optimal pH working condition, SMases are classified into three subtypes: acid, neutral, and alkaline; among these the acid SMase (ASM) and neutral SMase (NSM) are the main forms involved in Cer production in case of stress condition. Cer is a lipid mediator that can regulate cell growth and apoptosis. In particular, increased levels of Cers due to NSM induction bring to higher exosome secretion, that is known to be related to Aβ production, clearance and accumulation. In addition, exosomes are recognized as inflammatory mediators and crucial agents in oxidative stress during AD progression. Nowadays, it is confirmed that Aβ activates NSM but not ASM. However, ASM is associated with the onset of AD, especially

when ASM activity is elevated the autophagy-lysosome pathway (ALP) is altered, autophagy degradation is reduced and so the misfolded proteins tend to accumulate. For this reasons, in clinical treatments the interest towards NSM and ASM as targets is increasing also in the field of AD [29].

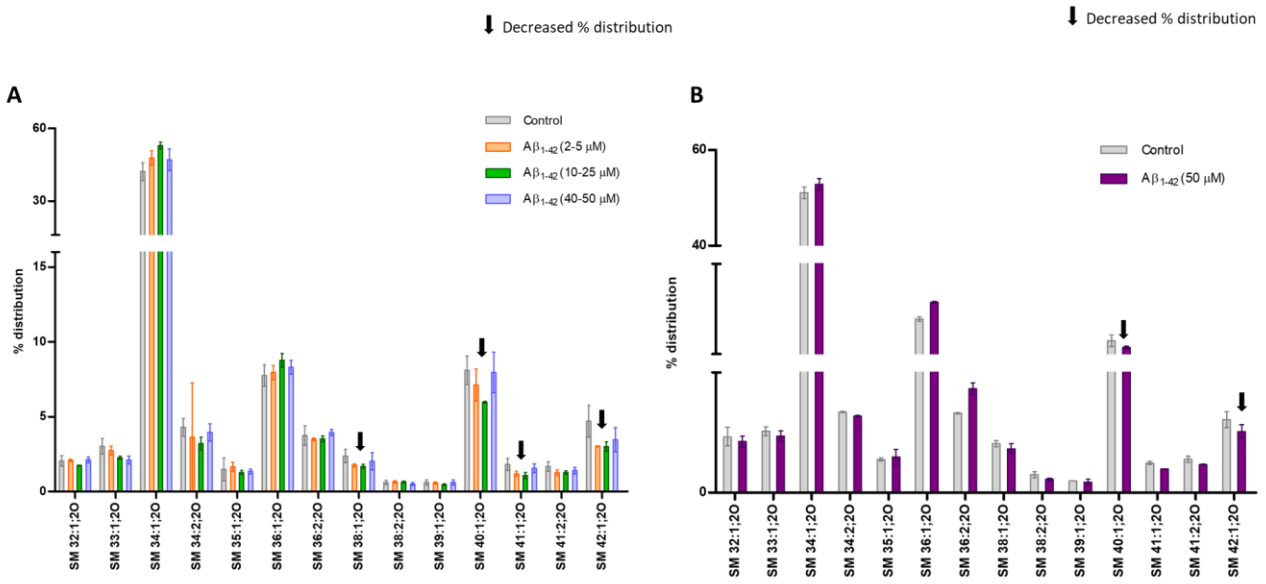

Figure 5.3.5-**5** Relative Sphingomyelin (SM) distribution in the lipid extract of differentiated SH-SY5Y cells treated with Aβ1-42. SH-SY5Y cells were incubated with Aβ1-42 (A) at increasing concentration (2-50 μM) for 24 h (B) at highest concentration (50 μM) for 48 h. Each bar represents means ± SEM of three independent experiments.

Our findings seem in line with all these assumptions because we found decreased level of SMs and increased amount of ceramides content in SH-SY5Y samples treated with $A\beta_{1\text{-}42}$ peptide. In particular, the percentage distribution of Cer 36:1;2O [Figure 5.3.5-6 (A)] seems significantly elevated increasing the $A\beta_{1\text{-}42}$ peptide concentration treatment.

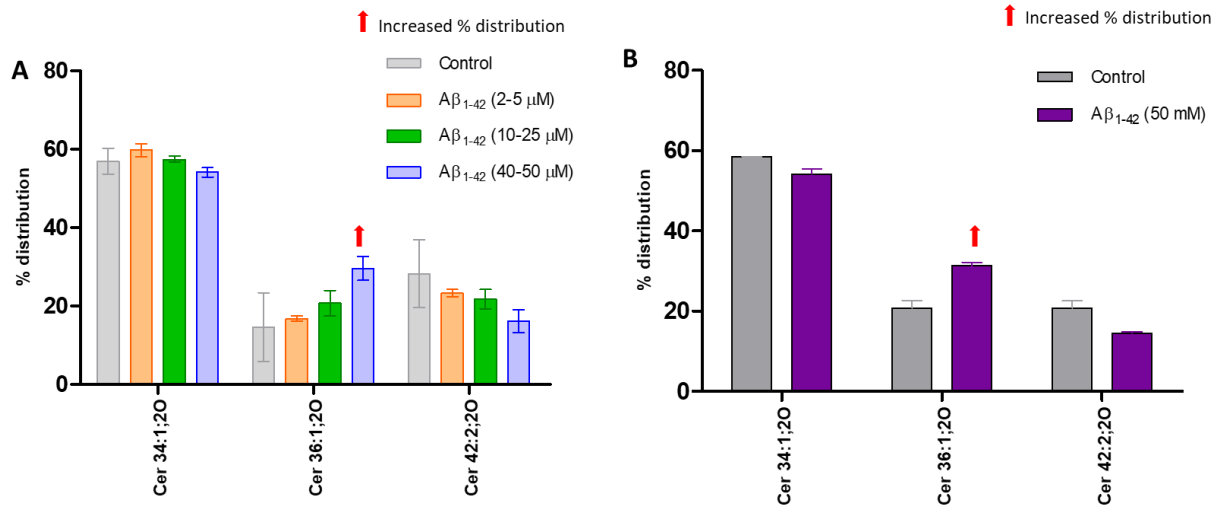

Figure *5.3.5*-**6** Relative Ceramide (Cer) distribution in the lipid extract of differentiated SH-SY5Y cells treated with $A\beta_{1-42}$. SH-SY5Y cells were incubated with $A\beta_{1-42}$ (A) at increasing concentration (2-50 µM) for 24 h (B) at highest concentration (50 µM) for 48 h. Each bar represents means ± SEM of three independent experiments.

In the second case study in which the same numbers of cells were incubated with $A\beta_{1-42}$ peptide at 50 µM for a longer time (48 h), the $A\beta_{1-42}$ determined a substantial toxic effect and cell death [figure 5.2.5-**1** (B)]. A decrease of the percentage distribution of the following PCs species: PC (18:0-18:1); PC (18:1-18:1); PC (18:0-20:4) and PC (16:0-22:5) [figure 5.3.5-**1** (B)], SM species: SM 40:1;2O, SM 42:1; 2O [figure 5.3.5-**5** (B)] and an increase of saturated FAs containing LPC species: LPC 16:0; LPC 18:0 [figure 5.3.5-**3** (B)] and Cer 36:1;2O [figure 5.3.5-**6** (B)] were observed.

These results are relevant considering the awareness that the dysregulated lipid homeostasis contributes greatly to the pathogenesis of AD. In fact, FAs and their metabolites are involved in synaptic plasticity, inflammation, cerebrovascular function and oxidative stress.

5.4 Conclusions

The lipidomic approach developed was found suitable to monitor some lipid metabolism alterations that might be correlated to $A\beta_{1-42}$ oligomers toxicity. The results showed potential biomarkers for targeting and testing AD by *in vitro* cell assays. It was supposed that these alterations in PC and LPC level might be due to the activation of Phospholipase A2 (PLA2) enzymes that hydrolyses the sn-2 ester bond of the membrane glycerophospholipids to generate MUFAs containing Lyso-phospholipids and polyunsaturated fatty acids (PUFAs). Both are biologically active lipid mediators in particular arachidonic acid that plays a critical central role in neuroinflammation.

Concerning the alterations in the SM profile it was hypothesised the activation of SM-degrading enzyme Sphingomyelinase (SMase) that hydrolyses the phosphocholine-headgroup of Sphingomyelins producing proapoptotic ceramides.

Recent studies have demonstrated the correlation between these enzymes and AD pathogenesis. Therefore, these enzymes could represent interesting targets for AD drug discovery. Furthermore, the method if will be validated could also be applied to the elucidation of amyloid aggregation inhibitors mechanism of action, able not only to inhibit the aggregation process, but also to avoid the lipid homeostasis alterations, in view of the AD research of new drugs for therapy.

This pilot study will guide future study designs and allow for proper selection of cell numbers, $A\beta_{1-42}$ peptide concentrations, incubation times, amongst others, for performing advanced investigations of the role of Aβ peptides on the lipidome of neuronal cells as well as its potential utilization to monitor effects of potential AD drug candidates.

References:

(1) Kao, Y. C.; et al. Lipids and Alzheimer's Disease. *International Journal of Molecular Sciences*. **2020**, *21*(4), 1505 https://doi.org/10.3390/ijms21041505.

(2) Cline, E. N.; et al. The Amyloid-β Oligomer Hypothesis: Beginning of the Third Decade. *Journal of Alzheimer's Disease*. **2018**, *64*(s1), S567-S610 https://doi.org/10.3233/JAD-179941.

(3) De Simone, A.; et al. Investigating in Vitro Amyloid Peptide 1−42 Aggregation: Impact of Higher Molecular Weight Stable Adducts. *ACS Omega* **2019**, *4* (7), 12308–12318 https://doi.org/10.1021/acsomega.9b01531.

(4) Bartolini, M.; et al.Kinetic Characterization of Amyloid-Beta 1-42 Aggregation with a Multimethodological Approach. *Anal. Biochem.* **2011**, *414* (2), 215-225 https://doi.org/10.1016/j.ab.2011.03.020.

(5) **Davani, L.; et al. Aß$_{1-42}$ Peptide Toxicity on Neuronal Cells: A Lipidomic Study in View of Alzheimer's Disease Drug Discovery. *J Pharm Biomed Anal* 2022 (*Submitted)***

(6) Fiori, J.; et al. Mass Spectrometry as an Efficient Tool for the Characterization of Amyloid β Peptide 25-35 Self-Assembly Species in Aggregation and Inhibition Studies. *Eur. J. Mass Spectrom.* **2013**, *19* (6), 483-90.https://doi.org/10.1255/ejms.1255.

(7) Bartolini, M.; et al. Insight into the Kinetic of Amyloid β (1-42) Peptide Self-Aggregation: Elucidation of Inhibitors' Mechanism of Action. *ChemBioChem* **2007**, 8 (17) 2152-2161 https://doi.org/10.1002/cbic.200700427.

(8) Tsugawa, H.; et al. MS-DIAL: Data-Independent MS/MS Deconvolution for Comprehensive Metabolome Analysis. *Nat. Methods* **2015**, *12* (6), 523–526 https://doi.org/10.1038/nmeth.3393.

(9) Pérez-Areales, F. J.; et al. Design, Synthesis and Multitarget Biological Profiling of Second-Generation Anti-Alzheimer Rhein-Huprine Hybrids. *Future Med. Chem.* **2017**, *9* (10), 965-981 https://doi.org/10.4155/fmc-2017-0049.

(10) Petry, F. dos S.; et al. Genistein Protects against Amyloid-Beta-Induced Toxicity in SH-SY5Y Cells by Regulation of Akt and Tau Phosphorylation. *Phyther. Res.* **2019**, *34* (4), 796-807 https://doi.org/10.1002/ptr.6560.

(11) Wang, H.; et al. Amyloid-β_{1-42} Induces Reactive Oxygen Species-Mediated Autophagic Cell Death in U87 and SH-SY5Y Cells. *J. Alzheimer's Dis.* **2010**, *21* (2), 597–610. https://doi.org/10.3233/JAD-2010-091207.

(12) Xicoy, H.; et al.Lipid Analysis of the 6-Hydroxydopamine-Treated SH-SY5Y Cell Model for Parkinson's Disease. *Mol. Neurobiol.* **2020**, *57* (2), 848–859. https://doi.org/10.1007/s12035-019-01733-3.

(13) Shipley, M. M.; et al. Differentiation of the SH-SY5Y Human Neuroblastoma Cell Line. *J. Vis. Exp.* **2016**, *108*, 53193 https://doi.org/10.3791/53193.

(14) Krishtal, J.; et al. In Situ Fibrillizing Amyloid-Beta 1-42 Induces Neurite Degeneration and Apoptosis of Differentiated SH-SY5Y Cells. *PLoS One* **2017**, *12* (10), e0186636 https://doi.org/10.1371/journal.pone.0186636.

(15) Lambert, M. P.; et al. β/A4-evoked Degeneration of Differentiated SH-SY5Y Human Neuroblastoma Cells. *J. Neurosci. Res.* **1994**, *39* (4), 377-385 https://doi.org/10.1002/jnr.490390404.

(16) Bligh, E. G.; Dyer, W. J. A Rapid Method of Total Lipid Extraction and Purification. *Can. J. Biochem. Physiol.* **1959**, *37* (8), 911-7 https://doi.org/10.1139/o59-099.

(17) Jakubec, M.; et al. Fast and Quantitative Phospholipidomic Analysis of SH-SY5Y Neuroblastoma Cell Cultures Using Liquid Chromatography-Tandem Mass Spectrometry and 31P Nuclear Magnetic Resonance. *ACS Omega* **2019**, *4* (25), 21596–21603. https://doi.org/10.1021/acsomega.9b03463.

(18) Montanari, S.; et al. A. Multitarget Strategy to Address Alzheimer's Disease: Design, Synthesis, Biological Evaluation, and Computational Studies of Coumarin-Based Derivatives. *ChemMedChem* **2016**, *11* (12), 1296-1308 https://doi.org/10.1002/cmdc.201500392.

(19) Belluti, F.; et al. Fluorinated Benzophenone Derivatives: Balanced Multipotent Agents for Alzheimer's Disease. *Eur. J. Med. Chem.* **2014**, *78*, 157-66 https://doi.org/10.1016/j.ejmech.2014.03.042.

(20) Montanari, S.; et al. Discovery of Novel Benzofuran-Based Compounds with Neuroprotective and Immunomodulatory Properties for Alzheimer's Disease Treatment. *Eur. J. Med. Chem.* **2019**, *178*, 243-258 https://doi.org/10.1016/j.ejmech.2019.05.080.

(21) Rampa, A.; et al. Chalcone-Based Carbamates for Alzheimer's Disease Treatment. *Future Med. Chem.* **2017**, *9* (8), 749-764 https://doi.org/10.4155/fmc-2017-0029.

(22) Bogie, J. F. J.; et al. Fatty Acid Metabolism in the Progression and Resolution of CNS Disorders. *Adv. Drug Deliv. Rev.* **2020**,*159*, 198-213 https://doi.org/10.1016/j.addr.2020.01.004.

(23) Mapstone, M.; et al. Plasma Phospholipids Identify Antecedent Memory Impairment in Older Adults. *Nat. Med.* **2014**, *20* (4), 415-8 https://doi.org/10.1038/nm.3466.

(24) Butterfield, S. M.; Lashuel, H. A. Amyloidogenic Protein-Membrane Interactions: Mechanistic Insight from Model Systems. *Angewandte Chemie - International Edition.* **2010**, *49* (33), 5628-54 https://doi.org/10.1002/anie.200906670.

(25) Sheikh, K.; et al. Differing Modes of Interaction between Monomeric Aβ1-40 Peptides and Model Lipid Membranes: An AFM Study. *Chem. Phys. Lipids* **2012**, *165* (2), 142-150 https://doi.org/10.1016/j.chemphyslip.2011.11.011.

(26) Gunn, A. P.; et al. Amyloid- Peptide A-3pE-42 Induces Lipid Peroxidation, Membrane Permeabilization, and Calcium Influx in Neurons. *J. Biol. Chem.* **2016**, *291* (12) 6134-6145https://doi.org/10.1074/jbc.M115.655183.

(27) Palavicini, J. P.; et al. Oligomeric Amyloid-Beta Induces MAPK-Mediated Activation of Brain Cytosolic and Calcium-Independent Phospholipase A2 in a Spatial-Specific Manner. *Acta Neuropathol. Commun.* **2017**, *5* (1), 56 https://doi.org/10.1186/s40478-017-0460-6.

(28) Alessenko, A. V.; et al. Connection of Lipid Peroxide Oxidation with the Sphingomyelin Pathway in the Development of Alzheimer's Disease. In *Biochemical Society Transactions*; **2004**, *32* (1), 144–146 https://doi.org/10.1042/BST0320144.

(29) Xiang, H.; et al. Physiological Functions and Therapeutic Applications of Neutral Sphingomyelinase

and Acid Sphingomyelinase. *Biomed. Pharmacother*. **2021**, *139*, 111610. https://doi.org/10.1016/j.biopha.2021.111610

Conclusions

The aim of this Ph.D thesis was the development of advanced analytical techniques capable of evaluating the activity of new potential multi-target directed ligands (MTDLs) for AD therapy. Beside the research was focused on analytical methodologies suitable for the characterization of the processes underlying drug-protein bindings and for the study of protein-protein interactions involved in neurodegenerative pathways.

Each analytical methodology investigated in the projects resulted able to support AD drug discovery.

In fact, the *in vitro* high-throughput luminescent assay proved to be suitable to evaluate the activity of the first series of potential GSK-3β-HDAC dual inhibitors designed by the Medicinal Chemistry group at *Department for Life Quality Studies* and it reliably and quickly identified true positive hit compounds. In addition, during the characterization of the Amaryllidaceae alkaloids towards GSK-3β the luminescent kinase assay resulted able to screen natural compounds and it allow to identify in these compounds an interesting natural scaffold for GSK-3β dual inhibitors. In both case this method provides information to perform structure activity relationships in view of the development and optimization of a lead structure with improved activity and bioavailability properties.

The multi-methodological approach, applied for the study of CORMs-$A\beta_{1-42}$ interaction, gave more innovative insights about the mechanism of toxicity of $A\beta_{1-42}$ aggregation, that is a crucial aspect in AD pathogenesis. Combination of ThT assay, ESI-MS analysis, and CD studies granted reliable information on the overall fibrilization process and it allowed to characterize the new potential aggregation inhibitors in a comprehensive way. CORMs were found able to generate stable adducts with $A\beta_{1-42}$ amino acidic chain, delaying in this way the transition of $A\beta_{1-42}$ monomers from α-helix to β-sheet secondary structure. CORM-3 emerged as a promising amyloid anti-aggregating agent, and the optimal CORM-3/$A\beta_{1-42}$ ratio for the best inhibitory effect was identified. This multimethodological approach explained a molecular additional mechanism of CORMs that are already known for their neuroprotective and anti-inflammatory effects.

Finally, in the research of new methods for diagnostic purposes in AD, the lipidomic approach developed was found suitable to monitor some lipid metabolism alterations that might be correlated to $A\beta_{1-42}$ oligomers toxicity. The identification and the relative quantification of some lipid altered species due to Aβ toxicity could be useful in the characterization of new biomarkers for the early detection of AD and in the therapeutic monitoring. The method developed allowed to obtain results that will guide future experiments with optimized conditions in terms of cell numbers, $A\beta_{1-42}$peptide concentrations, incubation times in order to carry on further investigations. Moreover, if the cell model will be validated, it could be exploited to elucidate amyloid aggregation inhibitors mechanism of action, able not only to inhibit the aggregation process, but also to reduce lipid alterations in view of AD new drugs discovery.